


For Reference

NOT TO BE TAKEN FROM THIS ROOM

Ex LIBRIS
UNIVERSITATIS
ALBERTAEASIS





Digitized by the Internet Archive
in 2023 with funding from
University of Alberta Library

<https://archive.org/details/Rusnak1971>

THE UNIVERSITY OF ALBERTA

NMR LINE BROADENING STUDY OF SOME PARAMAGNETIC
SCHIFF BASE AND PORPHYRIN COMPLEXES

by



Leonard Lawrence Rusnak

A THESIS

SUBMITTED TO THE FACULTY OF GRADUATE STUDIES
IN PARTIAL FULFILMENT OF THE REQUIREMENTS FOR THE DEGREE
OF DOCTOR OF PHILOSOPHY

Department of Chemistry

Edmonton, Alberta

Fall, 1971

Thesis
1971 F
76D

THE UNIVERSITY OF ALBERTA
FACULTY OF GRADUATE STUDIES

The undersigned certify that they have read, and
recommend to the Faculty of Graduate Studies for
acceptance, a thesis entitled

NMR LINE BROADENING STUDY OF SOME PARAMAGNETIC
SCHIFF BASE AND PORPHYRIN COMPLEXES

submitted by Leonard Lawrence Rusnak in partial fulfilment
of the requirements for the degree of Doctor of Philosophy.

ACKNOWLEDGEMENTS

I wish to express my gratitude to Dr. Robert B. Jordan for his advice and guidance throughout the course of this work.

I also wish to thank Mrs. Lorraine Bendle for the excellent preparation of this manuscript.

Financial assistance from the University of Alberta and the National Research Council of Canada is gratefully acknowledged.

ABSTRACT

The solvent exchange reactions of manganese(III) protoporphyrin(IX)dimethyl ester ($\text{Mn}(\text{DMPPrPor})^+$), a series of tetragonally distorted Schiff base complexes of nickel(II) (NiCR^{2+} , NiCRMe^{2+} , NiTAAB^{2+}), manganese(II) (MnB^{2+}), cobalt(II) (CoCR^{2+} , $\text{Co}(\text{trans}[14]\text{diene})^{2+}$) and copper(II) (CuCR^{2+}) were investigated using the nmr line broadening method. The octahedral Schiff base complex (NiTRI^{2+}) was also studied.

Chemical exchange controlled line broadening of the bulk solvent proton resonance was observed for $\text{Mn}(\text{DMPPrPor})^+$ in methanol and N,N-dimethylformamide (DMF); NiCR^{2+} in water, methanol, DMF and acetonitrile; NiCRMe^{2+} in water and DMF; NiTAAB^{2+} and NiTRI^{2+} in DMF; and MnB^{2+} in water, methanol and DMF. For NiCR^{2+} in dimethylsulfoxide, CoCR^{2+} in DMF, $\text{Co}(\text{trans}[14]\text{diene})^{2+}$ in water, methanol and acetonitrile and CuCR^{2+} in water and DMF, chemical exchange controlled line broadening was not observed. For the former systems, the kinetic parameters for solvent exchange were obtained by resolving the effects due to chemical exchange and relaxation of proton nuclei in the inner and outer coordination spheres of the metal ion complex, but for the latter systems, only lower limits could be placed on the exchange rates. Line broadening results under conditions of rapid exchange were interpreted in terms of dipolar and

or hyperfine interactions using reasonable solvent proton-metal ion interaction distances, correlation times, and hyperfine coupling constants determined from the measured chemical shifts of the bulk solvent resonance. Wherever possible, these chemical shifts were also used to obtain the most self-consistent set of kinetic parameters. For most systems, measurements were made at 60 and 100 MHz to enable an unequivocal interpretation of the relaxation mechanism.

Some unusual features were observed for the NiCR^{2+} and NiCRMe^{2+} complexes. It was found that these complexes undergo a rapid diamagnetic-paramagnetic equilibrium change in the coordinating solvents used in the nmr study. Magnetic susceptibility (Evan's method) and ligand proton contact shift measurements were used to determine the equilibrium constants which were required to interpret the nmr line broadening and chemical shift results. In addition, it was observed that the dipolar relaxation mechanism for NiCR^{2+} and NiCRMe^{2+} is magnetic field dependent since the dipolar correlation time is determined, for the most part, by the magnetic field dependent electron spin relaxation time. An additional unusual feature was observed for the NiCR^{2+} -methanol system in that the OH and CH_3 proton resonances were shifted in opposite directions due to a large pseudocontact shift of the OH proton but only a contact shift of the CH_3 proton resonance. Finally, the solvent

exchange rates of these two nickel(II) complexes were found to be unusually rapid. Possible reasons for the high rates are discussed in the final chapter.

For MnB^{2+} in methanol, DMF and water, a magnetic field dependence of T_{2M} relaxation was also observed but for this complex the field dependence could be attributed to the hyperfine contribution to T_{2M} . The theory of Bloembergen was used to obtain the correlation time for modulation of the zero-field splitting in the MnB^{2+} -water and methanol systems.

In the final chapter, the kinetic results of this work are discussed in relation to the previously studied hexa-solvated systems.

TABLE OF CONTENTS

	<u>Page</u>
Acknowledgements	iii
Abstract	iv
Table of Contents	vii
List of Figures	xi
List of Tables	xvi
 I INTRODUCTION	 1
1. General Comments	1
2. NMR Theory	5
(a) General Theory	5
(b) Temperature Dependence of Relaxation Times and Chemical Shifts	 9
(c) Limiting Cases of the Swift and Connick Theory	 17
 II THE PREPARATION AND CHARACTERIZATION OF COMPLEXES, SOLVENT PURIFICATION, SAMPLE PREPARATION AND INSTRUMENTATION	 25
1. Purification of Solvents	25
2. Preparation and Characterization of Mn(DMP ₄ PrPor)Cl·OH ₂	 25
3. Preparation and Characterization of MnB(ClO ₄) ₂	 27

4.	Preparation and Characterization of the Various Salts of NiCR^{2+} and NiCRMe^{2+}	30
5.	Preparation and Characterization of $\text{NiTAAB}(\text{ClO}_4)_2$	38
6.	Preparation and Characterization of $\text{NiTRI}(\text{ClO}_4)_2$	40
7.	Preparation and Characterization of $\text{CoCR}(\text{ClO}_4)_2$	40
8.	Preparation and Characterization of $\text{CuCR}(\text{BF}_4)_2$	42
9.	Preparation and Characterization of $\text{Co}(\text{trans}[14]\text{diene})(\text{ClO}_4)_2$	43
10.	Sample Preparation	45
11.	Instrumentation	48

III	NUCLEAR MAGNETIC RESONANCE LINE BROADENING AND CHEMICAL SHIFT STUDIES OF SOME PARAMAGNETIC SCHIFF BASE AND PORPHYRIN COMPLEXES	50
1.	Solvent Proton NMR Line Broadening and Chemical Shift Study of $\text{Mn}(\text{DMP}r\text{Por})^+$ in Methanol and N,N -dimethylformamide	50
2.	Solvent Proton NMR Line Broadening and Chemical Shift Study of MnB^{2+} in N,N - dimethylformamide, Water and Methanol	68
3.	Magnetic Susceptibility and Ligand PMR	

Shift Study of the Paramagnetic-Diamagnetic Equilibrium of NiCR^{2+} and NiCRMe^{2+} in Several Coordinating Solvents	99
4. Solvent Proton NMR Line Broadening and Chemical Shift Study of NiCR^{2+} in N,N- dimethylformamide, Water, Acetonitrile, Methanol and Dimethylsulfoxide and NiCRMe^{2+} in N,N-dimethylformamide and Water	118
5. Solvent Proton NMR Line Broadening and Chemical Shift Study of NiTRI^{2+} and NiTAAB^{2+} in N,N-dimethylformamide	173
6. Solvent Proton NMR Line Broadening Study of $\text{Co}(\text{trans}[14]\text{diene})^{2+}$, CoCR^{2+} and CuCR^{2+} in Various Solvents	187
IV DISCUSSION	207
1. Kinetic Results	
(a) Methanol and DMF Exchange from $\text{Mn}(\text{DMP}^+\text{rPor})^+$	207
(b) Methanol, DMF and Water Exchange from MnB^{2+}	210
(c) Solvent Exchange from NiCR^{2+} , NiCRMe^{2+} , NiTAAB^{2+} and NiTRI^{2+}	213

Page

2. General Comments Regarding Relaxation

Results	224
Literature Cited	226
Appendix	233

LIST OF FIGURES

<u>Figure</u>	<u>Page</u>
1 NMR spectra at 60 MHz of $\text{NiCR}(\text{BF}_4)_2$ and $\text{NiCRMe}(\text{BF}_4)_2$ in trifluoroacetic acid.	37
2 Temperature dependence of $-\log(T_{2P}P_M)$ for the hydroxy and methyl protons of methanol solutions of $\text{Mn}(\text{DMP}r\text{Por})\text{ClO}_4$.	52
3 Temperature dependence of $(\Delta\omega_{\text{obsd}}/P_M)$ for the hydroxy and methyl protons of methanol solutions of $\text{Mn}(\text{DMP}r\text{Por})\text{ClO}_4$.	53
4 Temperature dependence of $-\log(T_{2P}P_M)$ for the formyl and high field methyl protons of N,N-dimethylformamide solutions of $\text{Mn}(\text{DMP}r\text{Por})\text{ClO}_4$.	54
5 Temperature dependence of $(\Delta\omega_{\text{obsd}}/P_M)$ for the formyl and high field methyl protons of N,N-dimethylformamide solutions of $\text{Mn}(\text{DMP}r\text{Por})\text{ClO}_4$.	55
6 Temperature dependence of $-\log(T_{2P}P_M)$ for the formyl and high field methyl protons of N,N-dimethylformamide solutions of $\text{MnB}(\text{ClO}_4)_2$.	70
7 Temperature dependence of $(\Delta\omega_{\text{obsd}}/P_M)$ for the formyl proton of N,N-dimethylformamide solutions of $\text{MnB}(\text{ClO}_4)_2$.	71
8 Temperature dependence of $-\log(T_{2P}P_M)$ for the water proton of aqueous solutions of $\text{MnB}(\text{ClO}_4)_2$.	78

<u>Figure</u>		<u>Page</u>
9	Temperature dependence of $(\Delta\omega_{\text{obsd}}/P_M)$ for the water proton of aqueous solutions of $\text{MnB}(\text{ClO}_4)_2$.	79
10	Temperature dependence of $-\log(T_{2P}^{P_M})$ for the hydroxy and methyl protons of methanol solutions of $\text{Mn}(\text{DMP}r\text{Por})\text{ClO}_4$.	88
11	Temperature dependence of $(\Delta\omega_{\text{obsd}}/P_M)$ for the hydroxy proton of methanol solutions of $\text{MnB}(\text{ClO}_4)_2$.	89
12	Temperature dependence of the molar magnetic susceptibilities of $\text{NiCR}(\text{PF}_6)_2$ and $\text{NiCRMe}(\text{ClO}_4)_2$ in N,N-dimethylformamide.	103
13	Temperature dependence of the molar magnetic susceptibilities of $\text{NiCR}(\text{BF}_4)_2$ and $\text{NiCRMe}(\text{BF}_4)_2$ in water.	104
14	Temperature dependence of the molar magnetic susceptibilities of NiCR^{2+} in methanol, acetonitrile and dimethylsulfoxide.	105
15	Temperature dependence of the azo-methine methyl proton chemical shifts of NiCR^{2+} in water, methanol, acetonitrile, dimethylsulfoxide and N,N-dimethylformamide and of NiCRMe^{2+} in water and N,N-dimethylformamide.	107
16	Temperature dependence of $-\log(T_{2P}^{P_M})$ for the formyl proton of N,N-dimethylformamide solutions of NiCR^{2+} (both ClO_4^- and PF_6^- salts).	122

FigurePage

- 17 Temperature dependence of $(\Delta\omega_{\text{obsd}}/P_M)$ for the formyl proton of N,N-dimethylformamide solutions of NiCR^{2+} (both ClO_4^- and PF_6^- salts). 123
- 18 Temperature dependence of $-\log(T_{2P}^{P_M})$ for the formyl proton of N,N-dimethylformamide solutions of $\text{NiCRMe}(\text{ClO}_4)_2$. 128
- 19 Temperature dependence of $(\Delta\omega_{\text{obsd}}/P_M)$ for the formyl proton of N,N-dimethylformamide solutions of $\text{NiCRMe}(\text{ClO}_4)_2$. 129
- 20 Temperature dependence of $-\log(T_{2P}^{P_M})$ for the water proton of aqueous solutions of $\text{NiCR}(\text{BF}_4)_2$. 133
- 21 Temperature dependence of $(\Delta\omega_{\text{obsd}}/P_M)$ for the water proton of aqueous solutions of $\text{NiCR}(\text{BF}_4)_2$. 134
- 22 Temperature dependence of $-\log(T_{2P}^{P_M})$ for the water proton of aqueous solutions of $\text{NiCRMe}(\text{BF}_4)_2$. 135
- 23 Temperature dependence of $-\log(T_{2P}^{P_M})$ for the methyl protons of acetonitrile solutions of $\text{NiCR}(\text{PF}_6)_2$. 139
- 24 Temperature dependence of $(\Delta\omega_{\text{obsd}}/P_M)$ for the methyl protons of acetonitrile solutions of $\text{NiCR}(\text{PF}_6)_2$. 140

FigurePage

- | | | |
|----|---|-----|
| 25 | Temperature dependence of $-\log(T_{2P}P_M)$ for the methyl protons of methanol solutions of $\text{NiCR}(\text{BF}_4)_2$. | 144 |
| 26 | Temperature dependence of $-\log(T_{2P}P_M)$ for the hydroxy proton of methanol solutions of $\text{NiCR}(\text{BF}_4)_2$. | 145 |
| 27 | Temperature dependence of $(\Delta\omega_{\text{obsd}}/P_M)$ for the methyl protons of methanol solutions of $\text{NiCR}(\text{BF}_4)_2$. | 146 |
| 28 | Temperature dependence of $(\Delta\omega_{\text{obsd}}/P_M)$ for the hydroxy proton of methanol solutions of $\text{NiCR}(\text{BF}_4)_2$. | 147 |
| 29 | Temperature dependence of $-\log(T_{2P}P_M)$ for the methyl protons of dimethylsulfoxide solutions of $\text{NiCR}(\text{PF}_6)_2$. | 160 |
| 30 | Temperature dependence of $(\Delta\omega_{\text{obsd}}/P_M)$ for the methyl protons of dimethylsulfoxide solutions of $\text{NiCR}(\text{PF}_6)_2$. | 161 |
| 31 | Temperature dependence of $-\log(T_{2P}P_M)$ for the formyl proton of N,N-dimethylformamide solutions of $\text{NiTRI}(\text{ClO}_4)_2$. | 175 |
| 32 | Temperature dependence of $(\Delta\omega_{\text{obsd}}/P_M)$ for the formyl proton of N,N-dimethylformamide solutions of $\text{NiTRI}(\text{ClO}_4)_2$. | 176 |

<u>Figure</u>		<u>Page</u>
33	Temperature dependence of $-\log(T_{2P}P_M)$ for the formyl proton of N,N-dimethylformamide solutions of NiTAAB^{2+} (both ClO_4^- and NO_3^- salts).	179
34	Temperature dependence of $(\Delta\omega_{\text{obsd}}/P_M)$ for the formyl proton of N,N-dimethylformamide solutions of $\text{NiTAAB}(\text{ClO}_4)_2$.	180
35	Temperature dependence of $-\log(T_{2P}P_M)$ for the proton resonances of water and methanol each containing $\text{Co}(\text{trans}[14]\text{diene})^{2+}$.	189
36	Temperature dependence of $-\log(T_{2P}P_M)$ for the methyl protons of acetonitrile solutions of $\text{Co}(\text{trans}[14]\text{diene})^{2+}$ and for the formyl proton of N,N-dimethylformamide solutions of $\text{CoCR}(\text{ClO}_4)_2$.	190
37	Temperature dependence of $(\Delta\omega_{\text{obsd}}/P_M)$ for the methyl protons of acetonitrile solutions $\text{Co}(\text{trans}[14]\text{diene})^{2+}$.	191
38	Temperature dependence of $-\log(T_{2P}P_M)$ for the water proton of aqueous solutions of $\text{CuCR}(\text{BF}_4)_2$ and for the formyl proton of N,N-dimethylformamide solutions of $\text{CuCR}(\text{BF}_4)_2$.	201
39	Temperature dependence of $(\Delta\omega_{\text{obsd}}/P_M)$ for the formyl proton of N,N-dimethylformamide solutions of $\text{CuCR}(\text{BF}_4)_2$.	202

LIST OF TABLES

<u>Table</u>		<u>Page</u>
I	Microanalytical results for various NiCR^{2+} and NiCRMe^{2+} salts.	33
II	Electronic spectral data for NiCR^{2+} in water.	34
III	Least-squares best fit parameters of the nmr line broadening data for $\text{Mn}(\text{DMPPrPor})\text{ClO}_4$ in methanol.	59
IV	Least-squares best fit parameters of the nmr line broadening data for $\text{Mn}(\text{DMPPrPor})\text{ClO}_4$ in N,N-dimethylformamide.	61
V	Least-squares best fit parameters of the nmr line broadening data for $\text{MnB}(\text{ClO}_4)_2$ in N,N-dimethylformamide.	72
VI	Least-squares best fit parameters of the nmr line broadening data for $\text{MnB}(\text{ClO}_4)_2$ in water.	80
VII	Least-squares best fit parameters of the nmr line broadening data for $\text{MnB}(\text{ClO}_4)_2$ in methanol.	90
VIII	Least-squares best fit parameters of the magnetic susceptibilities of NiCR^{2+} and NiCRMe^{2+} in several solvents.	110
IX	Least-squares best fit parameters of the azo-methine methyl proton chemical shifts of NiCR^{2+} and NiCRMe^{2+} in several solvents.	111

TablePage

X	Least-squares best fit parameters of the nmr line broadening and chemical shift data for NiCR^{2+} in N,N-dimethylformamide.	124
XI	Least-squares best fit parameters of the nmr line broadening and chemical shift data for $\text{NiCRMe}(\text{ClO}_4)_2$ in N,N-dimethylformamide.	130
XII	Least-squares best fit parameters of the nmr line broadening data for $\text{NiCR}(\text{PF}_6)_2$ in acetonitrile.	141
XIII	Least-squares best-fit parameters of the nmr line broadening and chemical shift data for $\text{NiCR}(\text{BF}_4)_2$ in methanol.	148
XIV	Observed and calculated nmr results for NiCR^{2+} and NiCRMe^{2+} in N,N-dimethylformamide and water.	167
XV	Observed and calculated nmr results for NiCR^{2+} in acetonitrile, methanol and dimethylsulf- oxide.	168
XVI	Least-squares best fit parameters of the nmr line broadening and chemical shift data for $\text{NiTRI}(\text{ClO}_4)_2$ in N,N-dimethylformamide.	177
XVII	Least-squares best fit parameters of the nmr line broadening and chemical shift data for NiTAAB^{2+} in N,N-dimethylformamide.	181

<u>Table</u>	<u>Page</u>
XVIII Observed and calculated nmr results for Co(trans[14]diene) ²⁺ , CoCR ²⁺ and CuCR ²⁺ in several solvents.	192
XIX Summary of the kinetic parameters for solvent exchange of Mn(DMPPrPor) ⁺ and of some other systems.	208
XX Summary of the kinetic parameters for solvent exchange of MnB ²⁺ and of some other manganese(II) complexes.	211
XXI Summary of kinetic parameters for solvent exchange of NiCR ²⁺ , NiCRMe ²⁺ , NiTAAB ²⁺ , NiTRI ²⁺ and of some other nickel(II) complexes.	214
XXII Temperature dependence of the proton line widths of water, acetonitrile, dimethylsulf- oxide, methanol and N,N-dimethylformamide.	234
XXIII Hydroxy and methyl proton line widths of methanol solutions of Mn(DMPPrPor)ClO ₄ .	235
XXIV Hydroxy and methyl proton chemical shifts of methanol solutions of Mn(DMPPrPor)ClO ₄ .	237
XXV Formyl and high field methyl proton line widths of N,N-dimethylformamide solutions of Mn(DMPPrPor)ClO ₄ .	239
XXVI Formyl and high field methyl proton chemical	

<u>Table</u>		<u>Page</u>
	shifts of N,N-dimethylformide solutions of $\text{Mn}(\text{DMPPrPor})\text{ClO}_4$.	241
XXVII	Solution magnetic susceptibilities for $\text{Mn}(\text{DMPPrPor})\text{ClO}_4$ in methanol.	242
XXVIII	Formyl and high field methyl proton line widths of N,N-dimethylformamide solutions of $\text{MnB}(\text{ClO}_4)_2$.	243
XXIX	Formyl proton chemical shifts for N,N- dimethylformamide solutions of $\text{MnB}(\text{ClO}_4)_2$.	245
XXX	Proton line widths for aqueous solutions of $\text{MnB}(\text{ClO}_4)_2$.	246
XXXI	Proton chemical shifts for aqueous solutions of $\text{MnB}(\text{ClO}_4)_2$.	248
XXXII	Solution magnetic susceptibilities for $\text{MnB}(\text{ClO}_4)_2$ in water.	249
XXXIII	Hydroxy and methyl proton line widths at 60 MHz for methanol solutions of $\text{MnB}(\text{ClO}_4)_2$.	250
XXXIV	Hydroxy and methyl proton line widths at 100 MHz for methanol solutions of $\text{MnB}(\text{ClO}_4)_2$.	253
XXXV	Hydroxy proton chemical shifts at 60 MHz for methanol solutions of $\text{MnB}(\text{ClO}_4)_2$.	254

<u>Table</u>		<u>Page</u>
XXXVI	Solution magnetic susceptibilities for $\text{NiCR}(\text{PF}_6)_2$ and $\text{NiCR}(\text{ClO}_4)_2$ in N,N-dimethylformamide.	255
XXXVII	Solution magnetic susceptibilities for $\text{NiCRMe}(\text{ClO}_4)_2$ in N,N-dimethylformamide.	257
XXXVIII	Solution magnetic susceptibilities for $\text{NiCR}(\text{BF}_4)_2$ and $\text{NiCRMe}(\text{BF}_4)_2$ in water.	258
XXXIX	Solution magnetic susceptibilities for NiCR^{2+} in methanol, acetonitrile and dimethylsulfoxide.	260
XL	Contact shifts of the azo-methine methyl protons for NiCR^{2+} and NiCRMe^{2+} in several solvents.	263
XLI	Formyl proton line widths for N,N-dimethylformamide solutions of $\text{NiCR}(\text{PF}_6)_2$.	267
XLII	Formyl proton chemical shifts for N,N-dimethylformamide solutions of $\text{NiCR}(\text{PF}_6)_2$.	271
XLIII	Formyl proton line widths for N,N-dimethylformamide solutions of $\text{NiCR}(\text{ClO}_4)_2$.	275
XLIV	Formyl proton chemical shifts for N,N-dimethylformamide solutions of $\text{NiCR}(\text{ClO}_4)_2$.	276
XLV	Formyl proton line widths for N,N-dimethylformide solutions of $\text{NiCRMe}(\text{ClO}_4)_2$.	277
XLVI	Formyl proton chemical shifts for N,N-dimethylformamide solutions of $\text{NiCRMe}(\text{ClO}_4)_2$.	282

<u>Table</u>	<u>Page</u>
XLVII Proton line widths for aqueous solutions of NiCR(BF ₄) ₂ .	286
XLVIII Proton chemical shifts for aqueous solutions of NiCR(BF ₄) ₂ .	288
XLIX Proton line widths for aqueous solutions of NiCRMe(BF ₄) ₂ .	289
L Proton line widths for acetonitrile solu- tions of NiCR(PF ₆) ₂ .	290
LI Proton chemical shifts for acetonitrile solutions of NiCR(PF ₆) ₂ .	292
LII Hydroxy and methyl proton line widths for methanol solutions of NiCR(BF ₄) ₂ .	294
LIII Hydroxy and methyl proton chemical shifts for methanol solutions of NiCR(BF ₄) ₂ .	299
LIV Proton line broadening and chemical shifts for dimethylsulfoxide solutions of NiCR(PF ₆) ₂ .	305
LV Formyl proton line widths for N,N-dimethyl- formamide solutions of NiTRI(ClO ₄) ₂ .	307
LVI Formyl proton chemical shifts for N,N-dimethyl- formamide solutions of NiTRI(ClO ₄) ₂ .	311
LVII Formyl proton line widths for N,N-dimethyl- formamide solutions of NiTAAB(ClO ₄) ₂ .	313
LVIII Formyl proton line widths for N,N-dimethyl- formamide solutions of NiTAAB(NO ₃) ₂ .	316

<u>Table</u>	<u>Page</u>
LIX Formyl proton chemical shifts for N,N-dimethylformamide solutions of $\text{NiTAAB}(\text{ClO}_4)_2$.	317
LX Solution magnetic susceptibilities of $\text{NiTAAB}(\text{ClO}_4)_2$ and $\text{NiTAAB}(\text{NO}_3)_2$ in N,N-dimethylformamide.	319
LXI Proton line widths for $\text{Co}(\text{trans}[14]\text{diene})^{2+}$ in water.	321
LXII Solution magnetic susceptibilities of $\text{Co}(\text{trans}[14]\text{diene})(\text{ClO}_4)_2$ in water.	323
LXIII Hydroxy and methyl proton line widths for methanol solutions of $\text{Co}(\text{trans}[14]\text{diene})(\text{BF}_4)_2$.	324
LXIV Proton line widths for acetonitrile solutions of $\text{Co}(\text{trans}[14]\text{diene})^{2+}$.	325
LXV Proton chemical shifts for acetonitrile solutions of $\text{Co}(\text{trans}[14]\text{diene})^{2+}$.	326
LXVI Formyl proton line widths for N,N-dimethylformamide solutions of $\text{CoCR}(\text{ClO}_4)_2$.	327
LXVII Proton line widths for aqueous solutions of $\text{CuCR}(\text{BF}_4)_2$.	328
LXVIII Formyl proton line widths for N,N-dimethylformamide solutions of $\text{CuCR}(\text{BF}_4)_2$.	329
LXIX Formyl proton chemical shifts for N,N-dimethylformamide solutions of $\text{CuCR}(\text{BF}_4)_2$.	331

CHAPTER I: INTRODUCTION

1. General Comments

The nmr line broadening method has been extensively applied in the determination of ligand exchange rates.^{1,2,3} Initially, attention was focussed on hexasolvated systems of various metal ions in order to determine a general lability order, solvent effects and mechanistic information regarding this class of reactions. Useful correlations with crystal field effects have been realized in many of the systems investigated^{1,4} and it appears that in at least the cobalt(II) and nickel(II) systems a separation of the enthalpies of solvent exchange into crystal field and solvation contributions may be possible.⁵ Further, a comparison of the solvent exchange rates with the rates of substrate binding has greatly clarified the mechanisms involved in the latter reactions.^{2,6}

More recently, considerable interest has been shown in determining the effect of non-exchanging ligands on the solvent exchange rates.^{3,7,8} In this connection, the results of $^{17}\text{OH}_2$ exchange studies of partially substituted nickel(II) and cobalt(II) aquo ions have indicated that the water exchange rates correlate roughly with the solvation number for each type of metal ion.³ This observation has been taken to mean that the electronic effects of the non-exchanging ligands, being approximately additive, are at

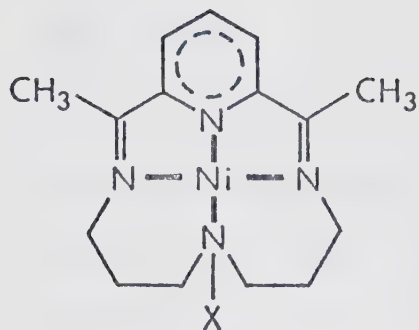
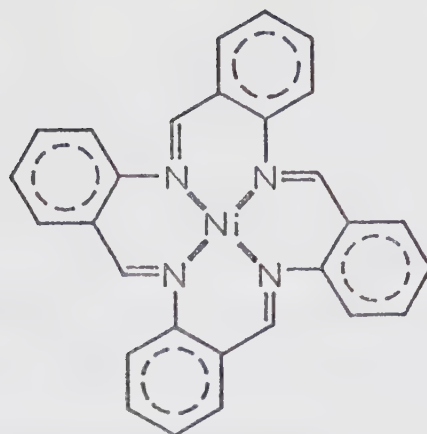
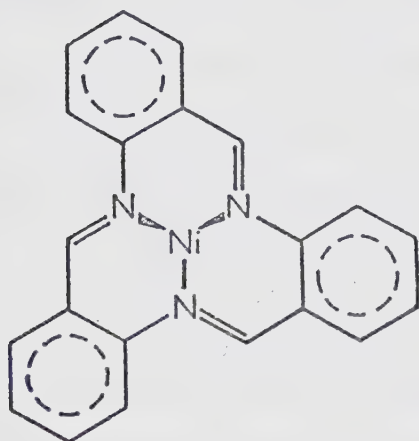
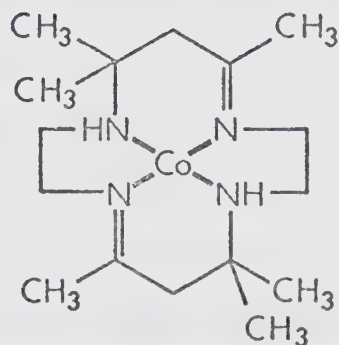
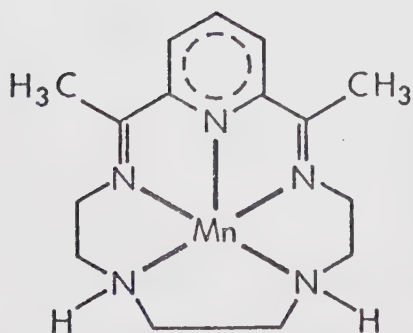
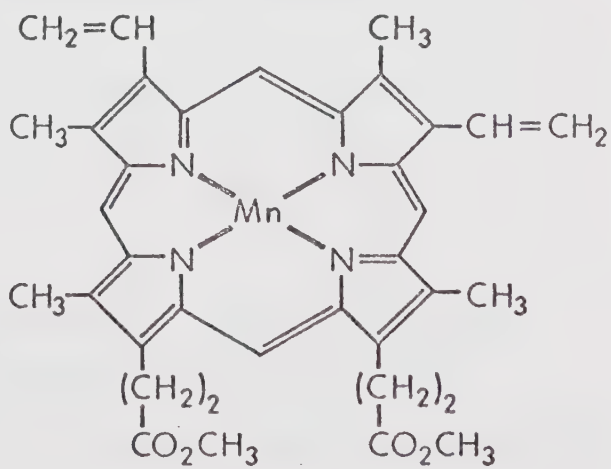
least partly responsible for the variation in the rate constants.

Comparatively few studies, however, have been made on the solvent exchange or substrate binding behaviour of complexes existing as tetragonally distorted pseudo-octahedral species in solution. This geometry is widely observed in biologically important metal ion complexes, as for instance in the porphyrins, phthalocyanines, and other related complexes having azo-methine donor nitrogen atoms. The exchange behaviour of ferriprotoporphyrin(IX) in ethanol and water mixed solvent⁹ and the studies of the rate of complexing of bis(β -diketonate)nickel(II) complexes with picoline derivatives^{10,11} are a few instances where the nmr method has been applied to complexes of this structure.

The work reported in this thesis is an attempt to gain more insight into the solvent exchange kinetics of tetragonally distorted complexes having a macrocyclic Schiff base or a porphyrin ligand. In using the nmr method, the usual chemical difficulties of complex solubility, thermal stability and polymerization are encountered. Perhaps the greatest limitation is that the exchange rate must be of the correct magnitude to have some effect on the nmr observations. The use of nonaqueous solvents with a long liquid temperature range is of some help in circumventing this difficulty. Since many nickel(II) complexes have exchange rates of a magnitude ideal for study by the nmr

method, much of the work in this and in previous studies has dealt with nickel(II) systems. The nickel(II) complexes studied here were: 2,12-dimethyl-3,7,11,17-tetraazabicyclo(11.3.1)heptadeca-1(17),2,11,13,15-pentaene nickel(II), NiCR^{2+} , shown as structure I(a); and its methylated analogue, NiCRMe^{2+} , structure I(b); tetrabenzo[b,f,j,n]-[1,5,9,13]tetraazacyclohexadecinenickel(II), NiTAAB^{2+} , structure II; and tribenzo[b,f,j][1,5,9]triazacyclododecinenickel(II), NiTRI^{2+} , structure III. The latter complex is a normal octahedral complex and was studied for purposes of comparison. The cobalt(II) and copper(II) complexes, CoCR^{2+} and CuCR^{2+} , were investigated in addition to the cobalt(II) complex, 5,7,7,12,14,14-hexamethyl-1,4,8,11-tetraazacyclotetradeca-4,11-dienecobalt(II), $\text{Co}(\text{trans}[14]\text{-diene})^{2+}$, shown as structure IV. The manganese(II), and manganese(III) complexes: 2,13-dimethyl-3,6,9,12,18-pentaazabicyclo[12.3.1]octadeca-1(18),2,12,14,16-pentaene-manganese(II), MnB^{2+} , structure V; and Mn(III)protoporphyrin(IX)dimethyl ester, $\text{Mn}(\text{DMPrPor})^+$, structure VI were also studied.

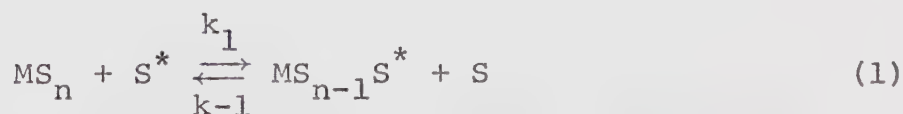
The temperature dependence of the magnetic susceptibility and ligand contact shift of the complexes NiCR^{2+} and NiCRMe^{2+} have been investigated, as well, in a series of solvents. These studies were necessary to characterize the diamagnetic-paramagnetic equilibrium in these two systems so that the nmr data could be interpreted properly.

I(a) $X=H$; $NiCR^{2+}$ I(b) $X=CH_3$; $NiCRMe^{2+}$ II $NiTAAB^{2+}$ III $NiTRI^{2+}$ IV $Co(trans [14] diene)^{2+}$ V MnB^{2+} VI $Mn(DMP\text{r}Por)^+$

2. NMR Theory

(a) General Theory

The time dependence of the net nuclear magnetization in a sample in terms of longitudinal and transverse relaxation processes is described by the Bloch phenomenological equations.^{12,13} These were subsequently extended by McConnell¹⁴ to take into account the effect of chemical exchange. Swift and Connick¹⁵ have solved these modified Bloch equations for nuclei exchanging between two chemically distinguishable sites for the particular case that the concentration of one of the exchange sites, the bulk solvent, is much greater than that of the other site, the equivalent coordination positions of a paramagnetic complex. This condition permits the total signal to be approximated by that of the pure solvent in the region of the solvent resonance. Their treatment of this type of system, which can be represented as



has been found to account adequately for the exchange effects observed in the various systems reported in this thesis. In eq 1 S^* represents an arbitrary bulk solvent molecule replacing any one of the n equivalent solvent molecules coordinated to the metal ion. Swift and Connick

have shown that the effect of chemical exchange and nuclear relaxation on the transverse relaxation time of solvent nuclei can be expressed as

$$(T_{2P}^{P_M})^{-1} = \frac{(T_{2obsd})^{-1} - (T_{2S})^{-1}}{P_M} = \frac{1}{\tau_M} \left\{ \frac{(\frac{1}{T_{2M}})^2 + (\frac{1}{T_{2M}\tau_M}) + \Delta\omega_M^2}{((\frac{1}{T_{2M}}) + (\frac{1}{\tau_M}))^2 + \Delta\omega_M^2} \right\} \quad (2)$$

The usual assumptions of slow passage and low radio frequency power level are made in the derivation of eq 2. In this equation T_{2S} and T_{2obsd} are the transverse nuclear relaxation times for the pure solvent, and for the bulk solvent in a solution containing one type of paramagnetic species, respectively. For a Lorentzian line shape T_2 is related to the full line width, $\Delta\nu$ in Hz, of the nmr absorption curve at half-maximum height by

$$T_2^{-1} = \pi\Delta\nu \quad (3)$$

The ratio of the number of coordinated to non-coordinated solvent molecules is defined by

$$P_M = \frac{n[m]}{[S] - n[m]} \quad (4)$$

where $[S]$ represents the total molal solvent concentration, $[m]$ is the molal concentration of the paramagnetic species, and n is the number of solvent molecules in the first co-

ordination sphere of the metal ion.

From the general definition of τ :

$$\tau = \frac{\text{concentration of a species}}{\text{rate of disappearance of that species}} \quad (5)$$

it can be readily shown by consideration of eq 1 that P_M is also related to τ_M , the lifetime of a solvent molecule in the first coordination sphere of the metal ion, and to τ_S , the lifetime of the solvent molecule in the bulk solvent, by means of the expression

$$P_M = \frac{\tau_M}{\tau_S} \quad (6)$$

It should be realized that τ_M^{-1} is a pseudo first-order rate constant which is related to the specific rate constants k_{-1} or k_1 of eq 1 by

$$\tau_M^{-1} = k \left\{ [S] - n[MS_n] \right\} \quad (7)$$

where $k_1 = k_{-1} = k$.

In eq 2 T_{2M} is the transverse relaxation time of nuclei in a solvent molecule coordinated to the metal ion, and $\Delta\omega_M$ represents the frequency shift in rad sec^{-1} between the resonance of the coordinated solvent molecules and the resonance for the pure solvent.

Equation 2 omits the line broadening arising

from the interaction between the paramagnetic ion and solvent molecules beyond the first coordination sphere. In this work this outer sphere broadening contribution was accounted for by adding a term T_{20}^{-1} to the right side of eq 2.

Under the same set of conditions used to derive eq 2, it was shown by Swift and Connick¹⁵ that the observed chemical shift ($\Delta\omega_{\text{obsd}}$), defined as the resonance frequency observed for the bulk solvent in a solution containing the paramagnetic species minus the resonance frequency of the pure solvent, is given by

$$-\Delta\omega_{\text{obsd}} = \frac{P_M \Delta\omega_M}{\left(1 + (\tau_M/T_{2M})\right)^2 + (\tau_M \Delta\omega_M)^2} \quad (8)$$

The definition of $\Delta\omega_{\text{obsd}}$ given above means that a downfield shift gives a positive value of $\Delta\omega_{\text{obsd}}$. Eq 8 is valid for dilute solutions ($P_M \ll 1$). This condition requires that $\Delta\omega_{\text{obsd}} \ll \Delta\omega_M$ and therefore permits the approximation to be made that $\Delta\omega_M$ is equal to the chemical shift of the coordinated solvent relative to the bulk solvent in the solution.

(b) Temperature Dependence of Relaxation Times and Chemical Shifts

The temperature dependence of each of the terms τ_M , T_{2M} and $\Delta\omega_M$ found in eqs 2 and 8 is known from theoretical considerations. For τ_M the temperature dependence according to transition state theory is given by

$$\tau_M^{-1} = \frac{kT}{h} \exp\left(\frac{-\Delta H^\ddagger + T\Delta S^\ddagger}{RT}\right) \quad (9)$$

where k is Boltzmann's constant, h is Planck's constant, T is the absolute temperature, R is the gas constant, ΔH^\ddagger and ΔS^\ddagger are the enthalpy and entropy of activation, respectively. It has been shown by Bloembergen¹⁶ that the Fermi contact shift can be expressed as

$$\Delta\omega_M = -\left(\frac{A}{\hbar}\right) \frac{\omega_0 \mu_{\text{eff}} \beta \sqrt{S(S+1)}}{3k\gamma_I T} \quad (10)$$

where $\left(\frac{A}{\hbar}\right)$ is the hyperfine coupling constant in rad sec^{-1} between the unpaired electrons on the metal and nuclei in the coordinated solvent molecule, ω_0 is the operating frequency of the nmr spectrometer, S is the spin quantum number of the paramagnetic ion, β is the Bohr magneton and γ_I is the nuclear magnetogyric ratio. It should be noted that according to the earlier definition of the sign

of the observed chemical shift, A/h is positive for a downfield shift. If μ_{eff} , the effective magnetic moment of the complex, is temperature independent then $\Delta\omega_M$ can be expressed as

$$\Delta\omega_M = - \frac{C_\omega}{T} \quad (11)$$

where C_ω contains the constants in eq 10.

The contact shift will have this simple temperature dependence if the complex has a relatively small zero-field splitting and there are no low lying electronic states which would be thermally accessible. However, there is the added possibility of a significant pseudocontact contribution to the observed shift, arising from the dipole-dipole interaction between the nuclear spin and electron spins in a paramagnetic ion having a large g factor anisotropy. Kurland and McGarvey¹⁷ have derived expressions for the contact and pseudocontact shifts in systems having large zero-field splittings in which there is appreciable orbital angular momentum contribution to the magnetic moment and appreciable mixing of ground and thermally populated excited electronic states. Assuming rapid thermal equilibrium between states, they have shown that for an $S = 1$ system with axial symmetry the pseudocontact shift should be more properly expressed as

$$\frac{\Delta\omega_M}{\omega_0} = - \frac{2\beta^2 (g_{\parallel}^2 - g_{\perp}^2) (3\cos^2\Omega - 1)}{9kTR^3} \left\{ 1 - \frac{(g_{\parallel}^2 + \frac{1}{2}g_{\perp}^2)D}{3k(g_{\parallel}^2 - g_{\perp}^2)T} \right\} \quad (12)$$

where g_{\parallel} and g_{\perp} are, respectively, the g factors parallel and perpendicular to the axis of symmetry of the complex, Ω is the angle between the symmetry axis and the radius vector connecting the metal ion center and the probe nucleus, R is the magnitude of this radius vector, and D is the zero-field splitting energy. It should be noted that eq 12 predicts that the pseudocontact shift may show both an inverse first and an inverse second power dependence on the absolute temperature if the second term in brackets is significant with respect to one.

Theoretical expressions for T_{2M} have been derived by Solomon and Bloembergen.^{18,19} Their account has shown that the magnetic interaction between nuclear and electron spins can be attributed to dipole-dipole and Fermi contact or hyperfine contributions. In the former, spin relaxation is a result of direct through-space interaction, whereas in the latter, spin relaxation is due to the finite probability of transferring electron spin density through chemical bonds to the probe nucleus. These two, dipolar and hyperfine, contributions to T_{2M} are represented by the first and second terms, respectively, in the equation

$$(T_{2M})^{-1} = \left\langle \frac{1}{r_i^6} \right\rangle \frac{\gamma_I^2 g^2 \beta^2 S(S+1)}{15} f_D(\tau_D) + \frac{1}{3} \left(\frac{A}{\hbar} \right)^2 S(S+1) f_e(\tau_e) \quad (13)$$

where $\left\langle \frac{1}{r^6} \right\rangle$ is the average magnitude of the reciprocal of the sixth power of the vector connecting the interacting spins.

The effective correlation times, $f_D(\tau_D)$ and $f_e(\tau_e)$, are functions of the dipolar (τ_D) and electronic (τ_e) correlation times, and in the limits $\omega_I \ll \omega_S$, $\omega_I^2 \tau_e^2 \ll 1$, $\omega_I^2 \tau_D^2 \ll 1$ they are given by²⁰

$$f_D(\tau_D) = \tau_{D1} + \frac{13\tau_{D2}}{1 + \omega_S^2 \tau_{D2}^2} \quad (14)$$

$$f_e(\tau_e) = \tau_{e1} + \frac{\tau_{e2}}{1 + \omega_S^2 \tau_{e2}^2} \quad (15)$$

where ω_I and ω_S are the Larmour frequencies of the nucleus under observation and the unpaired electrons, respectively.

Both the dipolar and hyperfine interactions can be modulated by electron spin relaxation or by chemical exchange, and in addition, the dipolar mechanism can be modulated by the rotation of the complex. Thus the various correlation times in eqs 14 and 15 are given by

$$\tau_{D1}^{-1} = \tau_{e1}^{-1} + \tau_r^{-1} = (\tau_{le}^{-1} + \tau_M^{-1}) + \tau_r^{-1} \quad (16)$$

$$\tau_{D2}^{-1} = \tau_{e2}^{-1} + \tau_r^{-1} = (T_{2e}^{-1} + \tau_M^{-1}) + \tau_r^{-1} \quad (17)$$

where τ_r is the rotational correlation time of the paramagnetic complex, T_{1e} and T_{2e} are the longitudinal and transverse electron spin relaxation times, respectively, and τ_M^{-1} is the solvent exchange rate discussed above.

Various theoretical developments have shown that T_{1e} and T_{2e} are functions of temperature, magnetic field, and zero-field splitting energy of the paramagnetic complex. According to the development of McLachlin²¹ the average electron spin relaxation times, $\langle T_{1e} \rangle$ and $\langle T_{2e} \rangle$, which define the average width of a composite electron spin resonance line, are given by

$$\langle T_{1e}^{-1} \rangle = C_e \left\{ \frac{\tau_C}{1 + \omega_S^2 \tau_C^2} + \frac{4\tau_C}{1 + 4\omega_S^2 \tau_C^2} \right\} \quad (18)$$

$$\langle T_{2e}^{-1} \rangle = \frac{C_e}{2} \left\{ 3\tau_C + \frac{5\tau_C}{1 + \omega_S^2 \tau_C^2} + \frac{2\tau_C}{1 + 4\omega_S^2 \tau_C^2} \right\} \quad (19)$$

In these equations, which are valid if $\tau_C < T_{2e}$, C_e is a function of the electron spin quantum number and of the zero-field splitting energy of the paramagnetic complex, and $\tau_C = \tau_r$ where τ_r was defined previously. Bloembergen and Morgan²² have derived the same functional dependence for T_{1e}^{-1} as that given by eq 18. In their treatment τ_C

was identified as the correlation time for distortion of the complex brought about by random molecular collisions.

Consideration of eqs 13 to 17 shows that the temperature dependence of $(T_{2M})^{-1}$ will correspond to that of the shortest correlation time controlling $f_D(\tau_D)$ or $f_e(\tau_e)$. If rotational tumbling of the complex provides the most rapid fluctuation, then the temperature dependence of τ_r , given by $\tau_r = \tau_r^0 \exp(E_r/RT)$, where τ_r^0 and E_r are constants, is sufficient to describe the temperature dependence of $(T_{2M})^{-1}$. For a correlation time controlled by electron spin relaxation, the exact temperature dependence of $(T_{2M})^{-1}$ can be quite complicated, in view of the functional form of T_{1e} and T_{2e} given by eqs 18 and 19, but it is generally assumed that here also a simple exponential temperature dependence applies. However, it should be noted that this assumption of exponential form is valid only for $\omega_S \tau_C \gg 1$ or $\omega_S \tau_C \ll 1$ and that between these two extremes the temperature dependence of T_{1e} will be small and nonexponential. Since in most instances $\tau_M \gg \tau_r, T_{1e}$, the temperature dependence of $(T_{2M})^{-1}$ can therefore be approximated by

$$(T_{2M})^{-1} = C_M \exp(E_M/RT) \quad (20)$$

where it is understood that E_M is an effective activation energy and C_M is a constant.

An expression for the outer sphere contribution to the

the observed line broadening has been derived by Luz and Meiboom²³ for the case that the lifetime of the solvent molecules beyond the first coordination sphere of the metal ion is short relative to the tumbling time of the complex. In the absence of significant hyperfine interaction and a well-defined second coordination sphere, Luz and Meiboom have shown that the outer sphere dipolar contribution can be obtained by averaging the inner sphere dipole-dipole interaction, described by the first term of eq 13, over equally populated distances from d_o , the average distance of closest approach between the probe nucleus in a second coordination sphere solvent molecule and the paramagnetic center, to an infinite distance to give

$$T_{2P}^{-1} = \frac{4\pi}{45} (10^{-3} \rho N[m]) \frac{S(S+1) \gamma_I^2 g^2 \beta^2 f_D(\tau_D)}{d_o^3} \quad (21)$$

In this expression the first term in brackets is the number of paramagnetic ions per cm^3 of solution, ρ is the solvent density, N is Avogadro's number and T_{2P} is defined by

$$(T_{2P})^{-1} = (T_{2\text{obsd}})^{-1} - (T_{2S})^{-1} \quad (22)$$

In the present work all observed $(T_{2P})^{-1}$ are normalized to $P_M = 1$, but since $(T_{2P})^{-1}$ for outer sphere solvent

molecules is proportional only to the metal ion concentration, and independent of solvent molality, it is convenient to rewrite eq 21 as

$$(T_{20})^{-1} = \frac{4.14 \times 10^{13} S(S+1) \rho f_D(\tau_D)}{d_o^3} \cdot \frac{[S]}{n} \quad (23)$$

where $(T_{20})^{-1}$ represents the outer sphere $(T_{2p})^{-1}$ normalized to $P_M = 1$. In eq 23 the substitutions for N , g , β and γ_I for the proton have been made.

The temperature dependence of $(T_{20})^{-1}$ is also generally assumed to be described by

$$(T_{20})^{-1} = C_0 \exp (E_0/RT) \quad (24)$$

where C_0 is a constant and E_0 is the effective activation for outer sphere broadening.

An alternative theoretical interpretation of outer sphere dipolar broadening is possible if it is assumed that a well-defined second coordination sphere exists to which the first term of eq 13 can be applied. However, this approach has been found to be unsuccessful.²⁴

(c) Limiting Cases of the Swift and Connick Theory

The temperature dependence of $(T_{2p})^{-1}$ and $\Delta\omega_{\text{obsd}}$ is readily broken down into one of five unique limiting conditions, four of which were considered by Swift and Connick.¹⁵ The fifth condition applies only to the effect of the paramagnetic complex on $(T_{2p})^{-1}$ for outer sphere solvent molecules. The observed line broadening can be affected by the solvent exchange rate, and in addition, it can be influenced by two types of relaxation mechanisms: relaxation by a T_{2M} process and relaxation by the chemical shift, $\Delta\omega_M$. In the T_{2M} mechanism, discussed previously, nuclei in a solvent molecule coordinated to the paramagnetic complex are relaxed by a modulation of the dipolar or hyperfine interaction with the unpaired electrons of the metal ion. In the relaxation mechanism arising from the chemical shift, nuclear relaxation occurs because solvent nuclei which are in phase coherence with the radiofrequency field become dephased with respect to the bulk solvent nuclei upon coordination of the solvent molecule to the paramagnetic complex. This dephasing of nuclear spins is due to the different precessional frequency of nuclei in the two sites. The "dephased" solvent molecules then return to the bulk solvent and give rise to a reduced net transverse magnetization and a smaller T_{2p} . The most efficient of these two mechanisms will be the predominating relaxation mode. It is obvious that the observed relaxation time will be controlled

by the solvent exchange rate or the rate of relaxation, depending on which is the slowest process. Thus, if the solvent exchange rate is slow, solvent molecule nuclei will be effectively relaxed by either of the two mechanisms each time the solvent molecule coordinates to the metal ion, and the effective relaxation time is simply τ_M . On the other hand, if solvent exchange is fast, the lifetime of solvent nuclei in the inner coordination sphere of the metal ion is too short for effective relaxation by either mechanism and the relaxation time is determined by the rate of relaxation.

In view of the two basic types of relaxation mechanisms, the limiting conditions of $(T_{2p})^{-1}$ and $\Delta\omega_{\text{obsd}}$ are most easily understood in terms of Cases A and B discussed below. This breakdown is justified since in reality one or the other of the relaxation mechanisms is generally most efficient. In each of the cases the limiting conditions are arranged according to their order of occurrence as the temperature is lowered in a typical nmr solvent-exchange study.

CASE A: Relaxation by the chemical shift mechanism at intermediate temperatures

$$(i) \quad \frac{1}{T_{2M} \tau_M} \gg \left(\frac{1}{T_{2M}} \right)^2, \Delta\omega_M^2; \quad \frac{1}{T_{2P}} = \frac{P_M}{T_{2M}} \quad \text{and} \quad (25a)$$

$$- \Delta\omega_{\text{obsd}} = P_M \Delta\omega_M$$

Here the exchange of solvent molecules between the inner coordination sphere of the metal ion and the bulk solvent is fast and $(T_{2P})^{-1}$ is controlled by an inner sphere dipole-dipole or hyperfine T_{2M} relaxation process. The chemical shift relaxation mechanism is ineffective since the lifetime of solvent molecules in the inner coordination sphere of the metal ion is too short to enable nuclei to lose phase coherence with respect to the bulk solvent nuclei. The theoretical expression given as eq 13 is used to interpret the line broadening in this region. The observed shift may be large and is not affected by exchange. As the temperature is lowered the mean lifetime of solvent molecules at the metal ion site increases to the point when the chemical shift relaxation mechanism begins to become effective. Limiting condition (ii), below, then begins to apply.

$$(ii) \left(\frac{1}{\tau_M}\right)^2 \gg \Delta\omega_M^2 > \frac{1}{T_{2M}\tau_M} ; \quad \frac{1}{T_{2P}} = P_M \tau_M \Delta\omega_M^2 \text{ and}$$

(25b)

$$- \Delta\omega_{\text{obsd}} = P_M \Delta\omega_M$$

Chemical exchange is still fast but $(T_{2P})^{-1}$ is now controlled by the rate of relaxation brought about by the change in precessional frequency of nuclei in the exchanging solvent molecule. This region of line broadening is unique to Case A and it is frequency dependent. The observed shift is appreciable and only begins to decrease from the value $-P_M \Delta\omega_M$ when $(\tau_M \Delta\omega_M)^2$ approaches one. Limiting condition (ii) is then no longer strictly valid and condition (iii), below, begins to apply:

$$(iii) \Delta\omega_M^2 \gg \left(\frac{1}{T_{2M}}\right)^2, \left(\frac{1}{\tau_M}\right)^2 ; \quad \frac{1}{T_{2P}} = \frac{P_M}{\tau_M} \text{ and}$$

(25c)

$$- \Delta\omega_{\text{obsd}} = \frac{P_M}{\Delta\omega_M \tau_M^2}$$

Relaxation by a change in precessional frequency of nuclei in the solvent molecule is now very efficient due to the longer lifetime of solvent molecules in the inner coordination sphere of the metal ion. Chemical exchange is

slow and controls $(T_{2P})^{-1}$. The observed shift is small and decreases rapidly as the temperature decreases due mainly to the increase in τ_M .

$$(iv) \quad \frac{1}{T_{2P}P_M} = \frac{1}{T_{2O}} \quad (25d)$$

The rate of exchange of solvent molecules from the first coordination sphere has now decreased to the point when it is too slow to affect $(T_{2P})^{-1}$ and $\Delta\omega_{\text{obsd}}$. Therefore, $(T_{2P})^{-1}$ is controlled by outer sphere dipolar interaction. The theoretical expression given as eq 21 is used to interpret this region of line broadening. Due to the small hyperfine coupling constant for outer sphere solvent molecules, the observed shift is negligible.

CASE B: Relaxation never controlled by the chemical shift

(i) Limiting condition Case A (i) applies at high temperature where exchange is fast. Therefore,

$$\frac{1}{T_{2P}} = \frac{P_M}{T_{2M}} \quad \text{and} \quad (26a)$$

$$- \Delta\omega_{\text{obsd}} = P_M \Delta\omega_M$$

As the temperature is lowered relaxation by the chemical shift never becomes more effective than relaxation by T_{2M} . Eventually, the line broadening and chemical shift begin to show solvent exchange effects as shown in Case B (ii), below.

$$(ii) \left(\frac{1}{T_{2M}}\right)^2 \gg \Delta\omega_M^2, \left(\frac{1}{\tau_M}\right)^2; \quad \frac{1}{T_{2P}} = \frac{P_M}{\tau_M} \quad \text{and} \quad (26b)$$

$$- \Delta\omega_{\text{obsd}} = P_M \Delta\omega_M \left(\frac{T_{2M}}{\tau_M}\right)^2$$

At this point relaxation by a T_{2M} mechanism is fast and $(T_{2P})^{-1}$ is controlled by the rate of chemical exchange. The observed shift will be small since $\tau_M/T_{2M} > 1$ and will decrease rapidly with temperature due to the effect of τ_M .

(iii) Chemical exchange is now very slow and limiting condition Case A (iv), above, applies. That is,

$$\frac{1}{T_{2P}P_M} = \frac{1}{T_{2O}} \quad (26c)$$

It is readily observed that the relaxation mechanism differentiating Cases A and B might be identified by a study of a system at two frequencies. The frequency dependence of $(T_{2P})^{-1}$ predicted by limiting condition

Case A (ii) will not normally occur in Case B, unless T_{2M} is frequency dependent as a result of a magnetic field dependence of the correlation time controlling T_{2M} . It should also be noted that if $(T_{2P})^{-1}$ is observed in a system only in the regions defined by A (iii) or B (ii), the relaxation mechanism would be ambiguous. But, due to the opposite dependence of $\Delta\omega_{\text{obsd}}$ upon $\Delta\omega_M$ in these instances it is possible, in principle, to distinguish the cases by a study of $\Delta\omega_{\text{obsd}}$ at two frequencies.

Since each of the quantities τ_M , $\Delta\omega_M$, T_{2M} and T_{2O} contained in the general expression for $(T_{2P}^{P_M})^{-1}$ has a different temperature dependence, a plot of $-\log(T_{2P}^{P_M})$ against the inverse absolute temperature will provide a good indication of the process controlling $(T_{2P}^{P_M})^{-1}$, especially in view of the normally large differences in activation energies for relaxation (E_M or E_O) and chemical exchange (ΔH^\ddagger). The magnitude of the various parameters defining the limiting conditions then can be obtained from a graphical fit of the data. In this study a non-linear least-squares program²⁵ was used to fit the $(T_{2P}^{P_M})^{-1}$ and $\Delta\omega_{\text{obsd}}/P_M$ data to the general expressions 2 and 8, respectively, or to the appropriate reduced form of these equations, using initial guesses obtained from a graphical fit. The obvious difficulty with this approach is that due to the large number of adjustable parameters, it is not difficult to get an excellent fit of the data. An

added difficulty frequently arises in that one or more of the limiting regions is not well defined. However, a more internally consistent set of parameters can be obtained by making as many independent measurements as possible. In this regard, measurements of both the chemical shift and T_{2P}^{-1} , and also at two frequencies, if a frequency dependence should exist, are extremely valuable. Measurements performed on two different protons in the exchanging solvent molecule are also useful.

It should be noted, however, that although both T_{2M} and τ_M determine $\Delta\omega_{\text{obsd}}$ when chemical exchange is slow, it is not possible to determine the parameters defining both T_{2M} and τ_M from a computer fit of $\Delta\omega_{\text{obsd}}$ to eq 8, since in no case does T_{2M} alone control $\Delta\omega_{\text{obsd}}$. The greatest use of shift measurements is in an independent determination of $\Delta\omega_M$ when exchange is fast; and in an evaluation of ΔH^\ddagger and ΔS^\ddagger , using the T_{2M} parameters obtained from a fit of the $(T_{2P}P_M)^{-1}$ data, when exchange is slow.

CHAPTER II. THE PREPARATION AND CHARACTERIZATION OF COMPLEXES, SOLVENT PURIFICATION, SAMPLE PREPARATION AND INSTRUMENTATION

1. Purification of Solvents

The solvents, N,N-dimethylformamide (Raylo Reagent), dimethylsulfoxide (Fisher Reagent), acetonitrile (Baker Reagent), methanol (Macco Reagent) and 2,2,2-trifluoroethanol (Eastman Organic Chemicals) were all purified by double vacuum distillation from Linde 3A molecular sieves. Only the middle fraction of each distillation was retained. All nonaqueous solvents were stored under vacuum over molecular sieves. Subsequent transfers of a solvent onto a complex were performed under vacuum.

The water used for aqueous samples was also doubly distilled. The final distillation (from alkaline potassium permanganate) occurred in an all glass apparatus.

2. Preparation and characterization of (chloroaquo)- manganese(III)protoporphyrin(IX)dimethyl ester {Mn(DMPor)Cl·OH₂}

This complex was prepared from protoporphyrin(IX)-dimethyl ester (Sigma Chemical Co.) and manganous acetate tetrahydrate (Fisher Reagent) in glacial acetic acid solvent as described by Boucher.²⁶ The product, which was isolated as the chloride salt, was purified by Soxhlet extraction with benzene following Boucher's procedure.

Anal. Calc'd for $C_{36}H_{36}O_4N_4MnCl \cdot OH_2$: C, 62.02; H, 5.49; N, 8.04. Found: C, 62.88; H, 5.45; N, 7.53.

The compound was further characterized by comparison of its visible spectrum to that reported by Boucher. For $Mn(DMPPrPor)Cl \cdot OH_2$ in methanol absorption maxima, with extinction coefficients in parentheses, were observed at $27,000\text{ cm}^{-1}$ ($7.73 \times 10^4\text{ M}^{-1}\text{ cm}^{-1}$), $21,600\text{ cm}^{-1}$ ($5.90 \times 10^4\text{ M}^{-1}\text{ cm}^{-1}$) and $18,200\text{ cm}^{-1}$ ($1.1 \times 10^4\text{ M}^{-1}\text{ cm}^{-1}$) with a further weak band at $17,200\text{ cm}^{-1}$. These band positions are in agreement with those given by Boucher, however, the extinction coefficients appear to be slightly higher than those which can be read from Figure 5 of ref 26. The intensity ratio of 0.76 obtained here for the two most intense bands is in good agreement with the value of 0.75 given in Table III of ref 26. It has also been observed that the removal of chloride ion from methanol solutions of $Mn(DMPPrPor)Cl \cdot OH_2$, using silver perchlorate, causes no change in the visible spectrum. This result confirms Boucher's earlier conclusion that halide anion complexing does not occur in methanol. However, chloride ion, in addition to the coordinated water, was removed from all samples used in the nmr study in order to avoid any possible complexing in the temperature range employed.

The effective magnetic moment of $Mn(DMPPrPor)^+$ in methanol was measured between -60 and 40° , using the nmr

shift method suggested by Evans.²⁷ A 9.81×10^{-3} m solution was prepared under vacuum by treating $\text{Mn}(\text{DMP}r\text{Por})\text{-Cl}\cdot\text{OH}_2$ in methanol with AgClO_4 and molecular sieves as described subsequently. Cyclopentane was used as the internal standard. All the measured magnetic susceptibilities were corrected for the diamagnetism of the porphyrin ligand using a diamagnetic correction of -330×10^{-6} cgs units obtained from Pascal's constants.²⁸ The resulting effective magnetic moment was 5.03 BM, in agreement with the values 4.86 to 4.97 BM determined by Boucher²⁶ for various solid salts. Over the temperature range studied the solution magnetic susceptibilities obeyed a Curie law temperature dependence. Calvin and Loach²⁹ have found a similar temperature dependence for the susceptibility of solid (chloroaquo) manganese(III)haematoporphyrin(IX)dimethyl ester.

3. Preparation and characterization of 2,13-dimethyl-3,6,9,12,18-pentaazabicyclo[12.3.1]octadeca-1(18),2,12,-14,16-pentaenemanganese(II) perchlorate $\{\text{MnB}(\text{ClO}_4)_2\}$.

The procedure used in preparing this unusual complex having a pentadendate macrocyclic ligand was that first reported by Alexander, Heuvelen and Hamilton.³⁰ The self-condensation reaction of 2,6-diacetylpyridine (Aldrich Chemical Co.) with triethylenetetramine (Aldrich Chemical Co., technical grade) in the presence of manganese(II)-

chloride tetrahydrate (Fisher Reagent) in aqueous methanol solvent was allowed to occur for one hour at room temperature. The complex was first isolated as the chloride salt and then converted to the perchlorate complex by the addition of an aqueous solution of sodium perchlorate to a solution of MnBCl_2 in water. After cooling, the yellow product was filtered, redissolved in warm water and reprecipitated with aqueous sodium perchlorate. The $\text{MnB}(\text{ClO}_4)_2$ was filtered, washed first with cool water and then with ethanol and ether, and air dried. The addition of silver nitrate solution to a quantity of $\text{MnB}(\text{ClO}_4)_2$, prepared in this manner, indicated the absence of chloride ion.

Anal. Calc'd for $\text{MnC}_{15}\text{H}_{23}\text{N}_5(\text{OH}_2)_3(\text{ClO}_4)_2$: C, 31.00; H, 5.03; N, 12.05. Found: C, 31.01; H, 4.73; N, 12.14.

This aquo complex, which was subsequently used only for the water proton nmr study, was further characterized by its IR spectrum and by a magnetic susceptibility study at several temperatures using Evan's nmr method.²⁷

The IR spectrum of $\text{MnB}(\text{OH}_2)_2(\text{ClO}_4)_2 \cdot \text{H}_2\text{O}$, determined for a nujol mull, indicated bands characteristic of the imide and secondary amine groups at 1650 cm^{-1} and 3280 cm^{-1} , respectively. A band at 1590 cm^{-1} was attributed to the pyridine ring vibrations. In addition, a broad absorption at 3400 cm^{-1} and one in the region 1000 to 1150 cm^{-1}

marked the presence of coordinated water, and perchlorate ion, respectively.

Magnetic susceptibility measurements were made on an aqueous solution of $\text{MnB}(\text{OH}_2)_2(\text{ClO}_4)_2 \cdot \text{H}_2\text{O}$ over the temperature interval 2° to 84° . This solution was not degassed and acetone at a concentration of 5 vol % was used as the internal standard. Within the experimental error of the shift measurements, the molar susceptibilities corrected for the diamagnetism of the macrocyclic ligand²⁸ (-186×10^{-6} cgs units), adhered to a Curie temperature dependence and indicated an average effective magnetic moment of 5.9 BM. This value compares favorably with the spin only value for high-spin manganese(II) and reasonably well with the result of a previous magnetic susceptibility study³¹ of solid MnBCl_2 in which the magnetic moment was observed to be slightly temperature dependent, varying from 5.72 at 67° to 5.90 BM at -51° . This temperature dependence of the effective magnetic moment was not observed for aqueous solutions of the perchlorate salt reported here.

For the purpose of nonaqueous solvent proton nmr measurements a portion of the $\text{MnB}(\text{OH}_2)_2(\text{ClO}_4)_2 \cdot \text{H}_2\text{O}$ was dried in vacuo over P_4O_{10} at room temperature in order to remove the coordinated water. After several weeks of drying an IR spectrum of the complex indicated the absence of coordinated water. Further, as previously observed by

Alexander, et al,³⁰ the intense perchlorate band was now split, a result probably due to perchlorate ion coordination as suggested by these workers.

Anal. Calc'd for $\text{MnC}_{15}\text{H}_{23}\text{N}_5(\text{ClO}_4)_2$: C, 34.17;
H, 4.40; N, 13.28. Found: C, 34.51; H, 4.19;
N, 13.20.

4. Preparation and characterization of the various salts of 2,12-dimethyl-3,7,11,17-tetraazabicyclo(11.3.1)heptadeca-1(17),2,11,13,15-pentaenenickel(II) $\{\text{NiCR}^{2+}\}$ and its methylated analogue $\{\text{NiCRMe}^{2+}\}$

These two complexes were studied in several solvents and as a result of solubility limitations it was necessary to prepare various salts.

NiCRCl_2 was prepared from stoichiometric amounts of $\text{NiCl}_2 \cdot 6\text{H}_2\text{O}$ (Baker and Adamson), 2,6-diacetylpyridine and 3,3'-diaminodipropylamine (Matheson, Coleman and Bell), using Curry's procedure, as described by Karn and Busch.³² The product was recrystallized from warm water.

The hexafluorophosphate salt, which is much less water soluble than the chloride, was prepared by mixing saturated aqueous solutions of NiCRCl_2 and NaPF_6 (Alfa Inorganics). The yellow product was recrystallized from aqueous solution.

The very water soluble tetrafluoroborate salt was prepared by mixing solutions of AgBF_4 and NiCRCl_2 ; the

AgBF_4 being prepared by the addition of 25% HBF_4 (Baker and Adamson) to a solution of Ag_2CO_3 (Johnson Matthey and Mallory) until neutralization was complete. The AgCl was removed by filtration and the resultant solution was evaporated under vacuum until crystallization commenced. This solution was cooled and the product collected by filtration and then recrystallized twice from water. Alternatively, the tetrafluoroborate salt was prepared by using $\text{Ni}(\text{BF}_4)_2 \cdot 6\text{H}_2\text{O}$ (Alfa Inorganics) in place of $\text{NiCl}_2 \cdot 6\text{H}_2\text{O}$ in the original condensation reaction. Some care is necessary in the latter method since overheating or prolonged reaction time resulted in a mixture of fluoride and tetrafluoroborate salts. The dried tetrafluoroborate salt was brick red in color.

$\text{NiCR}(\text{ClO}_4)_2$ and $\text{NiCR}(\text{NO}_3)_2$ were prepared as described by Karn and Busch.³² $\text{NiCR}(\text{SbF}_6)_2$ was prepared from NiCRCl_2 and $\text{Ag}(\text{SbF}_6)$ (Pennisular Chemical Research Inc.) in a manner analogous to that used for $\text{NiCR}(\text{BF}_4)_2$.

NiCRMeCl_2 was prepared by the same procedure as that used for NiCRCl_2 , except that the amine, 3,3'-diamino N-methyldipropylamine (Ames Laboratories, Inc.), was used. The perchlorate and tetrafluoroborate salts were prepared using procedures analogous to those described above.

All of the salts were dried under vacuum over P_4O_{10} at room temperature until the resolved OH stretching bands at 3500 to 3600 cm^{-1} , in Nujol, had disappeared from the

infrared spectrum. The compounds were characterized by carbon, hydrogen, and nitrogen analyses given in Table I, and by their infrared, electronic and nmr spectra.

The infrared spectra of $\text{NiCR}(\text{BF}_4)_2$, $\text{NiCR}(\text{ClO}_4)_2$ and $\text{NiCR}(\text{PF}_6)_2$ in Nujol mulls were identical except for bands characteristic of the anion. Band positions were in general agreement with those reported by Rich and Stucky³³ for $\text{NiCR}(\text{ZnCl}_4)$. However, their spectra in KBr show a water absorption at 3380 cm^{-1} and fail to show the sharp N-H stretching absorption at 3230 cm^{-1} observed in the present work. The complex absorption, due to C=N stretching and pyridine ring vibrations, in the 1575 to 1595 cm^{-1} region, has been observed in the present and previous work. The infrared spectrum of $\text{NiCRMe}(\text{BF}_4)_2$ was almost identical with that of $\text{NiCR}(\text{BF}_4)_2$ except for the absence of the N-H stretching absorption at 3230 cm^{-1} , as expected, since this is now an N-CH₃ group. There is an additional peak at 1245 cm^{-1} , consistent with a C-N stretching vibration, and two different peaks at 850 and 780 cm^{-1} .

The peak maxima and molar extinction coefficients in the electronic spectra of $\text{NiCR}(\text{BF}_4)_2$ and $\text{NiCR}(\text{PF}_6)_2$ in water are given in Table II. The results for $\text{NiCR}(\text{BF}_4)_2$ are in good agreement with those given by Rich and Stucky,³³ except that the latter workers did not observe the band at 720 nm . Measurements on the perchlorate and nitrate salts at 396 nm gave extinction coefficients of $127\text{ M}^{-1}\text{cm}^{-1}$

TABLE I
Microanalytical results for various NiCR^{2+} and NiCRMe^{2+} salts

Compound	%C		%H		%N	
	Calc'd	Found	Calc'd	Found	Calc'd	Found
$\text{NiCR}(\text{PF}_6)_2$	29.70	29.67	3.65	3.90	9.23	9.19
$\text{NiCR}(\text{BF}_4)_2$	36.71	36.57	4.52	4.55	11.41	11.71
$\text{NiCR}(\text{ClO}_4)_2$	34.77	34.91	4.24	4.26	10.93	10.86
$\text{NiCR}(\text{SbF}_6)_2$	22.84	22.78	2.81	2.76	7.11	7.10
$\text{NiCRMe}(\text{ClO}_4)_2$	35.26	35.86	4.56	4.51	10.58	10.70
$\text{NiCRMe}(\text{BF}_4)_2$	38.15	38.01	4.80	4.70	11.13	10.70
$\text{NiCR}(\text{DMF})_2(\text{PF}_6)_2$ (a)	33.50	33.11	4.83	4.85	11.15	11.31

(a) This N,N-dimethylformamide (DMF) adduct was prepared from anhydrous $\text{NiCR}(\text{PF}_6)_2$ dissolved in DMF under vacuum with subsequent removal of the solvent.

TABLE II

Electronic spectrum of NiCR^{2+} in aqueous solution at 25°.

Band position, nm	$10^{-3} \times$ Extinction Coefficient, $\text{M}^{-1}\text{cm}^{-1}$	
	$\text{NiCR}(\text{BF}_4)_2$	$\text{NiCR}(\text{PF}_6)_2$
720	0.025	— (b)
396	0.124	0.148
300 (a)	2.26	2.32
266	5.14	5.20
230	15.4	15.6

(a) Shoulder

(b) The salt is too insoluble in water for this extinction coefficient to be measured.

and $122 \text{ M}^{-1}\text{cm}^{-1}$, respectively, in agreement with the value for the BF_4^- salt. However, the extinction coefficient of the PF_6^- salt at 396 nm is significantly greater than that of the BF_4^- salt. Recrystallization of the PF_6^- salt and addition of F^- or PF_6^- to solutions of the BF_4^- salt failed to affect the extinction coefficient. Since both salts were derived from the same NiCRCl_2 source and since the extinction coefficients agree at the other wavelengths, an impurity seems unlikely. No adequate explanation has been found for this phenomenon, but both the ClO_4^- and PF_6^- salts gave identical nmr results in DMF. Also the results of the nmr study on the BF_4^- and ClO_4^- salts in water were in agreement.

The spectrum of $\text{NiCRMe}(\text{BF}_4)_2$ in water at 25° is similar to that of $\text{NiCR}(\text{BF}_4)_2$. There are maxima at 750 and 396 nm with extinction coefficients of 12.7 and $595 \text{ M}^{-1}\text{cm}^{-1}$, respectively. The same values were obtained for the perchlorate salt in water. The large difference in extinction coefficients at 396 nm between NiCR^{2+} and NiCRMe^{2+} is mainly due to the greater percentage of diamagnetic species present in the latter system at 25° .

The nmr and magnetic susceptibility studies show that only the diamagnetic form of the complexes is present in trifluoroethanol. In this solvent the visible spectra of $\text{NiCR}(\text{BF}_4)_2$, $\text{NiCR}(\text{ClO}_4)_2$ and $\text{NiCR}(\text{PF}_6)_2$ show a maximum at 390 nm with extinction coefficients of 1.40×10^3 ,

1.32×10^3 and $1.44 \times 10^3 \text{ M}^{-1}\text{cm}^{-1}$, respectively. Under the same conditions $\text{NiCRMe}(\text{ClO}_4)_2$ and $\text{NiCRMe}(\text{BF}_4)_2$ also show a maximum at 390 nm with extinction coefficients of 1.36×10^3 and $1.30 \times 10^3 \text{ M}^{-1}\text{cm}^{-1}$, respectively.

It is clear from these results that the absorbance at 396 nm in aqueous solutions is strongly affected by the diamagnetic species. The temperature variations of the visible spectra, to be discussed later in connection with equilibrium constant measurements, are consistent with this assignment.

When either $\text{NiCR}(\text{BF}_4)_2$ or $\text{NiCRMe}(\text{BF}_4)_2$ is dissolved in trifluoroacetic acid, d_3 -nitromethane, or trifluoroethanol the macrocyclic ligand pmr of the diamagnetic complex is observed. The spectra are shown in Figure 1. The A_2B multiplet centered at $\sim 2\tau$ is due to the pyridyl protons and the peak at 7.46τ is readily assigned to the two equivalent CH_3 groups. The amine CH_3 in NiCRMe^{2+} is observed at 6.85τ . The integrated intensities of the peaks were completely consistent with this assignment. These chemical shifts are assigned to the pure diamagnetic form since they are independent of the non-coordinating solvent used and also temperature independent over the range -42° to 82°C in trifluoroethanol.

In coordinating solvents the pmr spectra of these complexes are very temperature dependent and this has enabled a quantitative characterization of the temperature

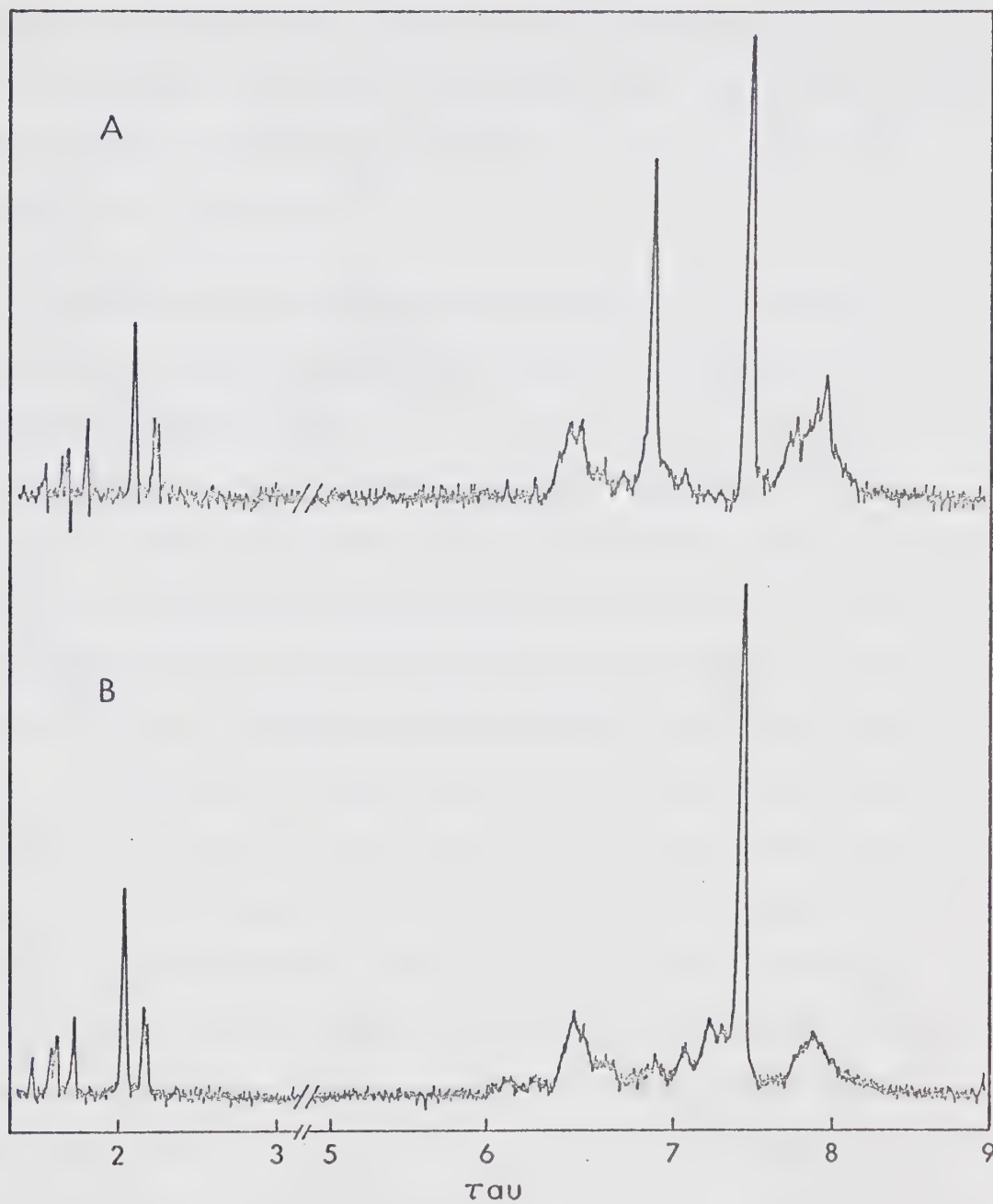


Figure 1: The 60 MHz pmr spectrum of $\text{NiCRMe}(\text{BF}_4)_2$ (A) and $\text{NiCR}(\text{BF}_4)_2$ (B) in trifluoroacetic acid. Spectra are calibrated in units of tau downfield from internal TMS.

dependence of diamagnetic-paramagnetic equilibrium which was observed to be present. The results of this study and of the related magnetic susceptibility studies are given in Chapter III, Section 3.

5. The preparation and characterization of tetrabenzo-[b,f,j,n][1,5,9,13]tetraazabicyclohexadecinenickel(II) perchlorate $\{\text{NiTAAB}(\text{ClO}_4)_2\}$

$\text{NiTAAB}(\text{NO}_3)_2$ was prepared by the self-condensation reaction of o-aminobenzaldehyde in the presence of $\text{Ni}(\text{NO}_3)_2 \cdot 6\text{H}_2\text{O}$ as described by Melson and Busch.³⁴ The o-aminobenzaldehyde was prepared by the method of Smith and Opie.³⁵ The reaction product, which contains a mixture of two different Schiff bases, was separated by the addition of a concentrated solution of sodium perchlorate as suggested by Melson and Busch;³⁴ the red $\text{NiTAAB}(\text{ClO}_4)_2$ immediately precipitating from solution. The filtrate containing yet another Schiff base was saved. The perchlorate salt isolated in this manner was converted to the nitrate salt using their procedure. Upon air drying, the following analyses were obtained.

Anal. Calc'd for $\text{NiC}_{28}\text{H}_{20}\text{N}_4(\text{OH}_2)_2(\text{NO}_3)_2$: C, 53.28; H, 3.83; N, 13.31. Found: C, 53.11; H, 3.70; N, 13.05.

A portion of the above nitrate salt was reconverted to the perchlorate salt by the addition of a sodium per-

chlorate solution to an aqueous solution of the nitrate salt. The product was filtered, washed with a solution of sodium perchlorate and finally with water. It was dried over P_4O_{10} at room temperature.

Anal. Calc'd for $NiC_{28}H_{20}N_4(ClO_4)_2$: C, 50.19; H, 3.01; N, 8.36. Found: C, 50.20; H, 3.02; N, 8.40.

The IR spectrum of each of these complexes was in agreement with that previously reported.³⁴

As a further characterization, magnetic susceptibility measurements, by the method of Evans,²⁷ were made on both $NiTAAB(NO_3)_2$ and $NiTAAB(ClO_4)_2$ in DMF. Both salts indicated molar susceptibilities having the same temperature dependence and the same limiting magnetic moment. At low temperatures the molar susceptibilities were observed to follow a Curie temperature dependence with a limiting magnetic moment of 3.14 BM. At higher temperatures the susceptibilities indicated the formation of a diamagnetic species as evidenced by the slight upward curvature in a plot of χ_M^{-1} against $T^\circ K$. Due to the small temperature dependence of the diamagnetic-paramagnetic equilibrium, the determination of the temperature dependence of the equilibrium constant from these results was only of limited accuracy. However, the results were of qualitative value in interpreting the solvent proton nmr study of $NiTAAB^{2+}$ in DMF.

6. The preparation and characterization of tribenzo[b,f,j]-[1,5,9]triazacyclododecinenickel(II) perchlorate {NiTRI(ClO₄)₂}

This complex, which is a co-product of NiTAAB²⁺ in the self-condensation reaction of o-aminobenzaldehyde, was prepared by the method of Bush and Melson^{34,36} as outlined in Part 5 above. The filtrate mentioned there was used in the present case. Both the nitrate and perchlorate salts were isolated using the procedure in ref 36. The complexes were air dried.

Anal. Calc'd for NiC₂₁H₁₅N₃(OH₂)₂(NO₃)₂: C, 47.76
H, 3.63; N, 13.26. Found: C, 47.22; H, 3.40;
N, 13.40.

Calc'd for NiC₂₁H₁₅N₃(OH₂)₃(ClO₄)₂: C, 40.61;
H, 3.41; N, 6.77. Found: C, 40.19; H, 4.14;
N, 6.97.

The complex was also identified by a comparison of its infrared spectrum to the spectral results previously published.³⁶

7. Preparation and characterization of 2,12-dimethyl-3,7,11,17-tetraazabicyclo(11.3.1)heptadeca-1(17),2,11,-13,15-pentaenecobalt(II) perchlorate {CoCR(ClO₄)₂}

The nitrate salt of this complex was prepared using the method of Long and Busch,³⁷ in which 2,6-diacetylpyri-

dine is condensed with 3,3'-diaminodipropylamine in the presence of $\text{Co}(\text{NO}_3)_2 \cdot 6\text{H}_2\text{O}$ (Baker and Adamson) in aqueous ethanol for 3-4 hrs. All solutions were purged with argon prior to being mixed and the reaction was allowed to proceed in an argon atmosphere. All subsequent handling of the complex was done with the rigorous exclusion of air. After excess solvent was removed under vacuum from the reaction mixture, a degassed solution of sodium perchlorate was added. The product, which precipitated immediately, was recrystallized from water and dried on the vacuum line. Crystals of dry $\text{CoCR}(\text{ClO}_4)_2$ were maroon in color.

Anal. Calc'd for $\text{CoC}_{15}\text{H}_{22}\text{N}_4(\text{ClO}_4)_2$: C, 34.90; H, 4.30; N, 10.85. Found: C, 35.04; H, 4.30; N, 11.27.

This complex was also identified by a comparison of its IR spectrum with that of $\text{NiCR}(\text{ClO}_4)_2$ and to previously reported results.³⁷ Also, the visible spectrum of a degassed methanol solution of $\text{CoCR}(\text{ClO}_4)_2$ was measured. In the resulting spectrum, which is very similar to the reflectance spectrum of $\text{CoCRBr}(\text{ClO}_4)_2$,³⁷ band maxima, with extinction coefficients in $\text{M}^{-1}\text{cm}^{-1}$ units shown in parentheses, were observed at 368 nm (1.36×10^3), 465 nm (1.56×10^3), 547 nm (1.0×10^3), 610 nm (8.3×10^3) and 700 nm ($\sim 3 \times 10^2$).

The magnetic moment of a degassed DMF solution of

$\text{CoCR}(\text{ClO}_4)_2$ was measured at only one temperature. A value of 1.85 BM was obtained at 35°. This is consistent with a low-spin electronic configuration for the cobalt(II).

8. Preparation and characterization of 2,12-dimethyl-3,7,11,17-tetraazabicyclo(11.3.1)heptadeca-1(17),2,11,13,15-pentaenecopper(II) tetrafluoroborate $\{\text{CuCR}(\text{BF}_4)_2\}$

CuCRCl_2 and subsequently the tetrafluoroborate salt were prepared using the method analogous to that used to obtain $\text{NiCR}(\text{BF}_4)_2$, with $\text{CuCl}_2 \cdot 2\text{H}_2\text{O}$ (Fisher) replacing $\text{NiCl}_2 \cdot 6\text{H}_2\text{O}$ in the preliminary reaction. The product was dried over P_4O_{10} in vacuo.

Anal. Calc'd for $\text{CuC}_{15}\text{H}_{22}\text{N}_4(\text{BF}_4)_2$: C; 36.36, H; 4.48, N; 11.31. Found: C; 36.44, H; 4.78; N, 11.12.

The visible and uv spectrum of an aqueous solution of $\text{CuCR}(\text{BF}_4)_2$ had band maxima at 560, 302 and 313 nm with extinction coefficients of 1.34×10^2 , 2.58×10^3 and $2.79 \times 10^3 \text{ M}^{-1}\text{cm}^{-1}$, respectively. In addition, a shoulder was present at 325 nm. These measurements are in agreement with the results reported for $\text{CuCR}(\text{ZnCl}_4)^{33}$ except that the band at 560 nm in the visible was reported to have an extinction coefficient of $110 \text{ M}^{-1}\text{cm}^{-1}$.

9. Preparation and characterization of 5,7,7,12,14,14-hexamethyl-1,4,7,11-tetraazacyclotetradeca-4,11-dienecobalt perchlorate $\{Co(trans[14]diene)(ClO_4)_2\}$

The metal-free Schiff base salt, $trans[14]diene \cdot 2HClO_4$, was prepared by the method of Curtus and Hay.³⁸ In the first stage, equimolar amounts of dilute $HClO_4$ and ethylenediamine (en) were mixed while being cooled in an ice bath. The product, $en_2 \cdot HClO_4$, was not isolated; instead, excess mesityl oxide (Eastman Organic Chemicals) was added to this solution and the reaction allowed to proceed without external heating. The resulting $trans[14]diene \cdot 2HClO_4$ was filtered and washed with acetone. A comparison of the IR spectrum with the results previously reported³⁹ and a determination of the integrated pmr spectrum served to identify this product. The cobalt(II) complex was prepared by the reaction of equimolar amounts of $trans[14]diene \cdot (HClO_4)_2$ and $Co(CH_3CO_2)_2 \cdot 4H_2O$ (Fisher Reagent) in aqueous methanol solvent at 70°. All solutions were initially purged with nitrogen and the reaction took place in a nitrogen atmosphere. After 2-3 hrs the resulting orange solution was evaporated down under vacuum until precipitation of the cobalt(II) Schiff base complex commenced. After further cooling the product was filtered in a glove bag and recrystallized twice from degassed water and finally from acetone. The yellow complex was dried over P_4O_{10} in vacuo at room temperature.

Anal. Calc'd for $\text{CoC}_{16}\text{H}_{32}\text{N}_4(\text{ClO}_4)_2$: C; 35.70, H; 5.99, N; 10.41, Co; 10.95. Found: C; 35.52, H; 6.11, N; 11.06, Co; 10.17.

Cobalt was analyzed for spectrophotometrically⁴⁰ as the thiocyanate complex after degradation of the Schiff base complex with potassium persulfate (AnalaR). The tetrafluoroborate salt of this complex was also prepared using an analogous procedure in which $\text{trans}[14]\text{diene} \cdot 2\text{HBF}_4$, prepared from dilute HBF_4 and ethylenediamine, was employed.

Anal. Calc'd for $\text{CoC}_{16}\text{H}_{32}\text{N}_4(\text{BF}_4)_2$: C; 37.46, H; 6.29, N; 10.92. Found: C; 37.42, H; 6.41, N; 10.54.

This complex was also identified by a comparison of its IR spectrum with previously reported results.³⁸ The visible spectrum of freshly prepared aqueous solutions of $\text{Co}(\text{trans}[14]\text{diene})(\text{ClO}_4)_2$ consisted of one band at 442 nm having an extinction coefficient of $97 \text{ M}^{-1}\text{cm}^{-1}$. Comparison of this spectrum with those of Endicott³⁹ for the corresponding cobalt(III) complex indicated that air oxidation of the complex, in the time taken to determine the spectrum, had not occurred. After several hours, however, the presence of Co(III) was detected and it was thus necessary to prepare all nmr and epr samples under vacuum.

Magnetic susceptibility measurements were made on

degassed aqueous solutions of $\text{Co}(\text{trans}[14]\text{diene})(\text{ClO}_4)_2$. The temperature dependence of the molar susceptibilities, corrected for the diamagnetism of the Schiff base ligand,²⁸ indicated a Curie-Weiss dependence with $\theta = 42^\circ\text{K}$. An effective magnetic moment of 2.07 BM was obtained from these measurements, thus indicating low-spin cobalt(II).

10. Sample Preparation

All nonaqueous solvent samples and also the aqueous samples of $\text{Co}(\text{trans}[14]\text{diene})^{2+}$ were prepared under vacuum using standard vacuum line techniques.

The general procedure consisted of placing a weighed amount of complex in a suitable flask which was then evacuated and weighed. The solvent was vacuum distilled onto the solid and the flask and contents were reweighed to determine the weight of solvent. An aliquot of the solution was poured into an nmr tube into which a small amount of internal standard was previously added. The nmr tube was then sealed.

In the case of the samples prepared from $\text{NiTRI}(\text{OH}_2)_3^-(\text{ClO}_4)_2$, $\text{NiTRI}(\text{OH}_2)_2(\text{NO}_3)_2$ and $\text{NiTAAB}(\text{OH}_2)_2(\text{NO}_3)_2$ the stock solutions, prepared in the above manner, were poured under vacuum into an evacuated vessel containing Linde 3A molecular sieves in order to remove the coordinated water. After several hours, these solutions were used to prepare the nmr samples.

Methanol and DMF solutions of $\text{Mn}(\text{DMP}r\text{Por})^+$ were prepared by placing a weighed amount of $\text{Mn}(\text{DMP}r\text{Por})\text{Cl}\cdot\text{OH}_2$ and a slight excess of AgClO_4 in the flask. After the vacuum preparation of these solutions, they were passed through a sintered glass filter to remove the AgCl and into another flask containing molecular sieves. These solutions were used after 2-3 hours to prepare the nmr samples.

Whenever dilute methanol solutions of either $\text{NiCR}(\text{BF}_4)_2$ or $\text{MnB}(\text{ClO}_4)_2$ were prepared, it was found necessary to add a very small amount of anhydrous 2,4-dinitrobenzenesulfonic acid (Eastman Organic Chemicals) to the nmr samples in order to collapse the coupling between methyl and hydroxy protons. The blank methanol sample was similarly prepared. However, it was observed that this addition of acid to methanol solutions of $\text{MnB}(\text{ClO}_4)_2$ resulted in significant acid hydrolysis of the complex, as evidenced by the slow increase with time of the nmr line broadening at higher temperatures, and by the eventual appearance of free Schiff base ligand in the nmr samples. To prevent this, freshly prepared samples were immediately cooled to -64° in a chloroform sludge and kept there between measurements. By taking this precaution it was possible to obtain reproducible results from several samples.

Much of the data for NiCR^{2+} and NiCRMe^{2+} was obtained using tetrafluoroborate or hexafluorophosphate salts. Due

to a concern over possible anion or fluoride ion effects on the magnetic susceptibility and nmr line broadening data, some of this data was checked against that of the perchlorate salt. For instance, the results from both the PF_6^- and ClO_4^- salts of NiCR^{2+} in DMF were identical within experimental error and similarly the results using the BF_4^- and ClO_4^- salts of NiCR^{2+} in water were in agreement. In the $\text{NiCR}(\text{BF}_4)_2$ -methanol study the poor solubility of the ClO_4^- salt prevented a similar comparison but it was found that both the nitrate and hexafluoroantimonate salts gave the same results.

Magnetic susceptibility measurements were made by Evan's nmr method²⁷ using precision made co-axial tubes (Wilmad Glass Co.). Solutions containing the paramagnetic complex along with ~5 vol % internal standard were added under vacuum to the inner tube and the pure solvent plus the internal standard were placed in the outer co-axial tube. Only the inner tube was sealed off. Whenever possible, the concentration of the complex was adjusted to give susceptibility shifts between the two internal standard peaks of 25 to 75 Hz.

In all DMF and methanol nmr and susceptibility samples cyclopentane (Aldrich) was used as the internal standard. Tetramethylsilane (TMS) or methoxybenzene (Matheson, Coleman and Bell) were used for dimethylsulfoxide (DMSO) and acetonitrile samples. For aqueous solutions t-butanol

(Matheson, Coleman and Bell), sodium 3-trimethylsilyl-1-propane sulfonate (DSS) (Eastman Organic Chemicals) or reagent acetone were used.

11. Instrumentation

The pmr spectra were recorded on Varian Associates A56/60 and HA-100 spectrometers equipped with model 4343 temperature control units. Temperatures were determined by a comparison of the peak to peak separation of pure methanol or ethylene glycol samples with calibration charts published by Varian Associates. Temperatures on the HA-100 spectrometer were measured by means of a copper-constantan thermocouple. In all cases the temperature was measured prior to a spectral run. Occasionally the temperature was remeasured after the determination of a spectrum and was found to be constant to $\pm 0.5^{\circ}\text{C}$. About 3-5 minutes was allowed for temperature equilibration in the nmr sample. The normal precautions were taken to prevent signal saturation and to ensure proper phasing. Linewidth measurements were reproducible on both instruments to ± 1 Hz.

EPR spectra were determined for $\text{Mn}(\text{DMP}r\text{Por})\text{ClO}_4$ and $\text{MnB}(\text{ClO}_4)_2$ in methanol, $\text{Co}(\text{trans}[14]\text{diene})(\text{BF}_4)_2$ in acetonitrile and $\text{CoCR}(\text{ClO}_4)_2$ in DMF in order to obtain an estimate of T_{1e} . These were obtained at X-band (~ 9000 MHz) on a Varian A-4502 EPR spectrometer. The

author wishes to thank Mr. G. Bigam and Mr. G. Miller for obtaining the epr spectra.

Electronic spectra were measured on a Cary 14 spectrophotometer and infrared spectra on a Perkin Elmer model 421 spectrophotometer.

CHAPTER III: NUCLEAR MAGNETIC RESONANCE LINE BROADENING
AND CHEMICAL SHIFT STUDIES OF PARAMAGNETIC
SCHIFF BASE AND PORPHYRIN COMPLEXES

1. Solvent Proton NMR Line Broadening and Chemical shift
Study of Manganese(III) Protoporphyrin(IX) Dimethyl Ester
in Methanol and N,N-dimethylformamide

The biological importance of metal porphyrin complexes is generally well recognized, and in the particular case of manganese, these compounds are believed to play a role in photosynthesis.^{29,41,42} Despite its importance, no information is available on the reaction rates of manganese porphyrins although kinetic studies of the rates of substrate binding to the more inert cobalt(III) and iron(III) hematoporphyrins have been reported.⁴³ Since a knowledge of the solvent exchange rate from the first coordination sphere of a metal ion is useful in establishing the general lability and mechanism of complexation to the metal ion,^{2,6} a study of the solvent exchange rates from manganese(III) protoporphyrin(IX) dimethyl ester, $\text{Mn}(\text{DMP}r\text{Por})^+$, was undertaken. This complex is shown as structure VI in the introduction to this thesis.

The results of this study also provide further information on the dependence of the solvent exchange rates on various metal ions. The manganese(III) in $\text{Mn}(\text{DMP}r\text{Por})^+$ is a high-spin d^4 ion and the exchange rates can be com-

pared to those of ferriprotoporphyrin(IX),⁹ which contains high-spin d^5 iron(III), in order to determine the importance of crystal-field effects in a d^4 system.

Due to the low solubility and possible polymerization of $\text{Mn}(\text{DMPPrPor})^+$ in aqueous solution, this solvent exchange study was restricted to the nonaqueous solvents, methanol and N,N-dimethylformamide (DMF). However, since a number of different metal ions have been studied in methanol, DMF, and water,² the results of this study can be used to infer the approximate water exchange rate on $\text{Mn}(\text{DMPPrPor})^+$.

The nmr measurements were made on solutions of $\text{Mn}(\text{DMPPrPor})\text{ClO}_4$ prepared *in situ* from $\text{Mn}(\text{DMPPrPor})\text{Cl}\cdot\text{OH}_2$ as described in the experimental section.

The temperature dependence of $(T_{2P}^{PM})^{-1}$ and $\Delta\omega_{\text{obsd}}/P_M$ for the hydroxy and methyl protons in the $\text{Mn}(\text{DMPPrPor})^+$ -methanol system are shown in Figures 2 and 3, respectively, while similar plots for the formyl and high field methyl protons in the $\text{Mn}(\text{DMPPrPor})^+$ -DMF study are shown in Figures 4 and 5. Since for DMF solutions of $\text{Mn}(\text{DMPPrPor})^+$ the overlap of the two DMF methyl resonances was considerable at low temperatures for the complex concentrations employed, the individual line widths were resolved by a computer fit of the absorption intensities to the sum of two Lorentzians. Only the results for the broader high field methyl resonance are given. Preliminary analysis of the line broadening results in these systems indicated

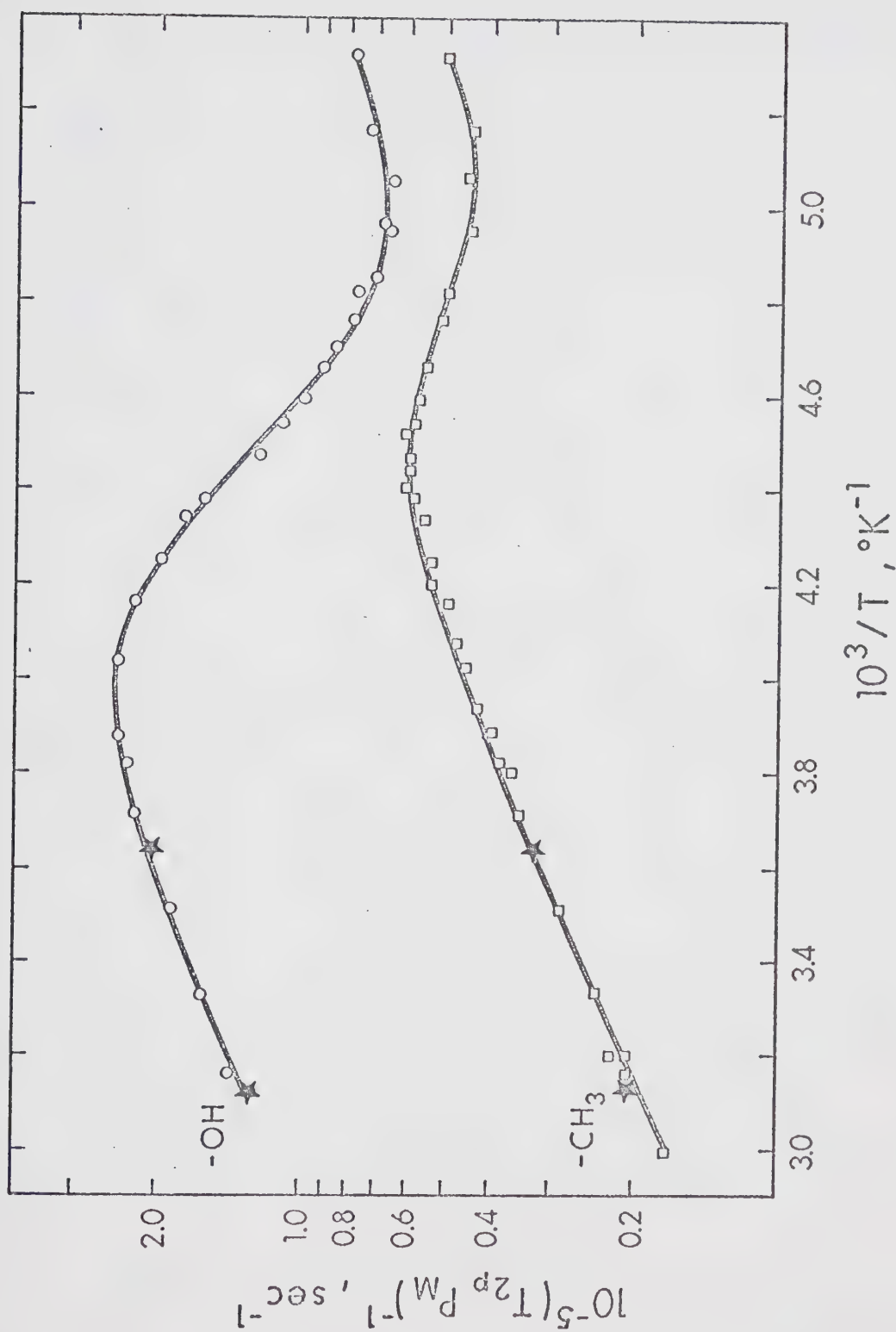


Figure 2: Temperature dependence of $-\log(T_{2p} P_M)$ for the hydroxy and methyl protons in methanol solutions of $\text{Mn}(\text{DMPPrPor})\text{ClO}_4$ at 60 MHz (o, \square) and 100 MHz (\star).

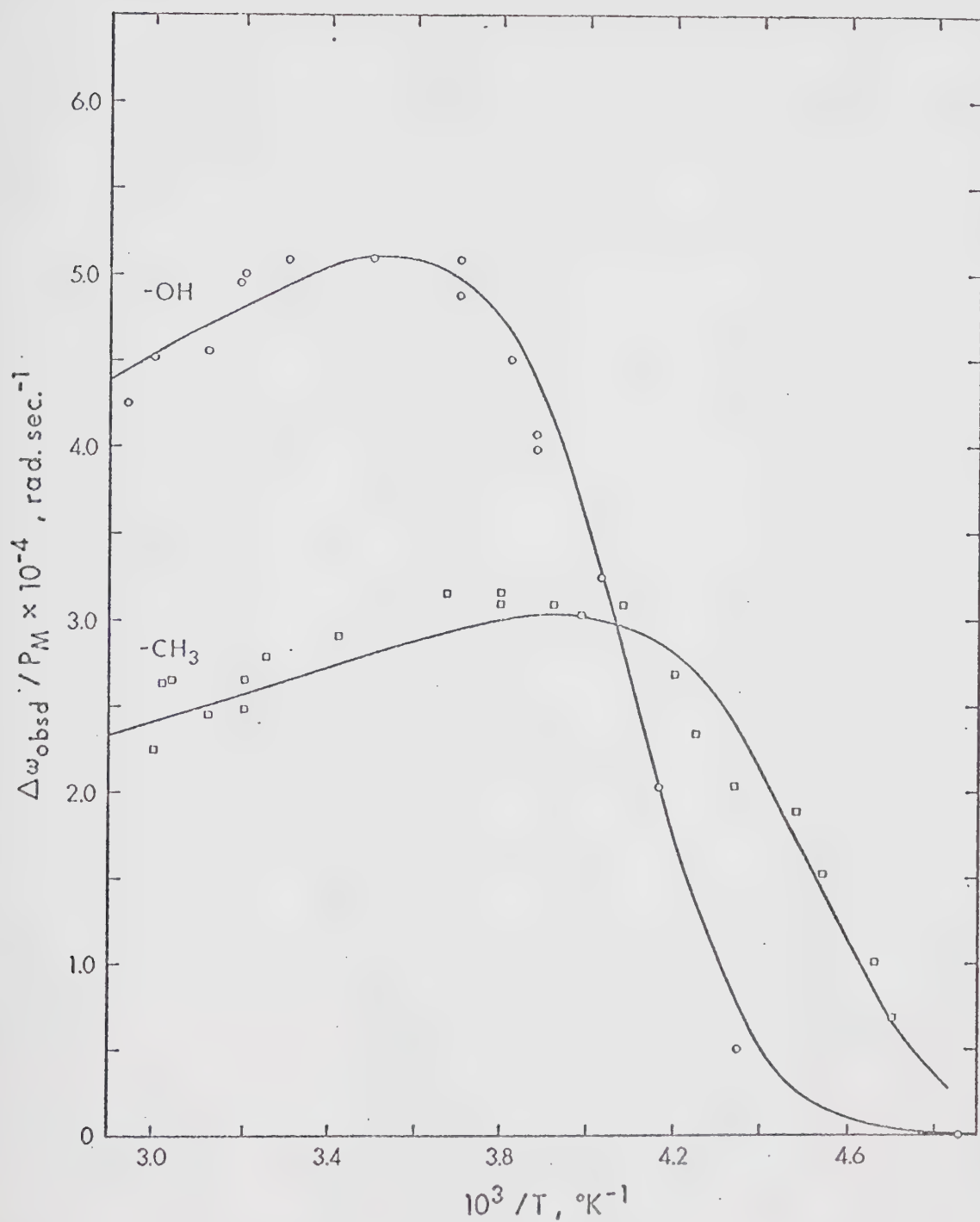


Figure 3: Temperature dependence of $(\Delta\omega_{\text{obsd}}/P_M)$ at 60 MHz for the hydroxy and methyl protons in methanol solutions of $\text{Mn}(\text{DMP}r\text{Por})\text{ClO}_4$.

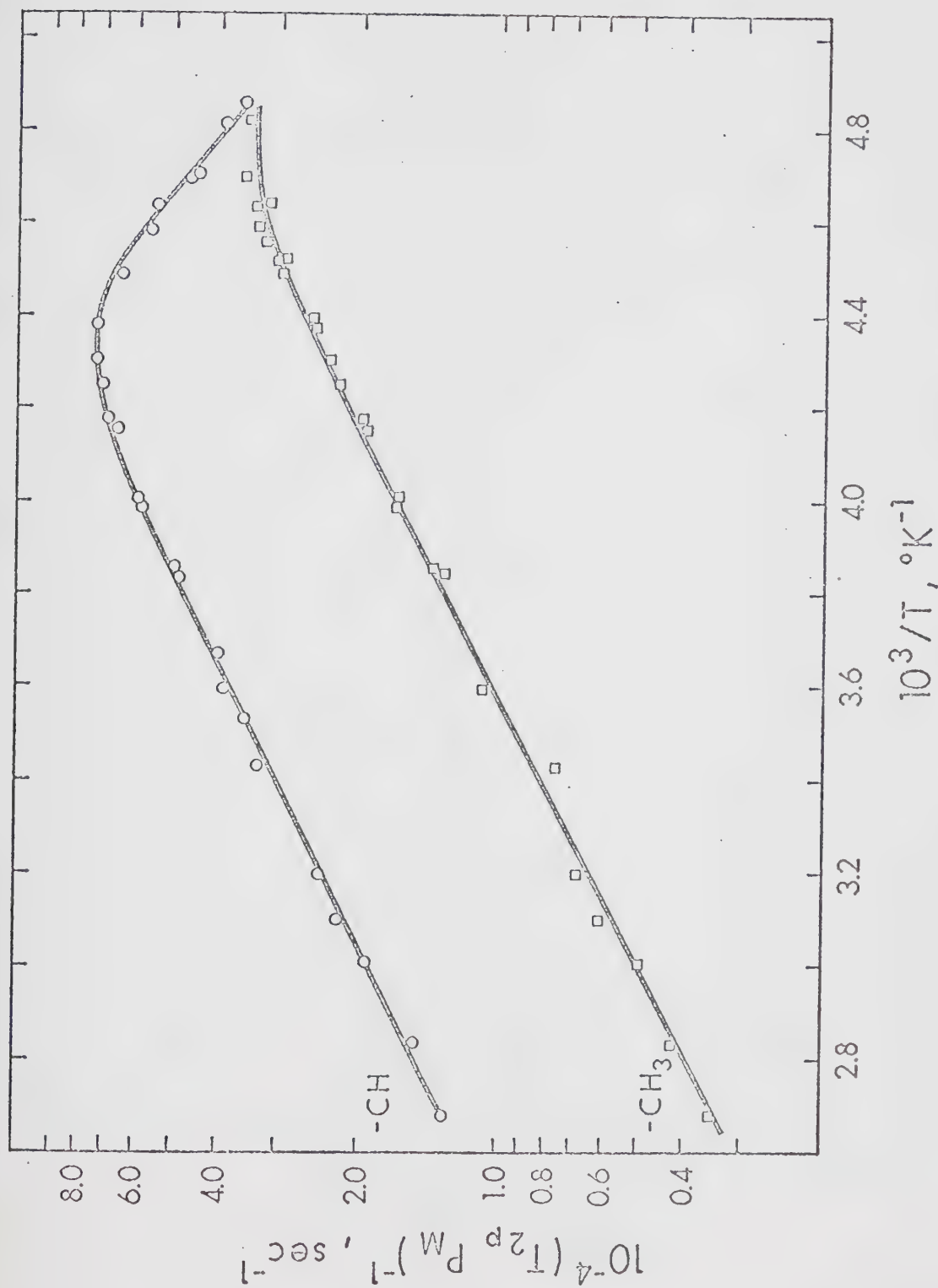


Figure 4: Temperature dependence of $-\log(T_{2P_M})$ at 60 MHz for the formyl and high field methyl protons in N,N-dimethylformamide solutions of $\text{Mn}(\text{DMPPrPor})\text{ClO}_4$.

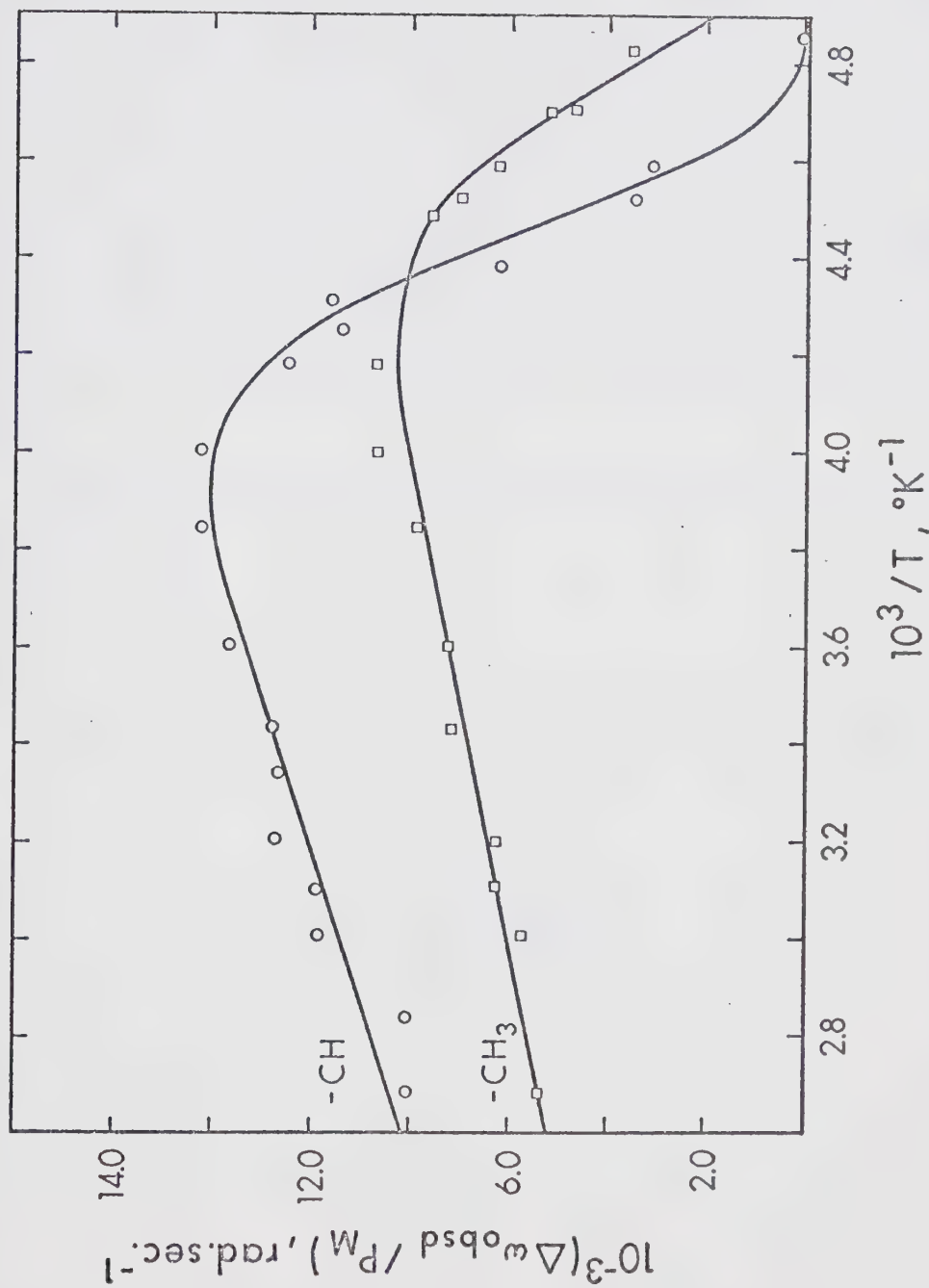


Figure 5: Temperature dependence of $(\Delta\omega_{\text{obsd}}/P_M)$ at 60 MHz for the formyl and high field methyl protons in N,N-dimethylformamide solutions of $\text{Mn}(\text{DMPPrPor})\text{ClO}_4$.

that either $(\tau_M)^{-2}$ or $(T_{2M})^{-2}$ was always greater than $\Delta\omega_M^2$. The absence of a frequency dependence and the low activation energy of the line broadening in the high temperature region, where $(T_{2P}P_M)^{-1}$ is independent of τ_M , is a further confirmation that limiting conditions 26(a) to 26(c) (Case B) apply. However, for $\text{Mn}(\text{DMP}r\text{Por})^+$ in DMF, no outer sphere line broadening region is observed since inner sphere solvent exchange broadening is very significant at the lowest temperature at which measurements could be made.

With the limiting conditions 26(a) to 26(c), eq 2 reduces to

$$(T_{2P}P_M)^{-1} = \frac{1}{\tau_M} \left\{ \frac{(1/T_{2M})^2 + (1/T_{2M}\tau_M)}{(1/T_{2M} + 1/\tau_M)^2} \right\} + (T_{2O})^{-1} \quad (27)$$

$$= \left(\frac{1}{T_{2M} + \tau_M} \right) + (T_{2O})^{-1}$$

and eq 8 becomes

$$- \frac{\Delta\omega_{\text{obsd}}}{P_M} = \frac{\Delta\omega_M}{((\tau_M/T_{2M}) + 1)^2} \quad (28)$$

In these expressions P_M is defined by eq 4 where it is as-

sumed that n has a value of two for $\text{Mn}(\text{DMPPrPor})^+$.

$\text{Mn}(\text{DMPPrPor})^+$ in Methanol

Considering the behaviour of $-\log(T_{2P}P_M)$ for $\text{Mn}(\text{DMPPrPor})^+$ in methanol, shown in Figure 2, it is readily seen that in the high temperature region ($1/T < 4 \times 10^{-3} \text{ } ^\circ\text{K}^{-1}$), $(T_{2M}\tau_M)^{-1} \gg (T_{2M})^{-2}$ and therefore $(T_{2P}P_M)^{-1}$ is controlled by $(T_{2M})^{-1}$. As the temperature decreases $(\tau_M)^{-1}$ becomes smaller than $(T_{2M})^{-1}$, and $(T_{2P}P_M)^{-1}$ is controlled by $(\tau_M)^{-1}$. Finally, $(T_{2O})^{-1}$ becomes the largest term in this equation as shown by the bending at low temperatures.

After the substitution of eq 9, 20, and 24 for the terms in eq 27 a least-squares fit of the $(T_{2P}P_M)^{-1}$ data was obtained for both the OH and CH_3 protons. Initial guesses for ΔH^\ddagger , ΔS^\ddagger , C_M , C_O , E_M and E_O were obtained from a graphical fit. It is not difficult to obtain an excellent fit of both sets of data to this six-parameter equation. Therefore, some discretion must be used in evaluating the resulting parameters, and it is of value to fix certain of them and examine the effect on the others. Both the OH and CH_3 data were tested to the assumption $E_M = E_O$ and a fit of the CH_3 data to the kinetic parameters obtained from a fit of the OH data was undertaken. A summary of the various least-squares fits is given in Table III.

It is apparent from Figure 2 that τ_M^{-1} is important for the CH_3 data over a relatively narrow temperature

range, and that it is never well resolved from $(T_{2M})^{-1}$ and $(T_{20})^{-1}$. Therefore, little confidence is attached to the ΔH^\ddagger and ΔS^\ddagger values obtained from the six-parameter fit D of the CH_3 data. However, a comparison of fits B and F shows that the ΔH^\ddagger and ΔS^\ddagger obtained from fit B of the OH data are completely consistent with the data for the CH_3 protons. Except for the parameters from fit D, all of the fits show general agreement of the various parameters and it is concluded that ΔH^\ddagger and ΔS^\ddagger are $8.0 \pm 0.3 \text{ kcal mol}^{-1}$ and $1.3 \pm 1.5 \text{ cal mol}^{-1}\text{deg}^{-1}$, respectively. The curves in Figure 2 correspond to fits B and F.

A qualitative analysis of the downfield chemical shifts for the OH and CH_3 protons, shown in Figure 3, shows that in the high temperature region where $\tau_M^{-1} \gg (T_{2M})^{-1}$, $\Delta\omega_{\text{obsd}} = -P_M \Delta\omega_M$. Therefore, the temperature dependence of $\Delta\omega_{\text{obsd}}$ is described by eq 11. As the temperature is decreased the term, τ_M/T_{2M} , in eq 28, becomes significant with respect to one and the shifts drop off rapidly. These observed chemical shifts were fitted to eq 28 after making the necessary substitutions from eq 9, 11 and 20. Since the frequency shifts are small and therefore inaccurate, no attempt was made to determine ΔH^\ddagger and ΔS^\ddagger independently from the shift data. However, the chemical shift results are completely consistent with the ΔH^\ddagger and ΔS^\ddagger from fit B as can be seen by a comparison of the calculated curve and data points in Figure 3. Only C_ω was

TABLE III

Least-Squares best fit parameters for Mn(DMPPrPor)ClO₄ in methanol

Proton	Fit	ΔH^\ddagger , kcal mol ⁻¹	ΔS^\ddagger , cal mol ⁻¹ deg ⁻¹	C_M' , sec ⁻¹	E_M' , kcal mol ⁻¹	C_O' , sec ⁻¹	E_O' , kcal mol ⁻¹
OH	A	8.26	2.25	5200	1.99	603	1.81
	B	7.72	-0.14	4950	2.04 (a)	323	2.04 (a)
	C	7.94	0.81	5098	2.02	313	2.05 (b)
CH ₃	D	10.53 (c)	7.07 (c)	908	1.78	201	2.05
	E	8.15	2.04	578	2.04 (d)	196	2.04 (d)
	F	7.72 (d)	-0.46	586	2.04 (d)	191	2.04 (d)

(a) Constrained by setting $E_M = E_O$.

(b) Held constant at value given by fit D.

(c) These values are not considered significant for reasons given in the text.

(d) Held constant at value given by fit B.

allowed to vary in evaluating this curve. The best-fit values of C_ω at 60 MHz are: $C_\omega(\text{OH}) = 1.52 \pm 0.18 \times 10^7$ rad sec⁻¹ °K and $C_\omega(\text{CH}_3) = 8.04 \pm 0.33 \times 10^6$ rad sec⁻¹ °K. If μ_{eff} is taken as 5.03 BM, as determined by the magnetic susceptibility measurements, then from eq 10 $(A/\hbar)_{\text{OH}} = 3.92 \times 10^6$ rad sec⁻¹ and $(A/\hbar)_{\text{CH}_3} = 2.07 \times 10^6$ rad sec⁻¹.

Mn(DMPPrPor)⁺ in N,N-dimethylformamide

The line width and frequency shift data for Mn(DMPPrPor)⁺ in DMF were treated in a manner analogous to that employed for the Mn(DMPPrPor)⁺ in methanol data, discussed above. It should be noted by a comparison of Figures 2 and 4 that the only qualitative difference between the two systems is the absence of a $(T_{20})^{-1}$ line broadening region for Mn(DMPPrPor)⁺ in DMF and also an absence of significant chemical exchange controlled effects on the high field methyl resonance of DMF.

The results of various least-squares fits of the formyl proton $(T_{2P}P_M)^{-1}$ data to eq 27 are summarized as fits A-E in Table IV, and they represent a good illustration of the ambiguity which can arise if the outer sphere contribution to the observed line broadening cannot be extrapolated from an observed $(T_{20})^{-1}$ controlled region. Fits A through C show the extreme sensitivity of ΔH^\ddagger and ΔS^\ddagger to the various assumptions regarding $(T_{20})^{-1}$ for the CH proton. Fit C is certainly not reasonable since some outer

Least-squares best fit parameters for Mn(DMPPrPor)⁺ in N,N-dimethylformamide

Proton	Fit	ΔH^\ddagger , kcal mol ⁻¹	ΔS^\ddagger , cal mol ⁻¹ deg ⁻¹	C_M' , sec ⁻¹	E_M' , kcal mol ⁻¹	C_O' , sec ⁻¹	E_O' , kcal mol ⁻¹
CH	A	10.50	12.40	509	2.30	92.3	2.25
	B	10.01	10.23	516	2.30 (a)	74.8	2.30 (a)
	C	6.36	- 5.72	513	2.40	0 (b)	-
	D	7.96	1.30	502	2.37 (a)	33.6 (c)	2.37 (a)
	E	7.96 (d)	0.74	605	2.22 (a)	93.5 (d)	2.22 (a)
CH ₃	F	7.96 (e)	1.30 (e)	57.2	2.37 (e)	83.5	2.37 (e)
	G	7.96 (e)	1.30 (e)	66.9 (f)	2.37 (e)	66.9 (f)	2.37 (e)
	H	10.50 (g)	12.40 (g)	63.4 (f)	2.43 (a)	63.4 (f)	2.43 (a)
	I	10.50 (g)	12.40 (g)	72.1 (h)	2.53 (a)	36.1 (h)	2.53 (a)
	J	10.50 (g)	12.40 (g)	82.3 (f)	2.30 (g)	82.3 (f)	2.30 (g)

(a) Constrained by setting $E_M = E_O$.

(b) Fixed at zero to give no outer sphere contribution.

(c) Calculated value held constant.

(d) Held constant to determine if ΔH^\ddagger from fit D and C_O from fit A are consistent with the data. The resulting fit was not acceptable.

(e) Held constant at value given by fit D.

(f) Constrained by setting $C_M = C_O$ in an attempt to resolve the anomaly in fit F.

(g) Held constant at value given by fit A.

(h) Constrained by setting $C_M = 2C_O$. The resulting fit was not acceptable.

sphere contribution must exist, but this fit demonstrates the maximum effect on ΔH^\ddagger and ΔS^\ddagger . If it is assumed that both inner and outer sphere nuclear relaxation are due to dipolar interactions, then the inner and outer sphere interaction distances of 3.1\AA and 5.75\AA , respectively, for VO^{2+} ion in DMF⁴⁴ can be used in eq 23 and the first term of eq 13 to estimate the relative magnitude of the outer sphere contribution. From the $(T_{2M})^{-1}:(T_{2O})^{-1}$ ratio a value of 33.6 sec^{-1} was calculated for C_0 assuming that $E_M = E_O$ and that $C_M \approx 509\text{ sec}^{-1}$. This value was used in fit D. As expected, the ΔH^\ddagger and ΔS^\ddagger values fall between those for fits A and C. However, this calculation of C_0 is too approximate to allow it to be used with any great confidence.

In order to determine which of the fits of the formyl proton data is most reasonable, fits of the high field methyl proton $(T_{2P}^{\text{PM}})^{-1}$ data were undertaken. It is obvious, however, that the CH_3 proton measurements cannot yield an independent measure of the solvent exchange parameters. Fits F - J of Table IV represent the various attempts to obtain a good fit of the CH_3 proton data by means of kinetic parameters which would be consistent with any one of the fits A, B or D of the CH proton data. It was observed that the ΔH^\ddagger and ΔS^\ddagger values obtained from fit D of the CH proton data are not acceptable in view of the anomaly, $(C_0)_{\text{CH}_3} > (C_0)_{\text{CH}}$, introduced by fit F.

However, the values of $10.5 \text{ kcal mol}^{-1}$ and $12.4 \text{ cal mol}^{-1} \text{ deg}^{-1}$ obtained by fit A for ΔH^\ddagger and ΔS^\ddagger , respectively, were found to be consistent with the CH_3 proton data if it is assumed that for the latter $C_O \approx C_M$. It should be noted that the analysis of both the CH and CH_3 proton measurements yields essentially the same value for $E_M = E_O$ since the small differences indicated in Table IV are not judged to be significant.

The downfield chemical shifts for the CH and CH_3 protons are shown in Figure 5. These were fitted to eq 28 using the parameters from fits A and H for the CH and CH_3 proton data, respectively. Only C_ω was allowed to vary. The values obtained were: $(C_\omega)_{\text{CH}} = 3.16 \pm 0.10 \times 10^6 \text{ rad sec}^{-1} \text{ } ^\circ\text{K}$ and $(C_\omega)_{\text{CH}_3} = 2.02 \pm 0.08 \times 10^6 \text{ rad sec}^{-1} \text{ } ^\circ\text{K}$. If μ_{eff} is taken as 5.03 BM, then $(A/\hbar)_{\text{CH}} = 8.15 \times 10^5 \text{ rad sec}^{-1}$ and $(A/\hbar)_{\text{CH}_3} = 5.21 \times 10^5 \text{ rad sec}^{-1}$.

The values of the least-squares fit parameters defining $(T_{2M})^{-1}$ and $(T_{20})^{-1}$ for the OH and CH_3 protons of methanol and the CH and high field CH_3 protons of DMF can, in principle, be used to estimate either the interaction distances for the dipolar broadening or the correlation times controlling the relaxation process, if one or the other of these is known. In this regard, the values of r_i and d_O found for the $\text{VO}^{2+} - \text{DMF}^{44}$ and $\text{VO}^{2+} - \text{CH}_3\text{OH}^{45}$ systems should permit an estimation of the correlation times if the extent of the hyperfine interactions can be assessed. This,

of course, assumes that these interaction distances are applicable to the nonspherically symmetric solvated $\text{Mn}(\text{DMPPrPor})^+$ complex.

For $\text{Mn}(\text{DMPPrPor})^+$ in methanol and DMF, at the magnetic field used in this study, the expressions for the effective dipolar and electronic correlation times, given as eq 14 and 15, can be further simplified since $\omega_S^2 \tau_{D2}^2 \gg 1$ and $\omega_S^2 \tau_{e2}^2 \gg 1$, to a good approximation. Therefore, the $(T_{2M})^{-1}$ and $(T_{20})^{-1}$ expressions shown as eq 13 and 23 can be reduced to:

$$(T_{2M})^{-1} = \frac{11.5 \times 10^{16} S(S+1)}{\langle 1/r^6 \rangle^{-1}} \tau_{D1} + \frac{1}{3} \left(\frac{A}{\hbar} \right)^2 S(S+1) T_{1e} \quad (29)$$

$$(T_{20})^{-1} = \frac{2.9 \times 10^{14} S(S+1) \rho \tau_{D1}}{d_o^3} \cdot \frac{[S]}{n} \quad (30)$$

where all the symbols have been previously defined.

Attempts to rationalize the observed $(T_{2M})^{-1}$ and $(T_{20})^{-1}$ contributions in terms of reasonable values for the unknown quantities, τ_{D1} , T_{1e} , r_i and d_o in eq 29 and 30, were only partially successful.

For $\text{Mn}(\text{DMPPrPor})^+$ in methanol at 25°C, $(T_{2M})^{-1}$ for the OH and CH_3 protons is $1.55 \times 10^5 \text{ sec}^{-1}$ and $1.84 \times 10^4 \text{ sec}^{-1}$,

respectively. The ratio $(T_{2M(OH)})^{-1} : (T_{2M(CH_3)})^{-1} = 8.56$ obtained here, as compared to a value of ~ 5 for cobalt(II)²³ and nickel(II)⁴⁶ ions in methanol, where dipolar interactions are responsible for essentially all of the inner sphere broadening, suggests that there is a significant hyperfine contribution to $(T_{2M(OH)})^{-1}$ for $Mn(DMPPrPor)^+$ in methanol. Reasonable estimates of the dipolar correlation time (τ_{D1}), obtained from the observed outer sphere broadening contributions of $1.01 \times 10^4 \text{ sec}^{-1}$ and $5.99 \times 10^3 \text{ sec}^{-1}$ for the OH and CH_3 protons, respectively, also indicate that inner sphere hyperfine interactions are very important. For instance the $(T_{2O})^{-1}$ contributions at 25°C can be accounted for in terms of a correlation time of $3.0 \times 10^{-11} \text{ sec}$ and values of 4.0\AA and 4.76\AA for $d_O(OH)$ and $d_O(CH_3)$, respectively. The good agreement of these values with those obtained for VO^{2+} ion in methanol⁴⁵ is encouraging. However, using the above dipolar correlation time and the inner sphere interaction distances: $r_i(OH) = 2.95\text{\AA}$ and $r_i(CH_3) = 3.90\text{\AA}$,⁴⁵ one would predict relatively small dipolar contributions to $(T_{2M})^{-1}$ of $3.1 \times 10^4 \text{ sec}^{-1}$ and $5.9 \times 10^3 \text{ sec}^{-1}$ for the OH and CH_3 protons, respectively. In order for the hyperfine interaction to account for the remaining broadening, a value of $T_{1e} \approx 10^{-9} \text{ sec}$ is required, as was shown by a calculation employing the second term of eq 29 and the values of the hyperfine coupling constants obtained from the measured chemical shifts. However,

from the broad epr spectrum of $\text{Mn}(\text{DMPPrPor})^+$ in methanol a value of $\sim 10^{-10}$ sec was estimated for T_{2e} . Although it is expected that $T_{1e} > T_{2e}$, the large difference required here appears to be unusual. It should be noted, however, that the estimated T_{2e} , given above, may be too short due to the unresolved hyperfine coupling in the epr spectrum.

For the $\text{Mn}(\text{DMPPrPor})^+ - \text{DMF}$ system a value of 6.46 is obtained for the ratio, $(T_{2M}(\text{CH}))^{-1} : (T_{2M}(\text{CH}_3))^{-1}$, in agreement with Matwiyoff's result of ~ 6.5 for $\text{Co}(\text{DMF})_6^{2+}$ in DMF.⁴⁷ This implies that perhaps for $\text{Mn}(\text{DMPPrPor})^+$ in DMF the hyperfine contribution to $(T_{2M})^{-1}$ is not significant. A comparison of the hyperfine coupling constants for the OH proton of methanol and the CH proton of DMF, obtained from the chemical shift studies, shows that the ratio, $(A/\hbar)_{\text{OH}} : (A/\hbar)_{\text{CH}} \approx 5$, is also consistent with a much smaller hyperfine $(T_{2M})^{-1}$ term in the DMF system. As expected, calculations assuming only dipolar broadening were more successful. Using the $(T_{2O})^{-1}$ parameters from fit A of the CH proton data and a value of 5.75\AA for $(d_o)_{\text{CH}}$,⁴⁴ a value of 6.97×10^{-11} sec was calculated for τ_{D1} using eq 30. Then, on the basis of the corresponding $(T_{2M})^{-1}$ parameters which give $(T_{2M})^{-1} = 2.48 \times 10^4 \text{ sec}^{-1}$ at 25°C , a value of 3.53\AA was obtained for $(r_i)_{\text{CH}}$. This is to be compared with the value of 3.1\AA found for VO^{2+} in DMF.⁴⁴ For the high field CH_3 protons r_i is 4.8\AA , in agreement with the estimate of 4.7\AA given in ref 47 for

$\text{Co}(\text{DMF})_6^{2+}$ in DMF. Similarly, $d_{\text{O}(\text{CH}_3)}$ was calculated to be 5.9\AA but this number should be viewed with some suspicion since the assumption that $C_{\text{O}} = C_{\text{M}}$ was made in fitting the CH_3 proton data.

In the absence of a good estimate for T_{1e} it is difficult to determine the exact significance of the dipolar correlation time obtained in these calculations for $\text{Mn}(\text{DMP}r\text{Por})^+$ in DMF. The reasonable agreement of the $(T_{2M})^{-1}$ activation energy ($2.3 \text{ kcal mol}^{-1}$) with the value of $\sim 2.5 \text{ kcal mol}^{-1}$ expected for DMF viscosity suggests that $\tau_{\text{DL}} = 6.97 \times 10^{-11} \text{ sec}$ might be the rotational tumbling time for $\text{Mn}(\text{DMP}r\text{Por})^+$. However, since this value is a factor of ~ 1.6 smaller than $1.15 \times 10^{-10} \text{ sec}$, obtained in ref 44 for VO^{2+} ion in DMF, it is possible that both T_{1e} and τ_r are contributing to τ_{DL} . If this is the case, then an estimate of $1.15 \times 10^{-10} \text{ sec}$ for τ_r yields a value of $1.78 \times 10^{-10} \text{ sec}$ for T_{1e} .

The kinetic results of these two studies will be discussed and compared to those of other systems in Chapter IV.

2. Solvent Proton NMR Line Broadening Study of the Manganese(II) Schiff Base Complex, $\text{MnB}(\text{ClO}_4)_2$, in Methanol, N,N-dimethylformamide and Water.

As part of an investigation of the effects of Schiff base ligands on the lability of solvent molecules coordinated to a tetragonally distorted metal ion complex, the manganese(II) Schiff base complex, 2,13-dimethyl-3,6,9,12,18-pentaazabicyclo[12.3.1]octadeca-1(18),2,12,14,16-pentaene-manganese(II) perchlorate, referred to as $\text{MnB}(\text{ClO}_4)_2$, was studied. The inferred structure of this complex is shown in the introduction to this thesis.

X-ray studies⁴⁸ have established that the monomeric iron(III) complex of ligand B, $\text{FeB}(\text{NCS})_2\text{ClO}_4$, has a pentagonal-bipyramidal structure with the five donor nitrogen atoms and the iron atom being nearly coplanar. Although a similar study on any of the salts of the analogous manganese(II) complex has not been reported, conductimetric and pH measurements on MnBCl_2 ³⁰ have been found to be consistent with seven-coordinate manganese(II). It is assumed in the present investigation that MnB^{2+} also has this seven-coordinate geometry in the solvents N,N-dimethylformamide, water and methanol throughout the range of temperatures studied.

Previous work³¹ has shown that MnBCl_2 contains high-spin d^5 manganese. Magnetic susceptibility measurements, given in Table XXXII, on an aqueous solution of $\text{MnB}(\text{ClO}_4)_2$

further substantiate this result. Thus, the solvent exchange results obtained for MnB^{2+} can be compared with those for the normal high-spin octahedral manganese(II) ion in water^{15,50,51} methanol⁴⁹ and DMF¹ in order to determine the effect of the macrocyclic B ligand on the solvent exchange rates. It is also of interest to compare the results for MnB^{2+} with those of a related study⁵⁰ in which the effect of the o-phenanthroline ligand on the $^{17}\text{OH}_2$ exchange rates of $\text{Mn}(\text{phen})(\text{H}_2\text{O})_4^{2+}$ and $\text{Mn}(\text{phen})_2(\text{H}_2\text{O})_2^{2+}$ was examined. This latter study was confined to the aqueous systems for which only a small rate enhancement was observed.

In this investigation, line width measurements were made at 60 and 100 MHz since a consideration of some of the earlier studies^{22,51} on manganese(II) ion has shown that an interpretation of the results obtained at a single frequency is very often equivocal.

$\text{MnB}(\text{ClO}_4)_2$ in N,N-dimethylformamide

The temperature dependencies of $-\log(T_{2P}P_M)$ at 60 and 100 MHz for the formyl proton of DMF solutions of $\text{MnB}(\text{ClO}_4)_2$ are shown in Figure 6. Measurements of $(T_{2P}P_M)^{-1}$ were also made at 60 MHz on the broader, high field methyl proton resonance and these are also shown in Figure 6. Significant overlap of the two CH_3 resonances was avoided by using dilute solutions. Small downfield chemical shifts of the formyl proton signal were observed in this study. These

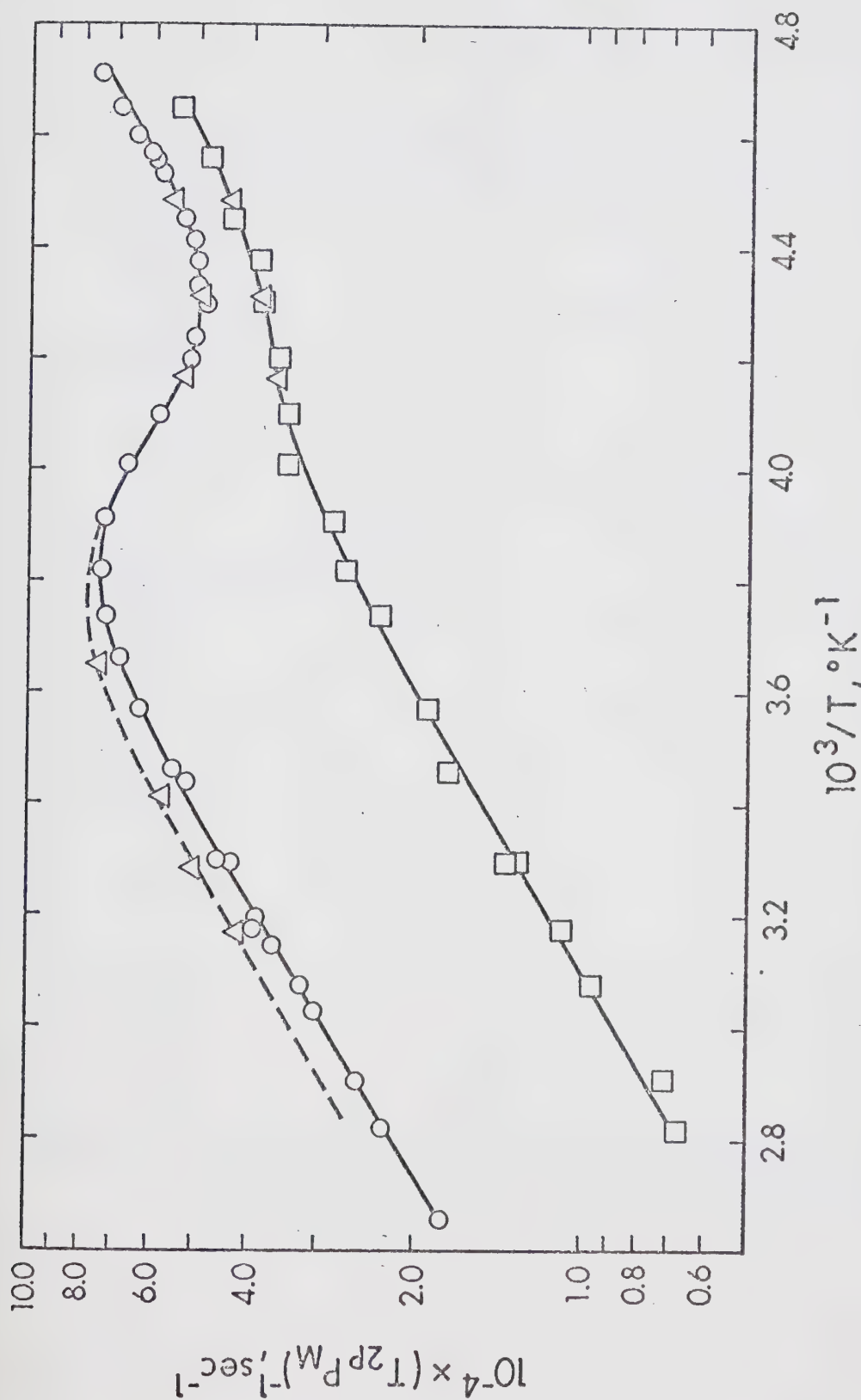


Figure 6: Temperature dependence of $-\log(T_{2P_M})$ for the formyl proton (upper two curves; \circ - 60 MHz, Δ - 100 MHz) and high field methyl protons (lower curve; \circ - 60 MHz, Δ - 100 MHz) of N,N-dimethylformamide solutions of $MnB(ClO_4)_2$.

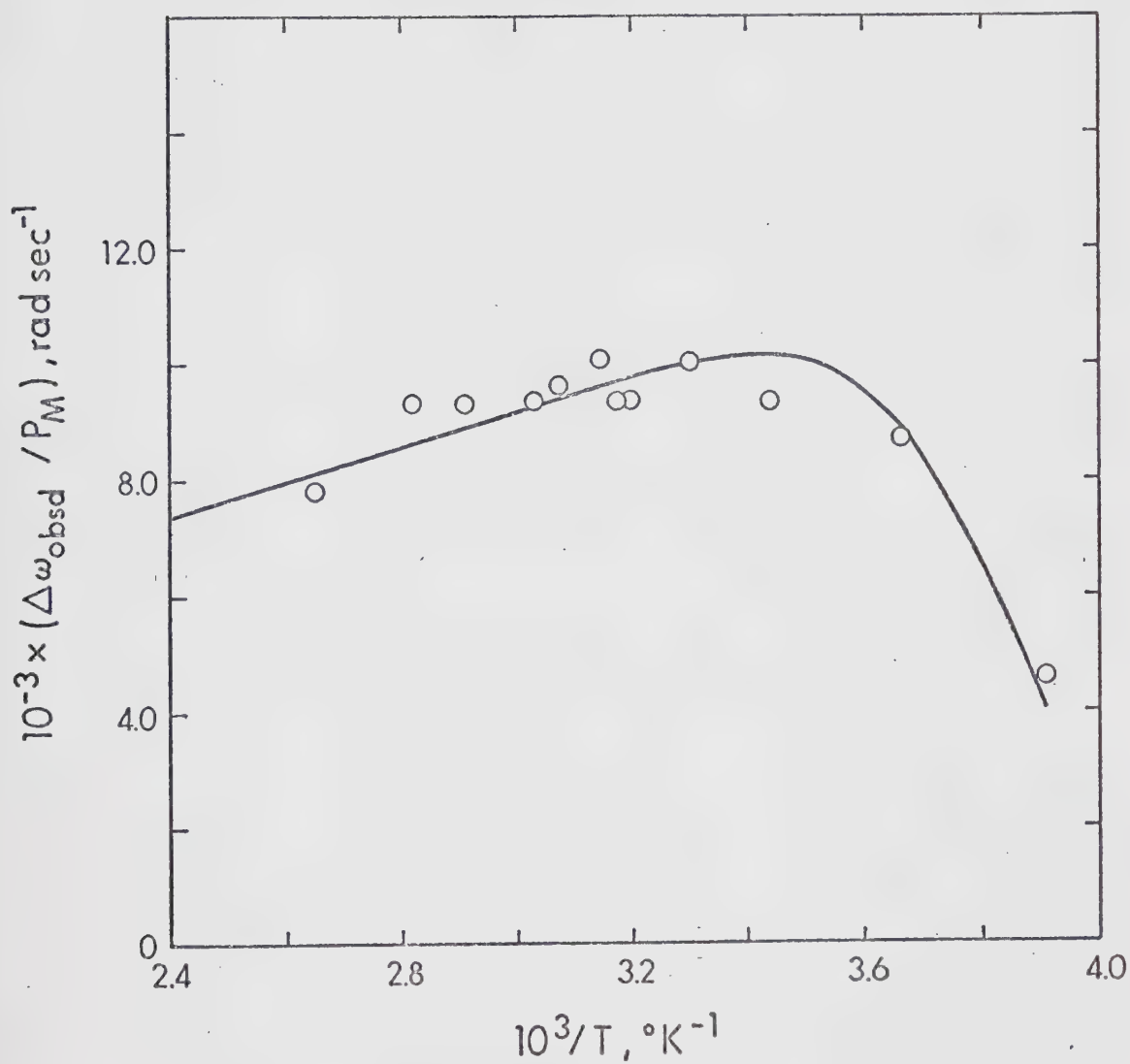


Figure 7: Temperature dependence of $(\Delta\omega_{\text{obsd}}/P_M)$ for the formyl proton of N,N-dimethylformamide solutions of $\text{MnB}(\text{ClO}_4)_2$ at 60 MHz.

TABLE V

Least-squares best fit parameters for $\text{MnB}(\text{ClO}_4)_2$ in N,N -dimethylformamide (a)

Proton	Fit	ΔH^\ddagger , kcal mol ⁻¹	ΔS^\ddagger cal mol ⁻¹ deg ⁻¹	C_M' sec ⁻¹	E_M' kcal mol ⁻¹	C_O sec ⁻¹	E_O' kcal mol ⁻¹
CH	A	13.1	16.3	359.8	2.74 (b)	109.4	2.74 (b)
	B	11.6	10.8	453.1	2.66	26.3	3.35
	C	13.3	17.1	383.0	2.70	107.0	2.75 (c)
	D	11.5 (d)	9.9	319.0	2.83	104.8	2.75 (c)
CH_3 (e)	E	13.1	16.3	53.7	2.74	85.4	2.74
	F	11.6	10.8	94.0	2.66	20.2	3.35
	G	11.5	9.9	55.8	2.74	83.8	2.74

(a) Only the 60 MHz $(T_{2P_M})^{-1}$ data was subjected to a curve-fitting process.

(b) Constrained by setting $E_M = E_O$.

(c) Held constant at the value expected for the activation energy of DMF viscosity.

(d) Held constant to determine the acceptability of a lower ΔH^\ddagger .

(e) In each of the fits E - G of the high field CH_3 proton data, all parameters except C_M and C_O were held constant at values obtained from either one of the fits A, B or D of the CH proton data.

chemical shifts were of value in estimating $(A/\hbar)_{\text{CH}}$, and therefore, a plot of $(\Delta\omega_{\text{obsd}}/P_M)$ against T^{-1} is given in Figure 7.

Qualitatively, the variation of $(T_{2P}P_M)^{-1}$ with temperature for $\text{MnB}(\text{ClO}_4)_2$ in DMF is analogous to that previously observed for $\text{Mn}(\text{DMP}r\text{Por})^+$ in methanol. That is, as the temperature is progressively lowered, $(T_{2P}P_M)^{-1}$ is controlled successively by $(T_{2M})^{-1}$, $(\tau_M)^{-1}$ and $(T_{2O})^{-1}$ according to eq 27. It is apparent, from Figure 6, however, that in contrast to the $(T_{2P}P_M)^{-1}$ results for $\text{Mn}(\text{DMP}r\text{Por})^+$, a small magnetic field dependence exists in only the $(T_{2M})^{-1}$ controlled line broadening region for $\text{MnB}(\text{ClO}_4)_2$ in DMF. The differences ($\sim 14\%$) in the 100 MHz and 60 MHz linewidths for the same solutions were reproducible and greater than the experimental error of the measurements. This field dependence of $(T_{2M})^{-1}$ has been attributed^{22,51} to a hyperfine contribution to $(T_{2M})^{-1}$ for which the correlation time is a magnetic field dependent electron spin relaxation time (see eq 29). The 100 MHz measurements shown in Figure 6 are included only to demonstrate, qualitatively, that the hyperfine contribution to the total $(T_{2M})^{-1}$ must be relatively small for the CH proton of DMF, a fact which is not true for the OH proton of methanol and water in the $\text{MnB}(\text{ClO}_4)_2$ -methanol and $\text{MnB}(\text{ClO}_4)_2$ -water systems, discussed in the following sections. Presumably, the DMF methyl proton data should be magnetic field dependent also, but

since it is expected that $(A/\hbar)_{\text{CH}_3} < (A/\hbar)_{\text{CH}}$, the field dependence would not be experimentally detectable.

A preliminary graphical analysis of the $(T_{2P}^{\text{PM}})^{-1}$ data for the CH proton, according to eq 27, indicated that the activation energies, E_M and E_O , were very nearly equal, as would be required if $(T_{2M})^{-1}$ is primarily controlled by the dipolar mechanism which accounts for the outer sphere broadening. As a result of this observation, the CH proton line broadening data were initially fitted to eq 27 with $E_M = E_O$. The resulting least-squares parameters are summarized as fit A in Table V. The value of $13.1 \text{ kcal mol}^{-1}$ obtained in this fit for ΔH^\ddagger is considered to be unusually large for a manganese(II) complex. In view of the absence of crystal field contributions to ΔH^\ddagger in a d^5 system, ΔH^\ddagger values in the range 8 to 10 kcal mol^{-1} are usually observed for solvent exchange on manganese(II). As a result of this anomaly, an alternative six-parameter fit (fit B) was attempted in which no restraints were placed on E_O . A comparison of the kinetic parameters from fits A and B indicates that ΔH^\ddagger and ΔS^\ddagger are extremely sensitive to the outer sphere activation energy, which can be anywhere in the range 2.74 to $3.35 \text{ kcal mol}^{-1}$ for this data, without affecting the quality of the resultant fit. This is quite understandable since the data shows that $\tau_M^{-1} < (T_{2M})^{-1}$ only over a narrow temperature range in which $(T_{2O})^{-1}$ contributes significantly. Fit B also shows that

the data are consistent with lower values of ΔH^\ddagger and ΔS^\ddagger than indicated by fit A, but the value of $E_O = 3.35 \text{ kcal mol}^{-1}$ appears to be slightly large, since the $(T_{20})^{-1}$ contribution at 25°C from fit A ($E_O = 2.75 \text{ kcal mol}^{-1}$) is much more consistent with an outer sphere interaction distance and a rotational correlation time obtained for the VO^{2+} -DMF system.⁴⁴ Also, a value of $2.75 \text{ kcal mol}^{-1}$ for E_O is in better agreement with the activation energy for viscosity of DMF. Therefore, there is no apparent justification for the higher value of E_O obtained in fit B and a value of $2.75 \text{ kcal mol}^{-1}$ was used in subsequent fits. The problem of the unusually large ΔH^\ddagger and ΔS^\ddagger encountered here also appears to be one of resolving ΔH^\ddagger from ΔS^\ddagger , since several additional fits of the CH proton $(T_{2P}^P)^{-1}$ data, in which E_O was held constant at $2.75 \text{ kcal mol}^{-1}$, have shown that the data can be fitted equally well with ΔH^\ddagger and ΔS^\ddagger being as low as $11.5 \text{ kcal mol}^{-1}$ and $9.9 \text{ cal mol}^{-1}\text{deg}^{-1}$, respectively (see fit D). The use of a ΔH^\ddagger less than $11.5 \text{ kcal mol}^{-1}$ would require the unacceptable result that E_M be greater than $E_O = 2.75 \text{ kcal mol}^{-1}$. Values of $E_M < E_O$ are foreseeable in the event of significant hyperfine contributions to $(T_{2M})^{-1}$, but for dipolar control of $(T_{2M})^{-1}$ and $(T_{20})^{-1}$, an $E_M > E_O$ is not justifiable. For all of the fits discussed above, the rate constant for DMF exchange at 25°C varies from 3.3×10^6 to $6.0 \times 10^6 \text{ sec}^{-1}$.

Unfortunately, the CH_3 proton $(T_{2P}^{P_M})^{-1}$ data, which shows negligible exchange effects, and the formyl proton chemical shifts, which are very small, are of little help in deciding on the most self-consistent set of parameters. It is therefore concluded that for this system ΔH^\ddagger and ΔS^\ddagger cannot be too accurately determined. All of the fits in Table V are consistent with a $\Delta H^\ddagger = 12.4 \pm 0.9 \text{ kcal mol}^{-1}$ and a $\Delta S^\ddagger = 13.5 \pm 3.6 \text{ cal mol}^{-1}\text{deg}^{-1}$.

The calculated curve shown in Figure 6 is based on the parameters from fit D, but as discussed above, all calculated curves from either of the fits A-D are within the experimental error of the data points. In the case of the methyl $(T_{2P}^{P_M})^{-1}$ data the curve shown in the figure has been calculated from fit G in which the parameters ΔH^\ddagger , ΔS^\ddagger , $E_M = E_O$ were held constant at the values given by fit D. However, from the quality of this fit it can only be concluded that the values of the fixed parameters used are at least not inconsistent with the CH_3 proton data.

From the observed downfield CH proton chemical shifts shown in Figure 7, a value of $3.1 \times 10^6 \text{ rad sec}^{-1}\text{°K}$ was estimated for C_ω at 60 MHz. This gives a hyperfine coupling constant of $5.5 \times 10^5 \text{ rad sec}^{-1}$ if $\mu_{\text{eff}} = 5.9 \text{ BM}$ in eq 10, but it should be noted that this (A/\hbar) is only of limited accuracy since the observed shifts were very small. The curve shown was calculated using the above value of C_ω and the parameters from fit D.

The values of $(T_{2M})_{CH}^{-1}$ and $(T_{2O})_{CH}^{-1}$ at 25°, defined by the parameters in fit D of Table V, can be interpreted in terms of hyperfine and dipolar contributions to $(T_{2M})^{-1}$ and only dipolar contributions to $(T_{2O})^{-1}$. If d_o is assumed to be 5.75 Å,⁴⁴ then a dipolar correlation time of 1.27×10^{-10} sec accounts for the outer sphere formyl proton broadening contribution of $1.10 \times 10^4 \text{ sec}^{-1}$. This correlation time can be interpreted as the rotational tumbling time (τ_r) of $\text{MnB}(\text{DMF})_2(\text{ClO}_4)_2$ since it is in reasonable agreement with the τ_r value of 1.15×10^{-10} sec found for the vanadyl ion in DMF.⁵³ In the case of the inner sphere $(T_{2M})^{-1}$ broadening, the hyperfine term was estimated to be $8.8 \times 10^3 \text{ sec}^{-1}$ from the measured value of $(A/h)_{CH} = 5.5 \times 10^5 \text{ rad sec}^{-1}$ and assuming that $T_{1e} = 1.0 \times 10^{-8}$ sec, the value found for MnB^{2+} in methanol (see subsequent section). The inner sphere dipolar contribution is therefore estimated to be $3.15 \times 10^4 \text{ sec}^{-1}$, consistent with $(r_i)_{CH} = 4.0 \text{ Å}$ and $\tau_c = 1.27 \times 10^{-10}$ sec. For the high field CH_3 protons, (r_i) and (d_o) were found to be 5.3 Å and 6.3 Å, respectively, if all of the observed broadening is assumed to be due to dipolar interactions.

$\text{MnB}(\text{ClO}_4)_2$ in Water

The $(T_{2P_M})^{-1}$ data at 60 and 100 MHz for aqueous solutions of $\text{MnB}(\text{ClO}_4)_2$ are shown in Figure 8. Small downfield chemical shifts were observed for the water proton resonance

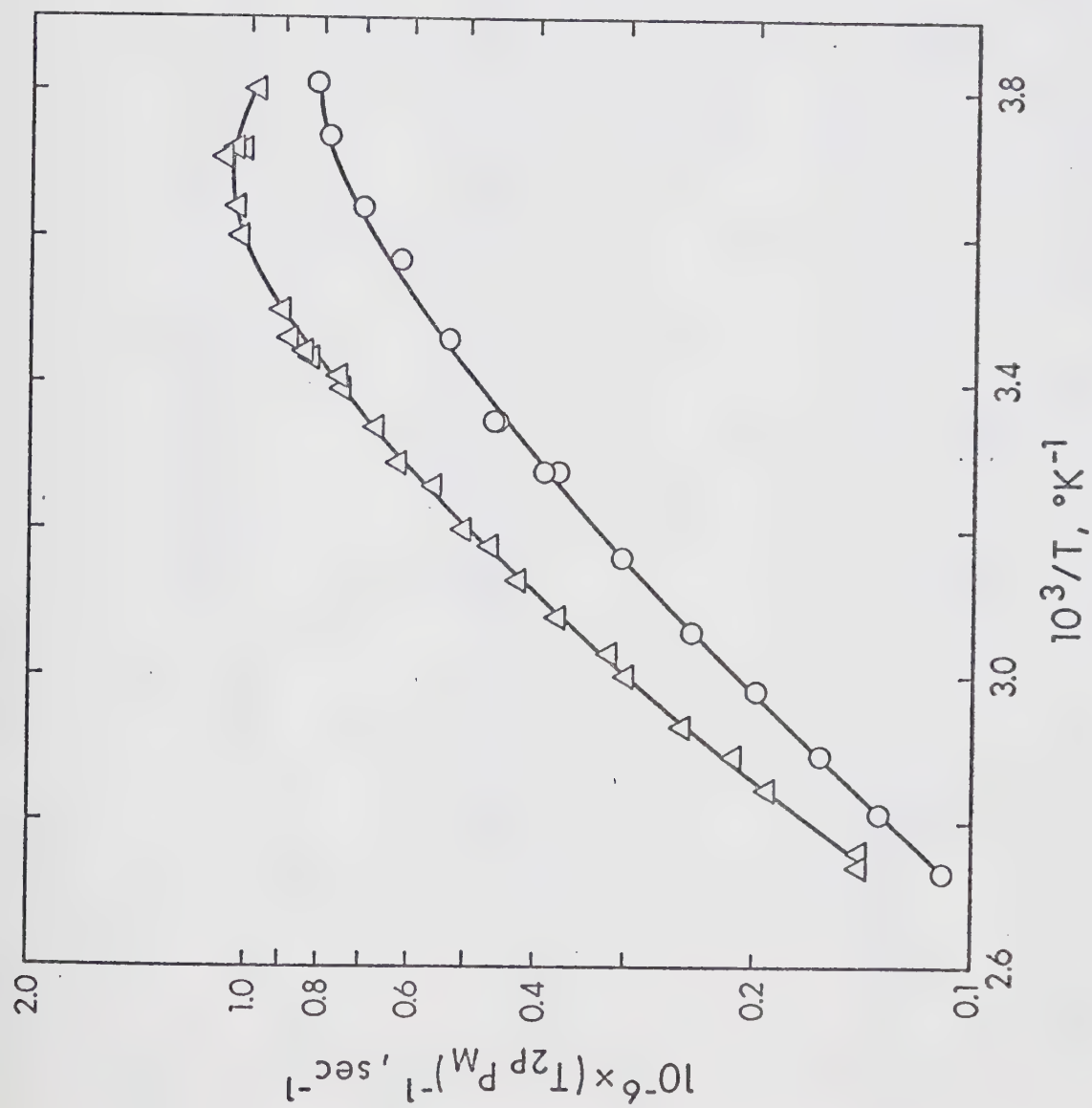


Figure 8: Temperature dependence of $-\log(T_{2P_M})$ at 60 MHz (o) and 100 MHz (Δ) for the water proton in aqueous solutions of $\text{MnB}(\text{ClO}_4)_2$.

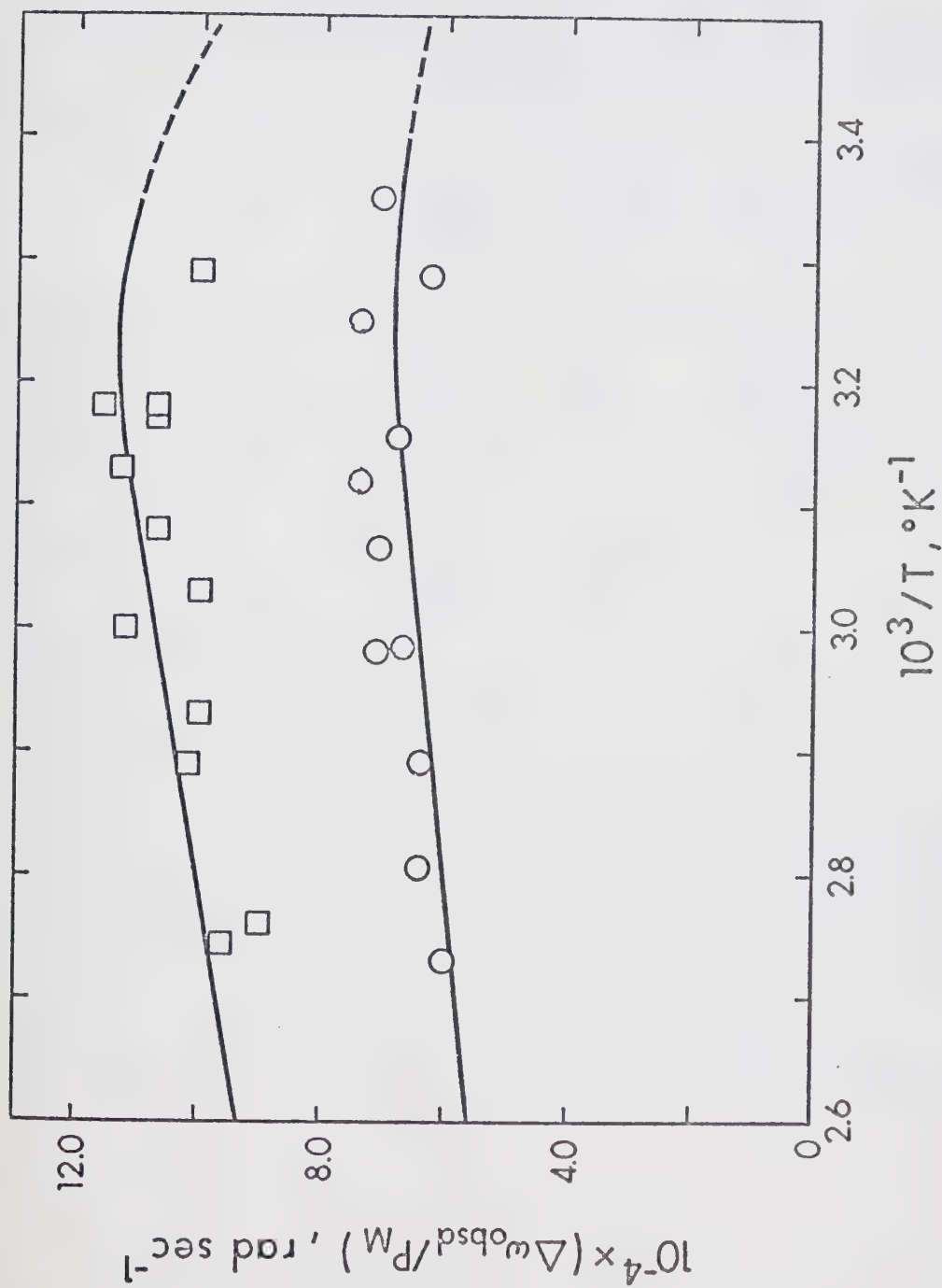


Figure 9: Temperature dependence of $(\Delta\omega_{\text{obsd}}/P_M)$ at 60 MHz (o) and 100 MHz (\square) for the water proton in aqueous solutions of $\text{MnB}(\text{ClO}_4)_2$.

TABLE VI

Least-squares best fit parameters of the $(T_{2P-M})^{-1}$
data for $MnB(ClO_4)_2$ in water.

	Temperature dependence used for T_{le}				
	eq 33-a		eq 18		
	100 MHz	60 MHz	100 MHz	60 MHz	
	A	B	C	D	E
ΔH^\ddagger , kcal mol ⁻¹	8.47	7.66	8.89	8.66	8.69
ΔS^\ddagger , cal mol ⁻¹ deg ⁻¹	2.57	0.01	4.09	3.88	4.16
E_C , kcal mol ⁻¹	—	—	3.90 ^(b)	3.90 ^(b)	3.90 ^(b)
E_a , kcal mol ⁻¹	3.64	3.64 ^(a)	—	—	—
$10^{11} \times T_{le}^o$, sec	3.88	2.01	—	—	—
$10^{14} \times \tau_C^o$, sec	—	—	1.08	1.32	1.08 ^(c)
$10^{-19} \times C_e$, sec ⁻²	—	—	3.89	3.41	2.89

(a) Held constant at the value indicated by 100 MHz fit A. When ΔH^\ddagger , ΔS^\ddagger , E_a and T_{le}^o were all unrestrained, the values obtained were 7.73 kcal mol⁻¹, 0.01 cal mol⁻¹ deg⁻¹, 3.0 kcal mol⁻¹ and 6.07×10^{-11} sec, respectively.

(b) Held constant at the value given in ref 22.

(c) Held constant at the value indicated by 100 MHz fit C.

and these are given in Figure 9. Only the chemical shifts in the fast exchange limit were large enough to be reproducible and therefore only these are shown in the figure.

A comparison of the temperature dependence of $(T_{2P}P_M)^{-1}$ observed here with that for $MnB(ClO_4)_2$ in DMF, discussed previously, reveals several interesting differences, the most obvious of which is the high activation energy characteristic of a chemical exchange process at high temperatures. Furthermore, the data at the lowest temperatures is only beginning to bend over into a τ_M^{-1} controlled region. As in the case of $MnB(ClO_4)_2$ in DMF, a magnetic field dependent $(T_{2P}P_M)^{-1}$ is observed but the effect is much greater here.

The manner in which the 60 and 100 MHz $(T_{2P}P_M)^{-1}$ data converge at high temperatures appears to suggest that for this system the frequency dependence results because of limiting condition 25(b) for which $(T_{2P}P_M)^{-1} = \tau_M \Delta\omega_M^2$. However, a preliminary fit of the data to the complete $(T_{2P})^{-1}$ equation, shown as eq 2, indicated that, although a satisfactory fit of the data could be obtained, the required coupling constant would have to be at least an order of magnitude greater than the value calculated from the observed chemical shifts. Therefore, it was concluded that a $\Delta\omega_M$ relaxation process will not account for the observed results. Instead, $(T_{2P}P_M)^{-1}$ is controlled by a T_{2M} mechanism with limiting conditions 26(a) and 26(b)

(Case B) applying in the high and low temperature regions, respectively. However, this system is somewhat different from the previously discussed Case B systems (MnB^{2+} in DMF and $\text{Mn}(\text{DMPPrPor})^+$ in DMF and methanol) in that the controlling correlation time for the hyperfine contribution to $(T_{2M})^{-1}$ is the solvent exchange rate. This type of behaviour has been observed previously for manganese(II) ion in water^{15,22} and ammonia⁵² and for mono and bis phenanthroline complexes in water.⁵⁰ Except for the study reported in ref 22, the field dependence of $(T_{2M})^{-1}$ observed here, had not been investigated in the above systems.

Since it will be shown that the neglect of the dipolar contribution is not completely justified for this system, eq 13, which represents the sum of the dipolar $((T_{2M})_{\text{DD}}^{-1})$ and hyperfine $((T_{2M})_{\text{HF}}^{-1})$ contributions to $(T_{2M})^{-1}$, permits eq 27 to be expressed as

$$(T_{2P}^{\text{PM}})^{-1} = \tau_M^{-1} \left\{ \frac{(T_{2M})_{\text{DD}}^{-1} + C_{\text{HF}} (\tau_M^{-1} + T_{1e}^{-1})^{-1}}{\tau_M^{-1} + (T_{2M})_{\text{DD}}^{-1} + C_{\text{HF}} (\tau_M^{-1} + T_{1e}^{-1})^{-1}} \right\} + (T_{20})^{-1} \quad (31)$$

where C_{HF} represents the constant $(A/\hbar)^2 S(S+1)/3$. The effective correlation time for the hyperfine interaction, $(\tau_M^{-1} + T_{1e}^{-1})^{-1}$, is obtained from eq 15 and the definition of τ_{e1} given by eq 16, if it is assumed that $\omega_s^2 \tau_{e2}^2 \gg 1$. This assumption is a very reasonable one for a manganese(II)

system at the operating frequencies dealt with here.

If it is assumed, for the sake of simplicity, that T_{2M} is determined solely by hyperfine interactions, then, neglecting the $(T_{20})^{-1}$ term, eq 31 reduces to the form

$$(T_{2P}P_M)^{-1} = \frac{1}{\tau_M + C_{HF}^{-1}(\tau_M^{-1} + T_{1e}^{-1})} \quad (32)$$

in terms of which the temperature dependence of $(T_{2P}P_M)^{-1}$, shown in Figure 8, can be qualitatively most readily understood. Thus, at low temperatures when exchange is slow, $T_{1e}^{-1} > \tau_M^{-1}$, and the rate of electron spin relaxation modulates the hyperfine interactions whereas at high temperatures, $\tau_M^{-1} > T_{1e}^{-1}$, and the rate of chemical exchange is the dominant correlation time for $(T_{2M})^{-1}$. A consideration of Figure 8 clearly shows that most of the data falls in the region between the above limiting conditions, for which both τ_M^{-1} and T_{1e}^{-1} contribute significantly. Therefore, at the highest temperature the frequency dependence of T_{1e} does not completely vanish. It should also be observed that, since there is only a slight bend in the data at low temperature, τ_M never becomes very significant relative to the second term in the denominator of eq 32.

Before the data of Figure 8 can be subjected to a curve-fitting process, it is necessary to estimate the relative importance of the frequency independent dipolar contribution to the total $(T_{2M})^{-1}$ and also the approximate

magnitude of $(T_{20})^{-1}$. Assuming the reasonable estimates of 2.90 Å, 4.65 Å, 4.2×10^{-11} sec for r_i , d_o and τ_r ,⁵³ respectively, then from eq 13 and 23 the inner and outer sphere dipolar contributions to $(T_{2P}^{PM})^{-1}$ at 25° are $0.711 \times 10^5 \text{ sec}^{-1}$ and $0.294 \times 10^5 \text{ sec}^{-1}$, respectively. Since the observed values of $(T_{2P}^{PM})^{-1}$ at this temperature are $4.45 \times 10^5 \text{ sec}^{-1}$ and $7.00 \times 10^5 \text{ sec}^{-1}$ at 60 and 100 MHz, respectively, the inner sphere dipolar contribution to $(T_{2M})^{-1}$, given above, contributes 16% at 60 MHz and 10% at 100 MHz to $(T_{2P}^{PM})^{-1}$. Although the $(T_{20})^{-1}$ contribution is very much smaller, it was included for the sake of completeness. The temperature dependence of the dipolar $(T_{2M})^{-1}$ and $(T_{20})^{-1}$ terms was assumed to be given by eq 20 and 24, respectively. A value of $3.9 \text{ kcal mol}^{-1}$, corresponding to the activation energy for the viscosity of water, was assumed for $E_M = E_O$ and the constants C_M and C_O were calculated from the above dipolar estimates of $(T_{2M})^{-1}$ and $(T_{20})^{-1}$.

It is also necessary to obtain an independent measurement of either the hyperfine coupling constant (A/\hbar) , or T_{le} and its temperature dependence, before the data can be meaningfully fitted to eq 31. In the present case, a fairly good estimate of A/\hbar could be obtained from the observed chemical shifts. Although the chemical shifts, shown in Figure 9, were small, both the 60 and 100 MHz measurements are consistent with a value $\sim 3.9 \times 10^6 \text{ rad}$

sec^{-1} for A/\hbar , calculated from the estimated values of C_ω and $\mu_{\text{eff}} = 5.9$ BM by means of eq 10. The Curie temperature dependence of the observed high temperature shifts is shown in Figure 9. The above value of A/\hbar was used to calculate C_{HF} which was held constant in all nonlinear least-squares fits of the $(T_{2P}P_M)^{-1}$ data to eq 31.

Finally, in regards to the temperature dependence of T_{1e} in eq 31, two approaches were used and compared as to their suitability in fitting the $(T_{2P}P_M)^{-1}$ data. In the one instance, the temperature dependence of T_{1e} was assumed to be given simply by

$$T_{1e} = T_{1e}^0 \exp(E_a/RT) \quad (33-a)$$

where T_{1e}^0 and E_a are constants. It should be noted from eq 18 that, since a frequency dependent T_{1e} is observed for this manganese(II) complex, $(\omega_s \tau_c)^2 \geq 1$. Equation 33(a) will therefore be applicable only in the event that $(\omega_s \tau_c)^2 > 1$. Alternatively, the complete expression for T_{1e} , given as eq 18, was used in eq 31. The temperature dependence of τ_c in eq 18 was taken to be

$$\tau_c = \tau_c^0 \exp(E_c/RT) \quad (33-b)$$

where E_c was held constant at a value of $3.9 \text{ kcal mol}^{-1}$, given in ref 22.

Computed nonlinear least-squares fits of the 60 and 100 MHz data to eq 31 were obtained using ΔH^\ddagger , ΔS^\ddagger , T_{1e}^0 and E_a as adjustable parameters in the first of the above approaches and ΔH^\ddagger , ΔS^\ddagger , τ_c^0 and C_e as the variable parameters in the second. A summary of the least-squares parameters is given in Table VI.

A comparison of the parameters from fits A and B with those from fits C and D indicates that excellent agreement is obtained for the ΔH^\ddagger and ΔS^\ddagger values from the 60 and 100 MHz data sets for the condition that T_{1e} is defined by the complete expression given by eq 18. The significantly poorer agreement in both ΔH^\ddagger and ΔS^\ddagger from fits A and B is attributed to the nonexponential temperature dependence of T_{1e} at high temperature where fits C and D indicate that $(\omega_s \tau_c)^2 \approx 1$. This problem is more serious at 60 MHz than at 100 MHz, and thus, the ΔH^\ddagger and ΔS^\ddagger values for the 60 MHz data are affected to a greater extent. At lower temperatures $(\omega_s \tau_c)^2 > 1$, and therefore, the activation energy of T_{1e} approaches that of τ_c , namely $3.9 \text{ kcal mol}^{-1}$. For most temperatures, the condition $(\omega_s \tau_c)^2 > 1$ is valid, and this accounts for the large apparent values of E_a indicated by fits A and B.

It should be noted that although the values of the constants, τ_c^0 and C_e , determined at 60 MHz (Fit D) do not agree perfectly with the values found at 100 MHz (Fit C), the agreement is as good as can be expected in view of the limited temperature range, the number of parameters neces-

sary to define the system, and the approximations made regarding the dipolar $(T_{2M})^{-1}$ and $(T_{2O})^{-1}$ contributions. However, since it is felt that the 100 MHz data defines each of the parameters more accurately, the value of τ_c^O indicated by 100 MHz fit C was held constant in the 60 MHz data. The resulting best-fit parameters for ΔH^\ddagger , ΔS^\ddagger and C_e are shown as fit E. Although the kinetic parameters are now in even better agreement with those from fit C, the difference in the C_e values is not resolved by this fit.

From the good agreement in the ΔH^\ddagger and ΔS^\ddagger values obtained in fits C and E, it is concluded that for MnB^{2+} in water, the solvent exchange parameters are: $\Delta H^\ddagger = 8.8 \pm 0.5$ kcal mol⁻¹ and $\Delta S^\ddagger = 4.5 \pm 1.0$ cal mol⁻¹deg⁻¹. The estimated uncertainties given above might seem to be larger than the variations indicated by the 60 and 100 MHz fits, but in view of the 14% disagreement between the C_e values at the two frequencies, the quoted errors appear to be reasonable. The curves of Figure 8 were calculated from the parameters given in fits C and E.

MnB(ClO₄)₂ in Methanol

The temperature dependencies of $(T_{2P_M})^{-1}$ at 60 and 100 MHz for the hydroxy and methyl protons of methanol solutions of $MnB(ClO_4)_2$ are shown in Figure 10. Small downfield chemical shifts of 0 to 6.5 Hz were observed for the OH proton and these are given in Figure 11. For the CH₃

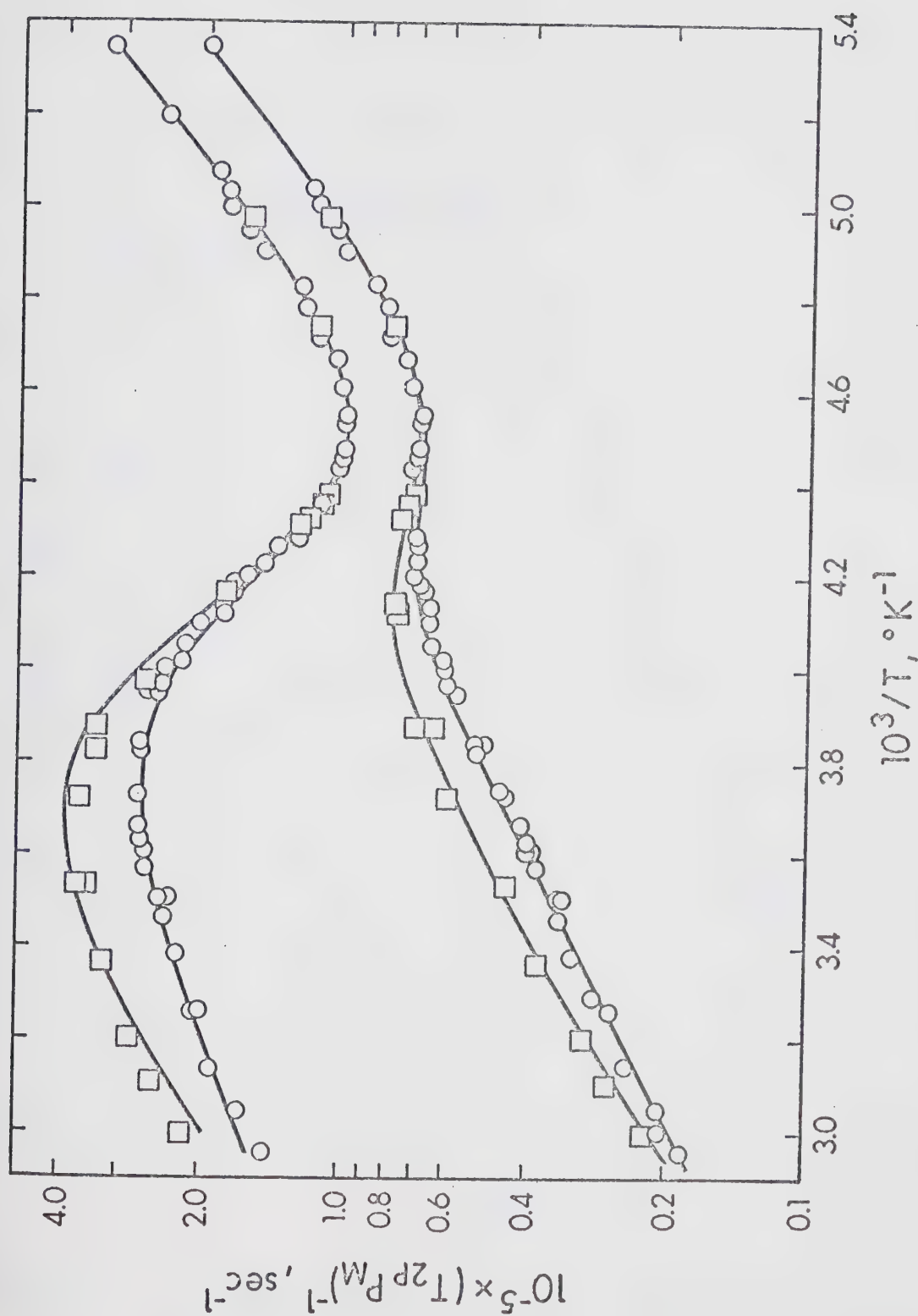


Figure 10: Temperature dependence of $-\log(T_{2P_M})$ at 60 MHz (o) and 100 MHz (\square) for the hydroxy proton (upper two curves) and methyl protons (lower two curves) of methanol solutions of $\text{MnB}(\text{ClO}_4)_2$.

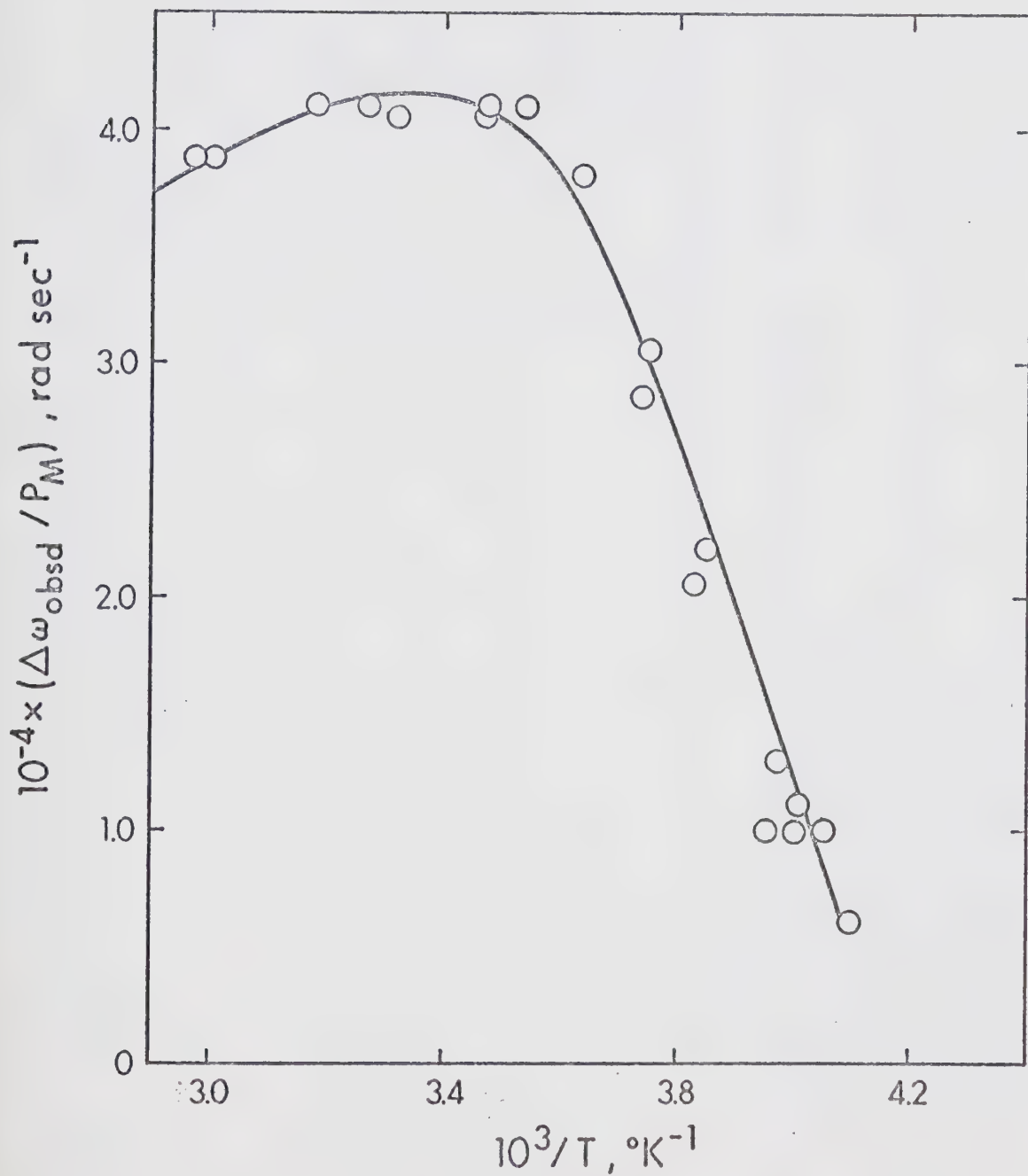


Figure 11: Temperature dependence of $(\Delta\omega_{\text{obsd}}/P_M)$ at 60 MHz for the hydroxy proton of methanol solutions of $\text{MnB}(\text{ClO}_4)_2$.

TABLE VII

Least-squares best fit parameters of the $(T_{2P_M})^{-1}$ data for $MnB(ClO_4)_2$ in methanol

	Model 1 (a)					Model 2 (b)				
	OH		CH ₃			OH		CH ₃		
	60 MHz	100 MHz	60 MHz	100 MHz	100 MHz	60 and 100 MHz	60 and 100 MHz	60 and 100 MHz	60 and 100 MHz	
ΔH^\ddagger , kcal mol ⁻¹	A	B	C	D	E	F	G			
ΔS^\ddagger , kcal mol ⁻¹ deg ⁻¹	9.92	9.30	9.92 (c)	9.92 (c)	9.92 (c)	8.87		8.87 (g)		
$10^{-3} \times C_M$, sec ⁻¹	7.35	4.53	7.11	7.80	7.35	2.82		2.18		
E_M , kcal mol ⁻¹	8.58	12.82	12.57	0.887	1.14	0.485 (e)		0.0902 (e)		
C_O , sec ⁻¹	1.90	1.90 (c)	1.90 (c)	1.96	1.96 (d)	3.00 (f)		3.00 (f)		
E_O , kcal mol ⁻¹	18.9	18.9 (c)	18.9 (c)	12.1	12.1 (d)	14.75		19.82		
$10^{14} \times \tau_C$, sec	3.62	3.62 (c)	3.62 (c)	3.62 (c)	3.62 (c)	3.71		3.43		
$10^{-19} \times C_e$, sec ⁻²						1.57		1.57 (g)		
$10^{-6} \times (A/\hbar)$, rad sec ⁻¹						1.74		1.74 (g)		
						2.30 (h)		0.56		

(a) The $(T_{2P_M})^{-1}$ results were fitted to eq 27, assuming that the temperature dependence of the total $(T_{2M})^{-1}$ is given by eq 20.

(b) The $(T_{2P_M})^{-1}$ results were fitted to eq 31 with T_{1e} being defined by eq 18. The 60 and 100 MHz data for each of the two different protons were fitted simultaneously.

(c) Held constant at the value obtained from fit A.

(d) Held constant at the value obtained from fit D.

(e) The constants C_M for the OH and CH₃ proton data were estimated as explained in the text.

(f) Held constant and E_C was set equal to E_M .

(g) Held constant at the value obtained from fit F.

(h) Held constant at the value indicated by the OH proton chemical shifts.

protons, the chemical shifts were too small to allow accurate measurements, and therefore, they are not given.

The temperature dependence of $(T_{2P}^{PM})^{-1}$ for this system is similar to that for $MnB(ClO_4)_2$ in DMF. The value of $(T_{2P}^{PM})^{-1}$ is controlled successively by $(T_{2M})^{-1}$, τ_M^{-1} and $(T_{2O})^{-1}$ as the temperature decreases. However, the magnetic field dependence observed for the two different protons at high temperature, shows that the hyperfine interactions contribute more significantly to the total $(T_{2M})^{-1}$ for MnB^{2+} in methanol than for MnB^{2+} in DMF. In this respect, this system is similar to MnB^{2+} in water. The greater magnetic field dependence which is observed for the OH proton than for the CH_3 protons, is qualitatively consistent with the fact that $(A/h)_{OH} > (A/h)_{CH_3}$.

It is apparent from the rather low effective energy of $(T_{2M})^{-1}$ for the OH and CH_3 protons that the exchange rate does not provide the predominant correlation time for the hyperfine interaction at high temperature. It was initially assumed that only T_{1e} controlled the hyperfine contribution to $(T_{2M})^{-1}$, and the $(T_{2P}^{PM})^{-1}$ data for each proton were fitted to eq 27 with the total $(T_{2M})^{-1}$ term (dipolar plus hyperfine) being defined by eq 20. A summary of the best-fit parameters can be found in Table VII (Model 1).

For the CH_3 protons, an independent determination of ΔH^\ddagger was not attempted since τ_M^{-1} is not well resolved from

$(T_{2M})^{-1}$ and $(T_{2O})^{-1}$. Instead, it is shown (fits D and E) that the observed $(T_{2P}^{PM})^{-1}$ for the CH_3 protons are completely consistent with the ΔH^\ddagger and ΔS^\ddagger values obtained from the OH proton data. Since a magnetic field dependence was not observed in the outer sphere line broadening region, the parameters defining $(T_{2O})^{-1}$ at 60 MHz were held constant in fitting the 100 MHz data. Although a fit of the 100 MHz OH proton data gave somewhat different values of ΔH^\ddagger and ΔS^\ddagger (compare fits A and B), it was found that the 100 MHz data could be fitted satisfactorily with the parameters shown in fit C.

At this stage, calculations were made to determine if τ_M should really be neglected as a correlation time for the hyperfine interaction. Using an iterative procedure in eq 29, it was found that, in order to properly account for the OH and CH_3 proton magnetic field dependence, the value of T_{1e} at 25°C at 60 and 100 MHz must be 8.6×10^{-9} and 1.48×10^{-8} sec, respectively, and that $\tau_r = 5.0 \times 10^{-11}$ sec for the inner sphere interaction distances: $(r_i)_{\text{OH}} = 2.95 \text{ \AA}$ and $(r_i)_{\text{CH}_3} = 3.9 \text{ \AA}$.⁴⁵ This calculation required that $(A/\hbar)_{\text{CH}_3}$ be $6.2 \times 10^5 \text{ rad sec}^{-1}$ if $(A/\hbar)_{\text{OH}} = 2.3 \times 10^6 \text{ rad sec}^{-1}$. The above value of $(A/\hbar)_{\text{OH}}$ was determined from the measured OH proton chemical shifts but $(A/\hbar)_{\text{CH}_3}$ could not be experimentally determined due to the small and inaccurate CH_3 proton chemical shifts. A comparison of the exchange rate at 25°C ($1.33 \times 10^7 \text{ sec}^{-1}$) from the values: $\Delta H^\ddagger = 9.9$

kcal mol⁻¹, $\Delta S^\ddagger = 7.35 \text{ cal mol}^{-1} \text{ deg}^{-1}$) with the above values of T_{1e} indicates that τ_M^{-1} contributes to the extent of ~10% and ~20% at 60 and 100 MHz, respectively. Thus, for a proper account of this system, the $(T_{2P}^{PM})^{-1}$ data should be fitted to eq 31 in a manner analogous to that used for MnB^{2+} in water.

In refitting the $(T_{2P}^{PM})^{-1}$ data for MnB^{2+} in methanol, according to eq 31, the complete temperature dependence of T_{1e} given by eq 18 was used. For the OH proton data, (A/\hbar) was held constant at the value indicated by the chemical shifts, but for the CH_3 proton data, $(A/\hbar)_{\text{CH}_3}$ was not restrained since the observed CH_3 proton chemical shifts were too small to give an accurate value of the hyperfine coupling constant. As for MnB^{2+} in water, it was necessary to obtain a good estimate of the dipolar contributions to $(T_{2M})^{-1}$. In this regard, the inner sphere interaction distances and dipolar correlation time given in the preceding paragraph were used to calculate the dipolar contribution to $(T_{2M})^{-1}$ at 25°C. It should be noted that the value of τ_r given above is in reasonable agreement with the value found for the VO^{2+} ion in methanol.⁵³ Using these estimates, the dipolar contribution to the total $(T_{2M})^{-1}$ at 25°C was found to be $7.63 \times 10^4 \text{ sec}^{-1}$ and $1.43 \times 10^4 \text{ sec}^{-1}$ for the OH and CH_3 protons, respectively. A value of 3.0 kcal mol⁻¹ was used for the inner sphere dipolar activation energy in order to calculate the values of the C_M constants for the

OH and CH_3 protons which were fixed in fitting the $(T_{2P}^{\text{PM}})^{-1}$ data. This was also the activation energy which was used for τ_c of eq 18. It might be expected that the activation energy for the outer sphere broadening, which is clearly defined for this system, would also be the activation energy which should be used for the inner sphere $(T_{2M})^{-1}$ dipolar contribution and for the process determining T_{1e} (eq 18). However, it was found by several additional fits that the activation energy required in the outer sphere $(T_{2O})^{-1}$ line broadening region, which is somewhat larger than the value expected for methanol viscosity ($\sim 3.0 \text{ kcal mol}^{-1}$)²⁴ gave unacceptable fits of all of the data when used to define the inner sphere dipolar $(T_{2M})^{-1}$ value and the value of T_{1e} . In order to obtain the over-all best set of parameters, the 60 and 100 MHz data for each proton were fitted simultaneously using two independent variables, the temperature and the electron spin precessional frequency (ω_s in eq 18), in the computer program. The values of the adjustable parameters ΔH^\ddagger , ΔS^\ddagger , C_e , τ_c^0 , E_o and C_o obtained from a fit of the OH proton $(T_{2P}^{\text{PM}})^{-1}$ data are given in Table VII (Model 2). For the CH_3 protons, ΔH^\ddagger , C_e , and τ_c^0 were held constant at the values obtained in fitting the hydroxy $(T_{2P}^{\text{PM}})^{-1}$ results and only the parameters ΔS^\ddagger , A/\hbar , E_o and C_o were allowed to vary. The values obtained for the adjustable parameters are also given in Table VII. The calculated curves for the OH and CH_3 proton, according to fits F and G, respectively,

are given in Figure 10.

Considering that the $(T_{2P}P_M)^{-1}$ data at the two frequencies were fitted simultaneously, the quality of the fits is quite satisfactory. It is also encouraging to find that the fit of the CH_3 proton $(T_{2P}P_M)^{-1}$ results is as good as it is in spite of the number of parameters which were restrained in obtaining a fit of this data. The value of $(A/\hbar)_{\text{CH}_3}$ predicted by fit G is also consistent with the very small shifts which were observed for the CH_3 proton resonance.

It should be noted that the values of $8.9 \text{ kcal mol}^{-1}$ and $2.5 \text{ cal mol}^{-1} \text{ deg}^{-1}$ for ΔH^\ddagger and ΔS^\ddagger , respectively, are somewhat smaller than those obtained using the simplified fitting procedure described earlier. The uncertainties in the values given are difficult to assess but considering the number of estimates which had to be made, in particular the estimate of the dipolar $(T_{2M})^{-1}$ term, errors of $\pm 0.5 \text{ kcal mol}^{-1}$ and $\pm 2 \text{ cal mol}^{-1} \text{ deg}^{-1}$ would not be unreasonable.

The observed chemical shifts of the hydroxy proton shown in Figure 11 were not used to obtain ΔH^\ddagger and ΔS^\ddagger since the shifts, being relatively small in the exchange region, were subject to considerable errors. Consequently, a value of $C_\omega = 1.28 \times 10^7 \text{ rad sec}^{-1} \text{ }^\circ\text{K}$ was estimated, graphically, from the chemical shifts in the fast exchange region and this value was used, along with the values of the parameters given in Table VII (fit F), to calculate the

shifts using eq 28. The calculated curve shown in Figure 11 indicates that the observed chemical shifts are consistent with the parameters obtained from the line broadening results. From the above value of C_ω and $\mu_{\text{eff}} = 5.9 \text{ BM}$, $(A/h)_{\text{OH}}$ was calculated to be $2.3 \times 10^6 \text{ rad sec}^{-1}$.

Magnetic Field Dependence of $(T_{2M})^{-1}$

The magnetic field dependence of $(T_{2M})^{-1}$ observed for MnB^{2+} in methanol, water and DMF is attributed to a field dependent hyperfine contribution. As shown previously, both τ_M and T_{1e} modulate this hyperfine interaction for MnB^{2+} in water and methanol, but for MnB^{2+} in DMF, $\tau_M > T_{1e}$, and thus, $\tau_e = T_{1e}$. For the latter system, the hyperfine contribution is relatively small. The magnetic field dependence of T_{1e} can be interpreted in terms of eq 18. In this section the parameters defining the field dependence of T_{1e} for MnB^{2+} in methanol and water are examined.

The values of τ_c^0 and E_c , which define the correlation time in eq 18, indicate that at 25°C , τ_c is $7.8 \times 10^{-12} \text{ sec}$ and $2.5 \times 10^{-12} \text{ sec}$, respectively, for MnB^{2+} in water and methanol. It should be noted that these values are much smaller than the rotational tumbling times⁵³ obtained for the VO^{2+} ion in water and methanol. It might be expected that the electronic relaxation mechanism proposed by Bloembergen and Morgan²² for the hydrated Mn^{2+} ion, and also found to be operative for the hydrated Fe^{3+} and Cr^{3+} ions,⁵⁴ is responsible for the small values of τ_c .

obtained here. For this mechanism, electron spin relaxation is due to the modulation of the zero-field splitting (ZFS) by random distortions of the inner solvation sphere as a result of molecular collisions with the bulk solvent. For complexes with cubic symmetry, and thus no permanent ZFS, the collisions provide a fluctuating ZFS averaging to zero. However, for complexes possessing a permanent distortion, as is the case for MnB^{2+} , it is expected that complex tumbling would also contribute to the modulation of the ZFS. For $\text{Mn}(\text{OH})_6^{2+}$, Bloembergen and Morgan obtained a value of 2.4×10^{-12} sec for τ_c at 300°K. Since the τ_c value for MnB^{2+} in water is considerably larger, it seems likely that both rotational tumbling and diffusional collisions contribute to a modulation of the ZFS.

Following McLachlin,²¹ the constant C_e in eq 18 is related to the ZFS energy term (Δ) and the electron spin quantum number by means of the expression

$$C_e = \frac{\Delta^2}{25} \left\{ 4S(S + 1) - 3 \right\} \quad (33-c)$$

From the value of the C_e constants given in Tables VI and VII, Δ is calculated to be $0.17 \pm 0.015 \text{ cm}^{-1}$ and 0.12 cm^{-1} for MnB^{2+} in water and methanol, respectively. These values of Δ are, as expected, considerably larger than the value 0.014 cm^{-1} found for the temporary ZFS energy in $\text{Mn}(\text{OH}_2)_6^{2+}$.⁵⁴ The values given above appear to be

consistent with the observation made by Alexander, *et al.*,³¹ that the $\text{MnBCl}_2 \cdot 6\text{H}_2\text{O}$ complex is characterized by a large zero-field splitting. It should be noted that the smaller Δ value obtained for MnB^{2+} in methanol than in water appears consistent with the result that τ_c is smaller for this system; the implication here being that the inherent ZFS for MnB^{2+} in methanol is smaller, and consequently, a greater contribution to the overall ZFS arises from the temporary distortion mechanism discussed above.

From $\tau_c(25^\circ)$ and C_e , T_{1e} for MnB^{2+} in methanol and water was calculated to be 1.0×10^{-8} and 7.2×10^{-9} sec, respectively, at 60 MHz (14.1 kG). For an independent estimate of T_{1e} , the epr spectrum of a degassed methanol solution of $\text{MnB}(\text{ClO}_4)_2$ was obtained at 25° . The spectrum consisted of 6 hyperfine lines superimposed on a broad background signal. The line width (~ 20 G) and coupling constant (~ 94 G) of the hyperfine lines are quite similar to those for $\text{Mn}(\text{CH}_3\text{OH})_6^{2+}$.^{49(b)} However, recrystallization of the complex failed to affect either the epr spectrum in methanol or the nmr line broadening in water. If it is assumed that $\text{Mn}(\text{CH}_3\text{OH})_6^{2+}$ is in equilibrium with MnB^{2+} , then relative intensity calculations indicate that the amount of $\text{Mn}(\text{CH}_3\text{OH})_6^{2+}$ is too small to account for the observed nmr results. If the hyperfine structure is actually a part of the MnB^{2+} epr spectrum, then eq 18 predicts that for $T_{1e} = 1.0 \times 10^{-8}$ sec at 14.1 kG, $T_{1e} = 2 \times 10^{-9}$ sec at the epr magnetic field (3500 G), in agreement with the value of 3×10^{-9} sec calculated for T_{2e} from the epr line width.

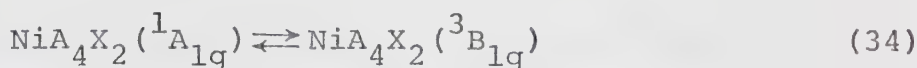
3. Magnetic Susceptibility and Ligand PMR Shift Study of the Paramagnetic-Diamagnetic Equilibrium of NiCR^{2+} and NiCRMe^{2+} in Several Coordinating Solvents

This section presents the results of a study of the diamagnetic-paramagnetic equilibrium for the solvated nickel(II) complex of 2,12-dimethyl-3,7,11,17-tetraazabicyclo(11.3.1)heptadeca-1(17),2,11,13,15-pentaene, NiCR^{2+} , and its methylated analogue, NiCRMe^{2+} . These complexes are shown in Chapter I as structures I(a) and I(b), respectively. It was necessary to study this equilibrium in order to interpret the solvent nmr line broadening properties of these nickel(II) complexes. For NiCR^{2+} , the diamagnetic-paramagnetic equilibrium was studied as a function of temperature in water, methanol, N,N-dimethylformamide (DMF), dimethylsulfoxide (DMSO) and acetonitrile. In the case of NiCRMe^{2+} , the equilibrium was studied in DMF and water. The equilibrium constants were determined from both magnetic susceptibility and ligand proton contact shift measurements.

The presence of a diamagnetic-paramagnetic equilibrium in the NiCR^{2+} system is not surprising in view of the earlier studies³² which have shown that in the solid state $\text{NiCR}(\text{ClO}_4)_2$ is diamagnetic while $\text{NiCR}(\text{OH}_2)_2(\text{ClO}_4)_2$, NiCRCl_2 and $\text{NiCR}(\text{SCN})_2$ are paramagnetic. It has also been observed that the iodide salt of the hydrogenated form of NiCR^{2+} shows a temperature-dependent spin-state equilibrium

in the solid state.⁵⁵ Similar observations on complexes less closely related to those studied here have been reviewed by Barefield, Busch and Nelson.⁵⁵

Several types of reactions have been associated with the diamagnetic-paramagnetic conversion in nickel(II) complexes. In the solid state, where ligand movement is restricted, a simple equilibrium between electronic states exists. For tetragonally distorted nickel(II) this would take the form



Such equilibria⁵⁵ normally have small values for ΔH° ($\sim 1 \text{ kcal mol}^{-1}$) and ΔS° ($\sim 1 \text{ cal mol}^{-1}\text{deg}^{-1}$).

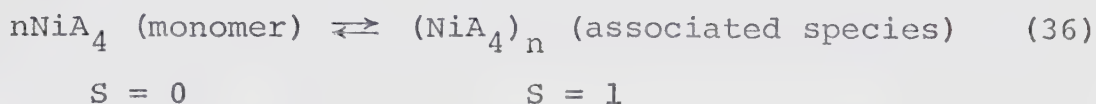
In solution a square planar-octahedral interconversion may occur according to the reaction



For $\text{Ni}(\text{CRH})^{2+}$ in water, where CRH is the hydrogenated CR macrocyclic ligand, ΔH° and ΔS° values⁵⁶ for equilibrium 35 are $-4.5 \text{ kcal mol}^{-1}$ and $-16 \text{ cal mol}^{-1}\text{deg}^{-1}$, respectively. Recently Kannan and Chakravorty⁵⁷ studied a series of 2-hydroxyacetophenimine complexes of nickel(II), with $\text{X} =$ pyridine, and found ΔH° values of -4 to $-11 \text{ kcal mol}^{-1}$ and

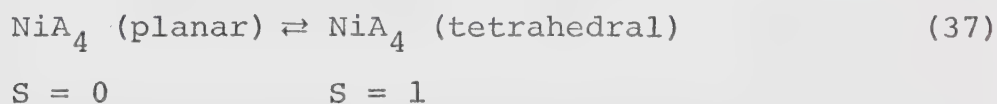
ΔS° values of -25 to -39 cal mol⁻¹deg⁻¹.

Several systems⁵⁵ have been found to exhibit the equilibrium



Such equilibria are characterized by their concentration dependence and sensitivity to steric factors in the A₄ ligand(s).⁵⁸

A final type of equilibrium (eq 37), involving a structural and spin-state change, has been observed.⁵⁹



The tetrahedral species can normally be detected from its characteristic electronic spectrum. Such an equilibrium seems unlikely with the fused ring quadridendate CR and CRMe ligands since it requires considerable ligand distortion. Therefore, equilibrium 37 will not be considered further here.

Preliminary studies on the NiCR²⁺ complex in water indicated that the visible spectrum was highly temperature dependent, with the extinction coefficient at 396 nm undergoing a reversible change from 76 M⁻¹cm⁻¹ at 5°C to 272

$M^{-1}cm^{-1}$ at $59.5^{\circ}C$. This type of observation indicates that an equilibrium exists in the system but is of little help in defining the type of change which is occurring. Therefore, studies of the temperature dependence of the magnetic susceptibility and of the ligand proton chemical shifts were undertaken.

The molar magnetic susceptibilities of $NiCR^{2+}$ and $NiCRMe^{2+}$, dissolved in several coordinating solvents, are shown in Figures 12, 13 and 14. These were determined by the method of Evans^{27,60} and were calculated from eq 2 of ref 27 which can be rewritten in the form

$$\chi_M = \left\{ \frac{3\Delta f}{2\pi f_0 [m] M \rho_t \times 10^{-3}} + \chi_0 \right\} M \quad (38)$$

where χ_M is the molar magnetic susceptibility, Δf is the magnetic susceptibility shift in Hz, f_0 is the spectrometer operating frequency (60 MHz in this study), $[m]$ is the solute molality, ρ_t is the solution density at $t^{\circ}C$, M is the molecular weight of the complex, and χ_0 is the solvent diamagnetic susceptibility in cgs units. The χ_M values shown in the figures have been corrected for the macrocyclic diamagnetic susceptibility (-163×10^6 cgs units).²⁸ However, for reasons to be discussed subsequently, ρ_t for each nonaqueous solvent system was assumed to be that of the solvent at 25° .

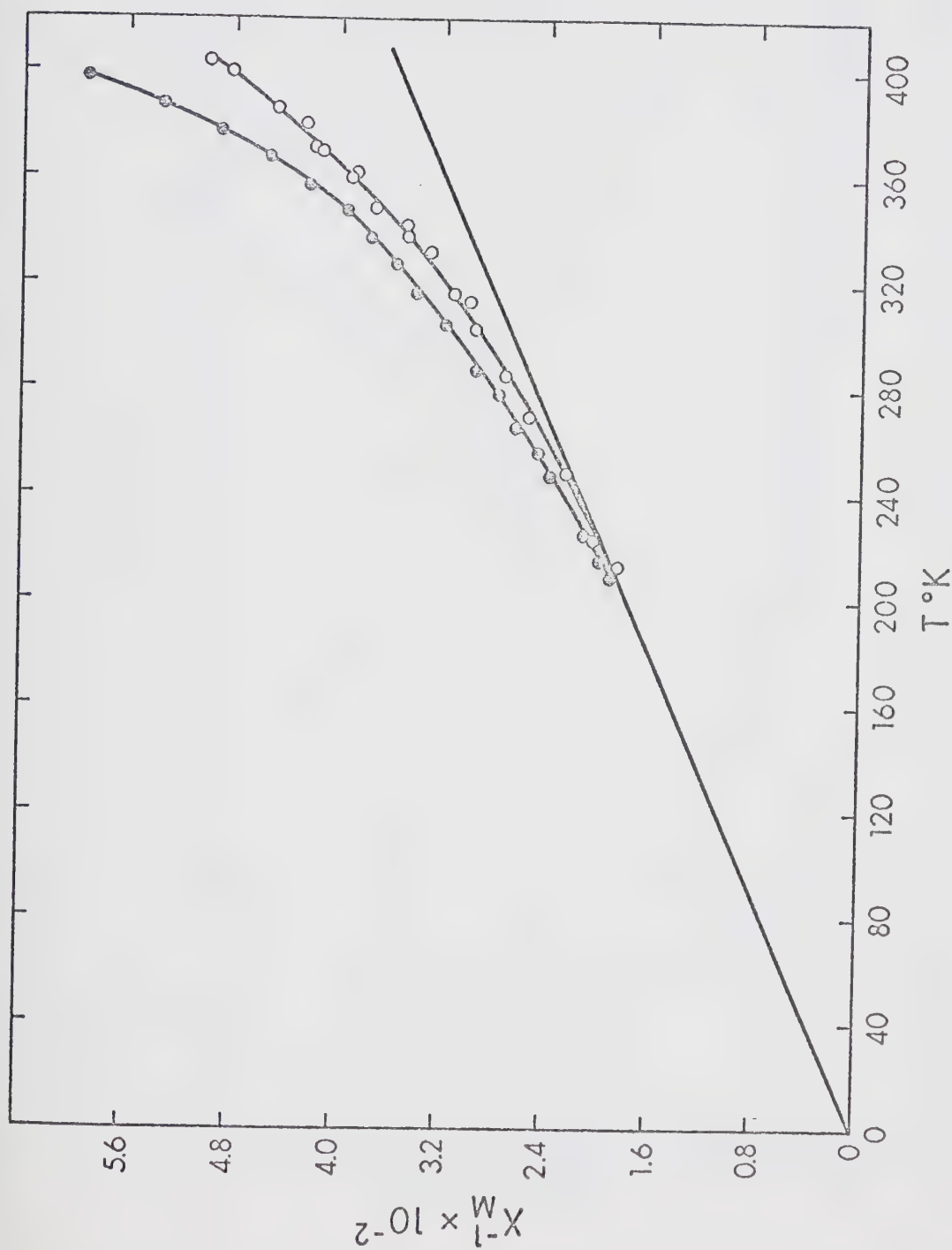


Figure 12: Temperature dependence of X_M^{-1} for $\text{NiCR}(\text{PF}_6)_2$ (o) and $\text{NiCRMe}(\text{ClO}_4)_2$ (●) in N,N-dimethylformamide.

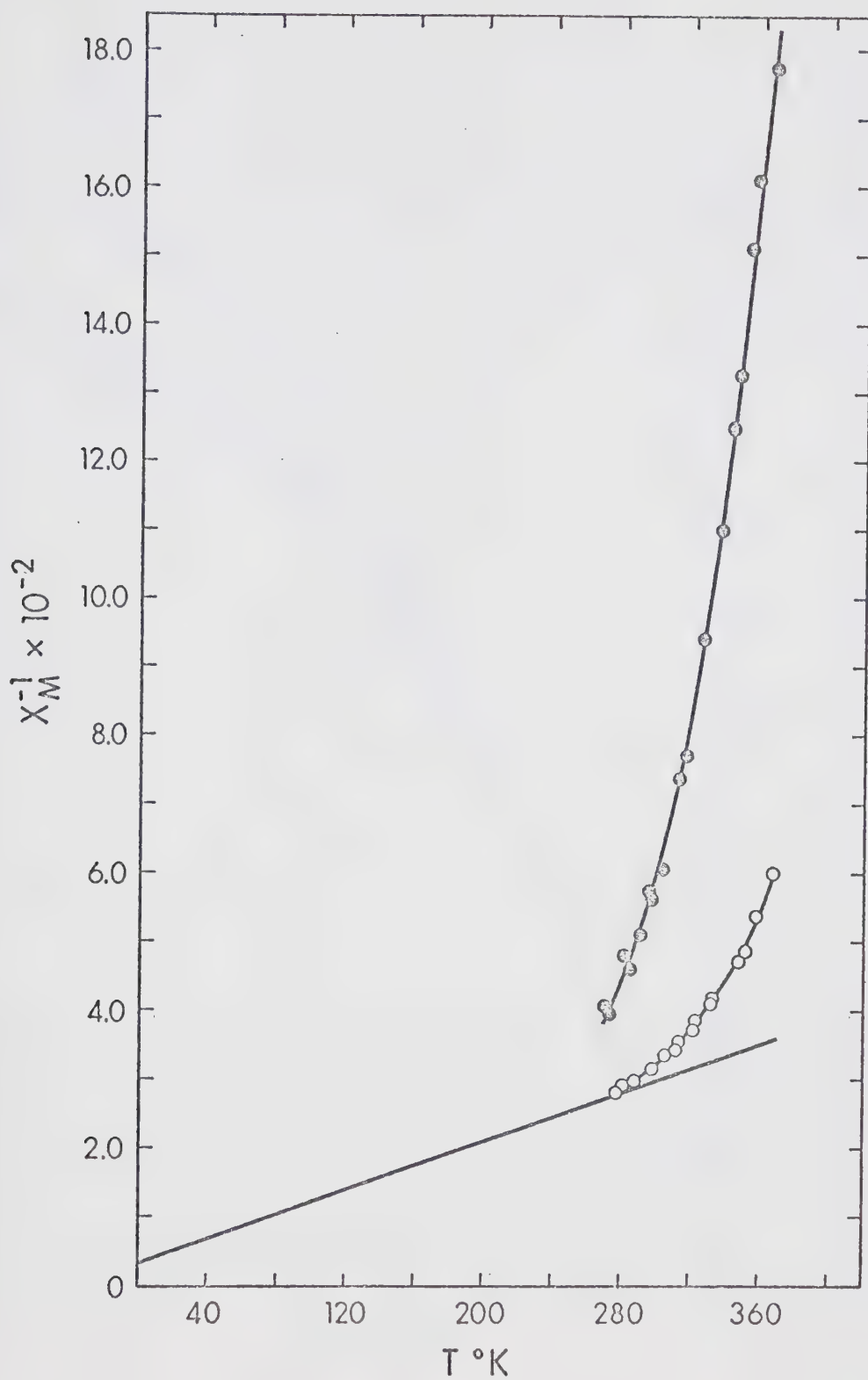


Figure 13: Temperature dependence of χ_M^{-1} for $\text{NiCR}(\text{BF}_4)_2$ (o) and $\text{NiCRMe}(\text{BF}_4)_2$ (●) in water.

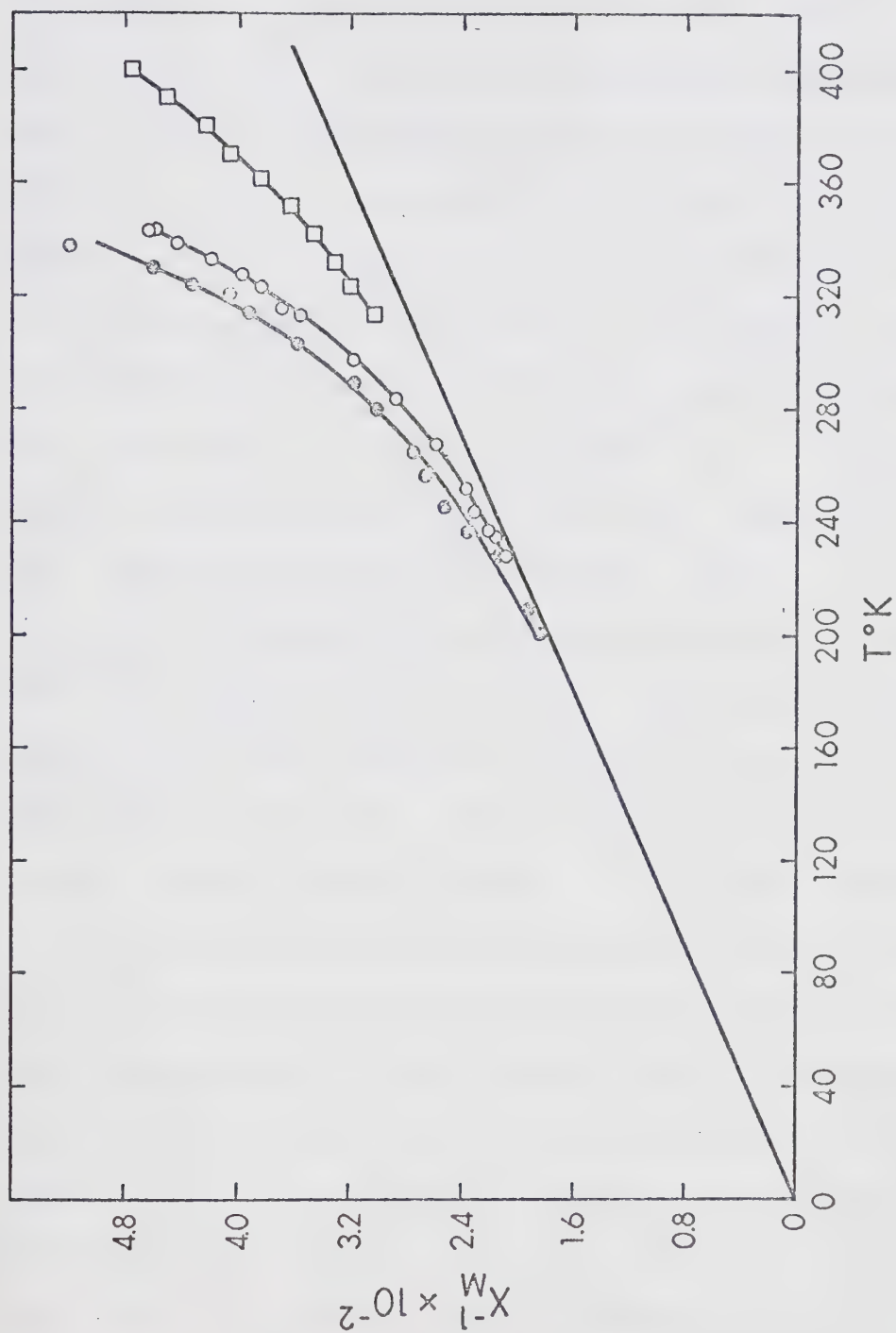


Figure 14: Temperature dependence of χ_M^{-1} for $\text{NiCR}(\text{PF}_6)_2$ in dimethylsulfoxide (\square), $\text{NiCR}(\text{PF}_6)_2$ in acetonitrile (\circ), and $\text{NiCR}(\text{BF}_4)_2$ in methanol (\bullet).

When the anhydrous NiCRMe^{2+} and NiCR^{2+} complexes were dissolved in a non-coordinating solvent, such as trifluoroacetic acid, the temperature-independent macrocyclic ligand pmr of the pure diamagnetic forms was obtained as shown by spectrum A and B, respectively, in Figure 1. On the other hand, when these complexes were dissolved in the coordinating solvents used in this study, the chemical shifts of the various resonances became very temperature dependent. For a solution of $\text{NiCR}(\text{PF}_6)_2$ in DMF at 60° , the pyridyl proton resonances appeared downfield, while the signals from the azo-methine methyl protons and the two types of CH_2 protons from the dipropylamine portion of the molecule were shifted upfield, the latter more than the former, relative to their diamagnetic positions shown by nmr spectrum B in Figure 1. The entire spectrum at this temperature occurred over a region of ~ 1800 Hz. Measurements of the temperature dependence of the sharpest resonance due to the azo-methine methyl protons were used to determine the position of the equilibrium. All shifts were found to be independent of concentration, at least in the range 0.3 to 0.8 m studied. The accuracy of the shifts was generally controlled by the line width and is estimated to vary from ± 2 Hz at the higher temperatures to ± 10 Hz at lower temperatures. The chemical shifts relative to the chemical shift in trifluoroacetic acid, which was taken as that of the pure diamagnetic form, are shown in Figure 15.

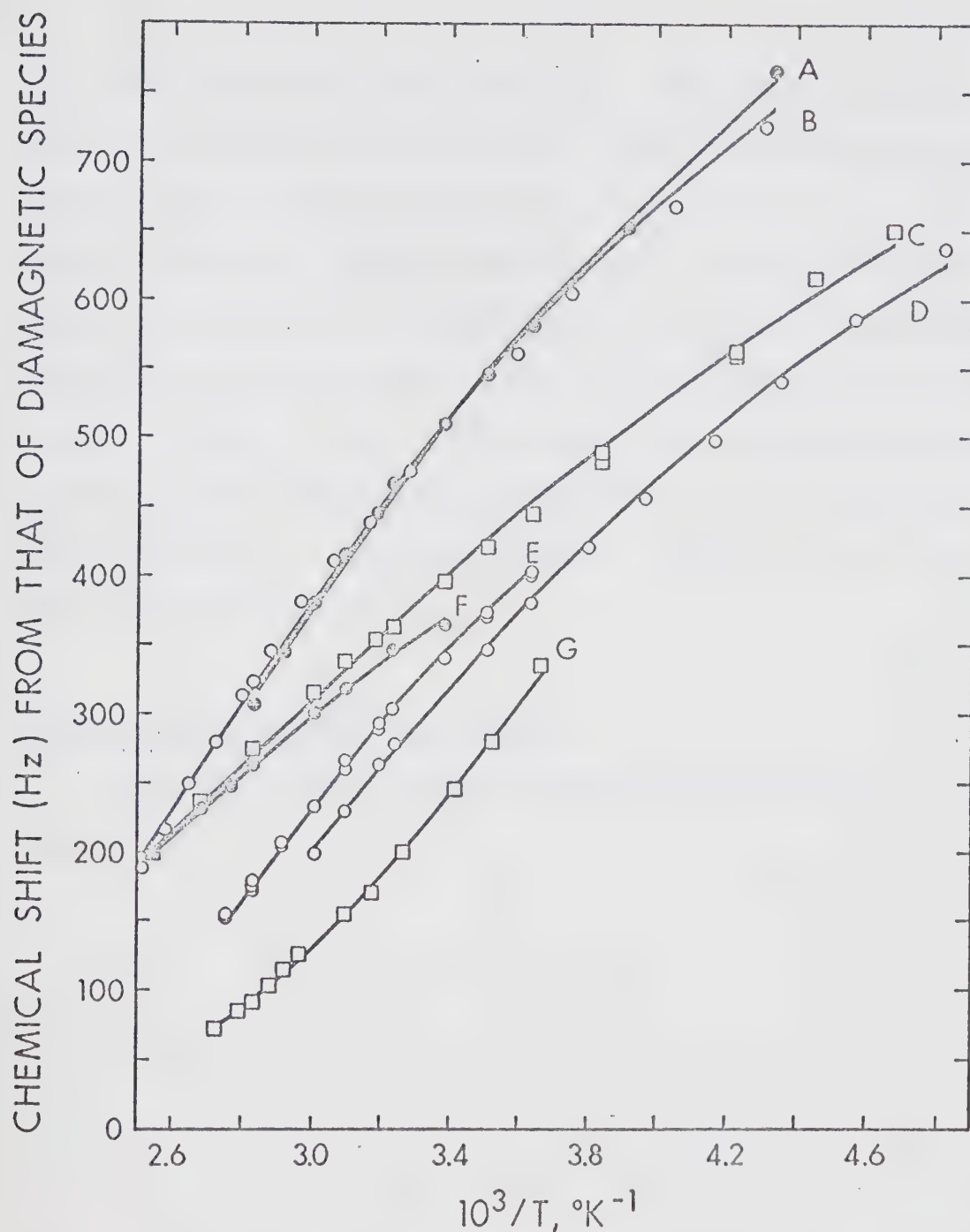
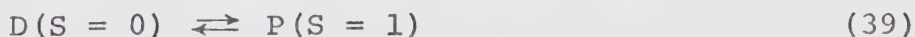


Figure 15: Temperature dependence of the chemical shift of the azo-methine methyl protons for NiCR^{2+} and NiCRMe^{2+} . A - $\text{NiCR}(\text{PF}_6)_2$ in acetonitrile, B - $\text{NiCRMe}(\text{ClO}_4)_2$ in N,N-dimethylformamide, C - $\text{NiCR}(\text{PF}_6)_2$ in N,N-dimethylformamide, D - $\text{NiCR}(\text{BF}_4)_2$ in methanol, E - $\text{NiCR}(\text{BF}_4)_2$ in water, F - $\text{NiCR}(\text{PF}_6)_2$ in dimethylsulfoxide, and G - $\text{NiCRMe}(\text{BF}_4)_2$ in water.

These magnetic susceptibility and chemical shift results indicate, unambiguously, that a diamagnetic-paramagnetic equilibrium exists, with the diamagnetic form being favored at higher temperatures. The measurements also show that it was not possible to obtain the chemical shifts and the magnetic susceptibilities of the pure paramagnetic forms. From the standpoint of improving the accuracy of the equilibrium constants, it would have been of considerable advantage if these limiting values could have been determined.

Magnetic Susceptibility Results

If the diamagnetic-paramagnetic equilibrium is represented by



then the equilibrium constant is given by

$$K = \frac{[P]}{[D]} = \exp\left(\frac{-\Delta H^\circ + T\Delta S^\circ}{RT}\right) . \quad (40)$$

The molar magnetic susceptibility can therefore be expressed as

$$\chi_M = \frac{\mu_\infty^2 N}{3k(T + \theta) \left(1 + \exp\left(\frac{\Delta H^\circ - T\Delta S^\circ}{RT}\right)\right)} \quad (41)$$

where μ_{∞} is the magnetic moment of the paramagnetic species in Bohr magneton units, N is Avogadro's number, and θ is the Weiss constant. A Curie-Weiss temperature dependence is assumed for μ_{∞} since previous work³² provides some guidelines as to the likely values for θ . Alternatively, a temperature independent term may be added to eq 41, with $\theta = 0^{\circ}\text{K}$; however, the two procedures are equivalent from the point of view of fitting the data, as long as $T \gg \theta$.

A nonlinear least-squares fit of the χ_M data to eq 41 would not give reasonable values for all the parameters: μ_{∞} , θ , ΔH° and ΔS° . However, fits to within the estimated experimental error of the χ_M values could be obtained using the assumptions summarized in Table VIII. A value of 3.00 BM was chosen for μ_{∞} , rather than the more normal value of 3.2 BM⁵⁵ for octahedral nickel(II), because it gave better agreement of ΔH° and ΔS° with the results of the chemical shift study and also gave smaller, more reasonable θ values. Although μ_{∞} may actually be slightly different for each system, as shown by fit A, the data do not permit such a refinement.

In fit C of Table VIII, an attempt was made to account for the changing solution density (eq 38) with temperature. Temperature density functions of the pure solvents⁶¹ were used. For the nonaqueous solvent systems, the ΔH° and ΔS° values do not agree with those from the chemical shift

TABLE VIII

Least-squares best fit parameters of the magnetic susceptibility data
for NiCR^{2+} and NiCRMe_2^{2+} in a series of solvents

Complex	Solvent	Fit A (a)			Fit B (b)			Fit C (c)		
		ΔH° , kcal mol ⁻¹	ΔS° , cal mol ⁻¹ deg ⁻¹	μ_∞ , BM	ΔH° , kcal mol ⁻¹	ΔS° , cal mol ⁻¹ deg ⁻¹	θ , °K	ΔH° , kcal mol ⁻¹	ΔS° , cal mol ⁻¹ deg ⁻¹	θ , °K
$\text{NiCR}(\text{BF}_4)_2$	Water	-7.29	-19.1	2.82	-6.97	-18.3	35.3	-6.81	-17.7	35.3
$\text{NiCR}(\text{BF}_4)_2$	CH_3OH	-4.63	-12.6	2.91	-4.26	-11.5	11.0	-5.00	-13.1	34.7
$\text{NiCR}(\text{PF}_6)_2$	CH_3CN	-4.28	-11.1	2.99	-4.28	-11.0	2.3	-4.90	-11.8	25.1
$\text{NiCR}(\text{PF}_6)_2$	DMF	-3.53	-6.8	3.00	-3.50	-6.7	0.4	-4.20	-7.1	15.9
$\text{NiCR}(\text{PF}_6)_2$	DMSO	-4.71	-9.3	2.95	-4.60	-9.2	9.7	-6.00	-11.1	16.8
$\text{NiCRMe}(\text{BF}_4)_2$	Water	-5.31	-17.0	2.62	-4.58	-15.3	35.3 (d)	-4.58	-15.3	35.3 (d)
$\text{NiCRMe}(\text{ClO}_4)_2$	DMF	-4.47	-10.0	2.91	-4.06	-9.1	12.4	-6.40	-14.0	18.0

(a) Fitted to eq 41 with $\theta = 0$.

(b) Fitted to eq 41 with $\mu_\infty = 3.00$ BM for each system. The data do not permit an independent determination of θ and μ_∞ .

(c) Fitted as in B but with a density correction taken from the pure solvent.

(d) θ fixed at 35.3 °K, as obtained for $\text{NiCR}(\text{BF}_4)_2$ in water, since the three-parameter fit gave an unreasonable value of $\theta = 78.5^\circ\text{K}$, with $\Delta H^\circ = -5.32$ kcal mol⁻¹ and $\Delta S^\circ = -17.2$ cal mol⁻¹deg⁻¹.

TABLE IX

Least-squares best fit parameters of the azo-methine methyl
chemical shift data for NiCR^{2+} and NiCRMe^{2+} in a series
of solvents ^(a)

Complex	Solvent	$\Delta H^\circ,$ kcal mol ⁻¹	$\Delta S^\circ,$ cal mol ⁻¹ deg ⁻¹	$10^{-5} \times A/\hbar,^{(b)}$ rad sec ⁻¹
$\text{NiCR}(\text{BF}_4)_2$	Water	-6.39	-17.9	-5.49
$\text{NiCR}(\text{BF}_4)_2$	CH_3OH	-4.09	-12.2	-6.20
$\text{NiCR}(\text{PF}_6)_2$	CH_3CN	-4.16	-10.8	-8.26
$\text{NiCR}(\text{PF}_6)_2$	DMF	-3.27	- 7.7	-6.57
$\text{NiCR}(\text{PF}_6)_2$	DMSO	-4.47	-10.0	-5.49
$\text{NiCRMe}(\text{BF}_4)_2$	Water	-4.60	-15.1	-5.91
$\text{NiCRMe}(\text{ClO}_4)_2$	DMF	-4.85	-12.6	-8.07

(a) Fitted to eq 42 with $\Delta = 0$.

(b) Calculated assuming $\bar{g}\sqrt{S(S+1)} = 3.00$ BM in eq 42.

TABLE IX

Least-squares best fit parameters of the azo-methine methyl
chemical shift data for NiCR^{2+} and NiCRMe^{2+} in a series
of solvents ^(a)

Complex	Solvent	$\Delta H^\circ,$ kcal mol ⁻¹	$\Delta S^\circ,$ cal mol ⁻¹ deg ⁻¹	$10^{-5} \times A/\hbar,^{(b)}$ rad sec ⁻¹
$\text{NiCR}(\text{BF}_4)_2$	Water	-6.39	-17.9	-5.49
$\text{NiCR}(\text{BF}_4)_2$	CH_3OH	-4.09	-12.2	-6.20
$\text{NiCR}(\text{PF}_6)_2$	CH_3CN	-4.16	-10.8	-8.26
$\text{NiCR}(\text{PF}_6)_2$	DMF	-3.27	- 7.7	-6.57
$\text{NiCR}(\text{PF}_6)_2$	DMSO	-4.47	-10.0	-5.49
$\text{NiCRMe}(\text{BF}_4)_2$	Water	-4.60	-15.1	-5.91
$\text{NiCRMe}(\text{ClO}_4)_2$	DMF	-4.85	-12.6	-8.07

(a) Fitted to eq 42 with $\Delta = 0$.

(b) Calculated assuming $\bar{g}\sqrt{S(S+1)} = 3.00$ BM in eq 42.

study. It would appear that the use of pure solvent densities for solutions containing from ~0.05 to ~0.2 m complex and ~5 vol % of internal standard is not justified. As expected, the inclusion of the temperature variation of the density of water for the aqueous systems has an insignificant effect on the fit parameters since the density of water does not have a very large temperature dependence.

Ligand Proton Chemical Shift Results

The temperature dependence of the chemical shift of the azo-methine methyl protons were also used to obtain the equilibrium constant for eq 39. If only the Fermi contact contribution to the shift is considered, then eq 40 of reference 17 can be used to obtain

$$\Delta\omega_P = \frac{A}{\hbar} \cdot \frac{\bar{g}\beta S(S+1)\omega_0}{3k\gamma_I T} \left(\frac{T - \Delta}{T} \right) \left\{ 1 + \exp\left(\frac{\Delta H^\circ - T\Delta S^\circ}{RT}\right) \right\}^{-1} \quad (42)$$

where $\Delta\omega_P$ is the measured chemical shift relative to that of the diamagnetic form, A/\hbar is the hyperfine coupling constant in rad sec^{-1} and ω_0 is the nmr operating frequency. The first term in brackets in eq 42 is obtained by rearrangement of the expression given by Kurland and McGarvey,¹⁷ with $\Delta = \left((g_{\parallel} - g_{\perp})D/9k\bar{g} \right)$, where D is the zero-field splitting energy and $\bar{g} = \frac{1}{3}(g_{\parallel} + 2g_{\perp})$. The

neglect of an additional pseudocontact shift (eq 12) appears to be justified for NiCR^{2+} and NiCRMe^{2+} since the angular geometry term, $(3\cos^2\Omega - 1)$, for the azo-methine methyl protons of NiCR^{2+} and NiCRMe^{2+} is expected to be small. It should also be observed from eq 12 that, since the pseudocontact shift has mainly a T^{-1} temperature dependence with only a small T^{-2} term, the omission of this contribution to the measured chemical shift in the present treatment should not affect the ΔH° and ΔS° values, but would affect the values of A/\hbar .

The frequency shift data of Figure 15 were originally fitted to eq 42 assuming $\Delta = 0$. With this condition eq 42 reduces to the form more normally used to fit contact shifts,⁶² in which a Curie law temperature dependence of the magnetic susceptibility is assumed. The results of these fits are summarized in Table IX. The ΔH° and ΔS° values are in good agreement with fit B of Table VIII, but not in such good agreement with fit C, except for the systems NiCR^{2+} and NiCRMe^{2+} in water. This indicates that the density corrections applied in fit C for the nonaqueous solvent systems are incorrect for reasons outlined earlier.

However, the agreement might be improved by inclusion of the non-Curie temperature dependence of the magnetic susceptibilities in fitting the contact shifts. The expression for the magnetic susceptibility of an $S = 1$ system, given by Kurland and McGarvey,¹⁷ can be used to show

that

$$\chi_{M/N} = \bar{\chi} = \frac{1}{3}(\chi_{\parallel} + 2\chi_{\perp}) = \frac{2\bar{g}^2\beta^2}{3kT} \left(\frac{T - \Delta'}{T} \right) \quad (43)$$

where $\bar{g}^2 = \frac{1}{3}(g_{\parallel}^2 + 2g_{\perp}^2)$ and $\Delta' = ((g_{\parallel}^2 - g_{\perp}^2)D/k\bar{g}^2)$. The Curie-Weiss law for the susceptibility may be written as

$$\chi_M = \frac{C}{T(1 + \theta/T)} \approx \frac{C}{T} (1 - \theta/T) \quad (44)$$

and then

$$\chi_M \approx \frac{C}{T} \left(\frac{T - \theta}{T} \right) \quad (45)$$

Comparison of eq 43 and 45 shows that the Weiss constant (θ) can be identified with Δ' . In the absence of known g values, a relationship for Δ in terms of θ cannot be obtained, but it can be shown that

$$\frac{\Delta'}{\Delta} = \frac{\theta}{\Delta} = 1 + 3 \left(\frac{g_{\parallel}}{g_{\perp}} + \frac{2g_{\perp}}{g_{\parallel}} \right)^{-1} \quad (46)$$

In the limit of a completely isotropic case $\Delta = 0.5\theta$ and it seems unlikely that $\Delta > 0.67\theta$. The contact shift data for the water systems, which have the largest θ values, were refitted to eq 42 assuming $\Delta = 0.67\theta$. The results for NiCR^{2+} are $\Delta H^\circ = -5.92 \text{ kcal mol}^{-1}$ and $\Delta S^\circ = -16.7 \text{ cal mol}^{-1}\text{deg}^{-1}$, and for NiCRMe^{2+} , $\Delta H^\circ = -4.61 \text{ kcal mol}^{-1}$ and

$\Delta S^\circ = -15.2 \text{ cal mol}^{-1}\text{deg}^{-1}$. These values for NiCR^{2+} are in poorer agreement with those from fit C, and the values for NiCRMe^{2+} are essentially unaffected. The overall fit was not significantly improved. Therefore, the inclusion of Δ in eq 42 will not significantly affect the results nor improve the agreement with the results of fit C.

It is somewhat difficult to estimate the magnitude of the errors for ΔH° and ΔS° because of the various approximations required and the number of parameters needed to fit the data. The ligand chemical shifts are least subject to these problems and experience with the fitting process indicates that an error of $\pm 0.5 \text{ kcal mol}^{-1}$ on ΔH° and $\pm 1 \text{ cal mol}^{-1}\text{deg}^{-1}$ on ΔS° is a reasonable estimate. Within these error estimates, the results from the magnetic susceptibility and ligand chemical shift studies are in agreement.

The values of ΔH° and ΔS° obtained for the diamagnetic-paramagnetic equilibrium are generally similar to those found previously^{55,56,57} for a square planar-octahedral equilibrium indicated by eq 35. Although it is possible that the paramagnetic species is only five-coordinate, the isolation of the bis-adduct, $\text{NiCR}(\text{DMF})_2(\text{PF}_6)_2$, for which the microanalytical results are given in Table I, provides some indirect evidence for the octahedral formulation. The magnitude of ΔH° and ΔS° argue strongly against an equilibrium such as that represented by eq 34. The lack of

any concentration dependence for the equilibrium precludes the possibility of complex association via the equilibrium represented by eq 36. Furthermore, in view of the absence of temperature dependent contact shifts of the ligand proton resonances in inert solvents, it is not likely that the formation of associated species would occur in coordinating solvents.

It would be expected that solvating power, steric effects, and ligand-field splitting might be contributing factors to the ΔH° values. However, except for NiCR^{2+} in water and DMF, the ΔH° and ΔS° values are quite similar, being about $4.4 \pm 0.4 \text{ kcal mol}^{-1}$ and $12 \pm 3 \text{ cal mol}^{-1}\text{deg}^{-1}$, respectively. Therefore, it seems that a number of compensating factors may be at work and a qualitative analysis of the ΔH° values is futile.

The ΔH° value for NiCR^{2+} in water is the most negative, consistent with the proposal by Busch⁵⁶ that solvent structure breaking is an important factor in determining the diamagnetic-paramagnetic equilibrium state. However, NiCRMe^{2+} in water has a rather normal ΔH° , and it seems unlikely that the introduction of a methyl group on the Schiff base ligand would have a significant effect on the solvent structure.

The hyperfine coupling constants (A/\hbar) in Table IX have all been calculated with the assumption that $\mu_\infty = \bar{g}\sqrt{S(S+1)} = 3.00 \text{ BM}$. It would seem likely that this as-

sumption is good to within at least $\pm 5\%$, and therefore, the variations in A/\hbar for different systems are real. The nature of the axial ligand, solvation of the octahedral complex, and minor changes in geometry of the macrocyclic ligand are likely to affect A/\hbar . Thus, the observed variations are not considered to be unusual.

The values of the equilibrium constant parameters determined in these studies are used in subsequent sections to correct the solvent proton chemical shifts and line broadenings for the diamagnetic form of the NiCR^{2+} and NiCRMe^{2+} complexes.

4. Solvent Proton NMR Line Broadening and Chemical Shift Study of the Nickel(II) Schiff Base Complexes, NiCR^{2+} and NiCRMe^{2+} , in Several Solvents

As a result of a number of recent nmr solvent exchange studies of normal octahedrally substituted nickel(II) complexes,^{2,3,7} it is now possible to qualitatively anticipate the effect of the non-exchanging ligands on the water exchange rates in such systems. However, there have been comparatively few studies of the kinetic properties of tetragonally distorted nickel(II) complexes. Thus, little is known regarding the relative importance of complex geometry and the effects of non-exchanging ligands in these systems. It was therefore of interest to study the solvent exchange properties of the Schiff base complex, NiCR^{2+} , in several solvents. The solvents chosen were: water, N,N-dimethylformamide, methanol, acetonitrile and dimethylsulfoxide.

For purposes of comparison of the solvent exchange and the relaxation results of NiCR^{2+} with those of another tetragonally distorted system, the Schiff base complex, NiCRMe^{2+} , was also studied in water and N,N-dimethylformamide. It should be noted from structures I(a) and I(b) that the only synthetic structural difference between these two complexes is that in the case of NiCRMe^{2+} a methyl group is substituted for the amine proton of the CR ligand.

It was shown in the previous section that a rapid dia-

magnetic-paramagnetic equilibrium is a characteristic property of NiCR^{2+} and NiCRMe^{2+} in the above coordinating solvents. The question therefore arises as to whether the solvent exchange behaviour of these complexes is also related to this equilibrium.

Chemical exchange effects on the nmr line broadening and frequency shifts were observed for both NiCR^{2+} and NiCRMe^{2+} in N,N-dimethylformamide and for NiCR^{2+} in methanol. Only the line broadening results for NiCR^{2+} in water and acetonitrile and for NiCRMe^{2+} in water show effects of chemical exchange. In the case of NiCR^{2+} in dimethylsulfoxide no chemical exchange controlled line broadening was observed. Measurements were made on all systems at both 60 and 100 MHz and in all cases a frequency dependence of the proton relaxation time in the first coordination sphere of the metal ion was observed. This behaviour is interpreted in terms of the magnetic field dependence of the electron spin relaxation time.

In order to include the effect of the temperature-dependent diamagnetic-paramagnetic equilibrium, represented by eq 35, on the concentration of the paramagnetic form of the complex in solution, P_M , previously defined by eq 4, is expressed as

$$P_M = \frac{nX_p [\text{Ni}^{2+}]_{\text{total}}}{[\text{S}] - nX_p [\text{Ni}^{2+}]_{\text{total}}} \quad (47)$$

where X_p is the mole fraction of the nickel complex in the paramagnetic form and is readily calculated from

$$\frac{X_p}{1 - X_p} = \exp \left(\frac{-\Delta H^\circ + T\Delta S^\circ}{RT} \right) \quad (48)$$

The values of ΔH° and ΔS° have been determined as described in section 3 of this chapter. A value of two has been assumed for n for both NiCR^{2+} and NiCRMe^{2+} , implying a pseudo-octahedral structure for the paramagnetic species. Indirect evidence supporting this assumption, at least for NiCR^{2+} , has been presented in the experimental section where it was shown that the bis-DMF adduct of $\text{NiCR}(\text{PF}_6)_2$ could be isolated. The characterization of the aquo-adduct, $\text{NiCR}(\text{OH}_2)_2(\text{ClO}_4)_2$, has also been reported.³² However, if n were actually one in solution, then the values of $(T_{2P}^{P_M})^{-1}$ and $\Delta\omega_{\text{obsd}}/P_M$ would have to be multiplied by a factor of two, essentially, since the second term in the denominator of eq 47 is small relative to $[S]$. Therefore, the calculated exchange rates and coupling constants would increase by a factor of two, and ΔS^\ddagger would increase by $1.4 \text{ cal mol}^{-1} \text{ deg}^{-1}$.

NiCR^{2+} in N,N -dimethylformamide

The temperature dependencies of $(T_{2P}^{P_M})^{-1}$ and $(\Delta\omega_{\text{obsd}}/P_M)$ for the formyl proton in DMF solutions of

NiCR^{2+} are shown in Figures 16 and 17, respectively. In this study most of the measurements were made on the hexafluorophosphate salt and these were found to be in agreement with data obtained for the perchlorate salt. All of the experimental points have been adjusted using in eq 48 the previously determined values of $-3.27 \text{ kcal mol}^{-1}$ and $-7.7 \text{ cal mol}^{-1}\text{deg}^{-1}$ for ΔH° and ΔS° , respectively. It may be noted that below -40°C the complex is $>96\%$ paramagnetic and the effect of the equilibrium on the concentration of paramagnetic species is quite small; however, at higher temperatures the effect is quite significant. At 120°C , for example, the complex is 43% in the diamagnetic form.

The temperature dependence of $(T_{2P}P_M)^{-1}$, shown in Figure 16, is typical of that observed for other nickel(II) systems. The value of $(T_{2P}P_M)^{-1}$ is primarily controlled successively by $(T_{2M})^{-1}$, $\tau_M\Delta\omega_M^2$ and finally $(\tau_M)^{-1}$ as the temperature is lowered. These limiting conditions were discussed as 25(a) to 25(d) (Case A) in Chapter I. It should be noted that no $(T_{2O})^{-1}$ controlled line broadening region is actually observed at low temperature but analysis of the data for this system and that of NiCRMe^{2+} in DMF, permitted the outer sphere term to be estimated. The results for $\text{Ni}(\text{DMF})_6^{2+}$ in DMF^{47} were also useful in this connection.

This system is unusual, however, in that the $(T_{2M})^{-1}$

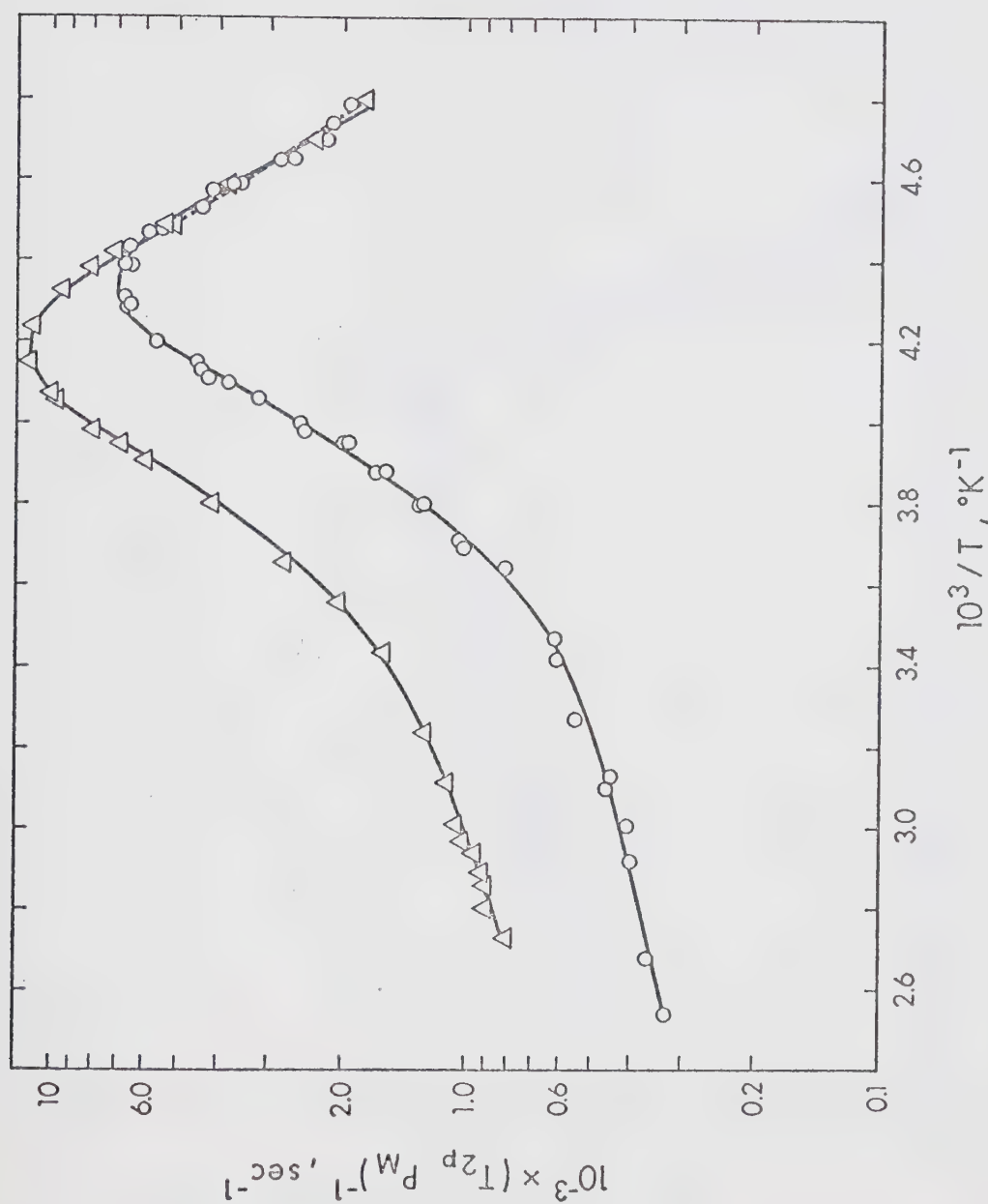


Figure 16: Temperature dependence of $-\log(T_{2p} P_M)$ for the formyl proton in N,N-dimethylformamide solutions of NiCR^{2+} (both PF_6^- and ClO_4^- salts), at 100 MHz (Δ), and 60 MHz (o).

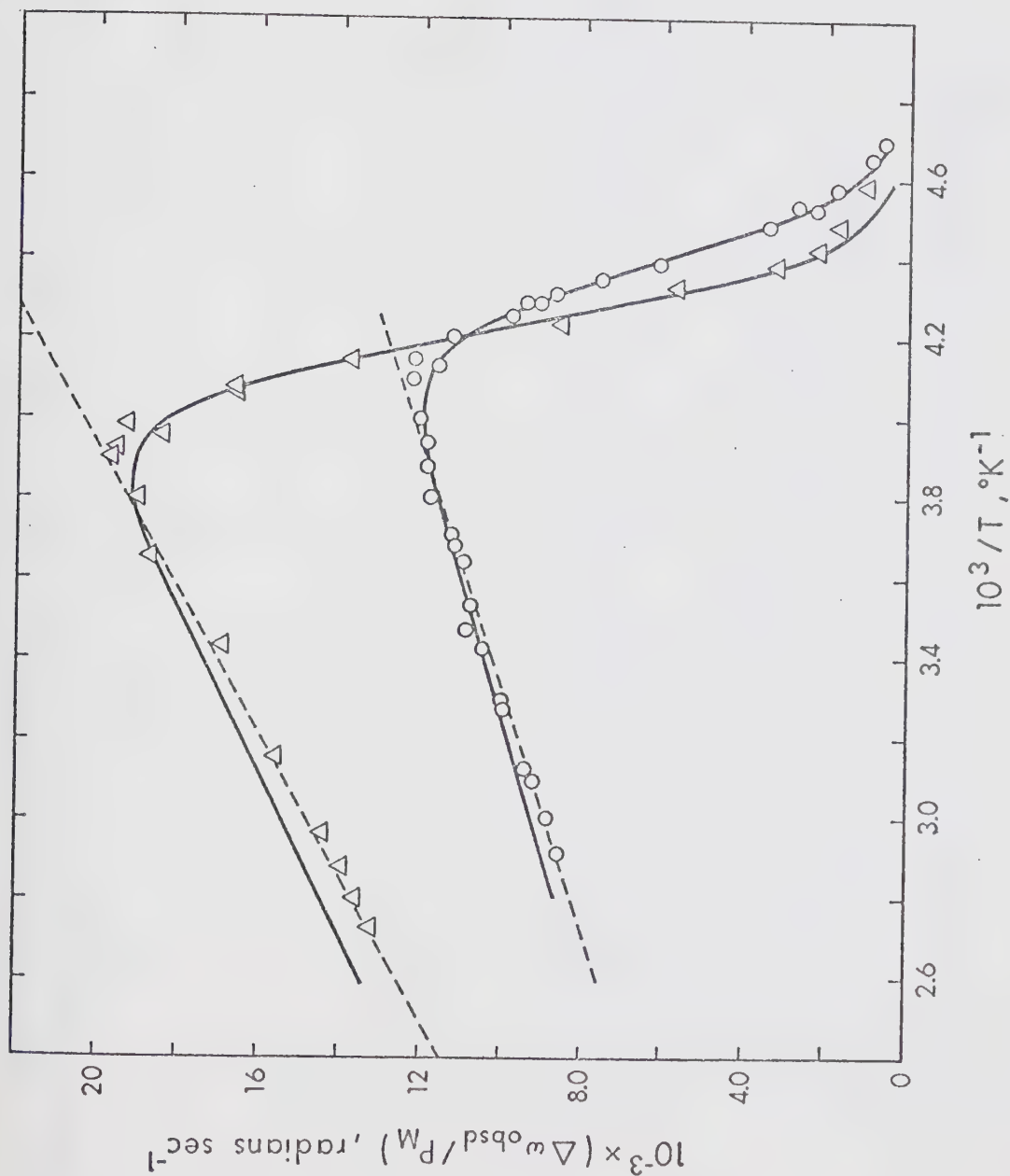


Figure 17: Temperature dependence of $(\Delta\omega_{\text{obsd}}/P_M)$ for the formyl proton in N,N-dimethylformamide solutions of NiCR^{2+} (both PF_6^- and ClO_4^- salts), at 100 MHz (Δ), and 60 MHz (o). The significance of the dashed and solid curves is explained in the text.

TABLE X

Least-squares best fit parameters for NiCR^{2+} in N,N-dimethylformamide

	$(T_{2P_M})^{-1}$ Data			$\Delta\omega_{\text{obsd}}$ Data	
	60 MHz	100 MHz	100 MHz	60 MHz	100 MHz
ΔH^\ddagger , kcal mol $^{-1}$	9.63	9.18	9.63 (d)	9.52	9.80
ΔS^\ddagger , cal mol $^{-1}\text{deg}^{-1}$	2.71	0.24	2.17	2.10	3.18
$10^{-6} \times C_\omega$, rad sec $^{-1}\cdot\text{K}$	3.08 (a)	5.36	5.14 (d)	3.08	5.14
$E_M = E_O$, kcal mol $^{-1}$	1.06 (b)	1.06	1.06 (e)	1.06 (e)	1.06 (e)
C_M , sec $^{-1}$	64.0 (c)	148.6	148.9	87.0	148.9 (g)
C_O , sec $^{-1}$	19.6 (c)	47.1	45.6	26.7	—

(a) Various 5 parameter fits gave C_ω between 3.04×10^6 and 3.17×10^6 depending on what value for C_O or E_M was chosen. The value tabulated was determined from $\Delta\omega_{\text{obsd}}$ analysis and held constant in this fit.

(b) Held constant at the value given by 100 MHz fit A. When allowed to vary E_M was in the range 1.1 to 1.3 kcal mol $^{-1}$, depending on the C_O value used.

(c) The ratio of C_M to C_O was held constant at 3.26 as indicated by 100 MHz fit B. This is consistent with values of ~ 3 obtained for $\text{Ni}(\text{DMF})_6^{2+}$ in DMF and $\text{NiCRMe}(\text{DMF})_2^{2+}$ in DMF.

(d) Held constant at values indicated by 60 MHz chemical shifts to test for consistency of 60 and 100 MHz data. ΔH^\ddagger was fixed as indicated by 60 MHz $(T_{2P_M})^{-1}$ data.

(e) Held constant at value from fit A.

(f) Held constant at value from 60 MHz $(T_{2P_M})^{-1}$ fit.

(g) Held constant at value from fit B.

value is frequency dependent. It is apparent from Figure 16 that, although $(T_{2M})^{-1}$ is the major contribution to $(T_{2P}P_M)^{-1}$ for $T^{-1} \lesssim 3.4 \times 10^{-3} \text{ } ^\circ\text{K}^{-1}$, the 60 and 100 MHz data do not converge at high temperature. This behaviour has been observed for NiCR^{2+} in several solvents and is attributed to a frequency dependence of the correlation time controlling the $(T_{2M})^{-1}$ relaxation. This phenomenon will be discussed subsequently. It has been assumed that the outer sphere relaxation has the same frequency dependence.

The $(T_{2P}P_M)^{-1}$ results have been fitted to eq 2, modified by the addition of a $(T_{2O})^{-1}$ term, with certain restrictions applied to the parameters as given in Table X.

Since the observed downfield chemical shifts of the bulk solvent formyl proton resonance were large for this system, this data was also used to evaluate the exchange parameters and to obtain an independent measure of C_ω . In addition, the temperature dependence of the observed chemical shifts in the fast exchange region, where $\Delta\omega_{\text{obsd}}$ is theoretically defined by limiting conditions 25(a) and 25(b), was used to qualitatively assess the validity of the corrections which have been made for the diamagnetic-paramagnetic equilibrium. It should be recalled, however, that the $\Delta\omega_{\text{obsd}}$ values are not useful in determining the parameters C_M and E_M defining $(T_{2M})^{-1}$ due to the difficulty of resolving T_{2M} from τ_M . The $(\Delta\omega_{\text{obsd}}/P_M)$ data at 60 and 100 MHz, given in Figure 17, were fitted to eq 8 with the

assumption that the temperature dependence of $\Delta\omega_M$ is given by eq 11. The parameters defining $(T_{2M})^{-1}$ were taken from the appropriate $(T_{2P}^P)^{-1}$ fit. The results are shown in Table X and the smooth curves calculated from these parameters are drawn in Figure 17. It should be noted that the predicted values are slightly higher than the observed values at higher temperatures. The dashed lines extrapolated through the observed high temperature data indicate a shift of -185 Hz at $T^{-1} = 0^\circ\text{K}^{-1}$. This discrepancy may be due to a slight error in correcting for the diamagnetic species, or to a non-Curie dependence of the chemical shift. Since the maximum discrepancy is only 8%, it is not possible to decide between these two alternatives. It is gratifying to find that the ΔH^\ddagger and ΔS^\ddagger obtained from the shift data are in good agreement with the values from the line broadening results.

Comparison of the values given in Table X indicates that the kinetic parameters for DMF exchange can be reasonably given as $\Delta H^\ddagger = 9.5 \pm 0.5 \text{ kcal mol}^{-1}$ and $\Delta S^\ddagger = 2.2 \pm 1.0 \text{ cal mol}^{-1}\text{deg}^{-1}$. These are the average values from the fits in which both ΔH^\ddagger and ΔS^\ddagger were allowed to vary. From the values: $C_\omega = 3.08 \times 10^6 \text{ rad sec}^{-1}^\circ\text{K}$ at 60 MHz and $\mu_{\text{eff}} = 3.00 \text{ BM}$, the hyperfine coupling constant for the CH proton was calculated to be $2.30 \times 10^6 \text{ rad sec}^{-1}$.

NiCRMe(ClO₄)₂ in N,N-dimethylformamide

For the NiCRMe(ClO₄)₂-DMF system the temperature dependencies of $(T_{2M}^{P_M})^{-1}$ and $(\Delta\omega_{\text{obsd}}/P_M)$ for the formyl proton are shown in Figures 18 and 19, respectively. The values given have been corrected for the formation of the diamagnetic species using $\Delta H^\circ = -4.85 \text{ kcal mol}^{-1}$ and $\Delta S^\circ = -12.55 \text{ cal mol}^{-1}\text{deg}^{-1}$. This correction is negligible at temperatures below -25° , but increases from 3 to 52% as the temperature increases from -25° to 115°C .

The results are qualitatively similar to those for NiCR²⁺ in DMF except that the $(T_{2M})^{-1}$ controlled relaxation at high temperature is more pronounced and the $\tau_M \Delta\omega_M^2$ region is consequently less well defined. As a result, it is not possible to obtain a good value of C_ω from the $(T_{2P}^{P_M})^{-1}$ data and the value obtained from the chemical shift measurements has been used in all of the $(T_{2P}^{P_M})^{-1}$ fits summarized in Table XI. It should also be noted that in the low temperature region the data from the 60 and 100 MHz studies do not converge as would be expected for τ_M^{-1} control of $(T_{2P}^{P_M})^{-1}$. This result appears to be due to the frequency dependence of the outer sphere relaxation which is significant but not dominant when $T^{-1} > 4.6 \times 10^{-3} \text{ }^\circ\text{K}^{-1}$. As in the case of NiCR²⁺, it has been found that E_M appears slightly larger at 100 MHz than at 60 MHz. The use of the best fit value of E_M from the 60 MHz data for the 100 MHz data or *vice versa* leads to a significantly poorer fit and poorer

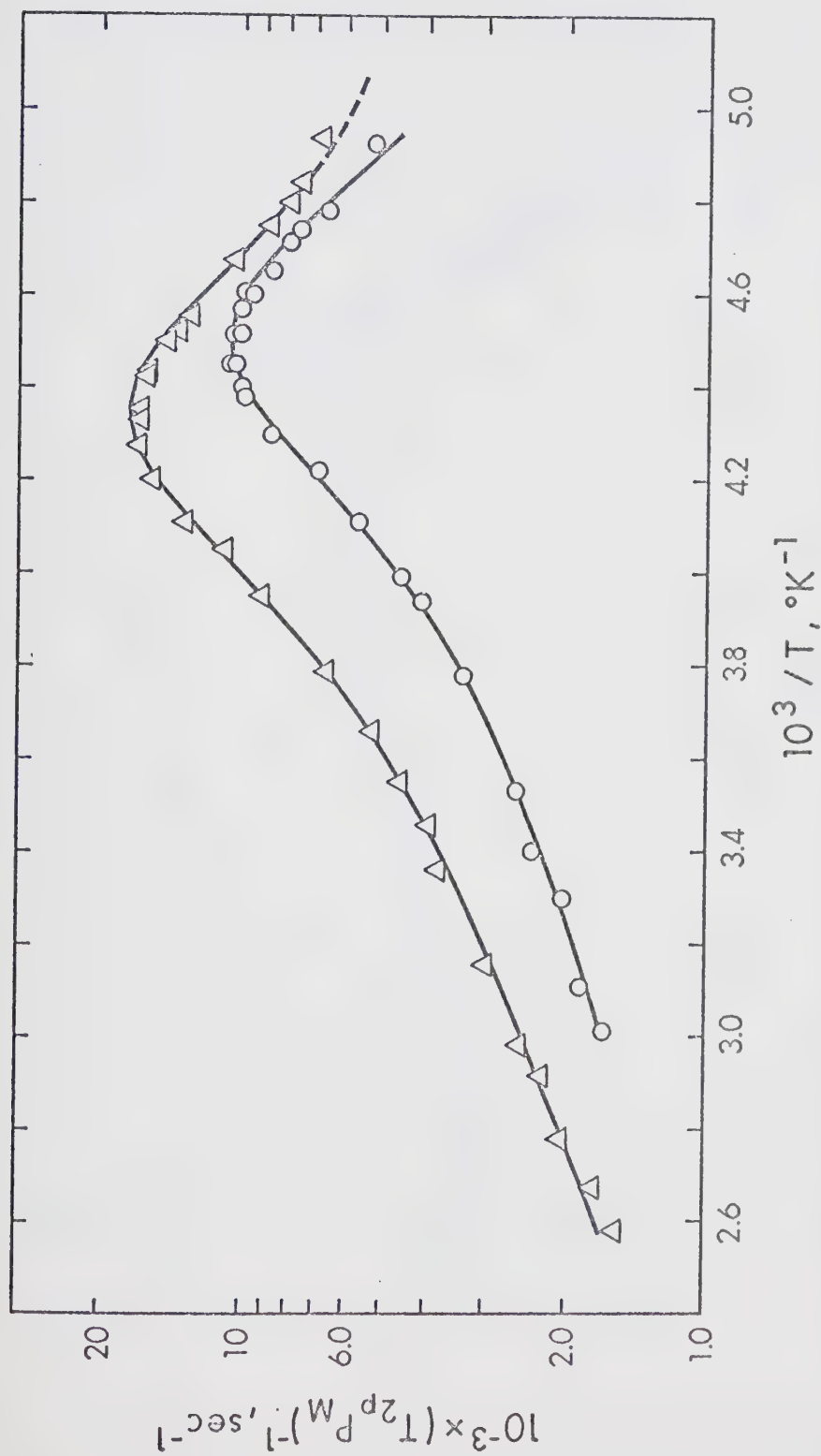


Figure 18: Temperature dependence of $-\log(T_{2pM})$ for the formyl proton in N,N-dimethylformamide solutions of $\text{NiCRMe}(\text{ClO}_4)_2$ at 100 MHz (Δ), and 60 MHz (\circ).

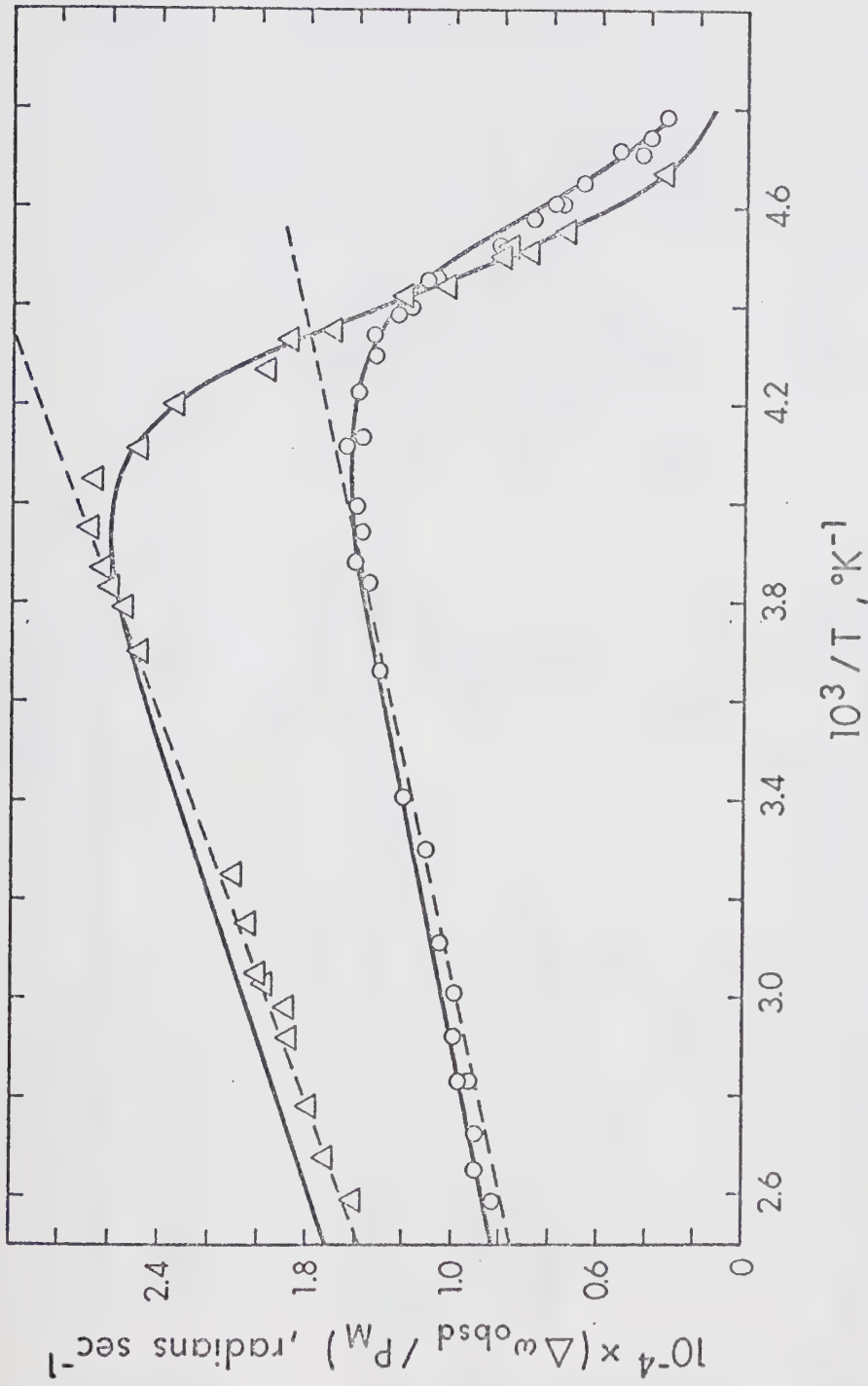


Figure 19: Temperature dependence of $(\Delta\omega_{\text{obsd}}/P_M)$ for the formyl proton in N,N-dimethylformamide solutions of $\text{NiCRM}(\text{ClO}_4)_2$ at 100 MHz (Δ), and 60 MHz (o). The significance of the dashed lines and solid curves is explained in the text.

TABLE XI

Least-squares best fit parameters for NiCRMe(ClO₄)₂ in N,N-dimethylformamide

	(T _{2P_M}) ⁻¹ Data			Δω _{obsd} Data	
	60 MHz	100 MHz	60 MHz	100 MHz	100 MHz
ΔH [‡] , kcal mol ⁻¹	7.84	7.86	8.15	7.24	7.84 (c)
ΔS [‡] , cal mol ⁻¹ deg ⁻¹	-2.84	-3.08	-0.65	-5.17	-2.52
10 ⁻⁶ x C _ω , rad sec ⁻¹ °K	4.06 (a)	6.77	4.06	6.86	6.86
E _M = E _O , kcal mol ⁻¹	1.35	1.77	1.35 (c)	1.77 (c)	1.77 (c)
C _M , sec ⁻¹	162.2	126.3 (b)	162.2 (c)	126.3 (c)	126.3 (c)
C _O , sec ⁻¹	53.4	41.5 (b)	—	—	—

(a) Held constant at value from 60 MHz Δω_{obsd} fit.

(b) The ratio of C_M to C_O was held constant at the value from the 60 MHz data.

(c) Held constant at value determined from the appropriate (T_{2P_M})⁻¹ data.

agreement between the ΔH^\ddagger and ΔS^\ddagger values from the two sets of data. This apparent frequency dependence of E_M will be discussed subsequently in connection with the frequency dependence of T_{2M} .

The chemical shift data were fitted as described above for the NiCR^{2+} -DMF system. For NiCRMe^{2+} in DMF, the high temperature chemical shifts at 60 and 100 MHz extrapolate to a shift of -520 Hz (dashed lines in Figure 19) rather than 0 when $T^{-1} = 0^\circ\text{K}^{-1}$. Again, this discrepancy might indicate non-Curie behaviour or may be due to a slight under correction for the diamagnetic-paramagnetic equilibrium. In any case the values of ΔH^\ddagger and ΔS^\ddagger are not significantly affected because the value of $\Delta\omega_M$, extrapolated in the region, $4.2 \times 10^{-3} \leq T^{-1} \leq 4.6 \times 10^{-3}$, is relatively insensitive to the assumed shift at $T^{-1} = 0^\circ\text{K}^{-1}$.

The values of ΔH^\ddagger and ΔS^\ddagger obtained from the shift and line broadening data are in good agreement. The average values from the fits in Table XI are $\Delta H^\ddagger = 7.8 \pm 0.5 \text{ kcal mol}^{-1}$ and $\Delta S^\ddagger = -2.9 \pm 2.5 \text{ cal mol}^{-1}\text{deg}^{-1}$. A value of $3.03 \times 10^6 \text{ rad sec}^{-1}$ is obtained for the hyperfine coupling constant for the formyl proton from both the 60 MHz and 100 MHz chemical shifts if μ_{eff} is taken as 3.00 BM in eq 10.

$\text{NiCR}(\text{BF}_4)_2$ and $\text{NiCRMe}(\text{BF}_4)_2$ in Water

The line broadening and chemical shift results for

$\text{NiCR}(\text{BF}_4)_2$ and $\text{NiCRMe}(\text{BF}_4)_2$ in water, corrected for the diamagnetic-paramagnetic equilibrium, are given in Figures 20, 21 and 22. The corrections were made using $\Delta H^\circ = -6.39$ kcal mol⁻¹ and $\Delta S^\circ = -17.9$ cal mol⁻¹deg⁻¹ for NiCR^{2+} , and $\Delta H^\circ = -4.58$ kcal mol⁻¹ and $\Delta S^\circ = -15.3$ cal mol⁻¹deg⁻¹ for NiCRMe^{2+} .

The solutions used to obtain the experimental data for these aqueous systems were unbuffered at pH \approx 4. Two samples, adjusted to pH 1.6 and 7.6, showed no difference in the line broadening. Both the perchlorate and tetrafluoroborate salts of NiCR^{2+} gave the same results, within experimental error.

It should be noted that no chemical shifts were observed in the NiCRMe^{2+} system. This result is probably due to the smaller percentage of paramagnetic form of NiCRMe^{2+} than NiCR^{2+} (52% versus 81% at 25°C). Thus the observed upfield chemical shifts of 3-9 Hz in the NiCR^{2+} system would be less than 5 Hz for NiCRMe^{2+} , even if the hyperfine coupling constants were the same.

The temperature dependence of $(T_{2P}^{\text{PM}})^{-1}$ in water is similar to that in DMF, however, no τ_M^{-1} controlled region is observed because of the more limited liquid range in water. With the limiting conditions: τ_M^{-2} , $(T_{2M}\tau_M)^{-1} \gg (T_{2M})^{-2}$, which are a combination of limiting conditions 25(a) and 25(b), eq 2 reduces to

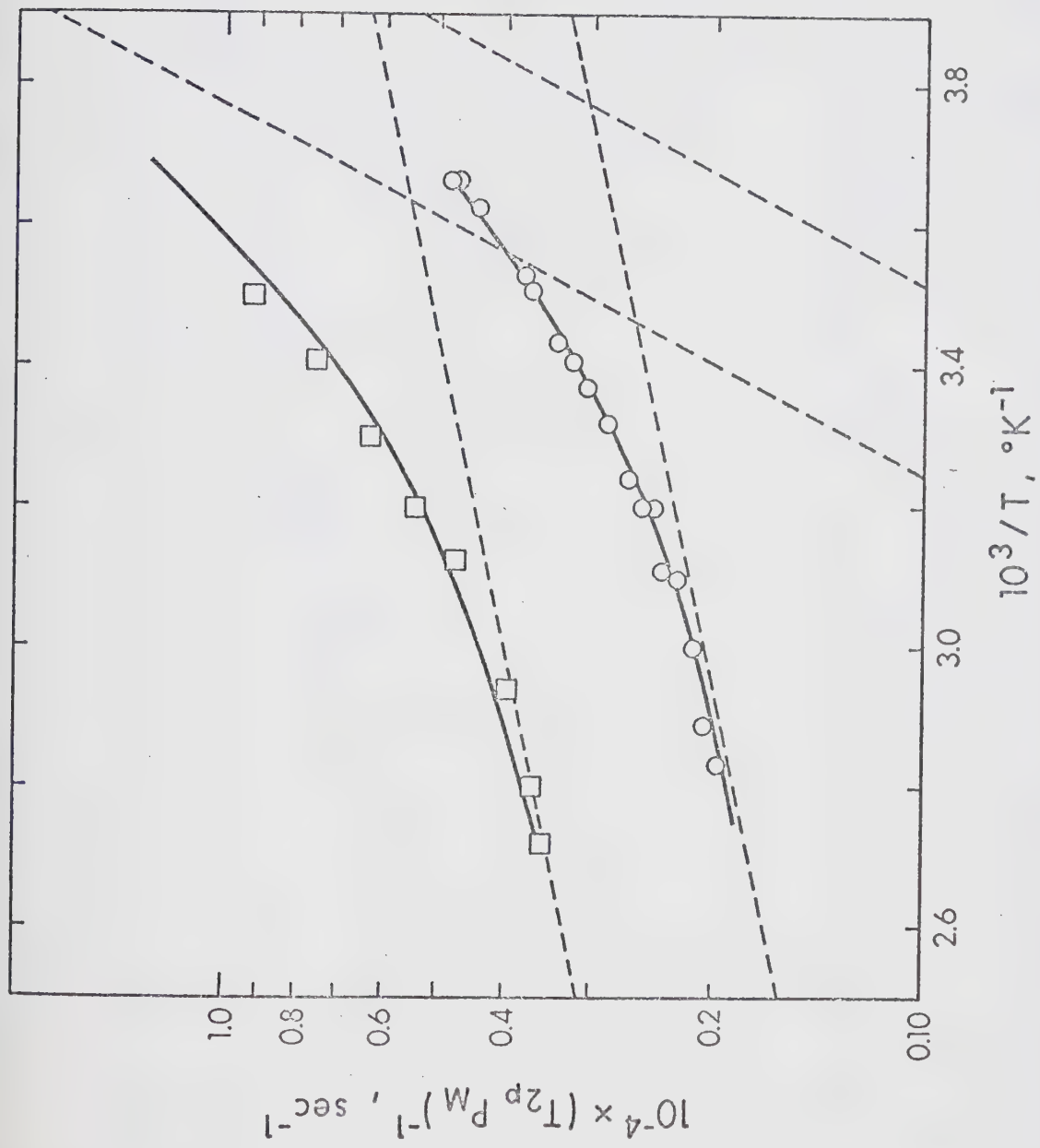


Figure 20: Temperature dependence of $-\log (T_{2p} P_M)$ for the water proton in aqueous solutions of $\text{NiCR}(\text{BF}_4)_2$ at 100 MHz (□), and 60 MHz (○). The dashed lines represent the $((T_{2M})^{-1} + (T_{2O})^{-1})$ and $\tau_M^2 \Delta \omega_M^2$ contributions.

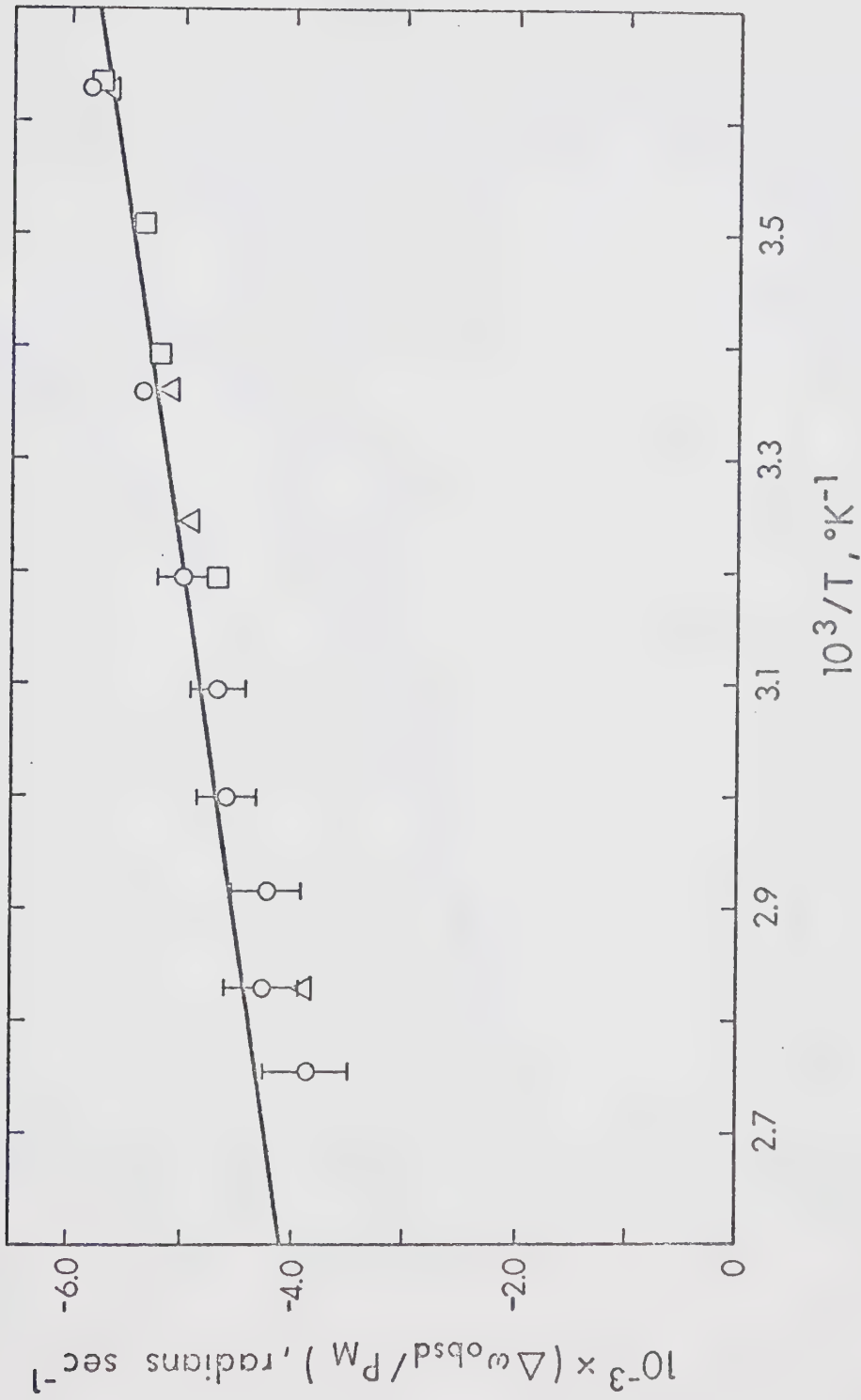


Figure 21: Temperature dependence of $(\Delta\omega_{\text{obsd}}/P_M)$ at 60 MHz for the water proton in aqueous solutions of $\text{NiCR}(\text{BF}_4)_2$. The result of a ± 0.5 Hz error in the measured shifts at high temperature are indicated.

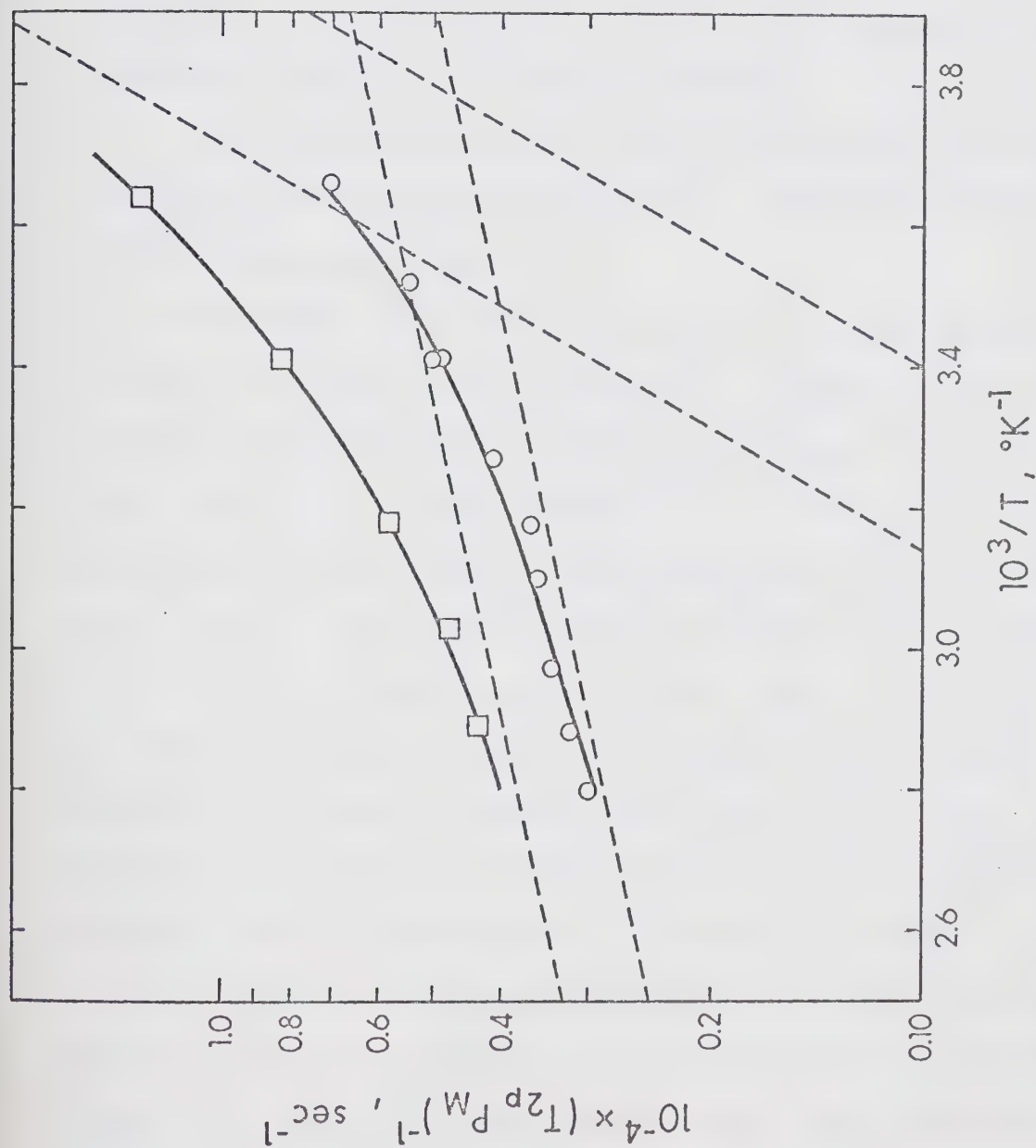


Figure 22: Temperature dependence of $-\log (T_{2p} P_M)$ for the water proton in aqueous solutions of $\text{NiCRMe}(\text{BF}_4)_2$ at 100 MHz (□), and 60 MHz (○). The dashed lines represent the $((T_{2M})^{-1} + (T_{2O})^{-1})$ and $\tau_M \Delta\omega_M^2$ contributions.

$$(T_{2P}^M)^{-1} = (T_{2M})^{-1} + \tau_M \Delta\omega_M^2 + (T_{2O})^{-1} \quad (49)$$

The term $(T_{2O})^{-1}$ is added to account for the outer sphere broadening but it is obvious that $(T_{2O})^{-1}$ cannot be distinguished from $(T_{2M})^{-1}$ for this system.

The chemical shifts for NiCR^{2+} do not show chemical exchange effects since $(\tau_M \Delta\omega_M)^2 \ll 1$ and consequently they are described by eq 11.

The results for NiCR^{2+} in water have been analyzed in terms of eq 49, with C_ω fixed at a value of -1.5×10^6 rad sec $^{-1}$ °K, as determined from the chemical shift measurements, and $E_M = E_O$ held constant at 1.0 kcal mol $^{-1}$. The least-squares fit of the 60 MHz data gave $\Delta H^\ddagger = 6.81$ kcal mol $^{-1}$, $\Delta S^\ddagger = -14.2$ cal mol $^{-1}$ deg $^{-1}$ and $(C_M + C_O) = 454.8$ sec $^{-1}$. The 100 MHz data were fitted with C_ω , $E_M = E_O$ and ΔH^\ddagger held constant at -2.5×10^6 rad sec $^{-1}$ °K, 1.0 kcal mol $^{-1}$ and 6.81 kcal mol $^{-1}$, respectively, and ΔS^\ddagger and $(C_M + C_O)$ varied to give the best fit values of -14.5 cal mol $^{-1}$ deg $^{-1}$ and 886.4 sec $^{-1}$, respectively. The good agreement between the ΔS^\ddagger values is at least partly fortuitous but it provides some justification for the assumption made regarding the $(T_{2M})^{-1}$ and $(T_{2O})^{-1}$ activation energy. From the above value of C_ω at 60 MHz and $\mu_{\text{eff}} = 3.00$ BM, the hyperfine coupling constant for this system is calculated to be -1.1×10^6 rad sec $^{-1}$.

The behaviour of $(T_{2P}P_M)^{-1}$ for NiCRMe^{2+} in water is very similar to that for NiCR^{2+} . However, due to the absence of chemical shifts, $\Delta\omega_M$ could not be determined and the exchange rate parameters cannot be extracted from the results. However, if it is assumed that the ratio of C_ω for NiCR^{2+} and NiCRMe^{2+} is the same in water and DMF, then the 60 MHz and 100 MHz data can be fitted with $\Delta H^\ddagger = 6.3$ kcal mol⁻¹, $\Delta S^\ddagger = -15.8$ cal mol⁻¹deg⁻¹, $E_M = 1.0$ kcal mol⁻¹. The value of $(C_M + C_O)$ is 6.97×10^2 sec⁻¹ and 9.29×10^2 sec⁻¹ at 60 and 100 MHz, respectively. These parameters were estimated by a graphical fit of the data according to the $((T_{2M})^{-1} + (T_{2O})^{-1})$ and $\tau_M \Delta\omega_M^2$ contributions shown in Figure 22, and are only included to show that the absence of any observed shift does not necessarily imply any unusual difference between NiCR^{2+} and NiCRMe^{2+} in water.

It should be noted that, for the aqueous systems, an alternative explanation based only on $(T_{2M})^{-1}$ control of $(T_{2P}P_M)^{-1}$ is possible, in principle. However, detailed consideration of this mechanism, given at the end of this section, indicates that this possibility will not quantitatively explain the results.

$\text{NiCR}(\text{PF}_6)_2$ in Acetonitrile

The variations of $-\log(T_{2P}P_M)$ and $(\Delta\omega_{\text{obsd}}/P_M)$ with T^{-1} for $\text{NiCR}(\text{PF}_6)_2$ in acetonitrile at 60 and 100 MHz are

shown in Figures 23 and 24, respectively. For this system, the equilibrium concentration of paramagnetic $\text{NiCR}(\text{CH}_3\text{CN})_2(\text{PF}_6)_2$ species was calculated at each temperature using, in eq 48, $-4.16 \text{ kcal mol}^{-1}$ and $-10.8 \text{ cal mol}^{-1}\text{deg}^{-1}$ for ΔH° and ΔS° , respectively. The values of P_M were calculated from eq 47 assuming $n=2$. As a result of the inclusion of the temperature dependence of the diamagnetic-paramagnetic equilibrium, the chemical shifts shown in Figure 24 adhere perfectly to a Curie law temperature dependence.

The temperature dependencies of $(T_{2P}P_M)^{-1}$ at the two frequencies are essentially the same as those observed previously for NiCR^{2+} and NiCRMe^{2+} in water. The line broadening is determined by $\tau_M \Delta\omega_M^2$ at low temperature and by the frequency dependent T_{2M} relaxation at high temperature. The complete temperature dependence is described by eq 49. However, in the present case, the low temperature line broadening region of kinetic interest is better defined due to the longer liquid range of acetonitrile. Also, for this system, the observed upfield chemical shifts were large and these permitted an accurate measurement of A/\hbar which is necessary for determining the kinetic parameters.

Both the 60 and 100 MHz $(T_{2P}P_M)^{-1}$ data were fitted by least-squares analysis to eq 49, with C_ω held constant at the values calculated from the chemical shifts. The best-fit parameters are given in Table XII (fits A and C). It should be noted that, despite the agreement of E_M at the

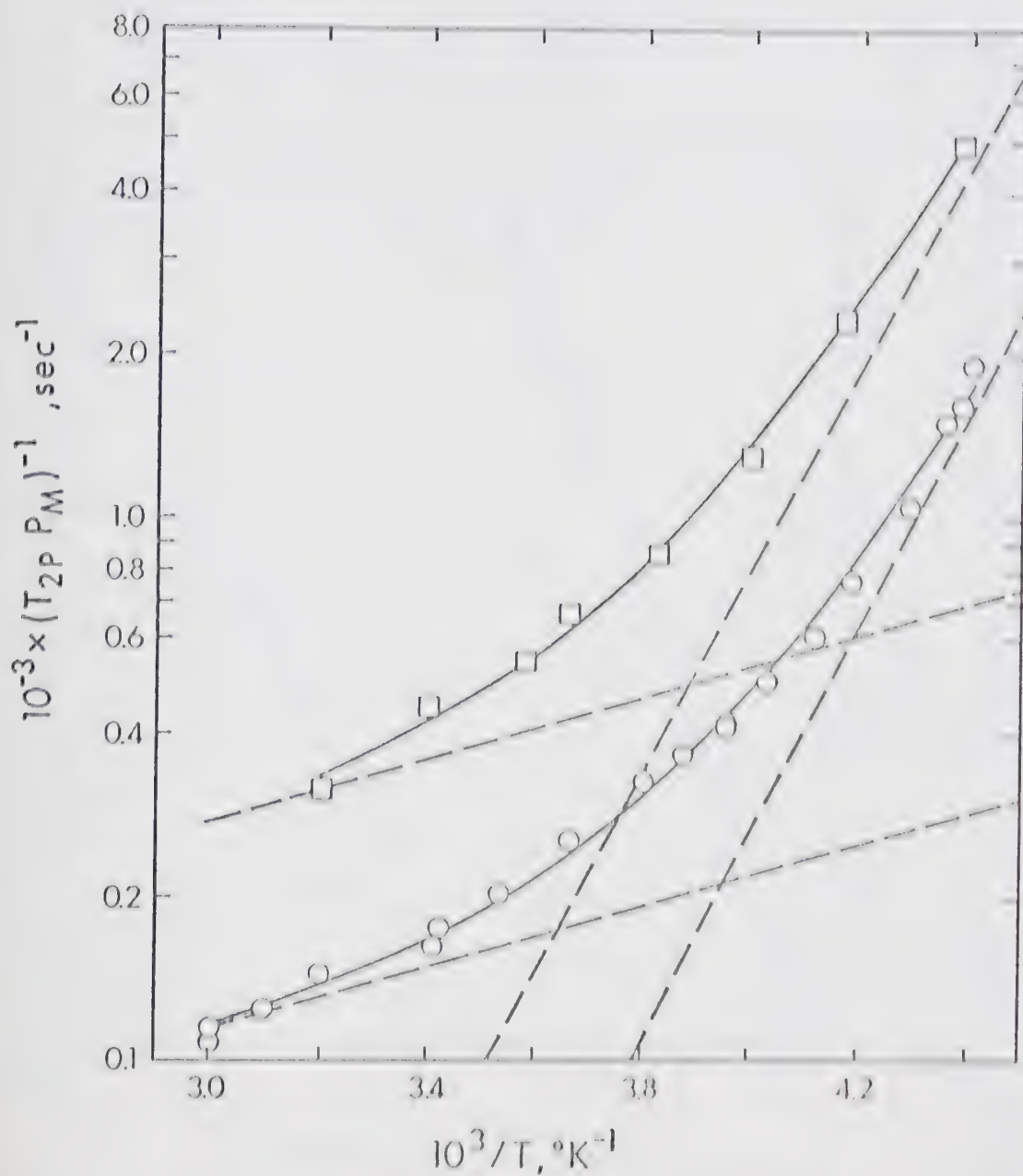


Figure 23: Temperature dependence of $-\log (T_2 P_M)$ for the methyl protons in acetonitrile solutions of $\text{NiCl}_2(\text{PF}_6)_2$ at 100 MHz (\circ), and 60 MHz (\square). The dashed lines represent the $(T_{2M})^{-1}$, $(T_{2O})^{-1}$ and $\tau_M \omega_M^2$ contributions.

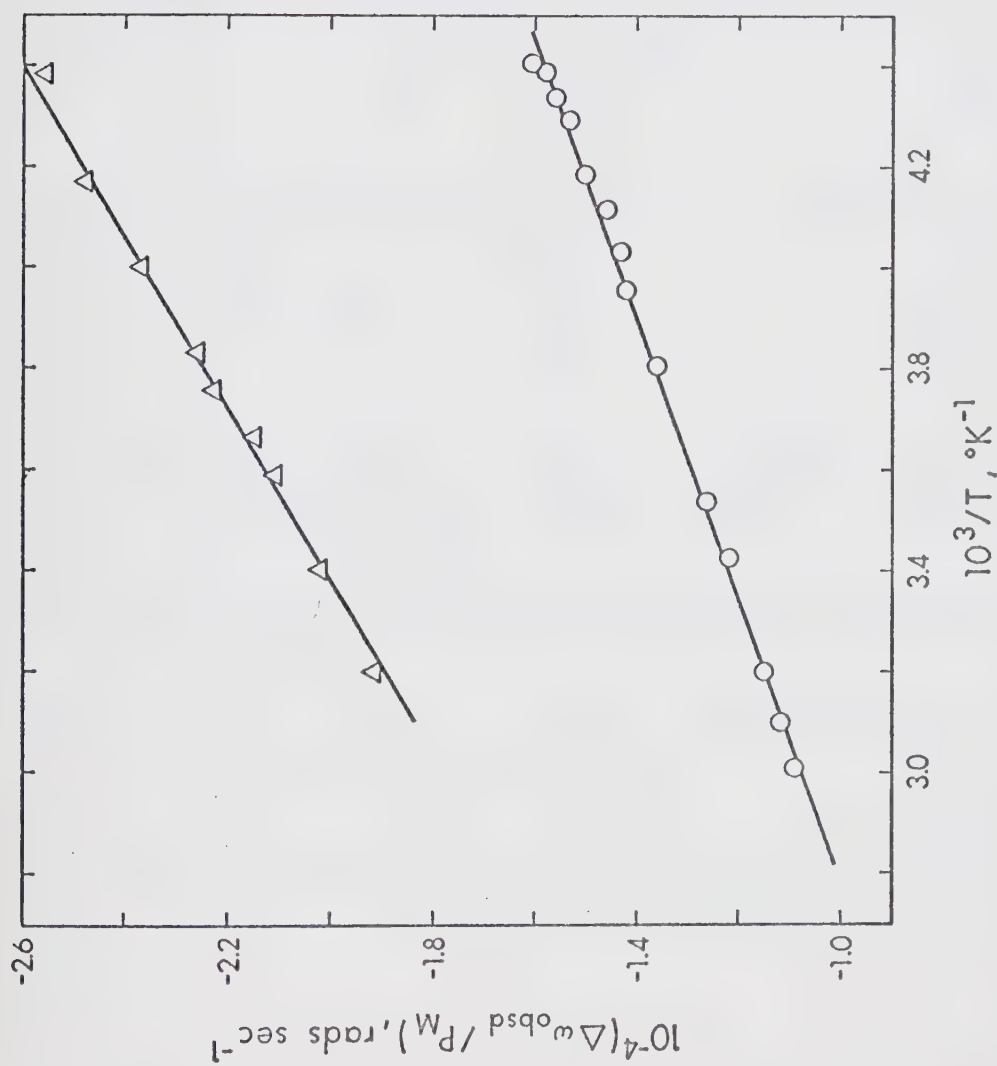


Figure 24: Temperature dependence of $(\Delta\omega_{\text{obsd}}/P_M)$ for the methyl protons in acetonitrile solutions of $\text{NiCR}(\text{PF}_6)_2$ at 100 MHz (Δ), and 60 MHz (o).

two frequencies, the values of ΔH^\ddagger and ΔS^\ddagger from the two data sets are not in acceptable agreement. Furthermore, since the $\tau_M \Delta \omega_M^2$ and $(T_{2M})^{-1}$ contributions to the line broadening are not well separated, a large value of 2.4 kcal mol⁻¹ was obtained for E_M in these fits. For the previously discussed NiCR^{2+} -DMF system, and for NiCR^{2+} in methanol, the results of which will be given subsequently, the $(T_{2M})^{-1}$ region of line broadening was better defined. Values of 1.0 to 1.3 kcal mol⁻¹ were observed for E_M in the latter two systems. Consequently, to resolve the difference between the kinetic parameters in fits A and C, the two sets of $(T_{2P}^P)^{-1}$ data were refitted using progressively lower values for E_M . As shown by fits B and D, acceptable agreement of ΔH^\ddagger and ΔS^\ddagger between the two data sets was obtained for $E_M = 1.33$ kcal mol⁻¹. The calculated curves for the latter two fits are shown in Figure 23.

Therefore, for NiCR^{2+} in acetonitrile, the $(T_{2P}^P)^{-1}$ data at the two frequencies are most consistent with values of 7.0 kcal mol⁻¹ and -3.6 cal mol⁻¹deg⁻¹ for ΔH^\ddagger and ΔS^\ddagger , respectively. Due to the difficulty of separating the two frequency dependent contributions to $(T_{2P}^P)^{-1}$, the errors on ΔH^\ddagger and ΔS^\ddagger are uncertain. From the measured chemical shifts, $(A/\hbar)_{\text{CH}_3}$ was calculated to be -2.66×10^6 rad sec⁻¹.

NiCR^{2+} in Methanol

Plots of $-\log(T_{2P}^P)$ versus T^{-1} at 60 and 100 MHz for the methyl and hydroxy protons of methanol solutions of

NiCR^{2+} are shown in Figures 25 and 26, respectively. The temperature dependencies of the chemical shifts for the two protons, each at 60 and 100 MHz, are shown in Figures 27 and 28, respectively. All of the data have been adjusted to include the effect of the diamagnetic-paramagnetic equilibrium on P_M , using $\Delta H^\circ = -4.26 \text{ kcal mol}^{-1}$ and $\Delta S^\circ = -11.5 \text{ cal mol}^{-1}\text{deg}^{-1}$ in eq 48.

Most of the line width and chemical shift data for this system were obtained using solutions of the tetrafluoroborate salt due to its greater solubility in methanol. Dilute solutions contained anhydrous 2,4-dinitrobenzenesulfonic acid, which was necessary to collapse the coupling of the OH and CH_3 protons. The absence of an acid dependence for this system was confirmed by comparing the results from more concentrated solutions of $\text{NiCR}(\text{BF}_4)_2$, requiring no acid, with the results from the acidified solutions. Some chemical shift measurements were also made on solutions of the nitrate and hexafluoroantimonate salts of NiCR^{2+} and these were found to be in agreement with the results for the BF_4^- salt. The latter solutions did not contain acid and this precluded a measurement of the true line widths.

Aside from the $(T_{2M})^{-1}$ frequency dependence, which is observed for NiCR^{2+} in various solvents, this system is very unusual in that both the $(T_{2P}^{P_M})^{-1}$ and $(\Delta\omega_{\text{obsd}}/P_M)$ data for the OH and CH_3 protons are vastly different. It should be noted from Figures 27 and 28 that the OH proton

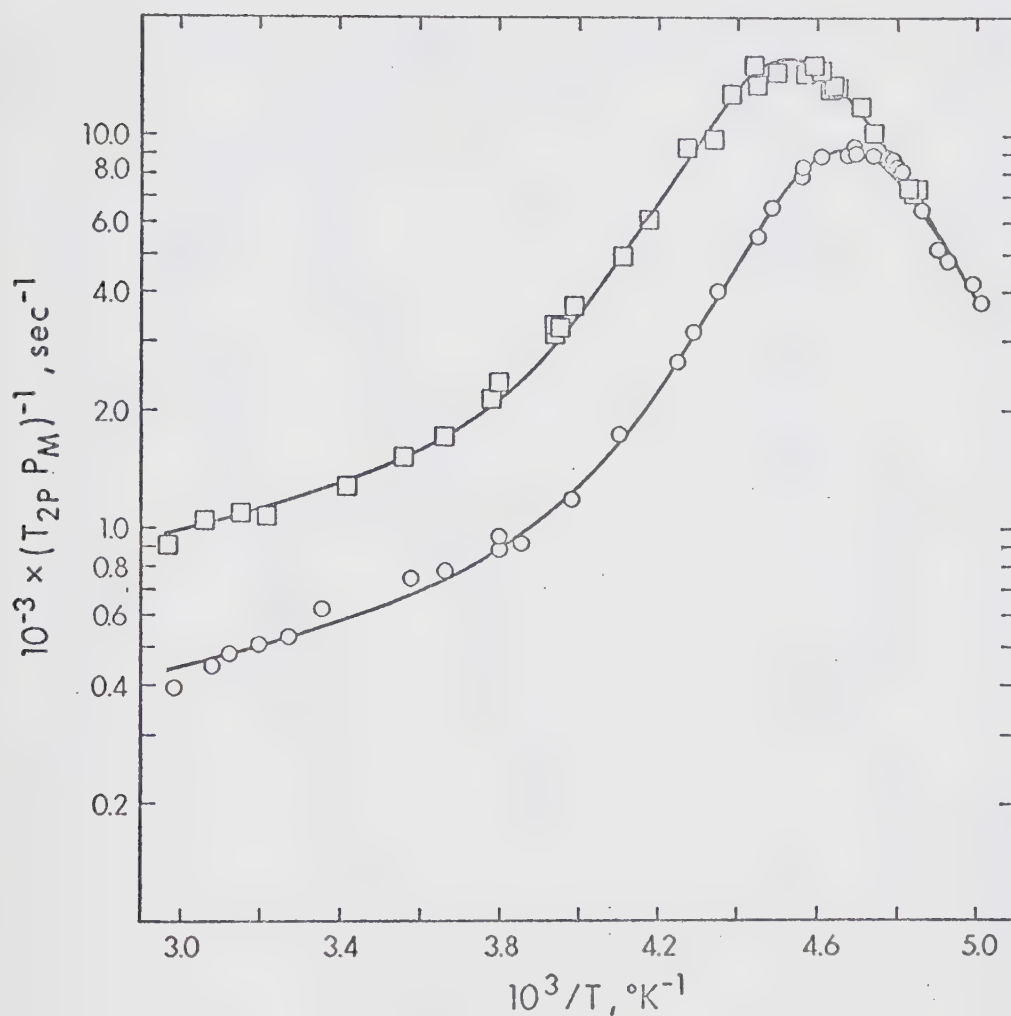


Figure 25: Temperature dependence of $-\log(T_{2P}P_M)$ for the methyl protons of methanol solutions of $\text{NiCR}(\text{BF}_4)_2$ at 60 MHz (o) and 100 MHz (□).

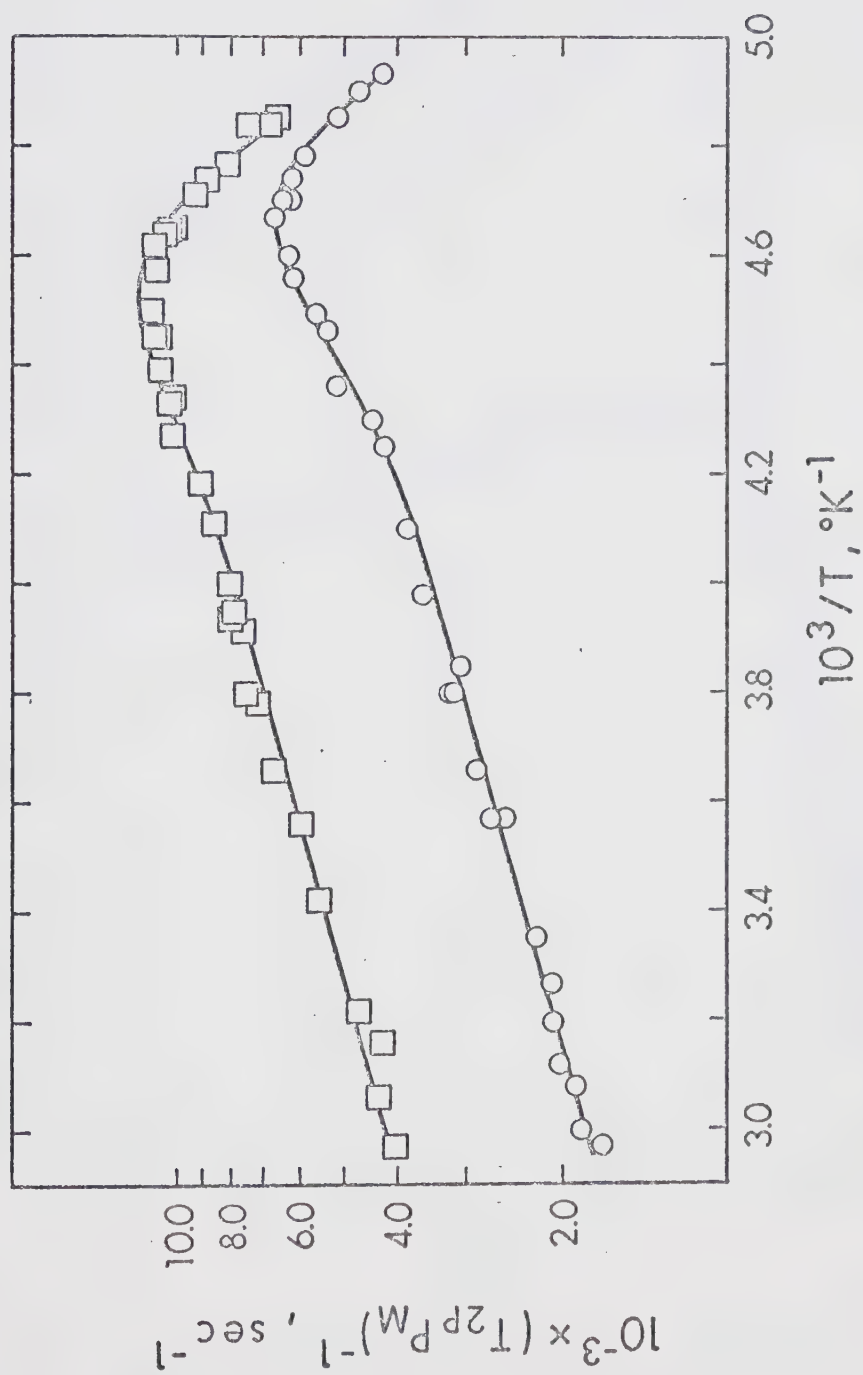


Figure 26: Temperature dependence of $-\log(T_{2P_M})$ for the hydroxy proton of methanol solutions of $\text{NiCR}(\text{BF}_4)_2$ at 60 MHz (o) and 100 MHz (□).

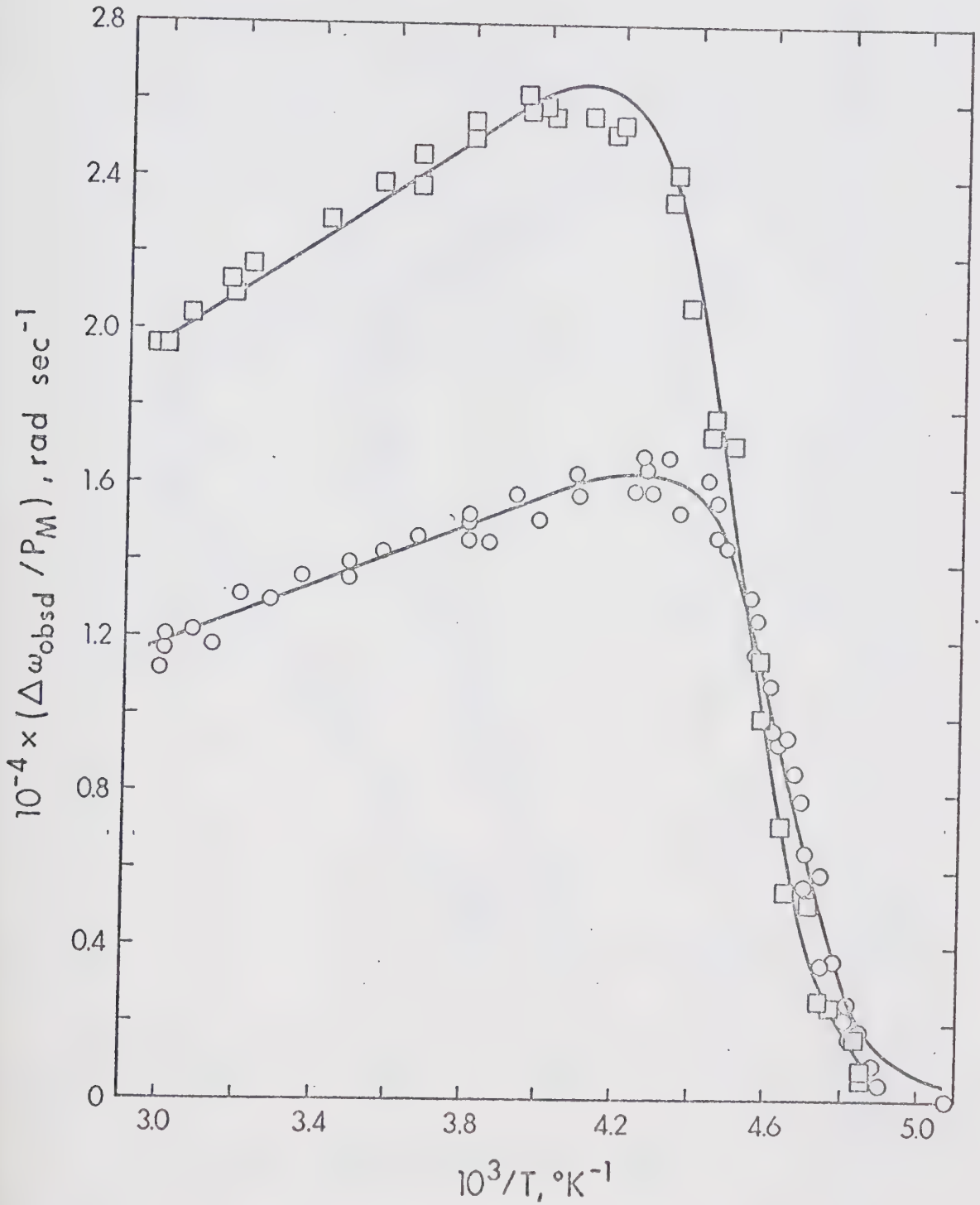


Figure 27: Temperature dependence of $(\Delta\omega_{\text{obsd}}/P_M)$ for the methyl protons of methanol solutions of $\text{NiCR}(\text{BF}_4)_2$ at 60 MHz (o) and 100 MHz (□).

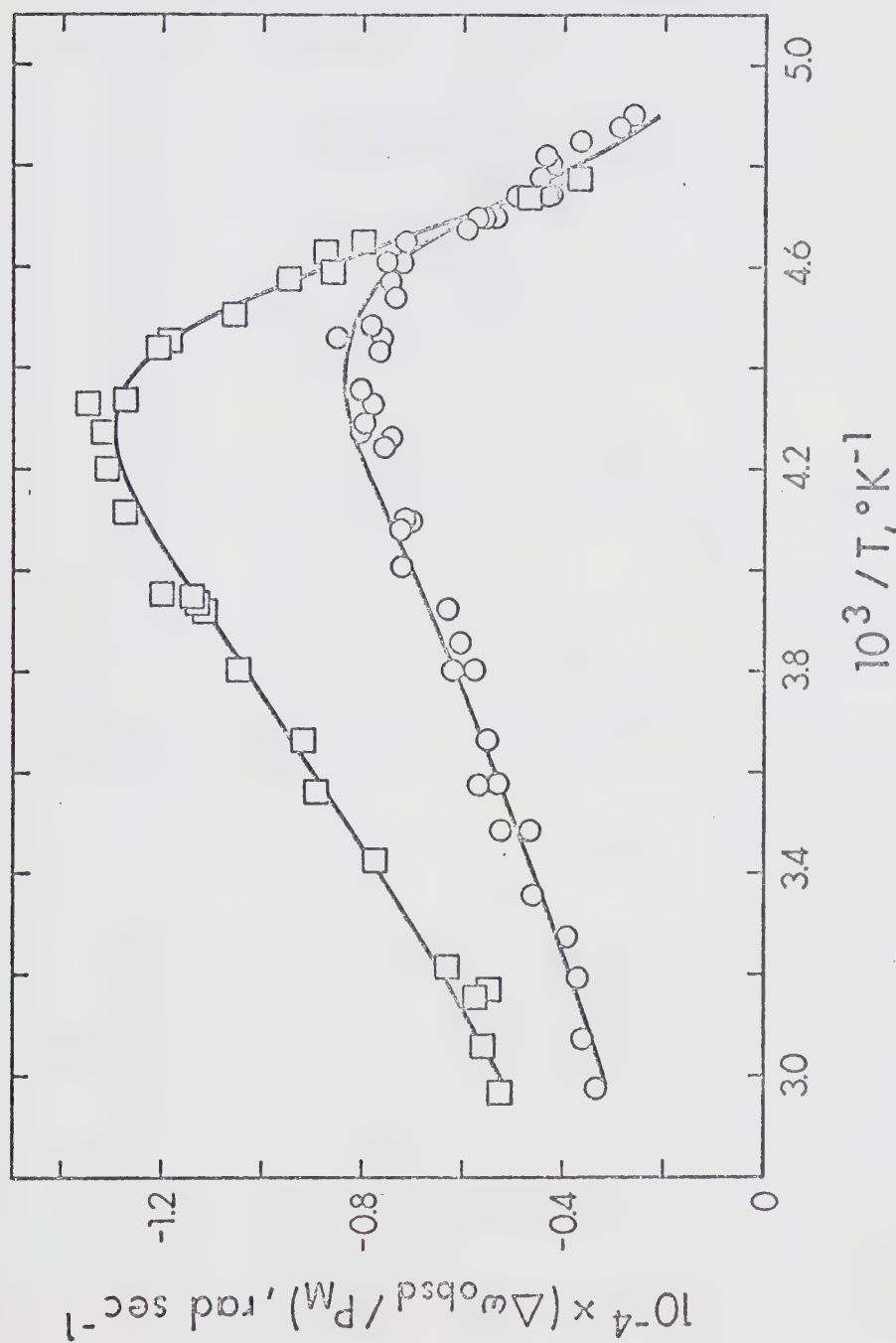


Figure 28: Temperature dependence of $(\Delta\omega_{\text{obsd}}/P_M)$ for the hydroxy proton of methanol solutions of $\text{NiCR}(\text{BF}_4)_2$ at 60 MHz (\circ) and 100 MHz (\square).

TABLE XIII

Least-squares parameters of the $(T_{2P_M})^{-1}$ and $(\Delta\omega_{\text{obsd}/P_M})$ data for NiCr^{2+} in methanol

Data	Proton	Frequency	Fit	$\Delta H, \ddagger$ kcal mol ⁻¹	$\Delta S, \ddagger$ cal mol ⁻¹ deg ⁻¹	C_M' sec ⁻¹	E_M' kcal mol ⁻¹	$10^{-6} \times C_\omega'$ rad sec ⁻¹ °K
$(T_{2P_M})^{-1}$	CH ₃	60 MHz	A	9.21	4.65	59.5	1.15 (a)	3.81
		100 MHz	B	9.52	6.12	58.9	1.15 (a)	3.96 (b)
			C	9.28 (c)	4.61	130.9	1.15 (a)	6.65
$\Delta\omega_{\text{obsd}/P_M}$	CH ₃	60 MHz	D	9.70	6.68	58.9 (d)	1.15 (d)	3.96
		100 MHz	E	9.28 (c)	4.53	130.9 (d)	1.15 (d)	6.57
$(T_{2P_M})^{-1}$	OH	60 MHz	F	9.28 (c)	4.66	284.3	1.17	— (e)
		100 MHz	G	9.28 (c)	4.57	639.8	1.18	— (e)
$\Delta\omega_{\text{obsd}/P_M}$	OH	60 MHz	H	9.28 (c)	5.36	284.3 (d)	1.17 (d)	— (e)
		100 MHz	I	9.28	5.52	639.8 (d)	1.18 (d)	— (e)

(a) This activation energy was obtained from fits of the 60 and 100 MHz OH proton $(T_{2P_M})^{-1}$ data for which ΔH^\ddagger was held constant at 9.52 kcal mol⁻¹.

(b) The value obtained from an analysis of the $(\Delta\omega_{\text{obsd}/P_M})$ data and held constant.

(c) The value obtained from an analysis of the 100 MHz $(\Delta\omega_{\text{obsd}/P_M})$ data and held constant.

(d) The parameters defining $(T_{2M})^{-1}$ were obtained from the least-squares fit of the $(T_{2P_M})^{-1}$ data at the appropriate frequency and were held constant in this fit.

(e) For the OH proton, the temperature dependence of $\Delta\omega_M$ given by $\Delta\omega_M = \frac{C_1}{T} + \frac{C_2}{T^2}$ was used. The constants, C_1 and C_2 , were restrained at the values given in the text.

chemical shifts are much smaller than those for the CH_3 proton, and also that the two different protons are shifted in opposite directions. The CH_3 proton resonance in methanol solutions of NiCR^{2+} is shifted downfield and the OH proton resonance is shifted upfield, relative to their diamagnetic positions in a blank methanol solution at the same temperature. This opposite sign of $\Delta\omega_{\text{obsd}}$ was maintained throughout the range of temperatures investigated. The temperature dependence of $(\Delta\omega_{\text{obsd}}/P_M)$ for the two protons at high temperature is also different. With the inclusion of the temperature dependence of the diamagnetic-paramagnetic equilibrium, the CH_3 proton chemical shifts at high temperature behave normally according to a Curie law temperature dependence. On the other hand, the OH proton frequency shifts in the fast exchange limit decrease more rapidly with increasing temperature. These differences in the behaviour of the chemical shifts of the two protons are attributed to a large upfield shift from a pseudocontact mechanism for the OH proton, the overall temperature dependence of which includes both T^{-1} and T^{-2} contributions (See eq 12). For the CH_3 protons, the downfield chemical shifts arise solely from the contact mechanism having only a T^{-1} temperature dependence. A further discussion of this pseudocontact shift of the OH proton will be given subsequently.

The temperature dependence of $(T_{2P}P_M)^{-1}$ for the CH_3

protons is qualitatively similar to that observed for the CH proton in DMF solutions of NiCR^{2+} and the same interpretation of the three limiting regions of line broadening applies. For the OH proton, the same processes account for the temperature dependence of $(T_{2P}P_M)^{-1}$, but due to the larger value of $(T_{2M})^{-1}$, and the apparently smaller value of $\Delta\omega_M$ for the OH proton than for the CH_3 protons, the $\tau_M\Delta\omega_M^2$ contribution is not resolved from the frequency dependent $(T_{2M})^{-1}$ contribution. A comparison of the data of Figures 25 and 26 shows that the same frequency dependence of $(T_{2M})^{-1}$ is observed for both protons. The poor separation of the relaxation processes for the OH proton, and the limited temperature range over which limiting condition 25(c) applies, prevents an independent determination of both ΔH^\ddagger and ΔS^\ddagger for the solvent exchange reaction using the OH data. However, it will be shown below that the exchange contributions to the line broadening and frequency shifts for both OH and CH_3 protons are completely consistent with only whole methanol molecule exchange.

The 60 and 100 MHz $(T_{2P}P_M)^{-1}$ methyl proton data were fitted to eq 2, modified by the addition of a $(T_{2O})^{-1}$ term. Since the outer sphere line broadening region was not experimentally attainable, a reasonable estimate of the magnitude of this contribution was made. In this regard, it was assumed that $E_O = E_M$ and that the ratio, $(T_{2M})_{\text{CH}_3}^{-1} : (T_{2O})_{\text{CH}_3}^{-1}$, has a value of ~ 3.1 . This value was estimated

from the T_{1M} measurements for nickel(II) in methanol, given in Figure 4 of ref 23. The $(\Delta\omega_{\text{obsd}}/P_M)$ measurements at each frequency were fitted to eq 8. In all of these fits of the CH_3 proton data, the temperature dependence of $\Delta\omega_M$ given by eq 11 was used. The results of the least-squares fits are summarized in Table XIII. It should be noted that a value of $1.15 \text{ kcal mol}^{-1}$ was used for the $(T_{2M})^{-1}$ activation energy as indicated by the OH proton $(T_{2P}P_M)^{-1}$ data. It is felt that this is justifiable since this parameter is more precisely defined for the OH proton due to the long temperature region in which only $(T_{2M})^{-1}$ contributes significantly. The OH proton data are also more accurate in this region due to the larger experimental line widths. The agreement in the parameters ΔH^\ddagger , ΔS^\ddagger and C_ω obtained from the various data sets is satisfactory and provides justification for the assumptions made.

In the case of the OH proton, the $(T_{2P}P_M)^{-1}$ and $(\Delta\omega_{\text{obsd}}/P_M)$ data were also fitted to eq 2 and 8, respectively, with the temperature dependence of $\Delta\omega_M$, according to eq 12, being now given by

$$\Delta\omega_M = \frac{c_1}{T} + \frac{c_2}{T^2} \quad (50)$$

The first term of eq 50 contains the combined contributions of the contact shift and the portion of the pseudocontact shift with a T^{-1} temperature dependence. The second term

of eq 50 arises only from the pseudocontact shift mechanism. In terms of the constants in eq 10 and 12, c_1 and c_2 are defined by

$$c_1 = - \left\{ \frac{A}{h} \frac{\omega_o \mu_{\text{eff}} \sqrt{S(S+1)}}{3k\gamma_I} + \frac{2\beta^2 \omega_o (g_{\parallel}^2 - g_{\perp}^2) (3\cos^2 \Omega - 1)}{9kR^3} \right\} \quad (51-a)$$

$$c_2 = \frac{2\beta^2 \omega_o D (g_{\parallel}^2 + g_{\perp}^2) (3\cos^2 \Omega - 1)}{27k^2 R^3} \quad (51-b)$$

The constants c_1 and c_2 were obtained from the intercept and slope, respectively, of a plot of $-(\Delta\omega_{\text{obsd}}/P_M)T$ versus T . This plot is linear in the high temperature region where $\Delta\omega_{\text{obsd}}/P_M = -\Delta\omega_M$. At 100 MHz, the constants are: $c_1 = -2.0 \times 10^6 \text{ rad sec}^{-1} \text{ } ^\circ\text{K}$ and $c_2 = 1.25 \times 10^9 \text{ rad sec}^{-1} \text{ } ^\circ\text{K}^2$. At 60 MHz, c_1 and c_2 are predicted to be 6/10 of the above values. An independent determination of c_1 and c_2 from the less accurate 60 MHz OH proton frequency shifts was not attempted, but no anomalies were introduced in the fitting process by assuming that these constants at 60 MHz are 6/10 of the values at 100 MHz.

The appropriate values of c_1 and c_2 were held constant in all fits of the 60 and 100 MHz $(T_{2P}^{P_M})^{-1}$ and $(\Delta\omega_{\text{obsd}}/P_M)$ data. As in the case of the fits of the CH_3 proton $(T_{2P}^{P_M})^{-1}$ results, an estimate of the outer sphere broadening contribution was made. Since the ratios $(T_{2M}^{\text{OH}})^{-1} : (T_{2M}^{\text{CH}_3})^{-1}$ and

$(T_{20})_{\text{OH}}^{-1} : (T_{20})_{\text{CH}_3}^{-1}$ have been observed in several instances^{23,46} to be 5.0 and 1.64, respectively, for systems in which dipolar interactions account for both inner and outer sphere broadening, these ratios along with the ratio, $(T_{2M})_{\text{CH}_3}^{-1} : (T_{20})_{\text{CH}_3}^{-1} \approx 3.1$, were used to estimate the magnitude of the $(T_{20})^{-1}$ term for the OH proton in the NiCR^{2+} -methanol system. Assuming that $E_O = E_M$, $C_O:C_M$ was estimated to be 0.106 and this value was used in the fitting process. Since it was not possible to obtain an independent value of ΔH^\ddagger from fits of the OH proton $(T_{2P}^{\text{PM}})^{-1}$ data, for reasons discussed earlier, the value of ΔH^\ddagger obtained from the analysis of the CH_3 proton results was used. The best-fit values of the adjustable parameters: ΔS^\ddagger , E_M and C_M for both the 60 and 100 MHz fits are given in Table XIII, and the calculated curves are shown in Figure 26. The good agreement of the values obtained here for ΔS^\ddagger with the values indicated by the CH_3 proton results, and also the quality of the fits, indicates that the OH and CH_3 protons exchange at the same rate.

The values of the $(T_{2M})_{\text{OH}}^{-1}$ parameters at 60 and 100 MHz, given in Table XIII, were used in fitting the OH proton $\Delta\omega_{\text{obsd}}/P_M$ results to eq 8. For the more accurate 100 MHz data, both ΔH^\ddagger and ΔS^\ddagger were allowed to vary and the best-fit values are given in Table XIII. These are in excellent agreement with the previous determinations. In the case of

the 60 MHz chemical shifts, it was necessary to restrain ΔH^\ddagger at the value indicated in Table XIII. Thus only ΔS^\ddagger was allowed to vary in obtaining the calculated curve shown in Figure 26. Although quite a few of the data points in the region $3.90 < 10^3/T < 4.55$ lie ~10% below the calculated curve, the quality of the fit is considered to be satisfactory in view of the fact that the 60 MHz OH proton chemical shifts were generally under 10 Hz at this frequency.

From the average of the several independent determinations of ΔH^\ddagger and ΔS^\ddagger indicated in Table XIII, it is concluded that for methanol exchange from NiCR^{2+} , ΔH^\ddagger and ΔS^\ddagger , together with their experimental uncertainties, are $9.4 \pm 0.5 \text{ kcal mol}^{-1}$ and $5.2 \pm 1.5 \text{ cal mol}^{-1}\text{deg}^{-1}$, respectively.

The coupling constant for the hyperfine interaction, which is assumed to be solely responsible for the chemical shift of the CH_3 protons, was calculated from eq 10 using the 60 MHz value of $3.96 \times 10^6 \text{ rad sec}^{-1}\text{°K}$ for C_ω and $\mu_{\text{eff}} = 3.00 \text{ BM}$. The value found for $(A/\hbar)_{\text{CH}_3}$ was $2.96 \times 10^6 \text{ rad sec}^{-1}$. For the OH proton, $(A/\hbar)_{\text{OH}}$ cannot be determined since the observed OH proton chemical shifts arise from both the hyperfine and pseudocontact mechanisms.

The absence of a significant pseudocontact contribution to the CH_3 proton chemical shifts in this system is ascribed to the fact that the angular geometry term,

$(3\cos^2\Omega - 1)$, is negligible for the CH_3 protons of the methanol molecule in the first coordination sphere of NiCR^{2+} . It should be noted that this condition is satisfied if the angle Ω between the line connecting the nickel(II) in $\text{NiCR}(\text{CH}_3\text{OH})_2^{2+}$ with the CH_3 protons and the symmetry axis is $\sim 55^\circ$. Since for NiCR^{2+} , the symmetry axis passes through the amine and pyridine nitrogens, coplanar with the approximate plane of the Schiff base complex, a value of $\sim 55^\circ$ for $(\Omega)_{\text{CH}_3}$ is consistent with a reasonable orientation of the coordinated methanol molecule in which the hydroxy proton points toward one of the azo-methine nitrogens. Therefore, $(\Omega)_{\text{OH}} \approx 90^\circ$, and this results in the largest possible negative value of -1 for the $(3\cos^2\Omega - 1)$ term, thus favoring a pseudocontact shift of the OH proton.

In principle, the values of c_1 and c_2 , determined from the study of the OH proton chemical shifts, can be used to evaluate some of the physical constants in the pseudocontact expression (eq 12). However, in view of the large number of unknown parameters, it is only possible to make a few estimates. It should be noted from eq 51-a that, in view of the sign of c_1 and the expected positive value for $(A/\hbar)_{\text{OH}}$, the second term in brackets arising from the pseudocontact contribution must be negative. Since the term, $(3\cos^2\Omega - 1)$, is negative, as discussed above, $(g_{\parallel}^2 - g_{\perp}^2)$ must be positive. Thus the positive value of c_2

in eq 51-b requires a negative value for the zero-field splitting term D . If it is assumed that $(A/\hbar)_{\text{OH}}$ is ~19% larger than $(A/\hbar)_{\text{CH}_3}$, as observed for nickel(II) ion in methanol,²³ and that: $(R)_{\text{OH}} = 2.95\text{\AA}$ and $(\Omega)_{\text{OH}} = 90^\circ$, then from the experimental value of c_1 , $(g_{\parallel}^2 - g_{\perp}^2)$ is calculated to be ~1.74. This requires a large anisotropy in the g values. In order to estimate g_{\parallel} , g_{\perp} and D , using the experimental value of c_2 in eq 51-b and the above value of $(g_{\parallel}^2 - g_{\perp}^2)$, the following relation⁶³ was employed:

$$D = \frac{\lambda}{2} (g_{\parallel} - g_{\perp}) \quad (51-c)$$

where λ is the spin-orbit coupling constant. Since it is required that the value of λ for $\text{NiCR}(\text{CH}_3\text{OH})_2^{2+}$ be greater than the free nickel(II) ion value of -322 cm^{-1} , a reasonable estimate of -300 cm^{-1} was assumed. Thus, it was found that g_{\parallel} , g_{\perp} and D are, respectively, 3.95, 3.72 and -34.1 cm^{-1} . Although the estimates given here are sensitive to the various assumptions regarding A/\hbar , R and Ω for the OH proton, and are also quite sensitive to the error (~25%) in c_1 , resulting from the long extrapolation required to obtain the intercept c_1 , it appears that additional factors are responsible for the unreasonably large estimates of g_{\parallel} and g_{\perp} given above. In particular, it might be expected that the absence of axial symmetry in the $\text{NiCR}(\text{CH}_3\text{OH})_2^{2+}$ complex may render eq 12 inapplicable for the present

system. To investigate this possibility further, the expression for the pseudocontact shift of a nonaxially symmetric system was developed⁶⁴ from the general expression for the pseudocontact shift, given as eq 17 by Kurland and McGarvey.¹⁷ It was found that:

$$\frac{\Delta\omega_M}{\omega_O} = - \frac{2\beta^2}{9kR^3T} \left\{ (3\cos^2\Omega - 1) \left[(g_z^2 - \frac{g_x^2 + g_y^2}{2}) - \right. \right. \quad (51-d)$$

$$\left. \frac{1}{6kT} \left(2Dg_z^2 + \frac{g_x^2(D - 3E) + g_y^2(D - E)}{2} \right) \right] -$$

$$\sin^2\Omega \cos 2\psi \left[\left(\frac{g_y - g_x}{2} \right) + \frac{1}{12kT} (g_y(D + 3E) - g_x(D - 3E)) \right] \right\}.$$

where g_x , g_y and g_z are the components of the g tensor, D is the zero-field splitting arising from the tetragonal distortion, E is the additional zero-field parameter characterizing the rhombic distortion, and ψ is the angle between the projection of the unit vector, which joins the metal ion nucleus with the ligand nucleus, onto the xy plane and the x axis. The zero-field splitting parameters D and E are related to the g tensor components by⁶³

$$D = \frac{\lambda}{2} \left(g_z - \left(\frac{g_x + g_y}{2} \right) \right) \quad (51-e)$$

$$E = \frac{\lambda}{4} (g_x - g_y) \quad (51-f)$$

In the case of axial symmetry, $E = 0$, $g_x = g_y = g_{\perp}$, $g_z = g_{\parallel}$, and therefore, the pseudocontact shift expression given by eq 51-d reduces to eq 12, as required.

It should be noted from the structure of NiCR^{2+} , given as I(a) in Chapter I, that if the inner sphere methanol molecule is orientated so that $(\Omega)_{\text{OH}} \approx 90^\circ$, then taking the x-axis to be the one perpendicular to the approximate plane of the molecule, the angle ψ , defined above, is $\ll 45^\circ$. Consequently, the term involving $\cos(2\psi)$ in eq 51-d does not vanish, as would be the case if $\psi = 45^\circ$. However, it was found that the contribution of this term to c_1 and c_2 is relatively small, and therefore, in the following discussion the term involving $\cos(2\psi)$ was neglected. With this assumption, the experimental value of c_1 is now defined by eq 51-a with the term $(g_z^2 - \frac{g_x^2 + g_y^2}{2})$ replacing $(g_{\parallel}^2 - g_{\perp}^2)$. The experimental value of c_2 is now given by

$$c_2 = \frac{2\beta^2 \omega_0 (3\cos^2 \Omega - 1)}{9k^2 R^3} \left\{ \frac{1}{6} (2g_z^2 D + \frac{g_x^2 (D-3E) + g_y^2 (D-E)}{2}) \right\} \quad (51-g)$$

Obviously, a closed solution for the constants: D , E , g_x , g_y , and g_z is not possible, but assuming that $\lambda = -300 \text{ cm}^{-1}$ and using the values of R , A/\hbar and Ω for the OH proton, given previously, it was found that one solution

is: $g_x = 2.00$, $g_y = 2.63$, $g_z = 2.68$, $D = -54.9 \text{ cm}^{-1}$ and $E = 47.1 \text{ cm}^{-1}$. The magnitude of the above g values are much more reasonable than those which were obtained previously assuming axial symmetry. These estimates also show that the g component in the direction of the azo-methine nitrogens (y -axis) is not much different from the g component in the direction of the pyridine nitrogen (z -axis). This does not appear to be unreasonable. It must be emphasized, however, that in view of the number of unknown parameters, the various assumptions made, and the errors in c_1 and c_2 , no great significance should be attached to the above estimated values. The only conclusion which can be reached is that the calculated results are consistent with a large pseudocontact shift of the OH proton in methanol solutions of NiCR^{2+} .

$\text{NiCR}(\text{PF}_6)_2$ in Dimethylsulfoxide

Figures 29 and 30, respectively, illustrate the temperature dependence of $-\log(T_{2P} P_M)$ and $(\Delta\omega_{\text{obsd}}/P_M)$, at 60 and 100 MHz, for $\text{NiCR}(\text{PF}_6)_2$ in DMSO. The data shown have been calculated from the observed line widths and chemical shifts assuming $n = 2$ in eq 4. It was found for this system that the equilibrium constants, calculated from the ΔH° and ΔS° values obtained from the magnetic susceptibility measurements (Table VIII) and from the azo-methine methyl proton contact shifts (Table IX), give rise

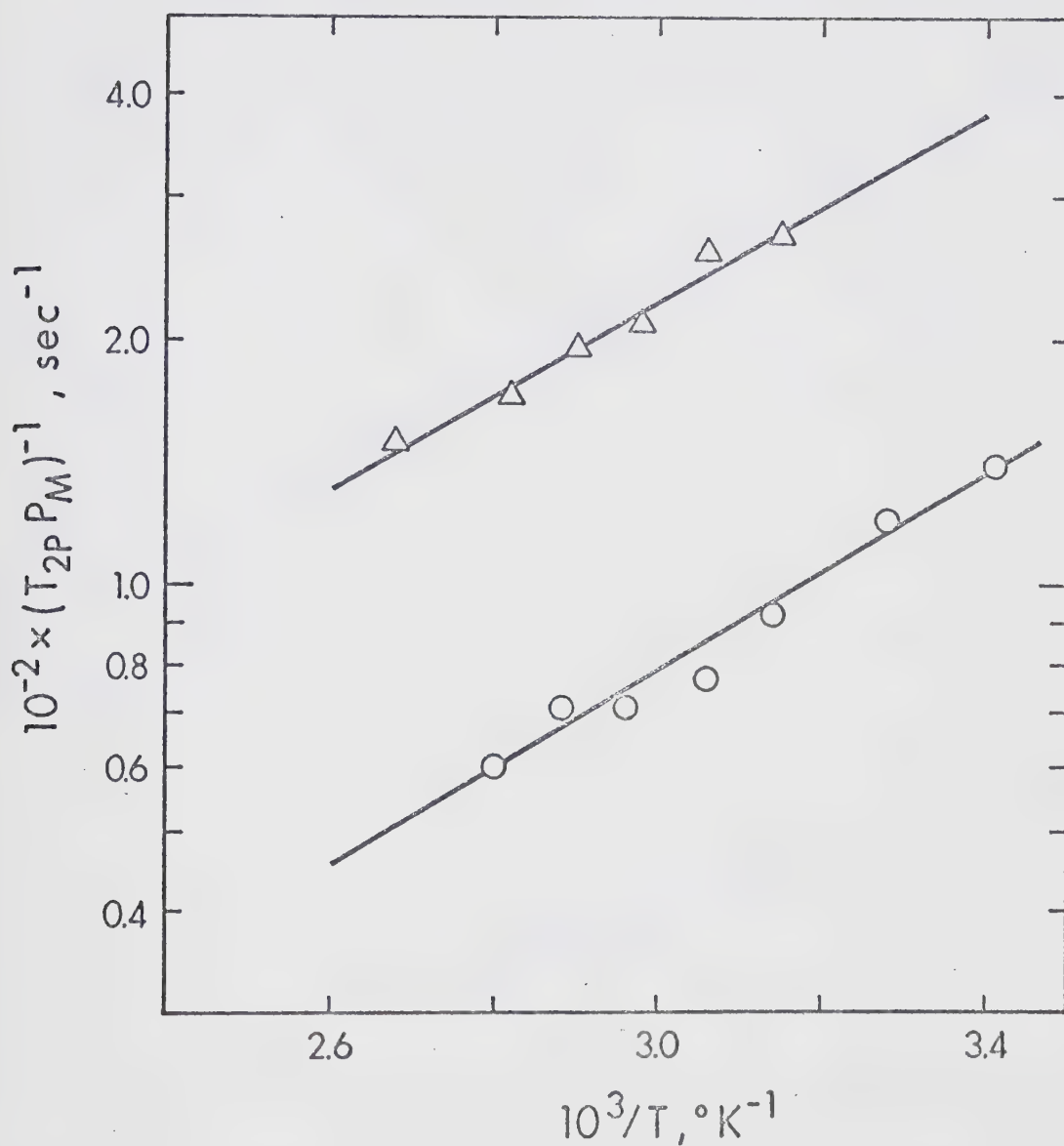


Figure 29: Temperature dependence of $-\log(T_{2P}P_M)$ at 60 MHz (o) and 100 MHz (Δ) for the methyl protons of dimethylsulfoxide solutions of $\text{NiCR}(\text{PF}_6)_2$.

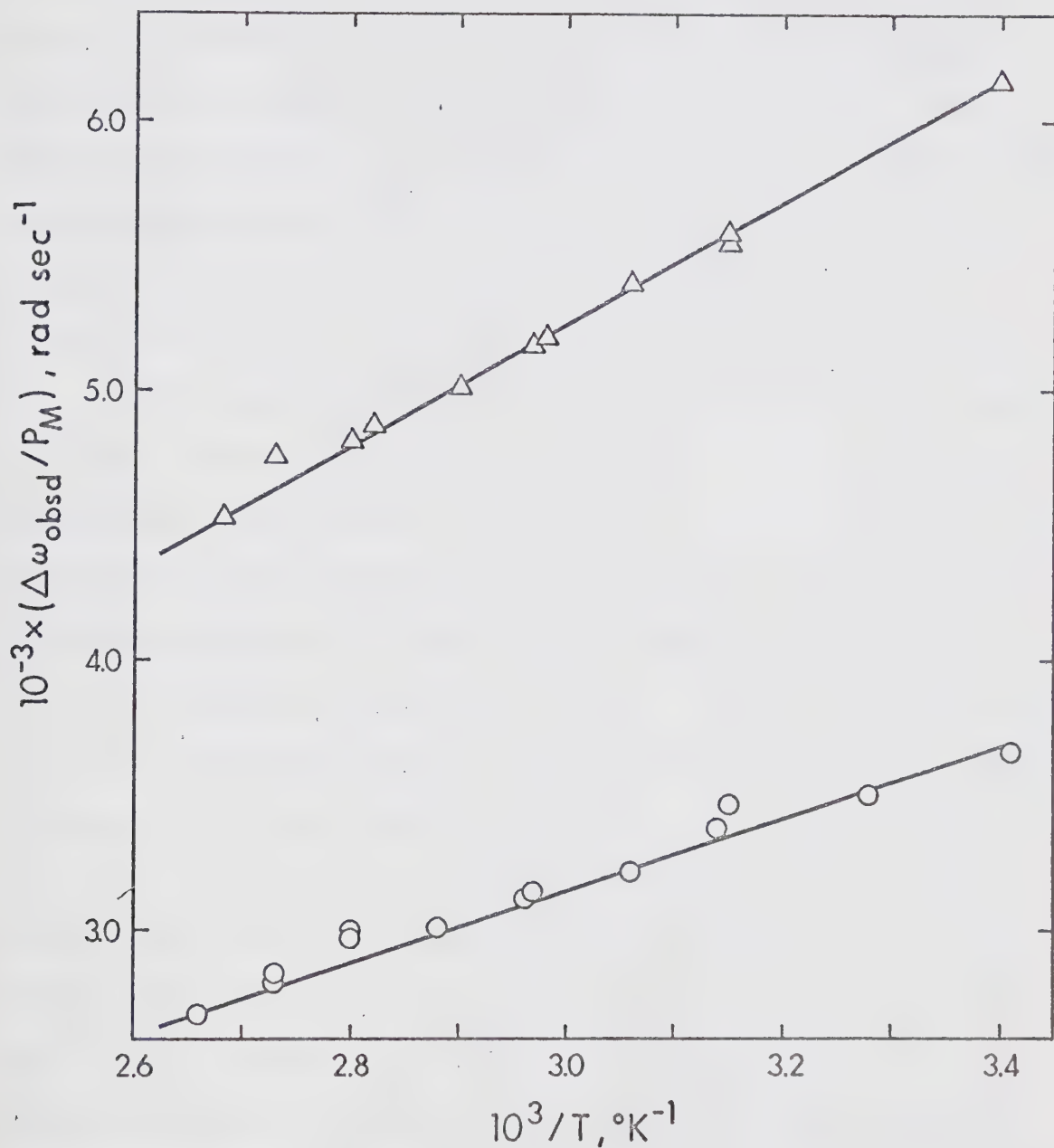


Figure 30: Temperature dependence of $(\Delta\omega_{\text{obsd}}/P_M)$ at 60 MHz (o) and 100 MHz (Δ) for the methyl protons of dimethylsulfoxide solutions of $\text{NiCR}(\text{PF}_6)_2$.

to an unreasonable over correction of the $(\Delta\omega_{\text{obsd}}/P_M)$ data, making the values almost temperature independent. Therefore, no corrections have been applied to the observed data for the diamagnetic-paramagnetic equilibrium. Although the magnetic susceptibility and ligand contact shift measurements both indicate values of approximately -4.5 kcal mol $^{-1}$ and -9.6 cal mol $^{-1}$ deg $^{-1}$ for ΔH° and ΔS° , respectively, the $(\Delta\omega_{\text{obsd}}/P_M)$ data appear to require $\Delta H^\circ \approx -4.5$ kcal mol $^{-1}$ and $\Delta S^\circ \approx -7.6$ cal mol $^{-1}$ deg $^{-1}$ in order for the corrected bulk solvent chemical shifts to be Curie dependent. These latter estimates of ΔH° and ΔS° were calculated from the solvent chemical shifts on the assumption that the percentage of diamagnetic species is negligible at $\sim 20^\circ\text{C}$. From the point of view of expected errors of ΔH° and ΔS° , determined by the susceptibility and contact shift measurements, the required difference of 2 cal mol $^{-1}$ deg $^{-1}$ for ΔS° would not be an unreasonable error, but it was found that a refit of the azo-methine methyl proton contact shifts with $\Delta H^\circ = -4.5$ kcal mol $^{-1}$ and $\Delta S^\circ = -7.6$ cal mol $^{-1}$ deg $^{-1}$ held constant, resulted in an unacceptable fit. No reasonable explanation has been found for the discrepancy discussed here. It would seem that since the two independent measurements of ΔH° and ΔS° gave essentially the same results, the discrepancy is related, for the most part, to the $(\Delta\omega_{\text{obsd}}/P_M)$ and $(T_{2P}^{P_M})^{-1}$ data which fail to decrease as rapidly at high temperature as is predicted by the results

of the equilibrium studies. However, since the measured bulk solvent chemical shifts were large (see Table LIV) and reproducible for two samples containing 0.125 m and 0.434 m $\text{NiCR}(\text{PF}_6)_2$, the problem is not one of inaccurate chemical shifts.

The presence of chemical shifts for this system, and the absence of chemical exchange effects in the $(T_{2P_M})^{-1}$ data of Figure 30, indicates that the temperature dependence of $(T_{2P_M})^{-1}$ is due to T_{2M} relaxation according to limiting condition 25(a) or 26(a). On the basis of the results for NiCR^{2+} in other solvents, discussed previously, the former of these limiting conditions is the most likely. The high melting point of DMSO (18°C) prevents the temperature from being lowered enough to observe any $\tau_M \Delta\omega_M^2$ contributions to $(T_{2P_M})^{-1}$. The T_{2M} relaxation for this system indicates an apparent activation energy of $\sim 2.6 \text{ kcal mol}^{-1}$ and a maximum frequency dependence of $(100/60)^2$. The significance of these two features will be discussed in the following section.

From the 100 MHz measurement of $(T_{2P_M})^{-1}$ at 25°C , a lower limit for DMSO exchange from NiCR^{2+} is estimated to be $3.6 \times 10^2 \text{ sec}^{-1}$. The hyperfine coupling constant for the CH_3 protons of DMSO is $8.1 \times 10^5 \text{ rad sec}^{-1}$ assuming $\mu_{\text{eff}} = 3.00 \text{ BM}$. This value of (A/\hbar) was calculated from the value of $(\Delta\omega_{\text{obsd}}/P_M)$ at 25° ; the latter being interpolated from the data of Figure 30 on the assumption that

the concentration of diamagnetic form is negligible at this temperature. Since the magnetic susceptibility and contact shift measurements indicate that 8% of $\text{NiCR}(\text{PF}_6)_2$ exists in the diamagnetic form at this temperature, the above value of (A/\hbar) may be in error by this amount also, but the amount of the correction remains uncertain as described in the preceding paragraph.

Magnetic Field Dependence of T_{2M} and T_{2O} for NiCR^{2+} and NiCRMe^{2+}

The Schiff base complexes, NiCR^{2+} and NiCRMe^{2+} , have been found to show a magnetic field dependence of the T_{2M} relaxation time for the solvent protons in the first coordination sphere of the metal ion. There is also a strong indication that this occurs in the second and higher or outer coordination spheres. Previous work has not indicated such a phenomenon for nickel(II) systems and some explanation seems to be required.

Consideration of the theoretical expressions for $(T_{2M})^{-1}$ and $(T_{2O})^{-1}$ (eq 13 and 23) and the definitions of the effective correlation times, $f_D(\tau_D)$ and $f_e(\tau_e)$ (eq 14 and 15), shows that if these correlation times are field dependent, then $(T_{2M})^{-1}$ and $(T_{2O})^{-1}$ should decrease on changing from an nmr operating frequency of 60 to 100 MHz, since ω_s changes from 2.48×10^{11} to 4.14×10^{11} rad sec⁻¹. However, the opposite effect was observed in this work,

and therefore, it must be concluded that the individual correlation times, defined by eq 16 and 17, are themselves field dependent. Since only T_{1e} and T_{2e} in eq 16 and 17 can be field dependent, it is necessary that $T_{1e} < \tau_r, \tau_M$. It should also be noted that the field dependence of $(T_{2M})^{-1}$, observed here for NiCR^{2+} and NiCRMe^{2+} , cannot arise exclusively from the hyperfine term of eq 13 since the values of (A/\hbar) determined from the chemical shifts would require electron spin relaxation times which would be unusually large for a nickel(II) complex. Instead, it is expected that both the dipolar and hyperfine terms of eq 13 contribute to the magnetic field dependence, the former much more than the latter.

Expressions for the field dependence of T_{1e} and T_{2e} have not been developed for the exact conditions found in this work. The equations of McLachlin, given as eq 18 and 19, have been developed with the assumption that $\tau_c < T_{1e}$, which appears not to be valid for the systems being considered. It seems likely that the functional form of the frequency dependence will be given by these equations, but complete quantitative agreement need not be expected. It is encouraging to note that eq 18 predicts a maximum ratio of 2.78 for the longitudinal electron spin relaxation times at 60 and 100 MHz and this ratio is never exceeded for the systems studied here. For NiCR^{2+} in DMSO, the ratio of $(T_{2M})^{-1}$ at 100 and 60 MHz is 2.78, but for the other

solvent systems, this ratio varies from 1.95 to 2.43. In the case of NiCRMe^{2+} , a smaller frequency dependence of $(T_{2M})^{-1}$ was observed; the above ratio being 1.33 for NiCRMe^{2+} in water and 1.59 for NiCRMe^{2+} in DMF.

In evaluating the experimental $((T_{2M})^{-1} + (T_{20})^{-1})$ results in terms of these equations, there are three unknowns: τ_r , C_e and d_o or r_i , assuming τ_c in eq 18 and 19 can be identified as τ_r , and two experimental numbers, the relaxation times at 60 and 100 MHz. An iterative procedure was used to determine these unknown constants using the ratio of the relaxation times at the two frequencies as a preliminary guide. Also, previous results from the study of the vanadyl ion in the various solvents^{24,53} provided some guide to reasonable values of τ_r , r_i and d_o . The results of these calculations for NiCR^{2+} and NiCRMe^{2+} in water and DMF are summarized in Table XIV along with the observed and calculated $(T_{2M})^{-1}$ and $(T_{20})^{-1}$ contributions at 25°C. Similar results for NiCR^{2+} in methanol, acetonitrile and DMSO are given in Table XV.

It is evident from the results in these Tables that, for NiCR^{2+} in the various solvents, the calculated T_{1e} values at 60 MHz, which fall in the range 3.1×10^{-12} to 7.1×10^{-12} sec, are in line with expected values for nickel(II) complexes^{20,23}. For NiCRMe^{2+} , the calculated T_{1e} values are larger but not unreasonably so. In all cases, except for NiCR^{2+} and NiCRMe^{2+} in DMF, an acceptable

TABLE XIV
Parameters and results of $T_{20}^{(a)}$ and $T_{2M}^{(a)}$ calculations
for NiCR^{2+} and NiCRMe^{2+} in DMF and water

		DMF		Water	
		NiCR^{2+}	NiCRMe^{2+}	NiCR^{2+}	NiCRMe^{2+}
$10^{-2} \times (T_{20})^{-1}^{(b)}$	60 MHz	1.18	5.19	6.15	9.43
	100 MHz	2.74	8.24	12.0	12.6
$d_o, \text{\AA}$		5.75	5.80	4.65	4.86
$10^{-2} \times (T_{2M})_{\text{obsd}}^{-1}$	60 MHz	3.83	15.8	18.5	28.3
	100 MHz	8.92	25.1	36.0	37.7
$10^{-2} \times (T_{2M})_{\text{calcd}}^{-1}^{(c)}$	60 MHz	3.83	15.8	18.5	28.9
	100 MHz	9.11	27.8	35.7	37.7
$10^{-2} \times (T_{2M})_{\text{HF}}^{-1}^{(d)}$	60 MHz	0.23	2.93	0.097	0.11 ^(e)
	100 MHz	0.67	8.08	0.27	0.18 ^(d)
$10^{11} \times \tau_c, \text{sec}$		5.80	5.80	1.75	1.00
$10^{11} \times T_{1e}, \text{sec}$ $10^{13} \times T_{2e}, \text{sec}$	60 MHz	0.65	4.7	0.415	0.918
		0.42	3.0	2.6	14.4
$10^{22} \times C_e, \text{sec}^{-2}$		27.5	3.8	13.4	3.68
$r_i, \text{\AA}$		3.94	4.10	2.80	2.86

(a) The T_{2M} and T_{20} values are given in sec.

(b) Since no outer sphere broadening was actually observed, the values given are based on reasonable estimates of the $(T_{20})^{-1} : (T_{2M})^{-1}$ ratio.

(c) The sum of the dipolar and hyperfine contributions calculated from eq 13.

(d) The hyperfine contribution calculated using the (A/h) values given in the text.

(e) The (A/h) used here was estimated as explained in the text.

TABLE XV
Parameters and results of $T_{20}^{(a)}$ and $T_{2M}^{(a)}$ calculations for
 NiCR^{2+} in methanol, acetonitrile and dimethylsulfoxide

		Methanol		Acetonitrile	Dimethylsulfoxide
		CH_3	OH		
$10^{-2} \times (T_{20})^{-1 (b)}$	$\left\{ \begin{array}{l} 60 \text{ MHz} \\ 100 \text{ MHz} \end{array} \right.$	1.34	2.20	0.43	0.42
		2.97	5.05	0.99	1.16
$d_o, \text{\AA}$		6.75	5.71	9.4	6.75
$10^{-2} \times (T_{2M})_{\text{obsd}}^{-1}$	$\left\{ \begin{array}{l} 60 \text{ MHz} \\ 100 \text{ MHz} \end{array} \right.$	4.11	20.6	1.00	0.88
		9.13	47.3	2.48	2.44
$10^{-2} \times (T_{2M})_{\text{calcd}}^{-1 (c)}$	$\left\{ \begin{array}{l} 60 \text{ MHz} \\ 100 \text{ MHz} \end{array} \right.$	4.12	20.6	1.01	0.88
		9.13	44.8	2.47	2.44
$10^{-2} \times (T_{2M})_{\text{HF}}^{-1 (d)}$	$\left\{ \begin{array}{l} 60 \text{ MHz} \\ 100 \text{ MHz} \end{array} \right.$	0.38	0.55 ^(e)	0.34	0.01 ₄
		1.08	1.51 ^(e)	0.93	0.03 ₈
$10^{11} \times \tau_c, \text{sec}$		3.7		5.8	$\gg T_{1e}$
$10^{11} \times T_{1e}, \text{sec}$	60 MHz	0.66		0.71	0.31
$10^{13} \times T_{2e}, \text{sec}$		1.0		0.46	—
$10^{22} \times C_e, \text{sec}^{-2}$		17.5		25.1	—
$r_i, \text{\AA}$		3.90	2.95	5.3	4.5

(a) The T_{2M} and T_{20} values are given in sec.

(b) Since no outer sphere broadening was actually observed, the values given for NiCR^{2+} in methanol are based on reasonable estimates of the $(T_{20})^{-1} : (T_{2M})^{-1}$ ratio used in fitting the $(T_{2P}^{\text{PM}})^{-1}$ data. For NiCR^{2+} in acetonitrile and DMSO, the estimated $(T_{20})^{-1}$ contribution was calculated using the outer sphere interaction distances given in ref 24 for vanadyl ion in these solvents.

(c) The sum of the dipolar and hyperfine contributions calculated from eq 13.

(d) The hyperfine contribution calculated using the (A/h) values given in the text.

(e) For the OH proton, (A/h) was assumed to be 19% greater than $(A/h)_{\text{CH}_3}$ as observed for nickel(II) ion in methanol.²³

account of the frequency dependence of $(T_{2M})^{-1}$ was obtained by using, in eq 13 and 23, inner sphere interaction distances which have been observed for hexasolvated metal ions. For NiCR^{2+} and NiCRMe^{2+} in DMF, the inner sphere interaction distances $(r_i)_{\text{CH}}$ are significantly larger than the value of 3.1\AA obtained for the VO^{2+} ion in DMF.⁴⁴ This feature, along with the observation that $(r_i)_{\text{CH}}$ is greater for $\text{NiCRMe}(\text{DMF})_2^{2+}$ than for $\text{NiCR}(\text{DMF})_2^{2+}$, is consistent with the presence of steric interaction between the Schiff base ligand and the inner sphere DMF molecules. This would be expected to increase upon substitution of a CH_3 group for the amine proton. The values of d_o for NiCR^{2+} in methanol are also larger than for normal octahedral systems but this may not be unreasonable in view of the presence of a large Schiff base ligand. It should be noted, however, that these outer sphere distances are merely estimates since no $(T_{20})^{-1}$ controlled line broadening was observed in any of the systems. For NiCR^{2+} and NiCRMe^{2+} in DMF and water, and for NiCR^{2+} in methanol, the indicated values of $(T_{20})^{-1}$ were calculated from the dipolar correlation times and the estimates of the ratio, $(T_{2M})^{-1} : (T_{20})^{-1}$, found to be acceptable in fitting the $(T_{2P}P_M)^{-1}$ data. In the case of NiCR^{2+} in acetonitrile and DMSO, the estimated $(T_{20})^{-1}$ contributions are based on the values of d_o reported in ref 24 for vanadyl ion in these solvents.

The values of τ_c obtained for NiCR^{2+} in methanol and

acetonitrile are in good agreement with the τ_r values of 4.1×10^{-11} sec and 6.2×10^{-11} sec determined from an analysis of the epr spectrum of the vanadyl ion in methanol and acetonitrile,⁵³ respectively. However, the τ_c values for NiCR^{2+} and NiCRMe^{2+} in water and DMF are about a factor of two smaller than the τ_r values given in ref 53 for the VO^{2+} ion in DMF and water. On the whole, the values are more reasonable than might have been expected considering the approximate nature of the theory.

It may be noted that for NiCR^{2+} in DMSO a value of τ_c cannot be calculated since for this system a maximum frequency dependence was observed, and consequently, the dipolar correlation time τ_D for the T_{2M} relaxation is determined exclusively by the electron spin relaxation time T_{1e} . In terms of eq 18 this maximum frequency dependence implies that $(\omega_s \tau_c)^2 \gg 1$, and therefore, T_{1e} is given by

$$T_{1e} = \frac{\omega_s^2 \tau_c}{2C_e} \quad (52-a)$$

The condition, $(\omega_s \tau_c)^2 \gg 1$, required here, is not unreasonable since for the vanadyl ion in DMSO the analysis of the epr spectrum gave a value of 1.2×10^{-10} sec for τ_r .⁵³ Thus, assuming $\tau_c = \tau_r$, the value of $(\omega_s \tau_c)^2$ at 60 MHz is 738. However, these considerations would lead to the conclusion that a maximum frequency dependence should also have been observed for NiCR^{2+} in DMF since

previous results⁵³ have shown that τ_r for the vanadyl ion in DMF is not significantly different from that in DMSO. Equation 52-a also suggests that the activation energy for the T_{2M} relaxation in the DMSO system should parallel that of τ_r if τ_c can be interpreted as τ_r . Although the activation energy of T_{2M} was greater for NiCR^{2+} in DMSO (2.6 kcal mol⁻¹) than for any of the other solvent systems, it is still significantly less than the expected activation energy for DMSO viscosity which is 3.5 kcal mol⁻¹. This disagreement would of course be greater if the $(T_{2P}P_M)^{-1}$ data were corrected for the diamagnetic-paramagnetic equilibrium which is evidently present on the basis of the magnetic susceptibility and contact shift results. Thus, the $(T_{2P}P_M)^{-1}$ values are not decreasing as rapidly with increasing temperature as is required by the results of the equilibrium constant measurements.

It was pointed out previously that the temperature dependence of $(T_{2P}P_M)^{-1}$ in the aqueous systems might be explained solely by a T_{2M} relaxation process. This could result since approximately

$$(T_{2P}P_M)^{-1} = (T_{2M})^{-1} \propto T_{1e} \propto \frac{1 + \omega_s^2 \tau_c^2}{\tau_c} \quad (52-b)$$

In the high temperature limit $(\omega_s \tau_c)^2 \ll 1$ and $(T_{2P}P_M)^{-1}$ should decrease as the temperature decreases, then vary slowly with temperature when $(\omega_s \tau_c)^2 \approx 1$, and finally,

$(T_{2P}P_M)^{-1}$ should increase as the temperature decreases further when $(\omega_s\tau_c)^2 \gg 1$. The results might be explained by assuming that the latter condition is approached in the lower temperature region in water. However, calculations indicate that, assuming $\tau_c = \tau_r$ and using reasonable values of 3.5 to 4.0 kcal mol⁻¹ for the apparent activation energy of τ_r , it is not possible to have both the low temperature and intermediate cases within the narrow liquid range of water. This is especially true at 100 MHz since at this frequency $(\omega_s\tau_r)^2$ must be significantly greater than one if it is also greater than one at 60 MHz.

Considerations similar to those above do provide an explanation for the higher apparent values of E_M at 100 MHz than at 60 MHz which were evident for $NiCR^{2+}$ and $NiCRMe^{2+}$ in DMF and water. At 100 MHz the system is closer to the limit $(\omega_s\tau_r)^2 > 1$ and therefore E_M will be closer to the value expected for the activation energy for τ_r , that is, 3.9 kcal mol⁻¹ in water and ~2.5 kcal mol⁻¹ in DMF.

The kinetic results for $NiCR^{2+}$ and $NiCRMe^{2+}$ will be discussed in relation to the results from other nickel(II) complexes in Chapter IV.

5. Solvent Proton NMR Line Broadening and Chemical Shift Study of the Nickel(II) Schiff Base Complexes, NiTRI^{2+} and NiTAAB^{2+} , in N,N-dimethylformamide

In this section the results of the proton nmr investigation of the N,N-dimethylformamide (DMF) solvent exchange rates of the two nickel(II) Schiff base complexes, tribenzo[b,f,j][1,5,9]triazabicyclododecinenickel(II), NiTRI^{2+} , and tetrabenzo[b,f,j,n][1,5,9,13]tetrazacyclohexadecinenickel(II), NiTAAB^{2+} , are presented. The complexes are shown as structures III and II, respectively, in Chapter I. It should be observed that unlike NiTAAB^{2+} , which exists as a tetragonally distorted pseudo-octahedral complex in coordinating solvents, NiTRI^{2+} coordinates three solvent molecules to form a normal octahedral complex. The study of these two structurally different nickel(II) Schiff base complexes was carried out in order to compare the effects of the two macrocyclic ligands on the solvent exchange rates and to compare NiTAAB^{2+} to the previously studied NiCR^{2+} and NiCRMe^{2+} complexes. The latter two complexes have quite high solvent exchange rates and the question arises as to whether this is generally true for all tetragonally distorted nickel(II) complexes or if specific electronic and steric effects are operative in the NiCR^{2+} and NiCRMe^{2+} systems. It was also of interest to determine if the similarity in the water exchange rates for $\text{Ni}(\text{OH}_2)_6^{2+}$ and $\text{NiTRI}(\text{OH}_2)_3^{2+}$ also extends to the DMF system.

NiTRI(ClO₄)₂ in N,N-dimethylformamide

Figures 31 and 32 show the temperature dependence of $(T_{2P}P_M)^{-1}$ and $(\Delta\omega_{\text{obsd}}/P_M)$, respectively, for the formyl proton in DMF solutions of NiTRI(ClO₄)₂. The investigation of this system was initially carried out on the nitrate salt but it was observed that the line broadenings were significantly different for NiTRI(NO₃)₂ and NiTRI(ClO₄)₂. Also, the downfield chemical shifts for the nitrate salt were considerably smaller than those for the perchlorate salt and they were found to be in disagreement with the line broadening study. These differences were attributed to nitrate complexing in DMF and only the results for the perchlorate salt are given here. The $(T_{2P}P_M)^{-1}$ results show the typical $(T_{2M})^{-1}$, $\tau_M\Delta\omega_M^2$, τ_M^{-1} and $(T_{2O})^{-1}$ regions of line broadening described by limiting conditions 25(a) - 25(d) (Case A). The results in the high temperature region clearly show that as the temperature increases the 100 MHz data is converging towards the 60 MHz measurements as $(T_{2M})^{-1}$ becomes the dominant term in eq 2. Since the $(T_{2M})^{-1}$ activation energy is not well defined, the assumption is made that the same mechanism determines $(T_{2M})^{-1}$ and $(T_{2O})^{-1}$, and consequently, $E_M = E_O$. The 60 and 100 MHz $(T_{2P}P_M)^{-1}$ data have been fitted to eq 2, modified by the addition of a term $(T_{2O})^{-1}$, and the $(\Delta\omega_{\text{obsd}}/P_M)$ measurements to eq 8. The parameters resulting from these least-squares fits are summarized in Table XVI.

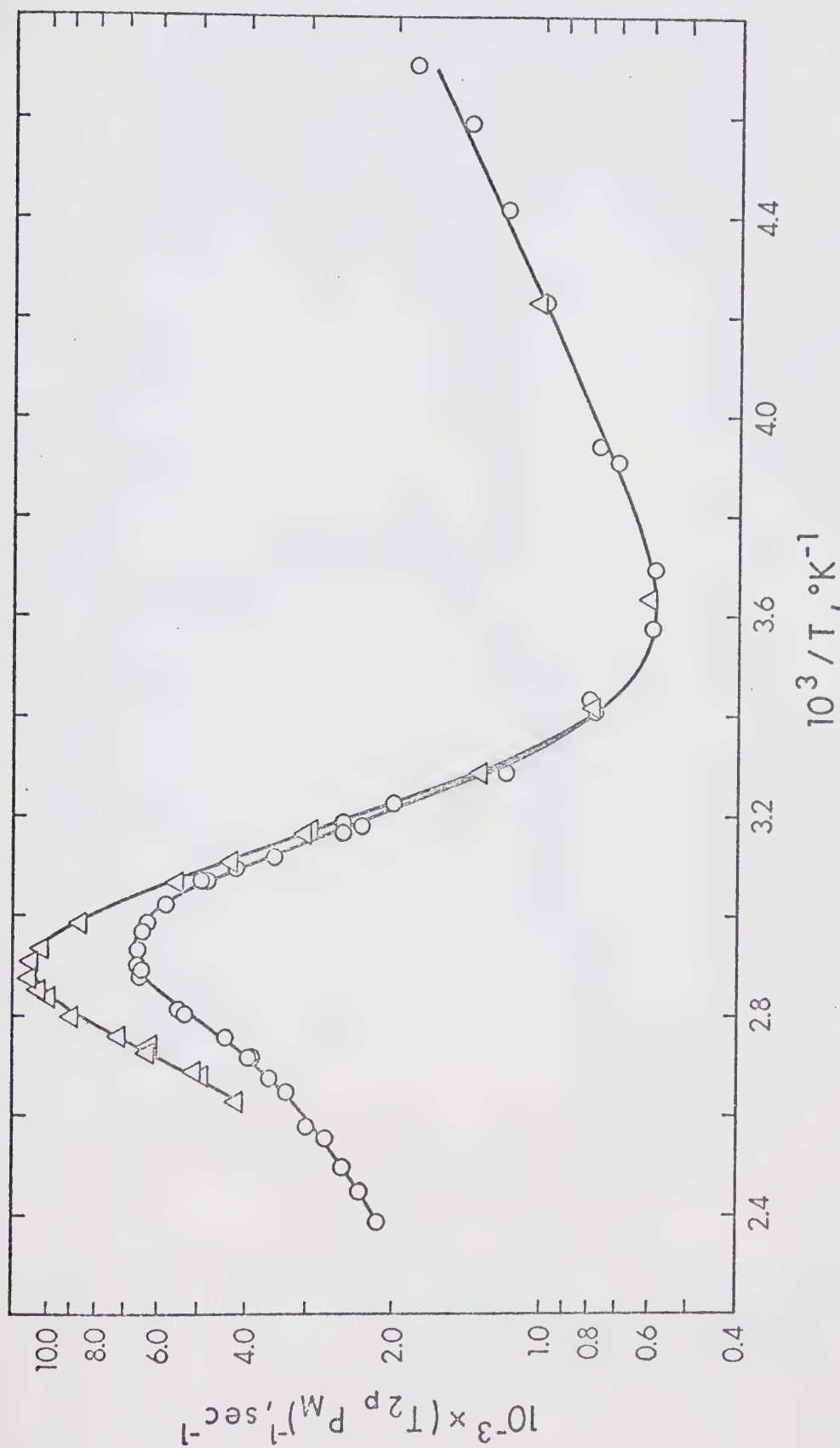


Figure 31: Temperature dependence of $-\log(T_{2p} P_M)$ for the formyl proton in N,N-dimethylformamide solutions of $\text{Ni}(\text{THI})(\text{ClO}_4)_2$ at 100 MHz (Δ), and 60 MHz (o).

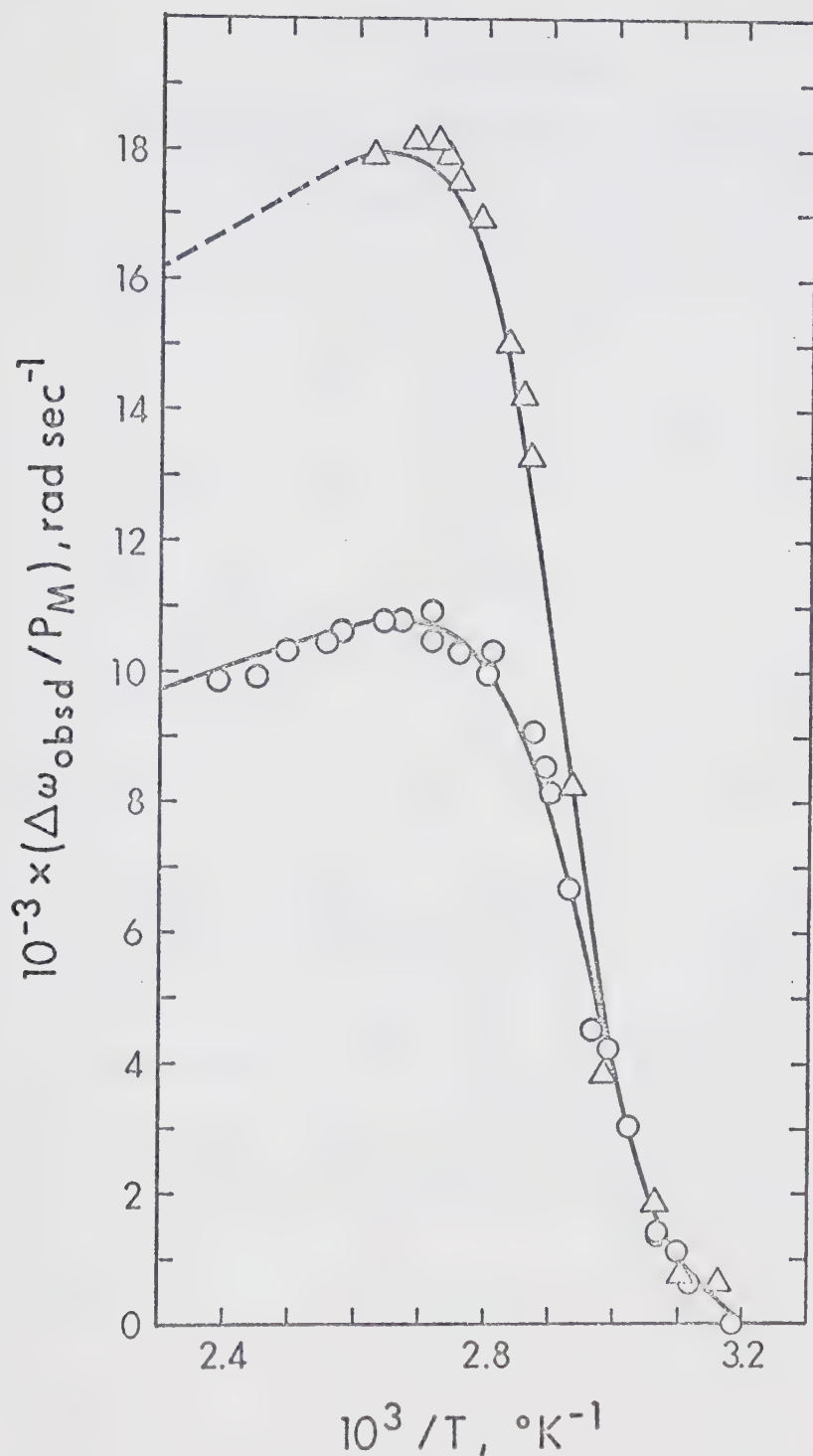


Figure 32: Temperature dependence of $(\Delta\omega_{\text{obsd}}/P_M)$ for the formyl proton in *N,N*-dimethylformamide solutions of $\text{Ni}(\text{TRI})(\text{ClO}_4)_2$ at 100 MHz (Δ), and 60 MHz (\circ).

TABLE XVI

Least-squares best fit parameters for
NiTRI(ClO₄)₂ in N,N-dimethylformamide

	(T _{2P_M}) ⁻¹ Data		Δω _{obsd} /P _M Data	
	60 MHz	100 MHz	60 MHz	100 MHz
ΔH [‡] , kcal mol ⁻¹	15.58	15.67	15.60	15.67 ^(c)
ΔS [‡] , cal mol ⁻¹ deg ⁻¹	6.28	6.66	6.37	6.56
10 ⁻⁶ x C _ω , rad sec ⁻¹ °K	4.13	7.15	4.20	7.00 ^(d)
E _M = E _O , kcal mol ⁻¹	2.14	2.14 ^(a)	2.14 ^(b)	2.14 ^(b)
C _M , sec ⁻¹	150.1	150.1 ^(a)	150.1 ^(b)	150.1 ^(b)
C _O , sec ⁻¹	10.6	10.6 ^(a)	—	—

- (a) The parameters defining (T_{2M})⁻¹ and (T_{2O})⁻¹ have been held constant as determined by the 60 MHz (T_{2P_M})⁻¹ fit.
- (b) Held constant at value given by 60 MHz (T_{2P_M})⁻¹ fit.
- (c) Held constant at value given by 100 MHz (T_{2P_M})⁻¹ fit.
- (d) Held constant at 100/60 of the value from the 60 MHz Δω_{obsd}/P_M fit.

Excellent agreement is obtained for the ΔH^\ddagger and ΔS^\ddagger values from the different data sets. It seems reasonable to conclude that ΔH^\ddagger and ΔS^\ddagger are 15.6 ± 0.25 kcal mol⁻¹ and 6.5 ± 0.5 cal mol⁻¹deg⁻¹, respectively. The value of 4.2×10^6 rad sec⁻¹°K for C_ω and 3.2 BM³⁶ for μ_{eff} yield a hyperfine coupling constant of 2.9×10^6 rad sec⁻¹ for the CH proton of DMF.

NiTAAB²⁺ in N,N-dimethylformamide

The line broadening and downfield chemical shift data for the formyl proton in DMF solutions of NiTAAB²⁺ are shown in Figures 33 and 34, respectively. Both the nitrate and perchlorate salts were studied and it was observed that both salts gave the same results, within experimental error, up to -10° ($10^3/T \approx 3.8^\circ\text{K}^{-1}$). Above this temperature, smaller broadenings and shifts were observed for the nitrate salt, and these shifts decreased more rapidly with increasing temperature. Again, this was attributed to nitrate complexing in DMF. As a result, the data obtained using NiTAAB(ClO₄)₂, and only that data for NiTAAB(NO₃)₂ which was in agreement with the results for NiTAAB(ClO₄)₂, were analyzed.

It should be noted from the chemical shift measurements shown in Figure 34 that an additional complication is observed for this system since the shifts in the fast exchange limit do not give an extrapolated zero shift at

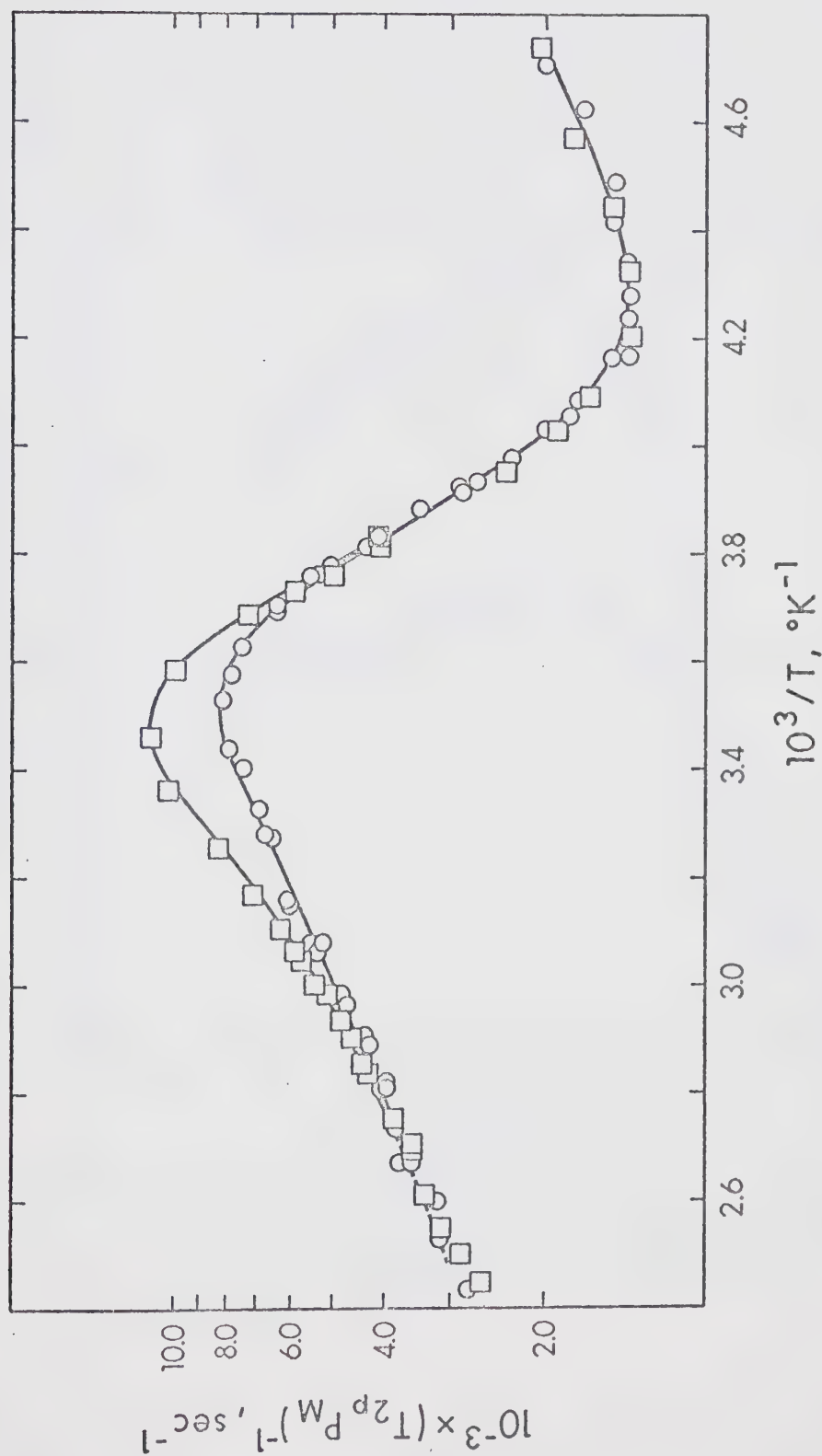


Figure 33: Temperature dependence of $-\log(T_{2p} P_M)$ for the formyl proton in N,N-dimethylformamide solutions of NiTAAB^{2+} (both ClO_4^- and NO_3^- salts), at 100 MHz (\square), and 60 MHz (\circ).

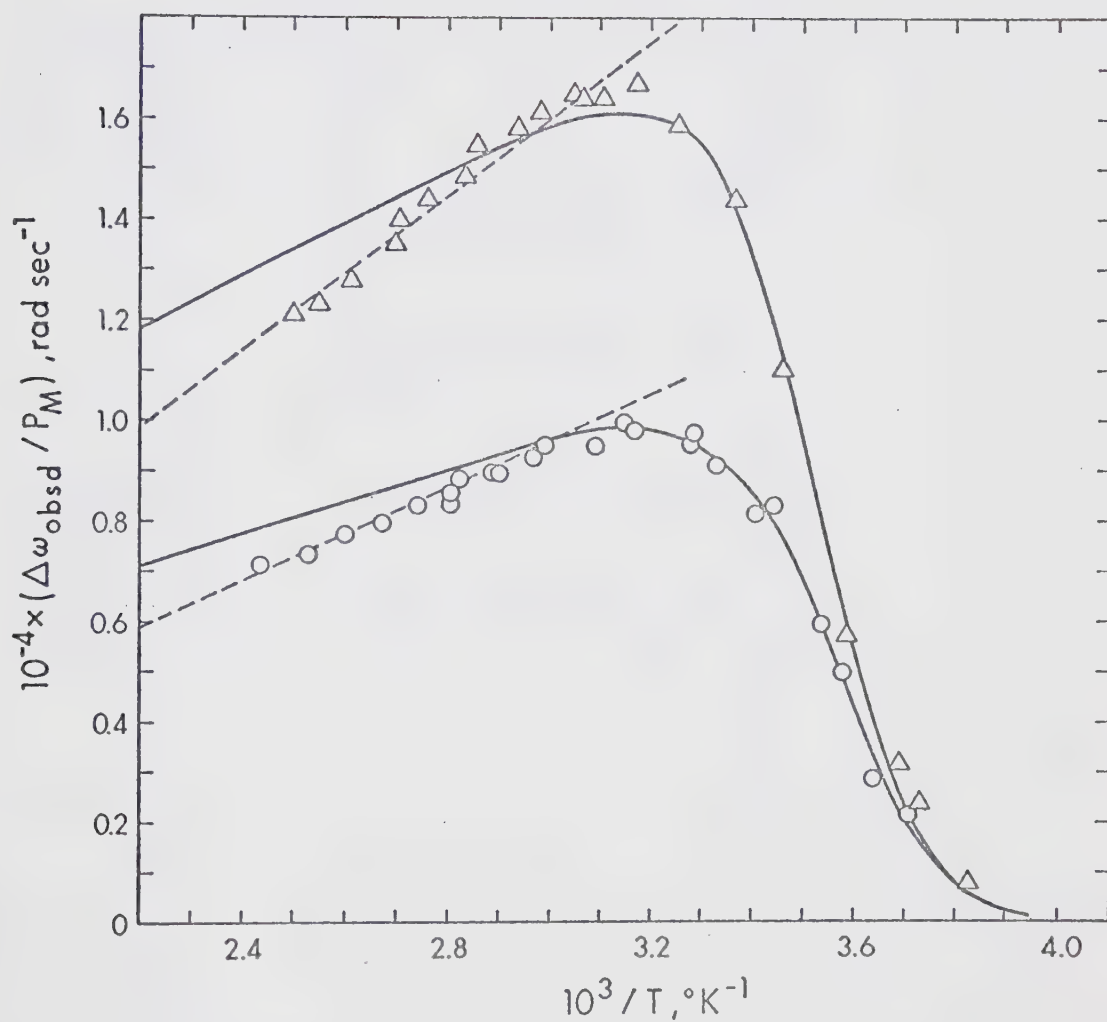


Figure 34: Temperature dependence of $(\Delta\omega_{\text{obsd}}/P_M)$ for the formyl proton in N,N-dimethylformamide solutions of $\text{NiTAAB}(\text{ClO}_4)_2$ at 100 MHz (Δ) and 60 MHz (o).

TABLE XVII

Least-squares best fit parameters for NiTAAB^{2+} in N,N -dimethylformamide

	$(T_{2pM})^{-1}$ Data				$(\Delta\omega_{\text{obsd}}/P_M)$ Data			
	60 MHz		100 MHz		60 MHz		100 MHz	
	A	B	C	D	E	F	G	H
ΔH^\ddagger , kcal mol ⁻¹	11.46	11.87	11.19	11.90	11.65	11.40	11.65 (f)	11.46
ΔS^\ddagger , cal mol ⁻¹ deg ⁻¹	2.24	3.68	0.96	3.46	2.65	1.68	2.79	2.18
$10^{-6} \times C_\omega$, rad sec ⁻¹ °K ⁻¹ (a)	3.21	3.21	5.35	5.35	5.35	5.35	3.22	5.35
E_M , kcal mol ⁻¹	1.78	1.78	2.13	2.34 (c)	2.18	1.78 (d)	1.78 (e)	1.78 (e)
E_O , kcal mol ⁻¹	2.85	2.34 (b)	2.77	2.34 (c)	2.34 (b)	2.34 (b)	—	—
C_M , sec ⁻¹	312.5	308.4	189.0	137.8	173.1	312.9	308.4 (e)	308.4 (e)
C_O , sec ⁻¹	2.30	7.63 (b)	2.82	7.63	7.63 (b)	7.63 (b)	—	—

(a) C_ω was held constant at the value determined by the 60 MHz shifts or at its corresponding 100 MHz value in all of the $(T_{2P_M})^{-1}$ fits.

(b) $(T_{2O})^{-1}$ parameters fixed as determined by fit D.

(c) $E_M = E_O$ assumed.

(d) E_M held constant at value indicated by fits A and B.

(e) $(T_{2M})^{-1}$ parameters held constant as determined by fit B.

(f) Held constant.

$T^{-1} = 0^\circ K^{-1}$. Measurements of the solution magnetic susceptibility of both $NiTAAB(ClO_4)_2$ and $NiTAAB(NO_3)_2$, using the method suggested by Evans,²⁷ have shown that the decreased chemical shift in the fast exchange limit is due to the presence of a diamagnetic-paramagnetic equilibrium with the diamagnetic species being formed at high temperatures. Within experimental error, the same temperature dependence of the molar magnetic susceptibilities was observed for both the nitrate and perchlorate salts. Since this susceptibility data (Table LX) and the solvent formyl proton chemical shifts of Figure 34 both indicate a small temperature dependence for the diamagnetic-paramagnetic equilibrium, a very accurate determination of the equilibrium constants is not possible. However, estimates of ΔH° and ΔS° for the equilibrium written as



were obtained. A fit of the susceptibility data to eq 41, with θ assumed to be zero, gave $\Delta H^\circ = -3.96 \text{ kcal mol}^{-1}$, $\Delta S^\circ = -7.42 \text{ cal mol}^{-1} \text{deg}^{-1}$ and $\mu_\infty = 3.14 \text{ BM}$. These values of ΔH° and ΔS° are in reasonable agreement with the values, $\Delta H^\circ = -4.1 \text{ kcal mol}^{-1}$ and $\Delta S^\circ = -5.6 \text{ cal mol}^{-1} \text{deg}^{-1}$, calculated from the observed formyl proton chemical shift data (dashed lines) and the predicted chemical shifts (solid curves) of Figure 34; the latter being calculated by fits

of the observed chemical shifts at lower temperatures to eq 8, assuming a normal temperature dependence for $\Delta\omega_M$ (eq 11).

The similarity of the ΔH° and ΔS° values obtained here with those found for NiCR^{2+} in DMF suggests that the diamagnetic species in the present study can be identified as square planar NiTAAB^{2+} . The paramagnetic species for the perchlorate salt is assumed to be $\text{NiTAAB}(\text{DMF})_2^{2+}$.

Aside from the complications due to the diamagnetic-paramagnetic equilibrium, outlined above, the line broadening and chemical shift temperature dependencies for NiTAAB^{2+} are qualitatively similar to those observed for NiTRI^{2+} . The same limiting conditions, 25(a) - 25(d), account for the four limiting regions of line broadening, however, the $(T_{2M})^{-1}$ contribution for NiTAAB^{2+} is more significant and not well resolved from $\tau_M \Delta\omega_M^2$, especially at 60 MHz. Consequently, the chemical shifts were essential in defining C_ω when the $(T_{2P}P_M)^{-1}$ results were fitted to eq 2, modified by the added $(T_{2O})^{-1}$ term. Because of the effect of the diamagnetic-paramagnetic equilibrium at higher temperatures, only the chemical shift data for temperatures below 90°C were fitted to eq 8. The parameters from the various least-squares fits of the line broadenings and frequency shifts are summarized in Table XVII.

It should be observed that the two five-parameter fits of the 60 and 100 MHz $(T_{2P}P_M)^{-1}$ data, shown as A and C,

both indicate that the approximation, $E_M = E_O$, does not appear to be completely justified for this system. In addition, the data at the two frequencies is most accurately fitted to the same kinetic parameters if E_M is allowed to be greater at 100 MHz (~ 2.2 kcal mol $^{-1}$) than at 60 MHz (1.78 kcal mol $^{-1}$). Although these differences between E_M at the two frequencies might be real, various fits show that ΔH^\ddagger and ΔS^\ddagger are not greatly affected by changes in E_M . On the basis of the reasonable fit of the 100 MHz data according to fit F, in which the $(T_{2M})^{-1}$ activation energy was held at 1.78 kcal mol $^{-1}$, and the unacceptable fit of the 60 MHz data with $E_M = 2.18$ kcal mol $^{-1}$, it is concluded that the former value for E_M is the most acceptable.

The average values of ΔH^\ddagger and ΔS^\ddagger , with their estimated uncertainties, are 11.5 ± 0.5 kcal mol $^{-1}$ and 2.5 ± 2 cal mol $^{-1}$ deg $^{-1}$, respectively. With $C_\omega(60 \text{ MHz}) = 3.21 \times 10^6$ rad sec $^{-1}$ °K and $\mu_{\text{eff}} = 3.14$ BM, the latter being the limiting magnetic moment estimated from the solution magnetic susceptibility study, the hyperfine coupling constant (A/h) of the CH proton is calculated to be 2.29×10^6 rad sec $^{-1}$.

T_{2M} and T_{2O} Considerations for $\text{NiTRI}(\text{ClO}_4)_4 \cdot 2$ and $\text{NiTAAB}(\text{ClO}_4)_4 \cdot 2$ in DMF

The values of $(T_{2M})^{-1}$ and $(T_{2O})^{-1}$ obtained in this study can be well accounted for in terms of the dipolar and

hyperfine contributions to $(T_{2M})^{-1}$ and only the dipolar contributions to $(T_{2O})^{-1}$, using eq 13 and 23, respectively. For $\text{NiTRI}(\text{DMF})_3^{2+}$, the observed outer sphere broadening of $3.94 \times 10^2 \text{ sec}^{-1}$ at 25°C predicts an electron spin relaxation time of $2.9 \times 10^{-11} \text{ sec}$ ($T_{1e} = T_{2e}$ assumed) if the outer sphere interaction distance $(d_o)_{\text{CH}}$ and the rotational correlation time are assumed to be 5.75\AA and $1.2 \times 10^{-10} \text{ sec}$,⁴⁴ respectively. The above electron spin relaxation time, an inner sphere interaction distance $(r_i)_{\text{CH}}$ of 3.29\AA , and the hyperfine coupling constant given earlier, predict dipolar and scalar contributions of $5.41 \times 10^3 \text{ sec}^{-1}$ and $1.67 \times 10^2 \text{ sec}^{-1}$ at 25°C , respectively. The observed $(T_{2M})^{-1}$ at 25°C is $5.58 \times 10^3 \text{ sec}^{-1}$. (60 MHz fit of Table XVI).

Similarly for $\text{NiTAAB}(\text{DMF})_2^{2+}$, the observed value of $6.22 \times 10^3 \text{ sec}^{-1}$ for $(T_{2M})^{-1}$, from fit B of Table XVII, is consistent with $(r_i)_{\text{CH}} = 3.02\text{\AA}$, $\tau_r = 1.2 \times 10^{-10} \text{ sec}$ and $T_{1e} = T_{2e} = 1.85 \times 10^{-11} \text{ sec}$. The outer sphere relaxation time of $3.98 \times 10^2 \text{ sec}^{-1}$ is consistent with $(d_o)_{\text{CH}} = 5.75\text{\AA}$. All of the interaction distances and electron spin relaxation times found here appear to be consistent with expected values for nickel(II) complexes. The significantly smaller interaction distances obtained in this study for $\text{NiTAAB}(\text{DMF})_2^{2+}$ and $\text{NiTRI}(\text{DMF})_3^{2+}$, compared to those observed for the complexes $\text{NiCR}(\text{DMF})_2^{2+}$ and $\text{NiCRMe}(\text{DMF})_2^{2+}$, are consistent with less steric influence from the Schiff

base ligands in the former complexes. Thus, on the basis of the value of $(r_i)_{CH}$ calculated for $NiTAAB(DMF)_2^{2+}$, longer interaction distances do not appear to be a general property of tetragonally distorted complexes.

The kinetic results from the study of these two Schiff base complexes of nickel(II) will be discussed and compared to the results for $NiCR^{2+}$ and $NiCRMe^{2+}$ in Chapter IV.

6. Solvent Proton NMR Line Broadening Study of the Cobalt(II) Schiff Base Complexes, $\text{Co}(\text{trans}[14]\text{diene})^{2+}$ and CoCR^{2+} , and of the Copper(II) Complex, CuCR^{2+} , in Various Solvents

The proton nmr line broadening studies reported in this section were undertaken in order to extend the solvent exchange studies of the nickel(II) and manganese(II) Schiff base complexes, discussed in the previous sections, to cobalt(II) and copper(II) systems. The temperature dependence of the nmr line broadening of water, methanol and acetonitrile solvents containing the cobalt(II) complex 5,7,7,12,14,14-hexamethyl-1,4,8,11-tetraazacyclotetradeca-4,11-dienecobalt(II), referred to as $\text{Co}(\text{trans}[14]\text{-diene})^{2+}$ and shown as structure IV, were investigated. In addition, the cobalt(II) and copper(II) complexes of the Schiff base CR ligand were studied in DMF and the copper(II) complex was also studied in water. In all of these systems no chemical exchange effects on the line broadening are observed, and therefore, discussion will center mainly on whether solvent exchange is fast and $(T_{2P})^{-1}$ is controlled by inner sphere T_{2M} relaxation or whether exchange is slow and $(T_{2P})^{-1}$ is determined exclusively by outer sphere T_{20} relaxation. A decision in this regard allows lower or upper limits to be placed on the solvent exchange rates. An attempt is also made to quantitatively explain the mechanism of the T_{2M} relaxation.

Co(trans[14]diene)²⁺ in Acetonitrile, Water and Methanol

The temperature dependencies of $-\log(T_{2P}P_M)$ for Co(trans[14]diene)²⁺ in water and in methanol are shown by the upper and lower curves, respectively, in Figure 35. The data for this complex in acetonitrile are shown in Figure 36 (lower curve). Only the tetrafluoroborate salt was studied in methanol, but both the tetrafluoroborate and perchlorate salts were used in water and in acetonitrile, and both salts gave the same temperature dependence of $(T_{2P}P_M)^{-1}$. Measurements were made at 60 MHz but for Co(trans[14]diene)²⁺ in water a few data points were also obtained at 100 MHz. No frequency dependence of $(T_{2P})^{-1}$ was observed in this system.

Measurable chemical shifts were observed only for Co(trans[14]diene)²⁺ in acetonitrile and these are shown in Figure 37. For the remaining systems, the frequency shifts were too small to be measured accurately at the complex concentrations employed.

All the $(T_{2P}P_M)^{-1}$ and $(\Delta\omega_{\text{obsd}}/P_M)$ data shown in the figures have been calculated from the observed line broadenings and chemical shifts assuming two inner sphere solvent molecules.

It should be noted that Co(trans[14]diene)²⁺ is a low spin cobalt(II) complex. Magnetic susceptibility measurements, which were made on an aqueous solution of the perchlorate salt at several temperatures, gave an effective

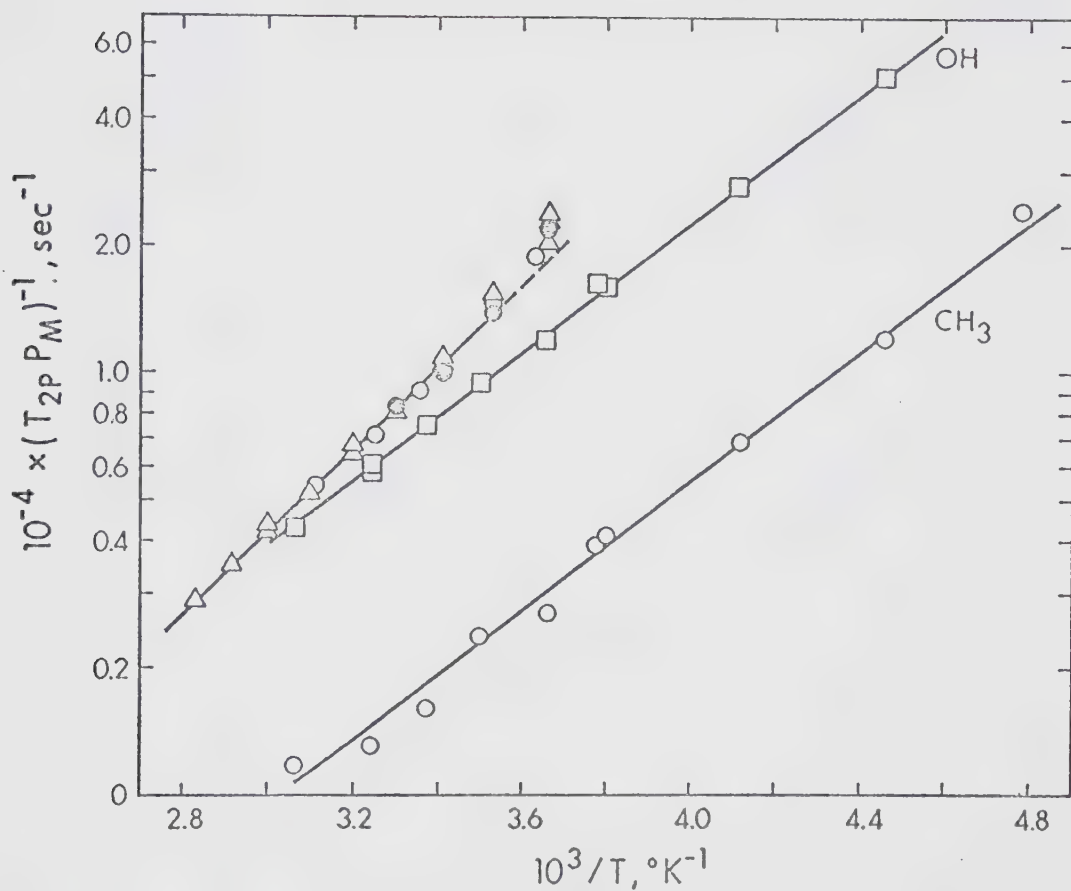


Figure 35: Temperature dependence of $-\log(T_{2P}P_M)^{-1}$ for the hydroxy and methyl protons in methanol solutions of $\text{Co}(\text{trans}[14]\text{diene})(\text{BF}_4)_2$ at 60 MHz (lower two curves), and for the water proton in aqueous solutions of the ClO_4^- (Δ) and BF_4^- (o) salts of $\text{Co}(\text{trans}[14]\text{diene})^{2+}$ at 60 MHz (upper curve). In the upper curve \bullet represents a 100 MHz measurement on the ClO_4^- salt.

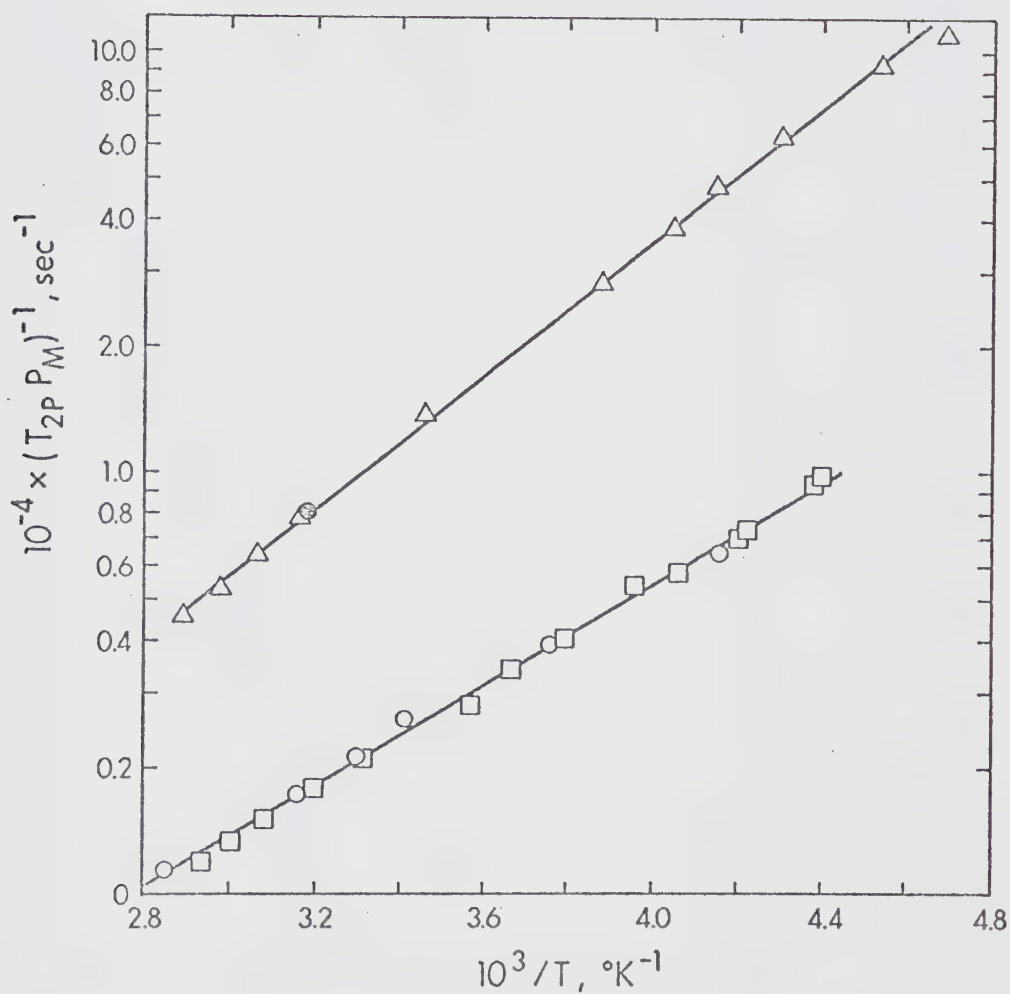


Figure 36: Temperature dependence of $-\log(T_{2P}P_M)$ for the methyl protons in acetonitrile solutions of the ClO_4^- (\square) and BF_4^- (\circ) salts of $\text{Co}(\text{trans}[14]\text{diene})^{2+}$ (lower curve) at 60 MHz; and for N,N -dimethylformamide solutions of $\text{CoCR}(\text{ClO}_4)_2$ (upper curve), at 60 MHz (Δ), and 100 MHz (\bullet).

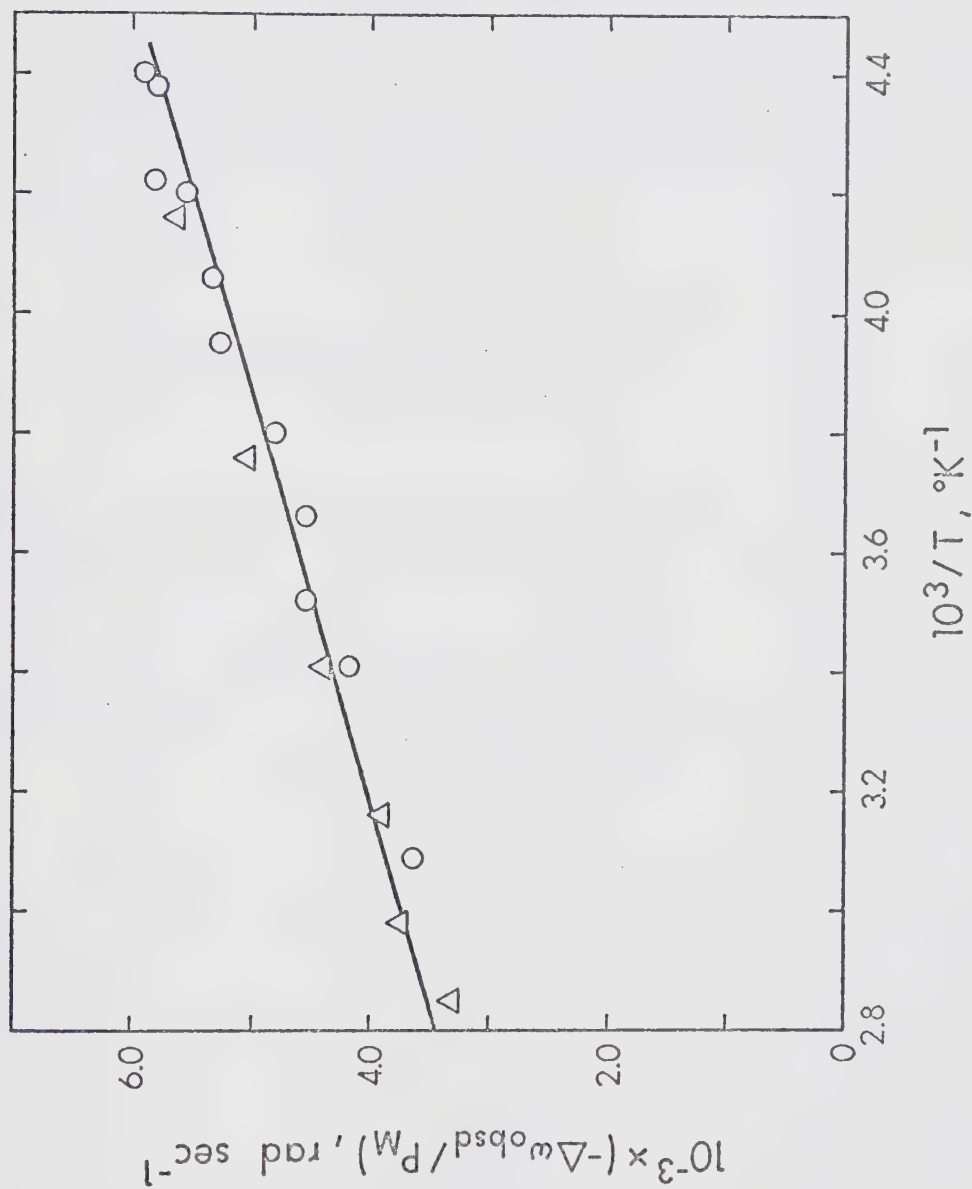


Figure 37: Temperature dependence at 60 MHz of $(\Delta\omega_{\text{obsd}}/P_M)$ for the methyl protons in acetonitrile solutions of the ClO_4^- (o) and BF_4^- (Δ) salts of $\text{Co}(\text{trans}[14]\text{diene})^{2+}$.

TABLE XVIII

NMR results and calculations for Co(trans[14]diene)²⁺, CoCR²⁺ and CuCR²⁺ in

several solvents

Complex	Co(trans[14]diene) ²⁺				CoCR ²⁺		CuCR ²⁺	
	Water	CH ₃ OH	CH ₃ CN	CH ₃	DMF	CH	Water	DMF
Solvent	OH	OH	CH ₃	CH ₃			OH	CH
Proton								
E _a , kcal mol ⁻¹	4.34	3.49	3.49	2.73	3.62		3.89	2.98
(C _M + C _O), sec ⁻¹	6.04	20.1	4.95	22.4	24.2		14.1	28.1
10 ⁻³ x(T _{2P_M}) ⁻¹ , sec ⁻¹ (a)	9.30	7.30	1.80	2.25	10.8		10.0	4.30
10 ⁻³ x(T _{2M_{DD}}) ⁻¹ , sec ⁻¹ (b)	6.55	4.86	0.89	0.23	9.10		5.44	2.60
10 ⁻³ x(T _{2M_{HF}}) ⁻¹ , sec ⁻¹ (c)	—	0.90(d)	—	1.71	—		—	—
10 ⁻³ x(T ₂₀) ⁻¹ , sec ⁻¹	2.75	1.55	0.90	0.31	1.70		4.56	1.70
r _i , Å	2.90	2.95(e)	3.9(e)	5.3(f)	3.20		2.90	3.95
d _O , Å	4.65	4.0(e)	4.8(e)	9.4(f)	5.75(g)		4.65	5.75(g)
10 ¹¹ xτ _r , sec ⁻¹	4.50	3.7	6.2(f)		11.5(g)		3.7	11.5(g)
10 ⁹ xT _{2e} , sec ⁻¹	1.2	—	1.4		0.3		—	—

(a) At 25°C assuming n=2 in the calculation of P_M for Co(trans[14]diene)²⁺ but n=1 for CuCR²⁺ and CoCR²⁺.(b) The dipolar contribution to (T_{2P_M})⁻¹.(c) The hyperfine contribution to (T_{2P_M})⁻¹.(d) Estimated from the observed (T_{2P_M})⁻¹ and the dipolar contribution to (T_{2M})⁻¹.(e) The interaction distances for VO²⁺ ion in methanol from ref 45.(f) The values obtained for VO²⁺ ion in acetonitrile, ref 44.(g) The values obtained for VO²⁺ in DMF, ref 44.

magnetic moment of 2.07 BM after correction of the observed molar magnetic susceptibilities (Table LXII) for the diamagnetism of the Schiff base ligand (-213 cgs units).²⁸

Although no previous measurement of μ_{eff} for this complex is available for comparison, the value obtained here is consistent with the values normally observed for low-spin cobalt(II) complexes.⁵⁵

The $(T_{2P}P_M)^{-1}$ results for each system were fitted graphically to the equation

$$(T_{2P}P_M)^{-1} = (C_M + C_O)\exp(E_a/RT) \quad (53)$$

and the best-fit values of the constant, $C_M + C_O$, and the effective activation energy, E_a , are given in Table XVIII.

However, it should be noted that, for $\text{Co}(\text{trans}[14]\text{diene})^{2+}$ in water, $(T_{2P}P_M)^{-1}$ increases more rapidly at low temperature than is predicted by eq 53. Only the data points

near 0°C deviate significantly from this exponential temperature dependence. Since the nmr line widths were independent of frequency, the nonexponential behaviour of

$(T_{2P}P_M)^{-1}$ at low temperatures cannot be ascribed to $\tau_M\Delta\omega_M^2$ effects (limiting condition 25(b)). Also, since the temperature variation of the magnetic susceptibilities did not indicate an unusual increase in μ_{eff} at low temperature, the above behaviour is not due to a temperature dependent magnetic moment. It is possible that the discrepancy is

due to a nonexponential increase in the viscosity of water at temperatures near the freezing point. For this system, the value of E_a and $(C_M + C_O)$ were estimated from the data at higher temperatures.

For $\text{Co}(\text{trans}[14]\text{diene})^{2+}$ in acetonitrile, the presence of chemical shifts, with the temperature dependence shown in Figure 37, indicates that solvent exchange is fast, and therefore, $(T_{2P_M})^{-1}$ is controlled by T_{2M} and T_{2O} relaxation. The close agreement of the value found here for E_a with the apparent activation energy of the viscosity of acetonitrile ($\sim 3.0 \text{ kcal mol}^{-1}$) might be taken to mean that both inner and outer sphere relaxation are due to dipolar interactions for which the correlation time is τ_r . However, substitution of reasonable estimates of r_i , d_o and τ_r , given in Table XVIII, into eqs 29 and 30 indicates that most of the observed broadening for this system is due to a hyperfine interaction. To account for the large hyperfine contribution using the hyperfine coupling constant, $-2.24 \times 10^6 \text{ rad sec}^{-1}$, determined from the measured chemical shifts, a value of $1.36 \times 10^{-9} \text{ sec}$ is required for T_{1e} at 25°C . This value of T_{1e} compares well with the experimental value of $1.4 \times 10^{-9} \text{ sec}$ obtained for T_{2e} . The latter was obtained from the epr spectrum of $\text{Co}(\text{trans}[14]\text{diene})(\text{BF}_4)_2$ in acetonitrile which will be discussed subsequently.

It should be noted that the observed chemical shifts for this system do not strictly adhere to a Curie law temp-

erature dependence as the extrapolated shift at $T^{-1} = 0^\circ\text{K}^{-1}$ is 120 Hz. As a result, the value of A/\hbar given above was calculated from the observed shift at 25°C , assuming $\mu_{\text{eff}} = 2.07 \text{ BM}$, instead of from the value of C_ω .

For $\text{Co}(\text{trans}[14]\text{diene})^{2+}$ in water, the $(T_{2P}P_M)^{-1}$ results are similar but no chemical shifts were observed for this system. Therefore, it is not possible to even estimate the hyperfine contribution to $(T_{2M})^{-1}$. However, calculations based on a primary solvent coordination number of two, using the reasonable interaction distances and correlation times listed in Table XVIII, indicate that $(T_{2P}P_M)^{-1}$ can be explained solely by inner and outer sphere dipolar interactions. In view of the T_{2e} estimate of 1.2×10^{-9} sec obtained from the epr spectrum of $\text{Co}(\text{trans}[14]\text{-diene})(\text{ClO}_4)_2$ in water, the negligible hyperfine interactions indicated by the above calculations must mean that A/\hbar for this system is small. From the acceptable agreement of the $(T_{2P})^{-1}$ activation energy with that expected for water viscosity ($3.9 \text{ kcal mol}^{-1}$) and the observation that $T_{2e} \gg \tau_r$, it is reasonable to conclude that the dipolar correlation time given in Table XVIII can be interpreted as τ_r . The value of τ_r obtained here is in good agreement with the value 4.1×10^{-11} sec obtained from an analysis of the epr spectrum of VO^{2+} ion in water⁵³.

In the case of $\text{Co}(\text{trans}[14]\text{diene})^{2+}$ in methanol, the observed $(T_{2P}P_M)^{-1}$ at 25°C for the hydroxy and methyl

protons were similarly interpreted in terms of $(T_{2M})^{-1}$ and $(T_{20})^{-1}$ contributions, assuming two rapidly exchanging inner sphere solvent molecules. Since measurable chemical shifts were not observed in this system, the hyperfine contribution to $(T_{2M})^{-1}$ cannot be calculated. However, the dipolar interaction distances and correlation time given in Table XVIII, which are all in good agreement with the values observed for VO^{2+} in methanol,⁴⁵ predict a small hyperfine contribution for the OH proton. The fact that the hyperfine contribution is small for the OH proton but negligible for the CH_3 protons was found to be compatible with the estimated value of T_{1e} , the absence of chemical shifts, and the large difference expected for the hyperfine coupling constants (A/\hbar) for the two different types of protons. Thus, if the values of A/\hbar for this system were different by a factor of 20, as was observed for Co^{2+} ion in methanol,²³ then the hyperfine contribution for the CH_3 protons would be less than 1% of the total $(T_{2M})^{-1}$. To account for the estimated hyperfine contribution for the OH proton, a value of $T_{1e} \approx 10^{-9}$ sec would necessitate an estimated $(A/\hbar)_{OH}$ of $\sim 6 \times 10^6$ rad sec⁻¹. For a 0.1 m solution this A/\hbar predicts a negligible OH proton chemical shift.

The nmr results for $Co(trans[14]diene)^{2+}$, discussed above, allow lower limits to be placed on the exchange rates of one solvent molecule. These limits for acetonitrile

trile, water and methanol exchange at 25°C are, respectively, $1 \times 10^4 \text{ sec}^{-1}$, $2.4 \times 10^4 \text{ sec}^{-1}$ and $7 \times 10^4 \text{ sec}^{-1}$.

EPR Results for $\text{Co}(\text{trans}[14]\text{diene})^{2+}$

In order to obtain the estimates of the electron spin relaxation times for $\text{Co}(\text{trans}[14]\text{diene})^{2+}$, which were used in the above discussion of the nmr results, the epr spectrum of this complex was obtained in acetonitrile and water at room temperature. Also, since in several instances well-resolved epr spectra for cobalt(II) systems have been observed only for oxygenated adducts,^{65,66} the possibility of oxygen coordination to $\text{Co}(\text{trans}[14]\text{diene})^{2+}$ was examined.

An epr spectrum of $\text{Co}(\text{trans}[14]\text{diene})^{2+}$ was initially determined for an aqueous solution of the perchlorate salt. This solution was not degassed and the spectrum was measured immediately after the sample was prepared. The resulting spectrum was well resolved into eight hyperfine lines due to coupling to the cobalt nucleus ($I = 7/2$) and was qualitatively similar to the fluid solution spectra observed by Hoffman and Basolo⁶⁵ for a series of oxygenated cobalt(II) Schiff base complexes, and to the spectra described by Yang and Oster⁶⁶ for several oxygenated cobalt(II) polyamines. However, in the spectrum obtained for $\text{Co}(\text{trans}[14]\text{diene})^{2+}$ the hyperfine coupling constant of 82 G is much larger than the characteristic value of ~13 G

found by the above workers for the monomeric oxygen adducts. This feature alone appears to indicate that $\text{Co}(\text{trans}[14]\text{diene})^{2+}$ does not bind molecular oxygen. As a further investigation in this regard, two additional epr spectra were obtained for $\text{Co}(\text{trans}[14]\text{diene})(\text{BF}_4)_2$ in acetonitrile. The first of these was determined for a thoroughly degassed solution, while the second was obtained for the same solution through which oxygen was bubbled. No difference was observed in the latter two spectra and both were similar to the spectrum of the perchlorate salt in aqueous solution, discussed above. However, for the spectrum of the tetrafluoroborate salt in acetonitrile the hyperfine splitting was not as well resolved; the splitting constant being 70 G as compared to 82 G obtained for the perchlorate salt in water. The line widths of the narrowest hyperfine components were ~ 48 G and ~ 43 G in acetonitrile and water, respectively. This gives values of $\sim 1.4 \times 10^{-9}$ sec and $\sim 1.2 \times 10^{-9}$ sec, respectively, for T_{2e} .

CoCR^{2+} in N,N-dimethylformamide

The temperature dependence of $(T_{2P_M})^{-1}$ for the formyl proton, determined for DMF solutions of the perchlorate salt, is shown by the upper curve in Figure 36. A graphical fit of this data to eq 53 gave the best-fit values of $(C_M + C_O)$ and E_a indicated in Table XVIII. The value of $(T_{2P_M})^{-1}$ at 25°C is most consistent with rapid solvent

exchange and dipolar T_{2M} and T_{20} contributions, but a somewhat better interpretation results if it is assumed that CoCR^{2+} is five-coordinate in DMF at this temperature. Thus, the value of 3.2\AA calculated for $(r_i)_{\text{CH}}$ assuming a primary solvent coordination number (n) of one and the values of d_o and τ_r , given in Table XVIII, would become 3.58\AA if n were assumed to be two. Although the former value is in better agreement with the value of 3.1\AA found for VO^{2+} in DMF⁴⁴ the argument for five-coordinate cobalt based on this evidence alone would be inconclusive. However, in view of the observation made by Long and Busch³⁷ that $\text{CoCR}(\text{ClO}_4)_2$ does not form bis-adducts with the strong Lewis bases, ammonia and pyridine, the calculation using $n=1$ appears to be the more consistent one. It should be noted, however, that the good agreement of r_i with the value 3.1\AA may be at least partly fortuitous because of the neglect of possible hyperfine interactions. There is also the possibility of a five-coordinate-six-coordinate equilibrium in this system since the E_a obtained here is unexpectedly larger than the apparent activation energy of the viscosity of DMF ($\sim 2.8 \text{ kcal mol}^{-1}$).

In order to further characterize this complex and to estimate the magnitude of the hyperfine contribution to $(T_{2M})^{-1}$, the magnetic susceptibility and the epr spectrum of $\text{CoCR}(\text{ClO}_4)_2$ were examined in DMF. A value of 1.85 BM was obtained for the effective magnetic moment after

applying a diamagnetic correction of -163 cgs units²⁸ to the measured susceptibility at 35°C . The epr spectrum of a degassed DMF solution of this low-spin cobalt(II) complex at room temperature consisted of only a broad line in which the hyperfine coupling was not resolved. A value of $\sim 3 \times 10^{-10}$ sec was estimated for T_{2e} from this spectrum. Therefore, for reasonable estimates of $(A/\hbar)_{\text{CH}}$, the above value of the electron spin relaxation time ($T_{1e} = T_{2e}$ assumed) would yield a hyperfine contribution which is $\sim 10\%$ of the total observed $(T_{2P}P_M)^{-1}$.

From the nmr results discussed above, a lower limit of $1 \times 10^5 \text{ sec}^{-1}$ is estimated for the DMF exchange rate of CoCR^{2+} at 25°C .

CuCR^{2+} in DMF and Water

The temperature dependencies of $(T_{2P}P_M)^{-1}$ for $\text{CuCR}(\text{BF}_4)_2$ in DMF and water are shown by the upper and lower curves, respectively, in Figure 38. Chemical shifts were observed only for CuCR^{2+} in DMF and these are given in Figure 39. Only the CH proton line widths and frequency shifts were studied for the DMF solutions. Measurements were made at 60 and 100 MHz and these indicated an absence of a frequency dependent T_{2P} value in the entire range of temperatures studied.

All of the data in Figures 38 and 39 were calculated from the observed T_{2P} and $\Delta\omega_{\text{obsd}}$ assuming that CuCR^{2+} is

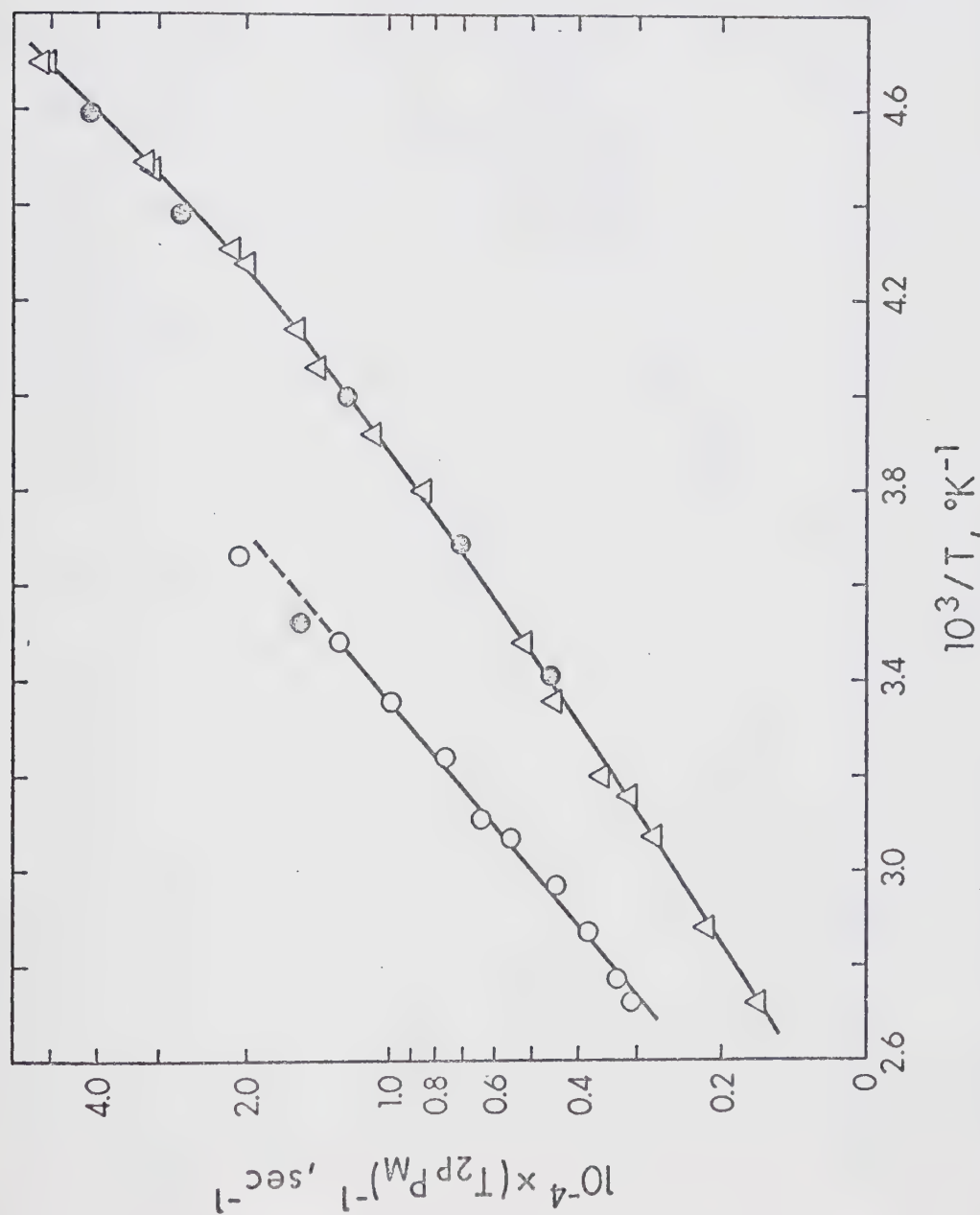


Figure 38: Temperature dependence of $-\log(T_{2PM})$ for the formyl proton in N,N-dimethylformamide solutions of $\text{CuCR}(\text{BF}_4)_2$ (lower curve), at 60 MHz (Δ), and 100 MHz (\bullet); and for the water proton in aqueous solutions of $\text{CuCR}(\text{BF}_4)_2$ (upper curve), at 60 MHz (o), and 100 MHz (\bullet).

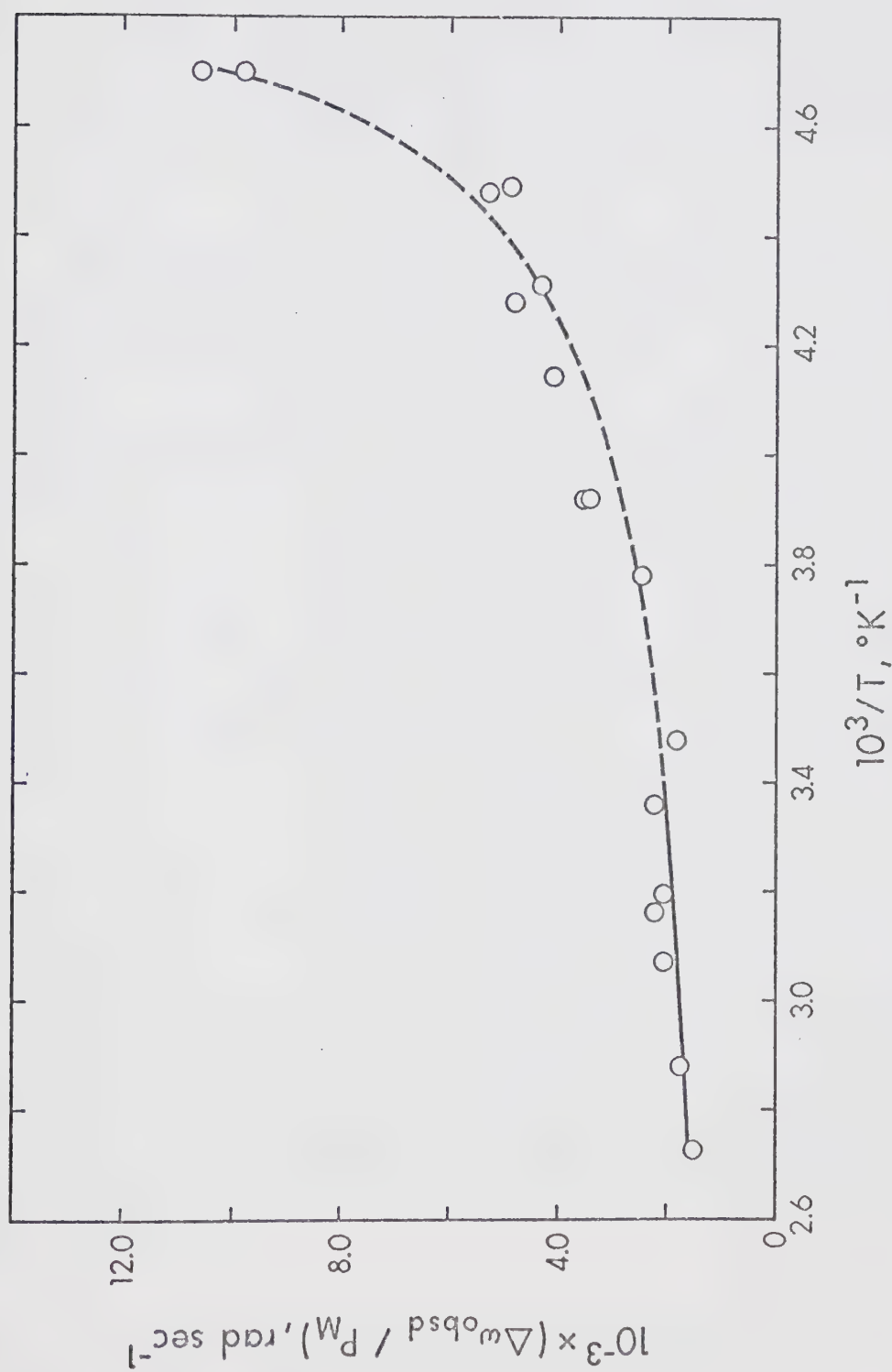


Figure 39: Temperature dependence at 60 MHz of $(\Delta\omega_{\text{obsd}}/P_M)$ for the formyl proton in N,N-dimethylformamide solutions of $\text{CuCR}(\text{BF}_4)_2$.

five-coordinate in these solvents over the complete temperature range studied. That is, a value of one was used for n in the calculation of P_M from eq 4. However, it will be shown below that this assumption is only partly justified.

The $(T_{2P}P_M)^{-1}$ data for CuCR^{2+} in DMF clearly indicates a gradual increase in the apparent activation energy of $(T_{2P}P_M)^{-1}$ with decreasing temperature. In view of the frequency independent T_{2P} , and the unusual temperature dependence of the CH proton chemical shifts, shown in Figure 39, it must be concluded that an equilibrium is present in solution. Since the chemical shifts in the high temperature region do not drop off to zero, but instead follow a Curie law temperature dependence, the species formed at high temperature cannot be predominantly CuCR^{2+} with no DMF molecules in its inner coordination sphere. From this point of view, outer sphere interactions could account for the observed $(T_{2P}P_M)^{-1}$ at high temperatures but would fail to explain the presence of chemical shifts in the high temperature region. On the other hand, both the chemical shifts and the line broadening data are consistent with the equilibrium



with the five-coordinate species, $\text{CuCR}(\text{DMF})$, being thermo-

dynamically favored at higher temperatures. Thus, the upward curvature in the chemical shifts and $(T_{2P_M})^{-1}$ data with decreasing temperature, indicated by the dashed lines in Figures 38 and 39, is due to a shift of equilibrium 54 to the right. From the high temperature chemical shifts the hyperfine coupling constant (A/\hbar) for $\text{CuCR}(\text{DMF})$ can be determined, but this chemical shift data do not permit measurement of A/\hbar for $\text{CuCR}(\text{DMF})_2$. Therefore, the temperature dependence of the equilibrium cannot be determined. The small observed chemical shifts of the broad formyl resonance at low temperatures are also a limitation in this regard. However, it should be noted that both the Curie dependence of the chemical shift for temperatures as high as $\sim 0^\circ\text{C}$ ($T^{-1} \approx 3.7 \times 10^{-3} \text{ }^\circ\text{K}^{-1}$), and the linear dependence of $-\log (T_{2P_M})$ with T^{-1} in the high temperature region, indicate that, essentially all of the complex exists in the five-coordinate form at temperatures $\geq 0^\circ\text{C}$. A graphical fit of the data in this linear line broadening region to eq 53 gave the values of $(C_M + C_O)$ and E_a indicated in Table XVIII.

The observed $(T_{2P_M})^{-1}$ at 25°C is interpreted in terms of rapid exchange of one DMF molecule giving rise to the $(T_{2M})^{-1}$ and $(T_{2O})^{-1}$ contributions shown in Table XVIII. The values of $(d_O)_{\text{CH}}$ and τ_r used to calculate $(T_{2O})^{-1}$ are those observed for the VO^{2+} -DMF system.⁴⁴ If all of the observed $(T_{2M})^{-1}$ is assumed to be due to dipolar inter-

actions, modulated by complex tumbling, then a value of 3.95\AA is obtained for $(r_i)_{\text{CH}}$. This is considerably larger than the 3.1\AA obtained in ref 44 for VO^{2+} in DMF but the agreement is not improved by assuming that the predominant copper species at 25°C is $\text{CuCR}(\text{DMF})_2$ instead of $\text{CuCR}(\text{DMF})$. It should be noted that the observed CH proton chemical shifts in the high temperature region give a large estimated value of $1.28 \times 10^6 \text{ rad sec}^{-1}$ for $(A/h)_{\text{CH}}$, if μ_{eff} is assumed to have a spin-only value of 1.73 BM. Thus, in order to justify neglecting the hyperfine contribution to $(T_{2M})^{-1}$, a value of 10^{-9} sec is required for T_{1e} . Although a T_{1e} of this order of magnitude was not confirmed by measurement of T_{2e} from the epr spectrum of CuCR^{2+} in DMF, a value of $\leq 10^{-9} \text{ sec}$ is reasonable for a copper(II) complex.⁶⁷

For $\text{CuCR}(\text{BF}_4)_2$ in water the $(T_{2P}P_M)^{-1}$ results are similar. However, since the line broadening is greater than in the $\text{CuCR}(\text{BF}_4)_2$ -DMF system, the chemical shifts are obscured, and thus it is not possible to tell whether the slight nonexponential increase of $(T_{2P}P_M)^{-1}$ at low temperatures is due to an increase in the primary solvent coordination number, as was proposed for CuCR^{2+} in DMF, or to a nonexponential increase in the viscosity of water. The variation of $-\log (T_{2P}P_M)$ with T^{-1} is essentially linear at higher temperatures and from this region the best-fit values of $(C_M + C_O)$ and E_a , shown in Table XVIII, were ob-

tained. For this system, the value of $(T_{2P}^{PM})^{-1}$ at 25°C can be adequately accounted for in terms of $(T_{2M})^{-1}$ and $(T_{2O})^{-1}$ dipolar interactions using the interaction distances and correlation time given in Table XVIII. It should be noted that the value of τ_r obtained here is in reasonable agreement with the value 4.5×10^{-11} sec obtained above for $\text{Co}(\text{trans}[14]\text{diene})^{2+}$ in water and that E_a agrees well with that expected for water viscosity.

Thus, the nmr results discussed above for CuCR^{2+} in DMF and water are consistent with the rapid exchange of one solvent molecule for which the lower limit of the exchange rate at 25°C is estimated to be $3 \times 10^4 \text{ sec}^{-1}$ and $1 \times 10^4 \text{ sec}^{-1}$ for DMF and water, respectively.

In conclusion, it should be noted that the estimates of the lower limits of the solvent exchange rates given here for $\text{Co}(\text{trans}[14]\text{diene})^{2+}$, CoCR^{2+} and CuCR^{2+} are quite conservative since they were estimated from the observed broadening at the lowest temperature for which measurements were made and therefore apply at low temperatures. Thus, a reasonable value of $\sim 9 \text{ kcal mol}^{-1}$ for ΔH^\ddagger for CoCR^{2+} and CuCR^{2+} in DMF would indicate higher values of the exchange rate at 25°C by at least a factor of 10^3 . Consequently, the rate of DMF exchange might be more like 10^8 sec^{-1} at 25°C for these two complexes in DMF.

Chapter IV. DISCUSSION

1. Kinetic Results(a) Methanol and DMF exchange from $\text{Mn}(\text{DMP}r\text{Por})^+$

The kinetic results from the study of manganese(III) protoporphyrin(IX) dimethyl ester are summarized in Table XIX together with the results of several other studies for comparison. For $\text{Mn}(\text{DMP}r\text{Por})^+$ in DMF, the uncertainties in the ΔH^\ddagger and ΔS^\ddagger values could not be estimated but they are expected to be greater than the error limits indicated for $\text{Mn}(\text{DMP}r\text{Por})^+$ in methanol since ΔH^\ddagger and ΔS^\ddagger were found to be very sensitive to assumptions regarding the outer sphere contributions to the observed line broadening. The values of ΔH^\ddagger and ΔS^\ddagger given were found to be the most internally consistent.

Manganese(III) protoporphyrin(IX) dimethyl ester is quite labile with rate constants of the order of 10^7 sec^{-1} at 25°C . Several reasons can be invoked to account for this lability. The manganese in this metalloporphyrin is a high-spin d^4 ion with a strong Jahn-Teller distortion and thus rapid ligand exchange rates are expected from crystal field considerations.⁴ Contributing to this effect, would be the reduction in metal ion charge as a result of the -2 charge on the porphyrin ligand. A further delocalization of charge in the metalloporphyrin due to porphyrin-metal d-orbital π interaction would also be ex-

TABLE XIX

A comparison of the kinetic parameters for solvent exchange of Mn(DMPor)⁺ with those of some other systems

System		$k(25^\circ\text{C}),$ sec^{-1}	$\Delta H^\ddagger,$ kcal mol^{-1}	$\Delta S^\ddagger,$ $\text{cal mol}^{-1}\text{deg}^{-1}$	Reference
Mn(DMPor) ⁺	CH ₃ OH	1.5×10^7	8.0 ± 0.3	1.3 ± 1	(a)
	DMF	6.4×10^7	10.5	12.4	(a)
Cr ²⁺	H ₂ O	$\geq 10^{10}$	—	—	(b)
Fe ³⁺	CH ₃ OH	4.3×10^3	10.1	-8.0	49(a)
	DMF	78	10.0	-16.4	68
		33	12.5	-10.0	69
	H ₂ O	1.5×10^2	—	—	(c)
	C ₂ H ₅ OH	2.0×10^4	6.2	-18	69
Fe(PrPor) ⁺	C ₂ H ₅ OH	1.8×10^6	6.2	-9.1	9
Co ²⁺	CH ₃ OH	1.8×10^4	13.8	7.2	23
	DMF	3.9×10^5	13.6	12.6	47
	H ₂ O	2.0×10^6	10.4	5.3	70

(a) This work.

(b) Quoted in ref 2.

(c) Quoted in ref 49(a).

pected to make the complex kinetically labile.

It was originally hoped that the measurement of the methanol exchange rate would permit at least an estimate of the water exchange rate on $\text{Mn}(\text{DMP}r\text{Por})^+$. Previous studies of cobalt(II), nickel(II) and manganese(II) ions (see Tables XIX, XX and XXI) have indicated that the water exchange rate is ~ 10 to 10^2 faster than the methanol exchange rate. However, the work of Breivogel on iron(III) in methanol^{49(a)} and ethanol⁶⁹ indicates that alcohol exchange is faster than water exchange by a factor of $\sim 10^2$. It may be noted, however, that the DMF and methanol exchange rates are similar for cobalt(II), nickel(II) and $\text{Mn}(\text{DMP}r\text{Por})^+$, and therefore, it may be justified to estimate the water exchange rate on $\text{Mn}(\text{DMP}r\text{Por})^+$, in analogy to the cobalt(II) and nickel(II) systems, as $\sim 10^8$ to 10^9 sec^{-1} . Although this estimate is an order of magnitude value at best, it accounts for Fleischer's⁴³ failure to observe complexing of CN^- , N_3^- and SCN^- to manganese(III) hematoporphyrin in a stopped-flow kinetic study. Relaxation methods similar to those used for copper(II)⁷¹ will be necessary to measure the ligand substitution rates of manganese(III) porphyrins.

From a consideration of the labilizing effect of porphyrin ligands on metal ion exchange rates, it is also possible to estimate the water exchange rate of hexaquomanganese(III). Fleischer⁴³ has observed that haematoporphyrin appears to enhance the rate of ligand substitution by $\sim 10^6$

in the more inert cobalt(III) and low-spin iron(III) systems. For high-spin iron(III), the solvent exchange rates given in Table XIX are generally consistent with the prediction that protoporphyrin(IX) increases the exchange rate on iron(III) by $\sim 10^4$. Thus, it is estimated that the water exchange rate of $\text{Mn}(\text{OH}_2)_6^{3+}$ would be $\sim 10^4$ to 10^5 sec^{-1} . This latter estimate appears consistent when the water exchange rates (see Tables XIX and XX) in the iso-electronic aquo manganese(II)-iron(III) and chromium(II)-manganese(III) systems are considered.

(b) Methanol, DMF and water exchange from $\text{MnB}(\text{ClO}_4)_2$

The kinetic results for $\text{MnB}(\text{ClO}_4)_2$, along with the solvent exchange results for all of the manganese(II) systems studied to date, are shown in Table XX.

A consideration of the data in this Table illustrates that the Schiff base B ligand does not have a significant effect on the solvent exchange rates for manganese(II). This is especially illustrated by the results for MnB^{2+} in water and DMF for which the exchange rates at 25°C are essentially identical to those for the hexasolvated ions. The results for MnB^{2+} in methanol might suggest that there is a significant labilizing effect by the Schiff base ligand in this system; however, the effect is somewhat uncertain because of the disagreement in the results from the two studies of manganese(II) ion in methanol. It should be

TABLE XX

Kinetic parameters for solvent exchange of MnB^{2+} and of other manganese(II) complexes.

Complex	$k(25^\circ\text{C})$ sec^{-1}	ΔH^\ddagger , kcal mol^{-1}	ΔS^\ddagger , $\text{cal mol}^{-1}\text{deg}^{-1}$	Reference
$\text{MnB}(\text{OH}_2)_2^{2+}$	2.1×10^7	8.8 ± 0.5	4.5 ± 1	(a)
$\text{Mn}(\text{phen})_2(\text{OH}_2)_2^{2+}$	8.7×10^7	9 ± 2	8 ± 9	50
$\text{Mn}(\text{phen})(\text{OH}_2)_4^{2+}$	5.3×10^7	9 ± 2	6 ± 7	50
$\text{Mn}(\text{OH}_2)_6^{2+}$	2.3×10^7	8.8 ± 1	5 ± 3	50
	3.0×10^7	8.1	2.9	15
$\text{MnB}(\text{CH}_3\text{OH})_2^{2+}$	7.7×10^6	8.8 ± 0.5	2.5 ± 2.5	(a)
$\text{Mn}(\text{CH}_3\text{OH})_6^{2+}$	3.7×10^5	6.2	-12	49(a)
	9.5×10^5	7.4	-6.4	49(b)
$\text{MnB}(\text{DMF})_2^{2+}$	4.4×10^6	12.4 ± 0.9	13.5 ± 3.6	(a)
$\text{Mn}(\text{DMF})_6^{2+}$	4.0×10^6	—	—	(b)
$\text{Mn}(\text{CH}_3\text{CN})_6^{2+}$	1.2×10^7	7.25 ± 0.25	-1.8 ± 0.8	72
$\text{Mn}(\text{NH}_3)_6^{2+}$	3.6×10^7	8 ± 0.5	5 ± 3	52

(a) This work.

(b) Quoted in ref 1. The ΔH^\ddagger and ΔS^\ddagger values have not been reported.

noted in this regard that the large negative entropy and the small ΔH^\ddagger obtained in ref 49(a) for methanol exchange from $\text{Mn}(\text{CH}_3\text{OH})_6^{2+}$ appears to be quite unusual when the results for the Mn^{2+} ion in the other solvents are considered. For MnB^{2+} in methanol, the ΔH^\ddagger and ΔS^\ddagger determined in this study appear to be more in line with the values observed for the other manganese(II) complexes.

Within the quoted experimental uncertainties, all of the manganese(II) complexes studied in water indicate the same ΔH^\ddagger and ΔS^\ddagger values, and thus, there are no significant detectable trends. The relative insensitivity of the kinetic parameters for water exchange from MnB^{2+} indicates that the electron donor properties of the amine nitrogens in the B ligand are not particularly different from the coordinated water molecules. It should be noted that this similarity in the kinetic parameters for manganese(II) complexes also extends to the $\text{Mn}(\text{NH}_3)_6^{2+}$ and $\text{Mn}(\text{CH}_3\text{CN})_6^{2+}$ systems.

The significantly larger ΔH^\ddagger and ΔS^\ddagger values observed for MnB^{2+} in DMF than in methanol or water might be taken to mean that the dissociative mode of activation is more important in the DMF system. A similar difference in the ΔH^\ddagger and ΔS^\ddagger values was observed for DMF and methanol exchange from $\text{Mn}(\text{DMP}r\text{Por})^+$. This trend may be contrasted to the similarity of the parameters for methanol and DMF exchange in the nickel(II) and also the cobalt(II) systems

(Tables XIX and XXI). Unfortunately, it is not possible to tell if the above difference is also common to the Mn^{2+} ion in DMF and methanol since the ΔH^\ddagger and ΔS^\ddagger values for DMF exchange from the Mn^{2+} ion have not been reported.

(c) Solvent exchange from NiCR^{2+} , NiCRMe^{2+} , NiTAAB^{2+} and NiTRI^{2+}

Table XXI summarizes the kinetic data for the four nickel(II) Schiff base complexes which were studied in the various solvents. The results from several other studies of normal octahedral nickel(II) systems are also shown for comparison.

A consideration of the solvent exchange results for NiCR^{2+} in DMF, methanol and acetonitrile and NiCRMe^{2+} in DMF indicates that the solvent exchange rates at 25°C are greater than for the hexasolvated systems by 5×10^2 to 1×10^4 . This greater exchange rate for these Schiff base complexes is due to the ΔH^\ddagger being lower by 6 to 7 kcal mol^{-1} . The increased rate does not involve the entropy factor since the ΔS^\ddagger values are lower by 3-5 cal $\text{deg}^{-1} \text{mol}^{-1}$ than for the octahedral systems. These results appear to be consistent with a dissociative mechanism in which steric interactions in the Schiff base complexes tend to weaken the solvent-metal ion interaction. The significant decrease in the ΔH^\ddagger value for $\text{NiCRMe}(\text{DMF})_2^{2+}$ over that for $\text{NiCR}(\text{DMF})_2^{2+}$ is also consistent with this proposal since it would be ex-

TABLE XXI

Kinetic parameters for solvent exchange of some nickel(II) complexes

Complex	k, sec ⁻¹ (25°C)	ΔH [‡] , kcal mol ⁻¹	ΔS [‡] , cal mol ⁻¹ deg ⁻¹	10 ⁻⁶ x(A/h), (a) rad sec ⁻¹	Reference
NiCR(DMF) ₂ ²⁺	1.9 × 10 ⁶	9.5	2.2	2.30	(b)
NiCRMe(DMF) ₂ ²⁺	2.8 × 10 ⁶	7.8	- 2.9	3.03	(b)
NiTAAB(DMF) ₂ ²⁺	7.3 × 10 ⁴	11.5	2.5	2.29	(b)
NiTRI(DMF) ₃ ²⁺	5.9 × 10 ²	15.6	6.5	2.94	(b)
Ni(DMF) ₆ ²⁺	3.8 × 10 ³	15.0	8.0	4.28	47
NiCR(CH ₃ OH) ₂ ²⁺	1.1 × 10 ⁷	9.4	5.2	2.96	(b)
Ni(CH ₃ OH) ₆ ²⁺	1.0 × 10 ³	15.8	8.0	3.58	23
Ni(C ₂ H ₅ OH) ₆ ²⁺	1.1 × 10 ⁴	10.8	- 4	-	69
NiCR(CH ₃ CN) ₂ ²⁺	7.4 × 10 ⁶	7.0	- 3.6	-2.66	(b)
Ni(CH ₃ CN) ₆ ²⁺	3.9 × 10 ³	10.9	- 8.8	-1.65	73
	2.8 × 10 ³	11.7	- 3.6	-5.09	74
	1.2 × 10 ⁴	11.8	- 0.2	-3.27	75
	2.7 × 10 ³	15.0	7.5	-3.3	76
	3.7 × 10 ³ (c)	15.1	8.5(c)	-	77
NiCR(OH ₂) ₂ ²⁺	4.5 × 10 ⁴	6.8	-14.4	-1.1	(b)
NiCRMe(OH ₂) ₂ ²⁺	5.2 × 10 ⁴	6.3	-15.8	(d)	(b)
Ni(OH ₂) ₆ ²⁺	3.2 × 10 ⁴	12.1	2.6	6.9(e)	78
NiTRI(OH ₂) ₃ ²⁺	3.8 × 10 ⁴	10.9	- 1.9	2.50	7
Nien ₂ (OH ₂) ₂ ²⁺	5.4 × 10 ⁶	9.1	2.6	-	80
Ni(NH ₃) ₃ (OH ₂) ₃ ²⁺	2.5 × 10 ⁶	10.2	5.0	-	81

(a) For the formyl proton in the DMF system, the methyl proton in the methanol and acetonitrile systems and for the water proton in the aqueous systems.

(b) This work

(c) The results in ref 77 are interpreted assuming that four acetonitrile molecules are co-ordinated to the Ni²⁺ ion. To permit a valid comparison to the previously obtained results, the value of ΔS[‡] and the rate constant at 25°C shown in this Table have been recalculated for a coordination number of six.

(d) The absence of chemical shifts in this system prevented a determination of (A/h). Consequently, the value of ΔS[‡] given was obtained as explained in the text using an estimated (A/h).

(e) From ref 79.

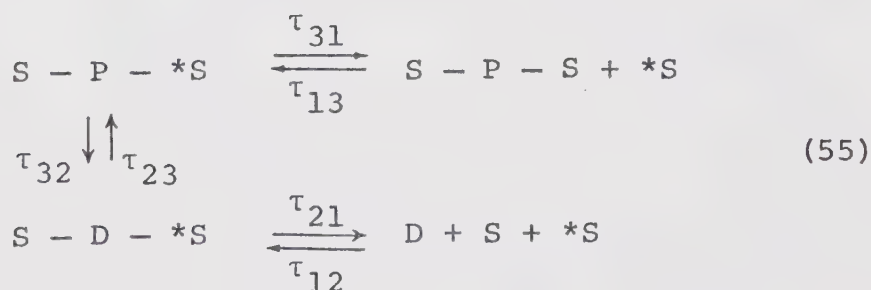
pected that the N-CH_3 group in the Schiff base CRMe ligand would increase the amount of steric interaction considerably. An additional labilization can also be expected to arise from electron donation from the CR and CRMe ligands. The studies of Hunt, *et al.*,³ on various aquo-amine nickel(II) complexes have shown that this latter effect can cause large rate enhancements operating through both a ΔH^\ddagger and ΔS^\ddagger change.

Similar arguments might be applied when considering the ΔH^\ddagger values for the aqueous systems. However, now the exchange rate is not greatly different from that for $\text{Ni}(\text{OH}_2)_6^{2+}$ because of a much less favorable ΔS^\ddagger in the Schiff base systems. In fact the large negative ΔS^\ddagger values are unusual for solvent exchange in nickel(II) systems and this might be taken to mean that some other mechanism is operative.⁸² Unfortunately, there is likely to be a rather large uncertainty in the ΔH^\ddagger and ΔS^\ddagger values for the aqueous systems since the $(T_{2M})^{-1}$ and $\tau_M \Delta \omega_M^2$ regions of line broadening are not independently well defined. However the water exchange rate and the value of ΔS^\ddagger are consistent with the correlations discussed below.

If the mode of activation for solvent exchange is primarily dissociative in these systems, as suggested above, then a correlation between the exchange rate constant (k_r) and the equilibrium constant (K^{-1}) for the paramagnetic to diamagnetic change (See Section 3) might be expected. In

fact, $\log k_r$ does vary directly in approximately a linear way with $-\log K$. The results for NiCRMe^{2+} in water and DMF show the same trend. The assumed dissociative mode of activation is consistent with the recently reported solvent exchange studies⁸³ of $\text{Co}(\text{DMSO})_6^{2+}$ and $\text{Ni}(\text{DMSO})_6^{2+}$ in the mixed solvents DMSO-nitromethane and DMSO-methylene chloride which have shown that the DMSO exchange parameters are independent of the composition of the mixed solvent, as expected for a dissociative mechanism.

The correlation of the diamagnetic-paramagnetic equilibrium results with the solvent exchange rates, discussed above, could be an indication (although not necessarily so) that the solvent exchange mechanism is coupled to the diamagnetic-paramagnetic equilibrium. If these systems are described by



where $\text{S} - \text{P} - \text{S}$ and $\text{S} - \text{D} - \text{S}$ refer to the solvated paramagnetic and diamagnetic forms, respectively, then the system can be treated as a three-site problem⁴⁵ with the bulk solvent as site 1, $\text{S} - \text{D} - * \text{S}$ as site 2 and $\text{S} - \text{P} - \text{S}$ as site 3. The τ_{31} , τ_{13} reaction would be the normal ex-

change path. If it is assumed that $\tau_{21}^{-1} \gg \tau_{23}^{-1}$, that is, that desolvation of the diamagnetic species is faster than its conversion to the paramagnetic form, and that the chemical shift in the diamagnetic form, $\Delta\omega_2 \ll \Delta\omega_3$, then

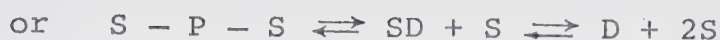
$$(T_{2P}^{PM})^{-1} = \frac{\left(\frac{1}{\tau_{32}} + \frac{1}{\tau_{31}}\right) \left\{ \frac{1}{T_{23}^2} + \frac{1}{T_{23}} \left(\frac{1}{\tau_{32}} + \frac{1}{T_{31}}\right) + \Delta\omega_3^2 \right\}}{\left(\frac{1}{T_{23}} + \frac{1}{\tau_{32}} + \frac{1}{\tau_{31}}\right)^2 + \Delta\omega_3^2} \quad (56)$$

A comparison of this equation to eq 2 shows that the effective exchange lifetime $\tau_M^{-1} = (\tau_{32}^{-1} + \tau_{31}^{-1})$. Therefore, the solvent exchange rate will be controlled by whichever process is faster, either direct exchange (τ_{31}^{-1}) or the S - P - S to S - D - S conversion (τ_{32}^{-1}). Unfortunately, no rate constants are available for the latter process; however, Wilkins, *et al.*⁸⁴ have given a lower limit of 10^5 sec^{-1} for this interconversion in $\text{Ni}(\text{trien})^{2+}$ and $\text{Ni}(2,3,2 \text{ tet})^{2+}$ in aqueous solution. It has also been found that tetrahedral-planar interconversions of nickel(II) complexes have rate constants in the range 10^5 to 10^6 sec^{-1} .^{85,86} Although the latter process is not really comparable to that observed here, it appears that structural and spin state changes have rate constants of this order of magnitude.

Other reaction paths are also possible such as



(57)



In these, the solvent exchange rate will be controlled by the first reaction and $S - P$ or $S - D$ could be intermediates for the solvent exchange and spin-state change. In the second reaction, the solvent exchange and spin-state change would proceed at the same rate and the solvent exchange rate might be expected to be unusual compared to a purely paramagnetic system.

The low exchange rate and unusually negative ΔS^\ddagger in the $NiCR^{2+}$ and $NiCRMe^{2+}$ aqueous systems might be rationalized by assuming that direct water exchange is sufficiently slow and thus the favored path is via the diamagnetic-paramagnetic equilibrium. It is hoped that future work may test this possibility by measurements of the rate of the diamagnetic to paramagnetic conversion.

The kinetic results for DMF exchange from $NiTAAB^{2+}$ and $NiTRI^{2+}$ are also shown in Table XXI. It should be recalled that the study of these two nickel(II) Schiff base complexes was undertaken to compare further the effects of Schiff base ligands on the solvent exchange rates in complexes having normal octahedral and tetragonally distorted structures.

The ΔH^\ddagger and ΔS^\ddagger values for $NiTRI(DMF)_3^{2+}$ are very similar to those for $Ni(DMF)_6^{2+}$; in fact, the similarity is

even more striking than for the aquo systems, $\text{NiTRI}(\text{OH}_2)_3^{2+}$ and $\text{Ni}(\text{OH}_2)_6^{2+}$. This confirms the previous conclusion⁷ that the tridendate TRI chelate does not greatly affect the solvent exchange kinetics from nickel(II). These observations also indicate that the TRI ligand is not particularly more or less electron donating than the DMF ligands. It is, therefore, reasonable to assume that the significantly lower ΔH^\ddagger value observed for DMF exchange from NiTAAB^{2+} is not due to greater electron donation from the macrocyclic TAAB ligand. Models indicate that steric interactions should not be important for $\text{NiTAAB}(\text{DMF})_2^{2+}$. It can only be concluded that the lower ΔH^\ddagger value and higher exchange rate may lie in the rather indeterminate solvation and crystal field effects for a tetragonally distorted system. However, it should be noted that the kinetic results for $\text{NiTAAB}(\text{DMF})_2^{2+}$ show that solvent exchange rates on tetragonally distorted nickel(II) complexes are not necessarily unusually rapid. Thus, the significantly lower ΔH^\ddagger values and larger exchange rates for NiCR^{2+} and NiCRMe^{2+} may be due to a combined effect of steric interactions, tetragonal distortion and electron donor properties of the non-reacting ligand. The significance of the latter factor is expected to be greater for CR and CRMe than for the TAAB ligand. Furthermore, the possibility of coupling of the solvent exchange path to the diamagnetic-paramagnetic equilibrium cannot be overlooked.

One of the original objectives in carrying out this

work was to determine if the trends in the solvent exchange parameters noted for the hexasolvated systems would persist for tetragonally distorted systems. If this were to be the case, then the exchange rate studies in nonaqueous solvents on other systems, porphyrins for example, could be used to determine the exchange rates in the more interesting aqueous system. Especially for porphyrins, solvent exchange studies in water are prevented by solubility and polymerization difficulties.

It has been found in the studies of NiCR^{2+} in several solvents that, qualitatively, the ΔH^\ddagger values do parallel those for the hexasolvated nickel(II) ion. The trend in ΔH^\ddagger is roughly $\text{DMF} \approx \text{CH}_3\text{OH} > \text{CH}_3\text{CN} \approx \text{H}_2\text{O}$. However, it should be pointed out that the recent results for the Ni^{2+} ion in acetonitrile^{76,77} cast considerable uncertainty onto the ΔH^\ddagger value for this system. The above trend in ΔH^\ddagger for the Ni^{2+} ion and NiCR^{2+} assumes that the earlier determinations of ΔH^\ddagger for $\text{Ni}(\text{CH}_3\text{CN})_6^{2+}$ are correct.

Several attempts have been made to obtain a more quantitative and useful correlation of the ΔH^\ddagger values with solvent properties. For instance, it seems likely that measures of the solvent basicity might provide a useful correlation parameter. It should be noted however that a direct correlation need not be expected since in a hexasolvated system the greater basicity of a solvent ligand will tend to labilize solvent exchange in a manner similar

to that observed by Hunt, *et al.*³ for various amines coordinated to the nickel(II) ion. At the same time the greater basicity would tend to increase the strength of the metal to solvent bond and thus make dissociation more difficult.

One such parameter of solvent basicity is Gutmann's⁸⁷ "donor number" (DN), which is a measure of the interaction of a covalent acceptor, SbCl_5 for example, with a solvent, and is defined to be the absolute value of the enthalpy for the reaction between the acceptor and the solvent. For MS_6 systems, where $\text{M} = \text{Co}^{2+}$ or Ni^{2+} and $\text{S} = \text{water, DMF, methanol}$ and acetonitrile, and also for NiCR^{2+} in these solvents, the values of ΔH^\ddagger for solvent exchange were found to roughly parallel $\text{DN}_{\text{SbCl}_5}$. The exceptions were the ΔH^\ddagger values for Ni^{2+} and Co^{2+} in ammonia, DMSO and also for the Ni^{2+} ion in acetonitrile if the redetermined value of ΔH^\ddagger ^{76,77} is used. These exceptions were so large so as to make the correlation dubious.

Another measure of solvent basicity may be derived for the C_B and E_B values used by Drago and co-workers to correlate the heats of reactions of acids and bases.^{88,89,90} The original workers proposed that C_B and E_B were related to the covalency and ionicity, respectively, of the interactions of the base with the acid. It might be expected that some combination of C_B and E_B would provide a measure of general basicity. It has been found empirically that a

good correlation exists between the product $C_B \cdot E_B$ and the activation enthalpies for solvent exchange. The $C_B \cdot E_B$ values used for NH_3 , DMSO, DMF and CH_3OH are 4.58,⁸⁸ 3.89,⁸⁹ 2.65⁸⁸ and 0.87,⁸⁸ respectively. The value for acetonitrile appears to be ~ 0.8 from the recent work by Drago, *et al.*,^{89,90} compared to the original value of 0.94. No value for water has been given but for the three metal ion systems, Ni^{2+} , Co^{2+} and NiCR^{2+} , a value of 0.7 has been found to most consistently predict the activation enthalpies for water exchange.

The empirical equation correlating $C_B \cdot E_B$ with ΔH^\ddagger for the NiS_6^{2+} systems is

$$\Delta H^\ddagger = \frac{51.8}{C_B E_B} (\log C_B E_B + 0.327) \quad (58)$$

which predicts activation enthalpies (in kcal mol^{-1}), with observed values in parenthesis, of 11.2(11.0), 12.1(12.2), 14.6(15.0), 15.8(15.8), 14.8(15,11.8), 12.6(12.1) for exchange of NH_3 , DMSO, DMF, CH_3OH , CH_3CN and H_2O , respectively.

Similarly for cobalt(II), the equation is

$$\Delta H^\ddagger = \frac{53.6}{C_B E_B} (\log C_B E_B + 0.283) \quad (59)$$

and the predicted and observed ΔH^\ddagger values in kcal mol^{-1} are 11.0(11.2), 12.0(12.2), 14.2(13.6), 13.7(13.8), 12.5(8.4,8.1), 9.8(10.4) for NH_3 , DMSO, DMF, CH_3OH , CH_3CN and

H₂O exchange, respectively.

For NiCR²⁺,

$$\Delta H^\ddagger = \frac{35.25}{C_B E_B} (\log C_B E_B + 0.291) \quad (60)$$

and the ΔH^\ddagger values are 9.50(9.50), 9.3(9.4), 8.6(7.0) and 6.9(6.8) for DMF, CH₃OH, CH₃CN and H₂O, respectively.

It may be noted that in general the agreement between the predicted and observed ΔH^\ddagger values is within 0.6 kcal mol⁻¹. The empirical equations have been arrived at without using the data for acetonitrile because of uncertainty in the $C_B E_B$ value and the ambiguity in the ΔH^\ddagger value brought about by the recent study of the Ni²⁺-acetonitrile system. The agreement of the calculated and observed ΔH^\ddagger values is much worse for the acetonitrile systems except for nickel(II) in acetonitrile where the recent value of 15 kcal mol⁻¹ for ΔH^\ddagger agrees with the predicted value of 14.8 kcal mol⁻¹ if $C_B E_B = 0.8$. On the other hand, if $C_B E_B$ is 0.68, then the predicted ΔH^\ddagger values are 12.0, 9.1 and 6.4 kcal mol⁻¹ for Ni²⁺, Co²⁺ and NiCR²⁺, respectively, and the general agreement is much better.

The general form of the empirical equations and the values of the parameters therein do not appear to have any obvious physical significance. The form of the equation is consistent with the idea proposed above that the ΔH^\ddagger should show both a direct and inverse dependence on the solvent

basicity. It may also be noted that the value of $-\log C_B E_B$ is relatively constant at ~ 0.3 when ΔH^\ddagger is zero for all systems. Intuitively, this does not seem unreasonable.

It is hoped that the ΔH^\ddagger -solvent basicity correlation discussed above can be experimentally tested on additional systems in future work.

2. General Comments Regarding Relaxation Results

It will have become apparent from the considerations in Chapter III that the relaxation effects of the various macrocyclic complexes studied can be accounted for rather well using standard theoretical T_{2M} and T_{20} expressions. The dipolar interaction distances and correlation times, obtained from these expressions by an iterative procedure, were in general similar to those observed for hexasolvated metal ion complexes.

Some empirical relationships between the T_{2M} values for different types of protons on a solvent molecule and also between the T_{2M} and T_{20} values for the same proton have been noted in some of the systems in which the hyperfine contributions are relatively insignificant. These are given in the various sections. For some of the systems, the relationships between T_{2M} and T_{20} found for hexasolvated metal ions were used to predict the outer sphere line broadening contributions for the purpose of increasing the accuracy of the ΔH^\ddagger and ΔS^\ddagger values for the solvent exchange

reaction. It is hoped that the empirical relationships noted in this study may provide at least a qualitative guideline for the interpretation of future work.

The determination of line width data at two frequencies, for several of the systems dealt with here, has led to the observation of a magnetic field dependent T_{2M} relaxation for two nickel(II) complexes (NiCR^{2+} and NiCRMe^{2+}) having large zero-field splitting energies. This phenomenon has also been recently observed, but to a more limited extent, in the Ni^{2+} -acetonitrile system.⁷⁷ This magnetic field dependence of the controlling correlation time, the electron spin relaxation time, has been interpreted in this work in terms of the T_{1e} and T_{2e} expressions of McLachlin which are not strictly valid for the conditions observed in nickel(II) complexes but which provide for a reasonable account of the observed results.

REFERENCES

1. T. R. Stengle and C. H. Langford, *Coordin. Chem. Rev.*, 2, 349 (1967).
2. D. J. Hewkin and R. H. Prince, *Coordin. Chem. Rev.*, 5, 45 (1970).
3. J. P. Hunt, submitted for publication in *Coordin. Chem. Rev.*
4. F. Basolo and R. G. Pearson, "*Mechanisms of Inorganic Reactions*", 2nd ed., John Wiley and Sons Inc., New York, (1967).
5. N. S. Angerman and R. B. Jordan, *Inorg. Chem.*, 8, 2579 (1969).
6. M. Eigen and R. G. Wilkins, "*Advances in Chemistry Series*", No. 49, American Chemical Society, Washington, D. C. 1965, pp 55-80.
7. J. E. Letter, Jr., and R. B. Jordan, *J. Amer. Chem. Soc.*, 93, 864 (1971).
8. D. Rablen and G. Gordon, *Inorg. Chem.*, 8, 395 (1969).
9. N. S. Angerman, B. B. Hasinoff, H. B. Dunford, and R. B. Jordan, *Can. J. Chem.*, 47, 3217 (1969).
10. R. W. Kluiber, R. Kukla and W. Dew. Horrocks, Jr., *Inorg. Chem.*, 9, 1319 (1970).
11. R. W. Kluiber, F. Thaller, R. H. Low and W. Dew. Horrocks, Jr., *ibid.*, 9, 2592 (1970).

12. R. K. Wangsness and F. Bloch, *Phys. Rev.*, 89, 728 (1953).
13. F. Bloch, *Phys. Rev.*, 102, 104 (1956).
14. H. M. McConnell, *J. Chem. Phys.*, 28, 430.
15. T. J. Swift and R. E. Connick, *J. Chem. Phys.*, 37, 307 (1962).
16. N. Bloembergen, *ibid.*, 27, 595 (1957).
17. R. J. Kurland and B. R. McGarvey, *J. of Mag. Res.*, 2, 286 (1970).
18. I. Solomon, *Phys. Rev.*, 99, 559 (1955).
19. N. Bloembergen, *J. Chem. Phys.*, 27, 572 (1957).
20. R. E. Connick and D. Fiat, *J. Chem. Phys.*, 44, 4103 (1966).
21. A. D. McLachlan, *Proc. Roy. Soc. (London)*, A280, 271 (1964).
22. N. Bloembergen and L. O. Morgan, *J. Chem. Phys.*, 34, 842 (1961).
23. Z. Luz and S. Meiboom, *ibid.*, 40, 2686 (1964).
24. N. S. Angerman, Ph.D. Thesis, University of Alberta (1969).
25. IBM Share Library Program, SDA 3094, 1964.
26. L. J. Boucher, *J. Amer. Chem. Soc.*, 90, 6640 (1968).
27. D. F. Evans, *J. Chem. Soc.*, 2003 (1959).
28. A. E. Earnshaw, "Introduction to Magnetochemistry", Academic Press Inc., New York (1968), p. 4-8.

29. P. A. Loach and M. Calvin, *Biochemistry*, 2, 361 (1963).
30. M. D. Alexander, Alan Van Heuvelen and H. G. Hamilton, Jr., *Inorg. Nucl. Chem. Letters*, 6, 445 (1970).
31. Alan Van Heuvelen, M. D. Lundeen, H. G. Hamilton, Jr., and M. D. Alexander, *J. Chem. Phys.*, 50, 489 (1969).
32. J. L. Karn and D. H. Busch, *Nature*, 211, 160 (1966).
33. L. R. Rich and G. L. Stucky, *Inorg. Nucl. Chem. Letters*, 1, 61, (1965).
34. G. A. Melson and D. H. Busch, *J. Amer. Chem. Soc.*, 86, 4834 (1964).
35. L. I. Smith and J. W. Opie, *Org. Syn.*, 28, 11 (1948).
36. G. A. Melson and D. H. Busch, *J. Amer. Chem. Soc.*, 87, 1706 (1965).
37. K. M. Long and D. H. Busch, *Inorg. Chem.*, 9, 505 (1970).
38. N. F. Curtis and R. W. Hay, *Chem. Commun.*, 524 (1966).
39. N. Sadasivan, J. A. Kernohan and J. F. Endicott, *Inorg. Chem.*, 6, 770, (1967).
40. R. E. Kitsen, *Anal. Chem.*, 22, 664 (1950).
41. G. M. Cheniae and I. F. Martin, *Energy Conversion by Photosynthetic Apparatus*, Brookhaven Symposia in Biology, 19, 406 (1967).
42. M. Calvin, *Rev. Pure Appl. Chem.*, 15, 1 (1965).
43. E. B. Fleischer, S. Jacobs, and L. Mestichelli, *J. Amer. Chem. Soc.*, 90, 2527 (1968).
44. R. B. Jordan and N. S. Angerman, *J. Chem. Phys.*, 48, 3983 (1968).

45. N. S. Angerman and R. B. Jordan, *Inorg. Chem.*, 8, 1824 (1969).
46. A. M. Chmelnick and D. Fiat, *J. Chem. Phys.*, 49, 2101 (1968).
47. N. A. Matwiyoff, *Inorg. Chem.*, 5, 788 (1966).
48. E. Fleischer and S. Hawkinson, *J. Amer. Chem. Soc.*, 89, 720 (1967).
49. (a) F. W. Breivogel, Jr., *J. Chem. Phys.*, 51, 445 (1969).
(b) H. Levanon and Z. Luz, *ibid.*, 49, 2031 (1968).
50. M. Grant, H. W. Dodgen and J. P. Hunt, *Inorg. Chem.*, 10, 71 (1971).
51. R. A. Bernheim, R. H. Brown, H. S. Gutowsky, and D. E. Woessner, *J. Chem. Phys.*, 30, 950 (1959).
52. M. Grant, H. W. Dodgen, and J. P. Hunt, *J. Amer. Chem. Soc.*, 91, 6318 (1969).
53. N. S. Angerman and R. B. Jordan, *J. Chem. Phys.*, 54, 837 (1971).
54. M. Rubinstein, A. Baram and Z. Luz, *Mol. Phys.*, 20, 67 (1971), and references therein.
55. E. K. Barefield, D. H. Busch, and S. M. Nelson, *Quart. Rev.*, 22, 457 (1968).
56. D. H. Busch, "Werner Centennial", *Advances in Chemistry Series No. 62*, American Chemical Society, Washington D. C. 1967, pp 616-

57. T. S. Kannan and A. Chakravorty, *Inorg. Chem.*, 9, 1153 (1970).
58. R. H. Holm and K. Swaminathan, *Inorg. Chem.*, 1, 599 (1962).
59. See ref 86 and the references quoted therein.
60. H. P. Fritz and K. E. Schwarzhans, *J. Organometal Chem.*, 1, 208 (1964).
61. (a) "International Critical Tables", Vol. 3, p. 27-28, NRC of U.S.A., McGraw-Hill Book Co. Inc., N.Y.
(b) J. Castell-Evans, "Physico-Chem. Tables", Vol. 1, p. 167, Charles Griffin and Co. Ltd., 2nd ed.
62. R. H. Holm, *Accounts Chem. Res.*, 2, 307 (1969).
63. B. R. McGarvey, "Transition Metal Chemistry", (R. L. Carlin, Ed.), Vol. 3, p. 89. Marcel Dekker, New York (1966).
64. The author gratefully acknowledges Dr. R. E. D. McClung and Dr. R. B. Jordan for this derivation.
65. B. M. Hoffman, D. L. Diemente and F. Basolo, *J. Amer. Chem. Soc.* 92, 61 (1972).
66. Nan-Loh Yang and G. Oster, *ibid.*, 92, 5266 (1970).
67. F. L. Lafferty, R. C. Jensen and J. C. Sheppard, *J. Inorg. Chem.*, 8, 1875 (1969).
68. J. Hodgkinson and R. B. Jordan, to be published.
69. F. W. Breivogel, Jr., *J. Phys. Chem.*, 73, 4203 (1969).
70. A. M. Chmelnick and D. Fiat, *J. Chem. Phys.*, 47, 3986 (1967).
71. R. L. Karpel, K. Kustin, A. Kowalak and R. F. Paster-

- nack, J. Amer. Chem. Soc., 93, 1085 (1971).
72. W. L. Purcell and R. S. Marianelli, *Inorg. Chem.*, 9, 1724 (1970).
 73. N. A. Matwiyoff and S. V. Hooker, *Inorg. Chem.*, 6, 1127 (1967).
 74. D. K. Ravage, T. R. Stengle and C. H. Langford, *ibid.*, 6, 1252 (1967).
 75. J. F. O'Brien and W. L. Reynolds, *ibid.*, 6, 2110 (1967).
 76. I. D. Campbell, J. P. Carver, R. A. Dwek, A. J. Nummelin and R. E. Richards, *Mol. Phys.*, 20, 913 (1971).
 77. I. D. Campbell, R. A. Dwek, R. E. Richards and M. N. Wiseman, *ibid.*, 20, 933 (1971).
 78. M. Grant, H. W. Dodgen and J. P. Hunt, *J. Amer. Chem. Soc.* 92, 2321 (1970).
 79. B. B. Wayland and W. L. Rice, *Inorg. Chem.*, 5, 54 (1966).
 80. A. G. Desai, H. W. Dodgen and J. P. Hunt, *J. Amer. Chem. Soc.*, 91, 5001 (1970).
 81. A. G. Desai, H. W. Dodgen and J. P. Hunt, *ibid.*, 92, 798 (1970).
 82. (a) It should be pointed out that proton exchange via an aquo-hydroxy equilibrium does not appear to be a likely possibility since pK_a of $Ni(OH_2)_6^{2+}$ is certainly >8 (ref 4) and proton exchange should have a rate constant of $\leq 10^2 \text{ sec}^{-1}$. The latter is consistent with the failure of Swift and Stephenson (ref 82-b) to observe this type of proton exchange for $Ni(OH_2)_6^{2+}$.

Amine substitution generally increases the pK_a of a coordinated water molecule, therefore, the proton exchange rate constant should be $<10^2 \text{ sec}^{-1}$ for $\text{NiCR}(\text{OH}_2)_2^{2+}$.

(b) T. J. Swift and T. A. Stephenson, *Inorg. Chem.*, 5, 1100 (1966).

83. L. S. Frankel, *Inorg. Chem.* 10, 814 (1971).
84. R. G. Wilkins, R. Yelin, D. W. Margeruni and D. C. Weatherburn, *J. Amer. Chem. Soc.*, 91, 4326 (1969).
85. L. H. Pignolet, W. Dew. Horrocks and R. H. Holm, *ibid.*, 92, 1855 (1970).
86. G. N. LaMar and E. O. Sherman, *ibid.*, 92, 2691 (1970).
87. V. Gutmann, "*Coordination Chemistry in Non-Aqueous Solutions*", Springer-Verlag, New York, (1968).
88. B. B. Wayland and R. S. Drago, *J. Amer. Chem. Soc.*, 87, 3571 (1965).
89. M. S. Nozari and R. S. Drago, *ibid.*, 92, 7086 (1970).
90. R. S. Drago, N. O'Brien and G. G. Vogel, *ibid.*, 92, 3925 (1970).

APPENDIX

Table XXII gives a representative sample of the proton magnetic resonance line widths at half-height for the pure solvents used in this study. In succeeding Tables, all of the observed bulk solvent proton magnetic resonance line widths and chemical shifts for solutions of the various complexes are given. The calculated $(T_{2P}P_M)^{-1}$ and $(\Delta\omega_{\text{obsd}}/P_M)$ data are also included. The solution magnetic susceptibility results for the various complexes can be found in Tables located near those giving the nmr data for that particular complex.

Table XXII

Temperature dependence of the proton line widths^(a) of
water, acetonitrile, dimethylsulfoxide (DMSO), methanol and
N,N-dimethylformamide (DMF).

t, °C	Water	Acetonitrile	DMSO	Methanol ^(b)		DMF	
				OH	CH ₃	CH	CH ₃ ^(c)
140			1.0			7.0	1.0
120			1.1			6.5	1.0
100	1.3		1.2			6.0	1.0
80	1.5	0.9	1.4			5.0	1.2
60	1.6	1.0	1.5	0.9	1.4	4.5	1.3
40	1.8	1.1	1.8	1.0	1.5	3.8	1.5
20	2.1	1.2	2.0	1.1	1.7	3.3	1.6
0	2.4	1.5		1.2	1.8	3.0	1.7
- 20		1.6		1.3	2.0	2.7	2.0
- 40		2.0		1.5	2.2	2.6	2.2
- 60				1.7	2.6	2.5	2.5
- 80				2.0	3.0		

(a) All line widths at half-height are expressed in Hz.

(b) Blank methanol sample contained a small amount of 2,4-dinitrobenzenesulfonic acid.

(c) High field methyl protons.

Table XXIII

Proton line broadening for Mn(DMPPrPor)⁺ in methanol (Figure 2). Frequency: 60 MHz.

*Frequency: 100 MHz.

10 ² x complex concn, molal	t, °C	10 ³ /T, °K ⁻¹	Δν _{obsd} , Hz		10 ⁻⁴ x (T _{2P_M}) ⁻¹ , sec ⁻¹	
			OH	CH ₃	OH	CH ₃
0.965	47	3.12	25.4*	5.8*	12.6*	2.09*
	43	3.16	28.8	5.6	14.0	2.07
	27.5	3.33	33.0	6.3	16.2	2.40
	12	3.51	38.1	7.3	18.7	2.90
	2	3.64	41.0*	8.4*	20.3*	3.23*
	- 3.5	3.71	45.0	8.5	22.3	3.49
	-15	3.88	48.5	9.3	24.0	3.92
	-25	4.03	48.5	10.6	24.0	4.52
	-33	4.16	45.0	11.9	22.2	4.96
	-38	4.25	40.3	14.4	19.8	5.34
	-42.5	4.34	36.0	13.1	17.6	5.59
	-49.5	4.47	25.6	14.4	12.2	6.05
	-52.5	4.54	23.3	14.0	11.0	5.84
	-58.5	4.66	19.5	14.0	9.05	5.59
	-71.5	4.96	15.7	12.7	6.70	4.52

Table XXIII (Cont'd).

$10^2 \times$ complex concn, molal	t, °C	$10^3/T, ^\circ K^{-1}$	$\Delta \nu_{\text{obsd}}, \text{ Hz}$		$10^{-4} \times (T_{2P_M})^{-1}, \text{ sec}^{-1}$	
			OH	CH ₃	OH	CH ₃
0.965	-79.5	5.16	18.0	13.5	7.36	4.46
	-85	5.32	20.1	15.9	7.89	5.08
0.981	-11	3.82	46.6	9.3	23.1	3.84
	-45	4.38	32.4	11.6	15.9	5.81
	-47.5	4.44	29.5	14.0	14.0	5.99
	-55	4.59	21.6	14.0	9.90	5.79
	-63	4.76	17.5	13.3	7.80	5.15
	-75.5	5.06	15.8	13.0	6.60	4.50
	-71	4.95	15.7	12.7	6.60	4.46
2.38	60	3.00		9.5		1.71
	39.5	3.20		11.5		2.06
	-10	3.80		20.1		3.62
	-18	3.92		22.7		4.16
	-28	4.08		25.8		4.79
	-35	4.20		28.6		5.38
	-46.5	4.42		32.6		6.17

Table XXIV

Proton chemical shifts of 9.65×10^{-3} (1), 9.8×10^{-3} (2), 2.38×10^{-2} (3), and 3.88×10^{-2} (4) molal solutions of $\text{Mn}(\text{DMPPrPor})^+$ in methanol (Figure 3). Frequency: 60 MHz.

t, °C	$10^3/T$, °K ⁻¹	obsd shift, Hz		$10^{-4} \times \Delta\omega/P_M$, rad sec ⁻¹	
		OH	CH ₃	OH	CH ₃
67	2.94	4.2 (1)		4.3	
60	3.00	11.0 (3)	5.5 (3)	4.5	2.3
55.5	3.04		10.5 (4)		2.65
43	3.16	4.5 (1)		4.6	
40	3.19	5.0 (2)		5.0	
39.5	3.20	12.0 (3)	10.0 (4)	5.0	2.52
32	3.28	5.0 (1)		5.1	
27.5	3.33	5.0 (1)		5.1	
19	3.42		11.5 (4)		2.90
15	3.47	4.7 (1)		4.8	
12	3.51	5.0 (1)		5.1	
- 0.5	3.68		12.5 (4)		3.15
- 3.5	3.71	4.8 (1)		4.9	
-10	3.80		12.5 (4)		3.15
-11	3.82	4.5 (2)		4.5	
-15	3.88	3.9 (1)		4.0	
-18	3.92		7.5 (3)		3.1
-22	3.98		12.0 (4)		3.0
-25	4.03	3.0 (1)		3.2	
-28	4.08		7.5 (3)		3.1
-33	4.17	2.0 (1)		2.0	
-35	4.20		6.5 (3)		2.7
-38	4.26		2.3 (1)		2.3
-42.5	4.34	0.5 (1)	2.0 (1)	0.5	2.0

Table XXIV (Cont'd).

t, °C	$10^3/T,$ °K ⁻¹	obsd shift, Hz		$10^{-4} \times \Delta\omega/P_M, \text{rad sec}^{-1}$	
		OH	CH ₃	OH	CH ₃
-50	4.48		7.5 (4)		1.9
-52.5	4.54		1.5 (1)		1.5
-58.5	4.66		1.5 (1)		1.0
-60	4.69		2.8 (4)		0.7

Table XXV

Proton line broadening for $\text{Mn}(\text{DMPPrPor})^+$ in N,N-dimethylformamide (Figure 4).

Frequency: 60 MHz.

$10^2 \times$ complex concn, molal	t, °C	$10^3/T, ^\circ\text{K}^{-1}$	$\Delta\nu_{\text{obsd}}, \text{Hz}$		$10^{-4} \times (T_{2P_M})^{-1}, \text{sec}^{-1}$	
			C-H	N-CH ₃ (a)	C-H	N-CH ₃ (a)
2.39	100	2.68	20.3	6.8	1.33	0.35
	80	2.83	21.8	6.0	1.51	0.42
	60	3.00	25.8	6.8	1.94	0.50
	50	3.10	28.5	8.1	2.21	0.61
	39.5	3.20	30.5	8.9	2.42	0.68
	19	3.42	40.3	9.7	3.32	0.75
	5	3.60	46.6	14.0	3.90	1.10
1.23	- 12.5	3.84	30.7	9.4	4.89	1.34
	- 23	4.00	37.3	11.4	5.94	1.66
	- 33.5	4.18	39.9	13.6	6.97	2.00
	- 40.5	4.30	45.0	15.3	7.35	2.29
	- 45	4.39		16.8		2.54
	- 51.5	4.51		19.6		2.98
	- 53	4.54		21.0		3.24
	- 57	4.63		21.0		3.25

Table XXV (Cont'd).

$10^2 \times$ complex concn, molal	t, °C	$10^3/T, ^\circ K^{-1}$	$\Delta\nu_{\text{obsd}}, \text{ Hz}$		$10^{-4} \times (T_{2P_M})^{-1}, \text{ sec}^{-1}$	
			C-H	N-CH ₃ (a)	C-H	N-CH ₃ (a)
1.23	- 60	4.69		23.0		3.59
0.688	10	3.53	14.2		3.50	
	- 0.5	3.67	15.9		4.03	
	- 13.5	3.85	18.8		5.00	1.39
	- 22	3.98	21.8	7.2	5.89	1.62
	- 32	4.15	24.2	8.4	6.68	1.96
	- 37.5	4.25	25.4	9.3	7.11	2.24
	- 44.5	4.38	26.3	10.2	7.35	2.53
	- 50	4.48	23.7	11.9	6.58	2.97
	- 55	4.59	21.2	13.3	5.81	3.38
	- 57	4.63	20.1	13.3	5.51	3.37
	- 60	4.69	17.0	14.0	4.65	3.56
	- 65	4.81	14.8	13.6	4.00	3.31
	- 67	4.85	14.4		3.62	

(a) High field CH₃

Table XXVI

Proton chemical shifts of 2.39×10^{-2} (1), 1.23×10^{-2} (2)
 and 6.88×10^{-3} (3) molal solutions of $\text{Mn}(\text{DMPPrPor})^+$
 in N,N-dimethylformamide (Figure 5). Frequency: 60 MHz.

t, °C	$10^3/T,$ °K ⁻¹	obsd shift, Hz		$10^{-3} \times \Delta\omega/P_M, \text{rad sec}^{-1}$	
		C-H	N-CH ₃ ^(a)	C-H	N-CH ₃ ^(a)
100	2.68	4.5 (1)	3.0 (1)	8.1	5.4
80	2.83	4.5 (1)	3.0 (1)	8.1	5.4
60	3.00	5.5 (1)	3.2 (1)	9.9	5.8
50	3.10	5.5 (1)	3.5 (1)	9.9	6.3
39.5	3.20	6.0 (1)	4.0 (1)	10.8	6.3
19	3.42	6.0 (1)	4.0 (1)	10.8	7.2
5	3.60	6.5 (1)	4.5 (1)	11.7	7.2
- 12.5	3.84	3.5 (2)	2.5 (2)	12.2	7.8
- 23	4.00	3.5 (2)	3.0 (2)	12.2	8.8
- 33.5	4.18	3.0 (2)	3.0 (2)	10.5	8.8
- 38	4.26	1.5 (3)		9.4	
- 40.5	4.30	2.8 (2)		9.6	
- 44.5	4.38	1.0 (3)		6.2	
- 50	4.48		1.2 (3)		7.6
- 51.5	4.51	1.0 (2)	2.0 (2)	3.5	7.0
- 55	4.59		1.0 (3)		6.2
- 60	4.69		1.5 (2)		5.2
- 65.5	4.82		1.0 (2)		3.5

(a) High field CH₃

Table XXVII

Magnetic susceptibilities of $\text{Mn}(\text{DMPrPor})\text{ClO}_4$ in methanol.

T, °K	$\Delta f, \text{Hz}$	(a)		(b)	
		$10^6 \times \chi_g,$	$10^3 \times \chi_{M(\text{cor})},$	μ_e, BM	(c)
		gm^{-1}	mol^{-1}		
313	10.0	13.2	10.1	5.05	
273	11.4	15.1	11.5	5.04	
252	12.3	16.3	12.5	5.03	
230.5	13.4	17.8	13.6	5.03	
213	14.5	19.4	14.7	5.03	

(a) At 60 MHz for a $9.81 \times 10^{-3} \text{M}$ solution prepared insitu from $\text{Mn}(\text{DMPrPor})\text{Cl} \cdot \text{OH}_2$ as described in the text.

(b) A diamagnetic correction of -330×10^{-6} cgs units has been applied.

(c) Calculated using $\mu_e = 2.839 \sqrt{\chi_{M(\text{cor})} T}$

Table XXVIII

Proton line broadening for $\text{MnB}(\text{ClO}_4)_2$ in
N,N-dimethylformamide (Figure 6).

Frequency: 60 MHz. *Frequency: 100 MHz.

$10^2 \times$ complex concn, m	t, °C	$10^3/T$, $^\circ\text{K}^{-1}$		$\Delta\nu_{\text{obsd}}$, Hz		$10^{-4} \times (T_{2P_M})^{-1}$, sec $^{-1}$	
				C-H	CH_3 (a)	C-H	CH_3 (a)
0.771	30.5	3.30		19.0	6.5	4.32	1.4
	16	3.46		23.0	7.9	5.52	1.8
	0	3.66		27.0		6.82	
	- 11	3.82		29.0	11.5	7.39	2.70
	- 24	4.01		26.5	14.5	6.69	3.48
	- 33	4.17		22.0*	15.0*	5.43*	3.59*
	- 35	4.20		21.0	15.0	5.15	3.59
	- 40.5	4.30		19.8	16.0	4.82	3.84
	- 41	4.31		20.2*	16.0*	4.94*	3.84*
	- 46.5	4.41		21.0		5.14	
	- 48.5	4.45		21.5	18.0	5.30	4.37
	- 50	4.48		23.0*	18.0*	5.57*	4.35*
	- 52.5	4.54		23.5		5.81	
	- 56	4.60		26.0		6.52	
	- 61	4.71		30.0		7.52	
0.402	7	3.57		13.8	4.8	6.30	1.9
	- 5.5	3.74		16.0	5.6	7.21	2.4
	- 17	3.91		15.8	6.5	7.34	2.8
	- 29	4.10		13.0	8.0	5.87	3.5
	- 44.5	4.38		11.3	9.3	5.01	3.9
	- 54	4.57		13.3	11.5	6.09	4.81
	- 58	4.65		15.5	13.0	6.94	5.45

Table XXVIII (Cont'd).

$10^2 \times$ complex concn, m	t, °C	$10^3/T$		$\Delta\nu_{\text{obsd}}$, Hz		$10^{-4} \times (T_{2P}^{PM})^{-1}$	
		°K ⁻¹		C-H	CH ₃ (a)	C-H sec ⁻¹	CH ₃ (a)
1.38	104	2.65		17.0		1.79	
	82	2.82		19.2	5.5	2.29	0.67
	71	2.91		20.5	5.8	2.55	0.72
	57	3.03		24.0		3.08	
	52	3.08		24.5	7.5	3.22	0.96
	45	3.14		27.0		3.62	
	42.5	3.17		31.0*	8.5	4.20*	1.1
	40	3.20		29.0		3.89	
	31.5	3.28		36.5*		5.09*	
	30	3.30		33.0	10.0	4.59	1.32
	20	3.41		40.5*		5.72*	
	17.5	3.44		37.0		5.21	
	1	3.65		51.0*		7.44*	
	0	3.66		47.0		6.85	
	- 17.5	3.91		50.0		7.30	
	- 37	4.24		36.0		5.13	
	- 42.5	4.33		35.5		5.05	
	- 54	4.56		42.0		6.06	

(a) High field methyl protons.

Table XXIX

Formyl proton chemical shifts at 60 MHz for
a 1.38×10^{-2} m solution of
 $\text{MnB}(\text{ClO}_4)_2$ in N,N-dimethylformamide (Figure 7).

t, °C	$10^3/T,$	obsd shift, Hz	$10^{-3} \times \Delta\omega_{\text{obsd}}/P_M,$
	°K ⁻¹		rad sec ⁻¹
104	2.65	2.5	7.8
82	2.82	3.0	9.4
71	2.91	3.0	9.4
57	3.03	3.0	9.4
52	3.08	3.1	9.7
45	3.14	3.5	10.8
42	3.18	3.0	9.4
30	3.30	3.5	10.8
0	3.66	2.8	8.7
- 17.5	3.91	1.5	4.7
17.5	3.44	3.0	9.4

Table XXX

Proton line broadening for $\text{MnB}(\text{ClO}_4)_2$ in

water (Figure 8). Frequency: 60 MHz. *Frequency: 100 MHz.

$10^3 \times \text{complex}$ concn, m	(a) t, °C	$10^3/T$, °K ⁻¹	$\Delta\nu_{\text{obsd}}$, Hz	$10^{-5} \times (T_{2P_M})^{-1}$, sec ⁻¹
5.23	46	3.13	27.0*	4.27*
	34	3.26	35.0*	5.58*
	26	3.34	42.0*	6.73*
	18.5	3.43	51.8*	8.35*
	17.5	3.44	52.0*	8.38*
	- 10	3.80	61.0*	9.82*
	- 4	3.72	65.0*	10.5*
5.23	92	2.74	10.1*	1.43*
	78.5	2.84	13.0*	1.91*
	68	2.93	16.5*	2.50*
	60.5	3.00	19.6*	3.01*
	52	3.08	24.6*	3.76*
	42.5	3.17	30.6*	4.76*
	40	3.20	32.0*	5.08*
	31	3.29	39.2*	6.28*
	22	3.39	46.5*	7.48*
	13	3.50	56.0*	9.05*
	4.5	3.60	63.5*	10.3*
	- 3.5	3.71	67.0*	10.8*
5.85	31.5	3.28	28.0	3.94
	25.5	3.35	32.0	4.52
	20	3.41	52.2*	7.52*
	16	3.46	37.0	5.35
	13	3.50	61.2*	8.85*

Table XXX (Cont'd).

$10^3 \times \text{complex}$ concn, m	(a) t, °C	$10^3/T,$ °K ⁻¹	$\Delta\nu_{\text{obsd}},$ Hz	$10^{-5} \times (T_{2P_M})^{-1},$ sec ⁻¹
5.85	7	3.57	43.5	6.21
	2	3.64	72.0*	10.4*
	2	3.64	49.5	7.09
	- 4	3.72	71.0*	10.3*
	- 5.5	3.74	55.0	7.89
	- 10.5	3.81	57.0	8.19
12.2	93	2.73	16.5	1.10
	90	2.76	21.2*	1.43*
	83.5	2.81	20.0	1.34
	73	2.89	24.2	1.63
	73	2.89	31.0*	2.12*
	63	2.98	29.2	1.99
	57.2	3.03	46.0*	3.18*
	53.5	3.06	35.5	2.43
	44	3.16	44.0	3.03
	41.5	3.18	66.8*	4.65*
	31.5	3.28	54.0	3.73
	25.5	3.25	66.0	4.58

(a) All samples contained 10 vol% acetone which served as the internal standard and which permitted measurements to be extended to -10°C.

Table XXXI

Proton chemical shifts for $\text{MnB}(\text{ClO}_4)_2$ in water (Figure 9).

Frequency: 60 MHz. *Frequency: 100 MHz.

$10^3 \times$ Complex concn, m	t, °C	$10^3/T$, °K ⁻¹	obsd shift, Hz	$10^{-4} \times (\Delta\omega_{\text{obsd}}/P_M)$
12.2	93	2.73	4.2	6.0
	90	2.76	6.3*	9.0*
	84	2.81	4.5	6.4
	73	2.89	7.2*	10.*
	73	2.89	4.5	6.4
	63	2.98	5.0	7.1
	57	3.03	7.0*	10.*
	54	3.07	5.0	7.1
	44	3.16	4.8	6.8
	42	3.18	7.5*	11.*
	32	3.29	4.4	6.3
	26	3.36	5.0	7.1
5.85	62	2.98	2.3	6.7
	47	3.12	2.5	7.4
	35	3.25	2.5	7.4
	26	3.35	2.4	7.1
5.23	92	2.74	2.9*	9.7*
	68	2.93	3.0*	10.*
	61	2.99	3.5*	12.*
	52	3.08	3.2*	11.*
	46	3.13	3.4*	11.*
	42	3.18	3.2*	11.*
	31	3.29	3.0*	10.*

Table XXXII

Magnetic susceptibilities of $\text{MnB}(\text{ClO}_4)_2$ in water.

T, °K	$\Delta f, \text{Hz}$ (a)	$10^6 \times \chi_g,$ gm ⁻¹	$10^3 \times \chi_{M(\text{cor})},$ (b) mol ⁻¹	μ_e, BM (c)
356.5	9.2	20.9	12.2	5.91
336	9.8	22.1	13.0	5.98
317	10.4	23.6	13.7	5.96
289	11.0	25.0	14.5	5.86
280	11.2	25.6	14.9	5.83
275	11.5	26.2	15.2	5.86

(a) At 60 MHz for a $5.85 \times 10^{-3} \text{m}$ solution containing 5 vol% acetone as the internal standard.

(b) A diamagnetic correction of -181×10^{-6} cgs units has been applied.

(c) Calculated using $\mu_e = 2.839 \sqrt{\chi_{M(\text{cor})} T}$.

Table XXXIII

Proton line broadening at 60 MHz for $\text{MnB}(\text{ClO}_4)_2$ in methanol (Figure 10).

$10^2 \times$ complex concn, m	t, °C	$10^3/T$, °K ⁻¹	$\Delta\nu_{\text{obsd}}$, Hz		$10^{-5} \times (T_{2P}^{PM})^{-1}$, sec ⁻¹	
			OH	CH ₃	OH	CH ₃
0.380	4	3.61	21.6	4.5	2.67	0.40
	- 12.5	3.84	22.0	5.2	2.71	0.52
	- 24	4.02	18.5	6.4	2.23	0.61
	- 86	5.35	27.0	19.0	3.20	2.00
0.385	33.5	3.26	17.0		2.06	
	22.5	3.38	18.5	3.8	2.23	0.32
	15	3.47	19.6		2.38	
	4	3.61	21.6	4.5	2.64	0.39
	- 20	3.95	20.5	5.5	2.48	0.55
	- 31	4.13	15.4	6.9	1.81	0.65
	- 76	5.08	17.0	12.2	1.91	1.20
1.547	33.5	3.26	64.0	9.5	2.00	0.263
	15	3.47	78.0	11.8	2.44	0.332
	2.5	3.63	87.0	14.0	2.72	0.399
	- 5	3.73	88.0	15.5	2.75	0.446
	- 12.5	3.84	94.0	17.0	2.74	0.505
	- 20	3.95	84.0	19.5	2.62	0.564
	- 24	4.02	71.0	20.9	2.21	0.606
	- 33	4.17	56.0	23.0	1.73	0.671
	- 36.5	4.23	49.0	24.0	1.51	0.696
	- 53	4.54	33.0	24.0	.997	0.690
0.836	0	3.66	48.0	8.5	2.75	0.416
	- 29	4.10	36.0	13.0	2.04	0.656

Table XXXIII (Cont'd).

$10^2 \times$ complex concn, m	t, °C	$10^3/T,$ °K ⁻¹	$\Delta\nu_{\text{obsd}}, \text{Hz}$		$10^{-5} \times (T_{2P} P_M)^{-1}, \text{sec}^{-1}$	
			OH	CH ₃	OH	CH ₃
0.836	- 38.5	4.26	25.0	14.0	1.39	0.706
	- 49.5	4.47	18.6	14.0	1.01	0.692
	- 59	4.67	19.6	15.0	1.06	0.738
	- 66	4.83	23.4	17.5	1.27	0.871
	- 74.5	5.04	33.0	23.0	1.82	1.18
1.325	65	2.96	40.0	6.0	1.44	0.185
	55	3.05	46.0	6.8	1.66	0.209
	45	3.14	53.0	7.9	1.92	0.240
	30.5	3.46		10.5		0.340
	- 11.5	3.82		16.0		0.518
	- 34	4.18	48.0	20.5	1.73	0.688
	- 48.5	4.45	29.0	21.0	1.02	0.702
0.972	7	3.57	54.0	8.9	2.67	0.38
	- 5.5	3.74		10.5		0.459
	- 11.5	3.82	55.0	12.0	2.72	0.524
	- 21	3.97	50.0	13.5	2.46	0.595
	- 23	4.00	50.0	13.8	2.45	0.610
	- 26	4.05	45.0	14.5	2.21	0.643
	- 35	4.20	33.0	16.0	1.60	0.711
	- 39.5	4.28	26.0	16.0	1.24	0.706
	- 43.5	4.36	23.8	16.0	1.13	0.706
	- 47.5	4.43	22.0	16.8	1.03	0.721
	- 52.5	4.54	21.5	16.0	1.01	0.693
	- 56	4.61	22.0	17.0	1.02	0.726
	- 61	4.72	25.0	19.0	1.16	0.806
	- 64	4.78	26.0	19.0	1.22	0.829

Table XXXIII (Cont'd).

$10^2 \times$ complex concn, m	t, °C	$10^3/T,$ °K ⁻¹	$\Delta\nu_{\text{obsd}}, \text{Hz}$		$10^{-5} \times (T_{2P_M})^{-1}, \text{sec}^{-1}$	
			OH	CH ₃	OH	CH ₃
0.972	- 69	4.90	32.0	23.0	1.51	1.01
	- 71	4.95	34.5	24.0	1.64	1.06
	- 73	5.00	39.0	27.0	1.81	1.16
	- 80.5	5.20	51.0		2.46	

Table XXIV

Proton line broadening at 100 MHz for $\text{MnB}(\text{ClO}_4)_2$
in methanol (Figure 10).

$10^2 \times$ complex concn, m	t, °C	$10^3/T$, °K ⁻¹	$\Delta\nu_{\text{obsd}}$, Hz		$10^{-5} \times (T_{2P_M})^{-1}$, sec ⁻¹	
			OH	CH ₃	OH	CH ₃
0.385	10	3.53	30.0		3.69	
	-11.5	3.82	27.5		3.38	
	-72	4.98	15.5	11.5	1.59	1.11
1.547	61.5	2.99	70.0	8.5	2.18	0.22
	49	3.11	82.0	10.0	2.56	0.269
	39	3.20	90.0	11.0	2.81	0.301
	24	3.37	103	13.5	3.23	0.380
	10	3.53	112	16.0	3.51	0.443
	-11.5	3.82		22.0		0.626
	-30	4.12	57.0	26.5	1.7	0.759
	-43.5	4.36	37.0	26.0	1.12	0.735
	-44.5	4.38	36.0	25.0	1.08	0.712
	-62	4.74	39.0	28.0	1.14	0.797
0.836	- 4	3.72	63.0		3.64	
	-15	3.87	58.0	14.0	3.34	0.703
0.972	-21	3.97	52.0		2.66	
	-33	4.17	36.5		1.78	
	-41	4.31	26.0		1.24	
1.32	- 4	3.72	103	18.0	3.77	0.591
	-31.5	4.14	50	23.0	1.81	0.775

Table XXXV

Hydroxy proton chemical shifts at 60 MHz for
 $\text{MnB}(\text{ClO}_4)_2$ in methanol (Figure 11).

$10^2 \times$ complex concn, m	t, °C	$10^3/T,$		$10^{-4} \times \Delta\omega_{\text{obsd}}/P_M,$ rad sec ⁻¹
		°K ⁻¹	obsd shift, Hz	
1.547 (a)	33.5	3.26	6.5	4.1
	15	3.47	6.5	4.1
	10	3.53	6.5	4.1
	2.5	3.63	6.0	3.8
	- 5	3.73	4.5	2.8
	- 12.5	3.84	3.5	2.2
	- 20	3.95	1.5	1.0
1.325	65	2.96	5.2	3.9
	16	3.46	5.5	4.1
	- 23	4.00	1.5	1.1
	- 34	4.19	0	0
0.972	29.5	3.31	4.0	4.1
	- 5.5	3.74	3.0	3.0
	- 11.5	3.82	2.0	2.0
	- 21	3.97	1.3	1.3
	- 23	4.00	1.0	1.0
	- 26	4.05	1.0	1.0
	- 35	4.20	0.5	0.5
0.836	60	3.00	3.3	3.9
	42.5	3.17	3.5	4.1
	0	3.66	1.5	1.8
	- 29	4.09	0.5	0.6

(a) Methyl proton chemical shifts for this sample were observed to be about 2.0 to 2.5 Hz at 33.5° to -5°C.

Table XXXVI

Magnetic susceptibilities of $\text{NiCR}(\text{PF}_6)_2$ (A) and $\text{NiCR}(\text{ClO}_4)_2$ (B)

in N,N-dimethylformamide (Figure 12).

10 x complex concn, molal (A)	(B)	T, °K	$\Delta f, \text{Hz}$		$10^6 \chi_{\text{g}}, \text{gm}^{-1}$		$10^3 \chi_{\text{M}}(\text{cor}), \text{mole}^{-1}$	
			(A)	(B)	(A)	(B)	(A)	(B)
0.655	0.696	403	16.8		3.03		2.00	
		390	18.5		3.40		2.23	
		371	19.8	20.0	3.68	4.17	2.39	2.32
		360	21.0	21.3	3.93	4.46	2.55	2.47
		348	22.0	22.5	4.14	4.76	2.68	2.62
		337	23.5	24.1	4.46	5.13	2.87	2.81
		325	24.0	25.3	4.57	5.40	2.94	2.95
		316	26.2	27.0	5.04	5.81	3.22	3.16
		303	27.4	28.5	5.29	6.16	3.37	3.35
		285	29.8	31.0	5.79	6.75	3.68	3.65
		269.5	31.8	33.2	6.21	7.28	3.94	3.92
		249	35.8	36.8	7.06	8.10	4.45	4.34
		233	39.0	40.3	7.75	8.92	4.87	4.67
		213	43.0	45.5	8.60	10.15	5.38	5.40

Table XXXVI (Cont'd).

10 x complex concn, molal (A)	T, °K (B)	$\Delta f, \text{Hz}$		$10^6 \chi_{\text{g}}, \text{gm}^{-1}$		$10^3 \chi_{\text{M}}(\text{cor}), \text{mole}^{-1}$	
		(A)	(B)	(A)	(B)	(A)	(B)
1.670	400	44.0		3.14		2.07	
	380.5	49.0		3.56		2.32	
	370.5	51.5		3.70		2.41	
	361	54.0		3.97		2.57	
	341.5	60.0		4.47		2.89	
	332	63.0		4.72		3.03	
	313	69.0		5.22		3.33	

Table XXXVII

Magnetic susceptibilities of $\text{NiCRMe}(\text{ClO}_4)_2$
 in $\text{N,N-dimethylformamide}$ (Figure 12).

Complex concn, T, molal °K	Δf , Hz	$10^6 \chi_g$, gm^{-1}	$10^3 \chi_{\text{M}(\text{cor})}$, mole^{-1}
8.05×10^{-2}	397	18.3	2.91
	387	20.0	3.24
	377	21.8	3.56
	367	23.5	3.89
	357	25.0	4.16
	347	26.8	4.50
	337	28.0	4.73
	327	29.8	5.05
	316	30.8	5.24
	304.5	33.0	5.66
	287	35.5	6.13
	278	37.5	6.50
	265.5	39.5	6.88
	255.5	41.8	7.32
	247	43.5	7.63
	237	46.0	8.10
	224.5	49.0	8.55
	215	52.0	9.21
	209	54.0	9.60

Table XXXVIII

Magnetic susceptibilities of NiCR^{2+} and
 NiCRMe^{2+} in water (Figure 13).

Complex	complex concn, m	T, °K	$\Delta f, \text{Hz}$	$10^6 \chi_g', (a)$ gm^{-1}	$10^3 \chi_M(\text{cor})'$ mole^{-1}
$\text{NiCR}(\text{BF}_4)_2$	0.151	352.5	41.5	3.87	2.06
		335	48.3	4.56	2.40
		323	52.3	4.97	2.60
		313	56.8	5.42	2.82
		305.5	60.0	5.77	2.99
		293	63.1	6.07	3.14
		282	68.5	6.64	3.42
		271.5	70.0	6.81	3.50
	0.173	368	38.8	3.08	1.67
		358	43.2	3.46	1.86
		348	49.0	3.99	2.12
		332.5	56.3	4.65	2.44
		322	62.0	5.18	2.70
		312	67.5	5.66	2.94
		298.5	73.0	6.15	3.18
		288	77.5	6.56	3.38
		277	82.0	6.97	3.58
$\text{NiCRMe}(\text{BF}_4)_2$	0.162	367	15.0	0.792	0.563
		357	16.3	0.907	0.621
		347	19.0	1.17	0.754
		337	22.3	1.48	0.911
		327	26.3	1.86	1.10
		317	30.3	2.26	1.30
		313	31.5	2.38	1.36
		304	37.5	2.95	1.65

Table XXXVIII (Cont'd).

Complex	complex concn, m	T, °K	Δf , Hz	$10^6 x \chi_g$, ^(a) gm ⁻¹	$10^3 x \chi_M(\text{cor})$, mole ⁻¹
NiCRMe(BF ₄) ₂	0.162	296.5	40.3	3.21	1.78
		290.5	44.0	3.57	1.96
		285	48.3	3.98	2.17
		278	55.5	4.68	2.52
	0.232	353	24.5	0.993	0.664
		343	28.5	1.26	0.801
		327	36.2	1.86	1.10
		295.5	56.5	3.15	1.75
		281	66.8	3.84	2.10

(a) The values tabulated have been corrected for the small temperature dependence of the density of water as explained in the text.

Table XXXIX

Magnetic Susceptibilities of NiCR^{2+} in methanol, acetonitrile and dimethylsulfoxide

(Figure 14).

Complex	Solvent	10xComplex concn, molal	T, °K	$\Delta f, \text{Hz}$	$10^6 \chi_{\text{g}}, \text{gm}^{-1}$	$10^3 \chi_{\text{M}}(\text{cor}), \text{mole}^{-1}$
$\text{NiCR}(\text{BF}_4)_2$	Methanol	0.981	336	20.0	3.66	1.96
			330	22.0	4.09	2.17
			324	22.2	4.13	2.19
			321	24.8	4.68	2.46
			313	26.2	5.01	2.62
			302.5	28.0	5.38	2.80
			289	31.2	6.08	3.15
			279	33.0	6.46	3.33
			265.5	35.8	7.05	3.62
			256	37.1	7.34	3.76
			245	39.0	7.75	3.96
			236.5	41.5	8.29	4.23
			228	46.0	9.26	4.70
			219	48.5	9.80	4.97
			209	51.0	10.33	5.23
			201	53.0	10.77	5.44

Table XXXIX (Cont'd).

Complex	Solvent	10xComplex concn, molal	T, °K	$\Delta f, \text{Hz}$	$10^6 \chi_{\text{g}}, \text{gm}^{-1}$	$10^3 \chi_{\text{M}}(\text{cor}), \text{mole}^{-1}$
$\text{NiCR}(\text{BF}_4)_2$	methanol	1.060	337	22.0	3.61	1.93
			330	24.2	4.05	2.15
			323.5	26.0	4.39	2.31
			318	28.0	4.77	2.60
			314.5	28.5	4.87	2.55
			289	34.2	5.97	3.09
			256	41.2	7.34	3.76
			236.5	46.0	8.26	4.21
$\text{NiCR}(\text{PF}_6)_2$	acetonitrile	1.03	343	24.8	3.33	2.18
			323	29.0	4.02	2.60
			313.5	31.0	4.35	2.80
			296.5	34.5	4.92	3.15
			283	38.0	5.48	3.49
			267.5	41.9	6.12	3.87
			252	45.5	6.70	4.23
			237	48.8	7.23	4.55
			228	51.5	7.67	4.82

Table XXXIX (Cont'd).

Complex	Solvent	10xComplex concn, molal	T, °K	$\Delta f, \text{Hz}$	$10^6 \chi_g, \text{gm}^{-1}$	$10^3 \chi_{M(\text{cor})}, \text{mole}^{-1}$
$\text{NiCR}(\text{PF}_6)_2$	acetonitrile	1.23	343	29.3	3.29	2.16
			338	30.5	3.46	2.26
			333	31.8	3.66	2.38
			327.5	33.3	3.86	2.51
			315.5	35.8	4.17	2.70
			244	55.3	6.83	4.30
			234.5	59.3	7.37	4.64
$\text{NiCR}(\text{PF}_6)_2$	DMSO	1.24	400	38.5	3.19	2.10
			390.5	40.5	3.38	2.22
			380.5	43.0	3.62	2.36
			370.5	44.5	3.77	2.45
			361	47.0	4.01	2.60
			352	50.0	4.27	2.76
			342	52.0	4.49	2.89
			332	54.0	4.68	3.01
			323	56.0	4.89	3.12
			313	59.0	5.16	3.30

Table XL

Chemical shifts at 60 MHz of the azo-methine methyl resonance relative to the diamagnetic shift for NiCR^{2+} and NiCRMe^{2+} in a series of solvents (Figure 15).

Complex	Solvent	t, °C	$\frac{10^3}{T}, ^\circ\text{K}^{-1}$	Chemical shift, Hz	
$\text{NiCR}(\text{BF}_4)_2$	water	2	3.64	402 ^(a)	403 ^(b)
		12	3.51	372	370
		22.5	3.38	340	
		36	3.24	304	
		40	3.20	293	289
		50	3.10	262	266
		60	3.03	234	233
		70	2.92	206	205
		80	2.83	178	176
		90	2.76	154	152
$\text{NiCRMe}(\text{BF}_4)_2$	water	0	3.66	336 ^(c)	
		11	3.52	279	
		20	3.41	245	
		33	3.27	200	
		42	3.18	171	
		50	3.10		155 ^(d)
		69.5	2.92		115
		74	2.88		104
		80	2.83		92.5
		84	2.79		85.5
		94	2.72		72.0
$\text{NiCR}(\text{PF}_6)_2$	acetonitrile	- 42.5	4.34	766 ^(e)	
		- 17.5	3.91	652	
		1.5	3.64	580	

Table XL (Cont'd).

Complex	Solvent	t, °C	$\frac{10^3}{T}, ^\circ\text{K}^{-1}$	Chemical shift, Hz
$\text{NiCR}(\text{PF}_6)_2$	acetonitrile	1.5	3.64	580
		12.	3.51	544
		22.5	3.38	510
		36	3.24	466
		41	3.18	444
		50	3.10	414
		60	3.00	380
		70	2.92	344
		80	2.83	306
$\text{NiCR}(\text{BF}_4)_2$	methanol	- 65.5	4.82	638 ^(f)
		- 54	4.57	586
		- 43.5	4.36	542
		- 33	4.17	498
		- 21	3.97	456
		- 10	3.80	420
		2	3.64	380 ^(g)
		12	3.51	346
		36	3.24	279
		40	3.20	264
		50	3.10	230
		60	3.00	198
$\text{NiCR}(\text{PF}_6)_2$	dimethyl- sulfoxide	22.5	3.38	367 ^(h)
		36	3.24	345
		50	3.10	318
		60	3.00	300
		80	2.83	262
		88	2.77	247
		100	2.68	230

Table XL (Cont'd).

Complex	Solvent	t, °C	$\frac{10^3}{T}, ^\circ\text{K}^{-1}$	Chemical shift, Hz
NiCR(PF ₆) ₂	dimethyl-sulfoxide	120	2.54	198
NiCR(PF ₆) ₂	N,N-dimethyl-formamide	- 59	4.67	651 (j)
		- 48.5	4.45	616
		- 36.5	4.23	560 (i) 562
		- 12.5	3.84	483 489
		1.5	3.64	444
		12.	3.51	421
		22.5	3.38	396
		36	3.24	363
		41	3.18	354
		50	3.10	338
		60	3.00	316
		80	2.83	274
		100	2.68	236
		120	2.54	200
NiCRMe(ClO ₄) ₂	N,N-dimethyl-formamide	- 41	4.31	734 (k)
		- 26	4.05	668
		- 8.5	3.78	604
		5	3.60	552
		31.5	3.28	474
		43	3.16	438
		54	3.06	410
		64	2.97	380
		74	2.88	345
		80	2.83	322

Table XL (Cont'd).

Complex	Solvent	t, °C	$\frac{10^3}{T}, ^\circ\text{K}^{-1}$	Chemical shift, Hz
NiCRMe(ClO ₄) ₂	N,N-dimethyl- formamide	84	2.80	322
		94	2.73	278
		104	2.65	248
		114	2.58	216
		124	2.52	188

- (a) Complex concn = 0.520 m, DSS internal standard.
- (b) Complex concn = 0.487 m, t-butanol internal standard.
- (c) Complex concn = 0.376 m, DSS internal standard.
- (d) Complex concn = 0.450 m, DSS internal standard.
- (e) Complex concn = 0.525 m, TMS internal standard.
- (f) Complex concn = 0.211 m, cyclopentane internal standard.
- (g) Complex concn = 0.343 m, cyclopentane internal standard.
- (h) Complex concn = 0.565 m, TMS internal standard.
- (i) Complex concn = 0.861 m, cyclopentane internal standard.
- (j) Complex concn = 0.476 m, cyclopentane internal standard.
- (k) Complex concn = 0.293 m, cyclopentane internal standard.

Table XLI

Formyl proton line broadening for $\text{NiCR}(\text{PF}_6)_2$ in N,N-dimethylformamide at 60 MHz
and at 100 MHz (Figure 16).

10 x Complex concn, molal	t, °C	$\frac{10^3}{T}, ^\circ\text{K}^{-1}$	x_p (a)	$\Delta\nu_{\text{obsd}}, \text{Hz}$		$10^{-3}x(\text{T}_{2\text{PM}})^{-1}, \text{sec}^{-1}$	
				60 MHz	100 MHz	60 MHz	100 MHz
5.55	77	2.86	0.69		21.9		0.903
	70	2.92	0.71	11.6		0.399	
	67	2.94	0.72		23.5		0.961
	60	3.00	0.74	12.3		0.408	
	57	3.03	0.75		26.3		1.06
	50	3.10	0.77	13.5		0.458	
	48	3.12	0.77		28.6		1.13
	40	3.20	0.80	15.0		0.513	
	36	3.24	0.81		32.0		1.26
	30	3.30	0.82	16.2		0.553	
- 1.5		3.69	0.90	28.8		1.03	
-10		3.80	0.91	36.4		1.31	
-15		3.88	0.92	45.6		1.66	
-20		3.95	0.93	53.4		1.95	

Table XLI (Cont'd).

10 x complex concn, molal	t, °C	$\frac{10^3}{T}, ^\circ\text{K}^{-1}$	x_p	(a)	$\Delta\nu_{\text{obsd}}, \text{Hz}$		$10^{-3}x(T_{2P_M})^{-1}, \text{sec}^{-1}$	
					60 MHz	100 MHz	60 MHz	100 MHz
5.55	-23	4.00	0.94		69.1		2.54	
	-30	4.11	0.95		116		4.28	
	-35	4.20	0.95		153		5.64	
	-55	4.59	0.98		100		3.57	
1.35	19	3.42	0.85		6.5		0.61	
	- 3.5	3.71	0.90		9.0		1.0	
	-29	4.10	0.94		25.5		3.80	
	-40	4.29	0.96		42.5		6.51	
	-45	4.39	0.96		42.5	52.5	6.48	8.09
	-47.5	4.43	0.97		43.0		6.54	
	-49.5	4.47	0.97		39.0		5.88	
	-50	4.48	0.97		36.5	35.6	5.48	5.33
	-55	4.59	0.98		25.8	26.3	3.73	3.81
	-56	4.61	0.98			22.0		3.12
	-58	4.65	0.98		19.0		2.64	
	-60	4.70	0.98		16.8	17.0	2.28	2.31

Table XLI (Cont'd).

10 x complex concn, molal	t, °C	$\frac{10^3}{T}, ^\circ\text{K}^{-1}$	X_p	(a)	$\Delta\nu_{\text{obsd}}, \text{Hz}$		$10^{-3} \times (T_{2P_M})^{-1}, \text{sec}^{-1}$	
					60 MHz	100 MHz	60 MHz	100 MHz
1.35	-62	4.74	0.98		16.5		2.23	
	-64	4.78	0.98		14.7	13.6	1.94	1.77
1.33	36	3.24	0.81			9.8		1.2
	18	3.44	0.85			11.7		1.58
	0.5	3.65	0.89			18.6		2.77
	-15	3.88	0.92		11.9		1.58	
	-31	4.13	0.95		29.0		4.44	
	-40	4.29	0.97		42.8		6.66	
	-45.5	4.39	0.97		43.3		6.70	
	-50	4.48	0.97		36.0		5.48	
	-54.5	4.58	0.97		27.9		4.14	
	-58	4.65	0.98		19.9		2.82	
1.24	-60	4.70	0.98		16.1		2.20	
	93	2.73	0.65			8.0		0.81
	84	2.80	0.67			8.2		0.91
	74	2.88	0.70			8.0		0.92

Table XLII

Formyl proton chemical shifts for $\text{NiCR}(\text{PF}_6)_2$ in N,N-dimethylformamide

at 60 MHz and at 100 MHz (Figure 17).

10 x complex concn, molal	t, °C	$10^3 \frac{T}{T}, ^\circ\text{K}^{-1}$	x_p (a)	obsd shift, Hz	$10^{-3} x(\Delta\omega_{\text{obsd}}/P_M), \text{rad sec}^{-1}$
				60 MHz 100 MHz	60 MHz 100 MHz
5.55	70	2.92	0.71	84	8.6
	60	3.00	0.74	89	8.8
	50	3.10	0.77	97	9.2
	40	3.20	0.80	103	9.39
	30	3.30	0.82	114	10.0
	10	3.54	0.87	131	10.8
	- 1.5	3.69	0.90	140	11.2
	-10	3.80	0.91	150	11.8
	-15	3.88	0.92	153	11.9
	-23	4.00	0.94	159	12.1
	-55	4.59	0.98	24	1.8
1.35	19	3.42	0.85	28.5	10.5
	- 3.5	3.71	0.90	32.5	11.3
	-29	4.10	0.94	37.0	12.3

Table XLII (Cont'd).

10 x complex concn, molal	t, °C	$\frac{10^3}{T}, ^\circ\text{K}^{-1}$	x_p (a)	obsd shift, Hz		$10^{-3} \times (\Delta\omega_{\text{Obsd}}/P_M), \text{rad sec}^{-1}$	
				60 MHz	100 MHz	60 MHz	100 MHz
1.35	-38	4.26	0.96	30.0		9.80	
	-40	4.29	0.96	29.0		9.45	
	-45	4.39	0.96	19.0	10.0	6.15	3.24
	-50	4.48	0.97	10.0	5.3	3.22	1.7
	-55	4.59	0.97	6.0	3.4	1.9	1.1
	-57	4.63	0.98	5.0		1.6	
	-58	4.65	0.98	3.0		0.95	
	-60	4.70	0.98	2.0		0.64	
1.33	18	3.44	0.85		45.4		16.9
	0.5	3.65	0.89		52.5		18.7
	-15	3.88	0.92	35.0		12.0	
	-18	3.92	0.93		57.3		19.6
	-31	4.13	0.95	34.6		11.6	
	-35	4.20	0.95	34.0		11.3	
	-40	4.29	0.97	27.5		9.09	
	-45.5	4.39	0.97	21.0		6.90	

Table XLII (Cont'd).

10 x complex concn, molal	t, °C	$10^3 \frac{\Delta\omega}{T}, ^\circ\text{K}^{-1}$	x_p (a)	obsd shift, Hz		$10^{-3} \times (\Delta\omega_{\text{obsd}}/P_M), \text{rad sec}^{-1}$	
				60 MHz	100 MHz	60 MHz	100 MHz
1.33	-50	4.48	0.97	10.5		3.43	
	-54.4	4.58	0.97	5.5		1.8	
	-58	4.65	0.98	3.5		1.1	
	-60	4.70	0.98	2.5		0.81	
1.24	93	2.73	0.65		25.0		13.2
	84	2.80	0.67		26.6		13.6
	74	2.88	0.70		28.5		13.9
	64	2.97	0.73		30.6		14.4
	44	3.16	0.79		35.7		15.6
	8	3.56	0.88		45.0		17.5
	-10	3.80	0.91		51.2		19.2
	-20	3.95	0.93		50.1		18.4
	-25.6	4.08	0.94		45.9		16.6
0.655	-16	3.91	0.93		28.1		19.7
	-22	3.98	0.94		27.8		19.3

Table XLII (Cont'd).

10 x complex concn, molal	t, °C	$10^3 \frac{1}{T}, ^\circ\text{K}^{-1}$	x_p (a)	obsd shift, Hz 60 MHz 100 MHz	$10^{-3} x(\Delta\omega_{\text{obsd}}/P_M), \text{rad sec}^{-1}$ 60 MHz 100 MHz
0.655	-27	4.06	0.94	24.0	16.6
	-32	4.15	0.95	20.1	13.8
	-37	4.24	0.96	12.6	8.57
	-42	4.33	0.96	8.4	5.7
	-47	4.42	0.97	3.3	2.2

(a) Mole fraction of paramagnetic $\text{NiCR}(\text{DMF})_2^{2+}$ species.

Table XLIII

Formyl proton line broadening for $\text{NiCR}(\text{ClO}_4)_2$ in
N,N-dimethylformamide at 60 MHz (Figure 16).

complex concn, m	t, °C	$10^3/T,$ °K ⁻¹	X_P (a)	$\Delta\nu_{\text{obsd}}$ Hz	$10^{-3} \times (T_{2P_M}^P)^{-1},$ sec ⁻¹
0.224 (b)	1.5	3.64	0.89	10.8	0.815
	-27	4.06	0.94	35.0	3.21
	-52	4.52	0.97	48.5	4.39
0.271 (c)	47	3.13	0.78	8.3	0.446
	32.5	3.27	0.82	9.2	0.546
	-10	3.80	0.91	18.0	1.27
	-22	3.98	0.94	33.0	2.48
0.131 (c)	15	3.47	0.86	6.3	0.62
	1	3.65	0.89	7.8	0.87
	-19	3.94	0.93	14.1	1.97
	-29	4.10	0.94	23.5	3.60
	-32	4.15	0.95	29.0	4.49
	-41	4.31	0.96	43.0	6.79
	-62	4.74	0.98	15.5	2.13

(a) Mole fraction of paramagnetic $\text{NiCR}(\text{DMF})_2^{2+}$ species.

(b) This sample was prepared insitu from anhydrous NiCRCl_2 and a slight excess of AgClO_4 . The solution was passed under vacuum through a synthered glass filter to remove the AgCl .

(c) This sample was prepared from isolated $\text{NiCR}(\text{ClO}_4)_2$.

Table XLIV

Formyl proton chemical shifts for $\text{NiCR}(\text{ClO}_4)_2$
in N,N-dimethylformamide at 60 MHz (Figure 17).

complex concn, m	t, °C	$10^3/T,$ °K ⁻¹	x_p (a)	obsd shift, Hz	$10^{-3} \times \Delta\omega_{\text{obsd}}/P_M,$ rad sec ⁻¹
0.224 (b)	1.5	3.64	0.89	52.8	11.0
	-27	4.06	0.94	63.0	12.4
	-52	4.52	0.97	12.0	2.29
0.271 (c)	60	3.00	0.74	42.5	8.85
	47	3.13	0.78	47.5	9.41
	32.5	3.27	0.82	53.0	9.98
	-10	3.80	0.91	71.0	11.9
	-22	3.98	0.94	76.0	12.4
0.131 (c)	15	3.47	0.86	29.0	10.9
	1	3.65	0.89	32.0	11.6
	-19	3.94	0.93	34.5	11.9
	-29	4.10	0.94	37.5	12.8
	-32	4.15	0.95	36.0	12.2
	-52	4.53	0.97	8.5	2.81
	-62	4.74	0.98	3.0	0.98

(a) Mole fraction of paramagnetic $\text{NiCR}(\text{DMF})_2^{2+}$ species.

(b) This sample was prepared from anhydrous NiCRCl_2 as described in footnote (b) of Table XLIII.

(c) This sample was prepared from isolated $\text{NiCR}(\text{ClO}_4)_2$.

Table XLV

Formyl proton line broadening for $\text{NiCRMe}(\text{ClO}_4)_2$ in N,N-dimethylformamide
at 60 MHz and at 100 MHz (Figure 18).

10 x complex concn, molal	t, °C	$\frac{10^3}{T}, ^\circ\text{K}^{-1}$	x_p	(a)	$\Delta\nu_{\text{obsd}}, \text{Hz}$		$10^{-3} \times (\tau_{2p_M})^{-1}, \text{sec}^{-1}$	
					60 MHz	100 MHz	60 MHz	100 MHz
2.93	114	2.58	0.50		13.0	16.2	1.08	1.55
	104	2.65	0.54		14.6		1.27	
	101	2.68	0.55			18.4		1.73
	94	2.72	0.58		16.0		1.35	
	87	2.78	0.62			22.0		2.03
	80	2.83	0.65		18.5		1.53	
	70	2.92	0.69		20.5	26.0	1.69	2.25
	62	2.98	0.73			29.5		2.50
	57	3.03	0.75			32.0		2.67
	44	3.15	0.80			37.5		2.99
1.40	35	3.25	0.83			43.0		3.36
	25	3.36	0.87			50.0		3.78
	80	2.83	0.65		10.3		1.48	
	59.5	3.01	0.74		12.0		1.64	

Table XLV (Cont'd).

10 x complex concn, molar	t, °C	$\frac{10^3}{T}, ^\circ\text{K}^{-1}$	x_p	(a)	$\Delta\nu_{\text{obsd}}, \text{Hz}$		$10^{-3}x(T_{2P_M})^{-1}, \text{sec}^{-1}$	
					60 MHz	100 MHz	60 MHz	100 MHz
1.40	45	3.14	0.80		13.0		1.76	
	30	3.30	0.85		15.0		2.04	
	10	3.54	0.91		18.5		2.55	
	- 8.5	3.78	0.95		24.0		3.36	
	- 19	3.94	0.96		29.0		4.10	
0.805	- 56	4.60	0.99		66.0		9.62	
	- 64	4.79	1.00		49.0		7.00	
	20.5	3.41	0.88		11.1		2.34	
0.805	16.5	3.46	0.89			16.5		3.94
	8.5	3.55	0.89			18.8		4.54
	0	3.66	0.93		13.8	21.0	3.06	5.24
	- 9	3.79	0.95			26.8		6.67
	- 12.5	3.84	0.96		16.0		3.65	
0.805	- 22.5	3.99	0.97		19.5		4.58	
	- 30	4.11	0.98		23.5		5.65	
	- 36	4.22	0.98		28.5		6.85	

Table XLV (Cont'd).

10 x complex concn, molal	t, °C	$\frac{10^3}{T}, ^\circ\text{K}^{-1}$	x_p (a)	$\Delta\nu_{\text{obsd}}, \text{Hz}$		$10^{-3}x(T_{2P_M})^{-1}, \text{sec}^{-1}$	
				60 MHz	100 MHz	60 MHz	100 MHz
0.805	- 36	4.22	0.98	28.5		6.85	
	- 40.5	4.30	0.98	34.5		8.71	
	- 45.5	4.40	0.99	40.0		10.0	
	- 48.5	4.45	0.99	41.0		10.1	
	- 51.5	4.51	0.99	41.0		10.2	
	- 58	4.65	0.99	35.5		8.76	
	- 61	4.72	1.00	31.5		7.65	
	- 64	4.78	1.00	27.5		6.63	
0.468	- 3	3.70	0.94		14.5		5.58
	- 12	3.83	0.96		17.2		6.98
	- 20	3.95	0.97		22.0		9.21
	- 26	4.05	0.97		25.8		10.9
	- 30	4.11	0.98		31.0		13.3
	- 35	4.20	0.98		36.0		15.6
	- 39	4.27	0.98		39.0		16.9
	- 42	4.33	0.99		38.4		16.6

Table XLV (Cont'd).

10 x complex concn, molal	t, °C	$\frac{10^3}{T}, ^\circ\text{K}^{-1}$	x_p (a)	$\Delta\nu_{\text{obsd}}, \text{Hz}$		$10^{-3}x(T_{2P}^P)^{-1}, \text{sec}^{-1}$	
				60 MHz	100 MHz	60 MHz	100 MHz
0.468	- 43	4.35	0.99		38.1		16.5
	- 45	4.38	0.99	24.0		9.93	
	- 47	4.42	0.99		37.5		16.1
	- 47.5	4.43	0.99		37.0		15.9
	- 51	4.50	0.99		34.0		14.5
	- 52	4.52	0.99		30.5		13.8
	- 53	4.55	0.99		30.5		12.9
	- 54.5	4.57	0.99	24.5		10.1	
	- 56	4.61	0.99	24.0		9.88	
	- 59	4.67	0.99		25.1		10.4
	- 62	4.74	1.00	19.0	21.8	7.56	8.85
	- 65	4.80	1.00		20.0		8.02
	- 66.5	4.85	1.00		19.0		7.55
	- 70	4.93	1.00	14.0	17.5	5.26	6.86
0.576	- 48.5	4.45	0.99	30.5		10.5	
	- 51.5	4.52	0.99	31.0		10.6	

Table XLV (Cont'd).

10 x complex concn, molal	t, °C	$\frac{10^3}{T}, ^\circ\text{K}^{-1}$	X _p (a)	$\Delta\nu_{\text{obsd}}, \text{Hz}$	$10^{-3} \times (T_{2P_M})^{-1}, \text{sec}^{-1}$
				60 MHz	100 MHz
				100 MHz	60 MHz
				100 MHz	100 MHz
0.576	- 56	4.61	0.99	29.0	9.86
	- 60.5	4.71	1.00	24.0	7.95

(a) Mole fraction of paramagnetic $\text{NiCRMe}(\text{DMF})_2^{2+}$ species.

Table XLVI

Formyl proton chemical shifts for $\text{NiCRMe}(\text{ClO}_4)_2$ in N,N-dimethylformamide

at 60 MHz and at 100 MHz (Figure 19).

10 x complex concn, molal	t, °C	$\frac{10^3}{T}, ^\circ\text{K}^{-1}$	x_p (a)	obsd shift, Hz			$10^{-4} x \Delta\omega_{\text{obsd}} / P_M, \text{rad sec}^{-1}$	
				60 MHz	100 MHz	60 MHz	60 MHz	100 MHz
2.93	114	2.58	0.50	36.0	55.2	1.04	1.60	
	104	2.65	0.54	42.0		1.11		
	101	2.68	0.55		66.4		1.72	
	94	2.72	0.58	45.0		1.10		
	87	2.78	0.62		76.9		1.79	
	80	2.83	0.65	53.0		1.17		
	70	2.92	0.69	58.0	90.9	1.19	1.87	
	62	2.98	0.73		96.2		1.88	
	57	3.03	0.75		104.0		1.98	
	55	3.05	0.76		106.6		2.00	
	44	3.15	0.80		115.0		2.04	
	35	3.25	0.83		123.9		2.10	
1.40	80	2.83	0.65	24.0		1.13		
	59.5	3.01	0.74	29.0		1.19		

Table XLVI (Cont'd).

10 x complex concn, molal	t, °C	$\frac{10^3}{T}, ^\circ\text{K}^{-1}$	x_p (a)	obsd shift, Hz		$10^{-4} \times \Delta\omega_{\text{obsd}}/P_M, \text{rad sec}^{-1}$	
				60 MHz	100 MHz	60 MHz	100 MHz
1.40	30	3.30	0.85	37.0		1.31	
	- 19	3.94	0.96	50.5		1.58	
	- 31	4.14	0.98	51.5		1.58	
	- 56	4.60	0.99	25.0		0.757	
	- 64	4.79	1.00	11.5		0.347	
0.805	20.5	3.41		23.5		1.41	
	16.5	3.46					
	8.5	3.55					
	0	3.66		26.5		1.50	
	- 9	3.79			45.7		2.54
	- 12.5	3.84		28.0		1.55	
	- 22.5	3.99		29.5		1.61	
	- 30	4.11	0.98	30.5		1.65	
	- 36	4.22	0.98	30.0		1.61	
	- 40.5	4.30	0.98	28.5		1.52	
	- 45.5	4.40	0.99	25.8		1.38	

Table XLVI (Cont'd).

10 x complex concn, molal	t, °C	$10^3 \frac{^\circ\text{K}^{-1}}{T}$	x_p	(a)	$10^{-4} x \Delta \omega_{\text{obsd}} / P_M, \text{rad sec}^{-1}$		
					obsd shift, Hz	60 MHz	100 MHz
0.805	- 48.5	4.45	0.99		24.6	1.31	
	- 58	4.65	0.99		12.5	0.664	
	- 61	4.72	1.00		10.0	0.531	
	- 64	4.78	1.00		7.0	0.37	
0.468	- 3	3.70	0.94		25.5		2.48
	- 12	3.83	0.95		27.2		2.60
	- 14.5	3.87	0.96		27.6		2.63
	- 20	3.95	0.97		28.4		2.68
	- 26	4.05	0.97		28.5		2.67
	- 30	4.11	0.98		26.6		2.48
	- 35	4.20	0.98		25.3		2.35
	- 39	4.27	0.98		21.3		1.97
	- 42	4.33	0.99		20.3		1.88
	- 43	4.35	0.99		18.4		1.70
	- 45	4.38	0.99			1.43	
	- 47	4.42	0.99		15.5		
					15.2		1.40

Table XLVI (Cont'd).

10 x complex concn, molal	t, °C	$\frac{10^3}{T}, ^\circ\text{K}^{-1}$	x_p (a)	obsd shift, Hz		$10^{-4} \times \Delta\omega_{\text{obsd}}/P_M, \text{rad sec}^{-1}$	
				60 MHz	100 MHz	60 MHz	100 MHz
0.468	- 51	4.50	0.99		10.9		1.00
	- 52	4.52	0.99		10.5		0.9666
	- 53	4.55	0.99		8.0		0.74
	- 54.5	4.58	0.99	9.5		0.87	
	- 56	4.61	0.99	8.5		0.78	
	- 59	4.67	0.99		3.7		0.34
	- 62	4.75	1.00	4.5			0.41
	- 67.5	4.86	1.00		1.6		0.14
	- 70.5	4.94	1.00		1.3		0.12
						1.61	
0.576	- 15.5	3.88		21.0			
	- 42.5	4.34		20.5		1.54	
	- 48.5	4.45		17.0		1.27	
	- 51.5	4.52		13.5		1.01	
	- 56	4.61		9.5		7.1	
	- 60.5	4.71		5.9		4.4	

(a) Mole fraction of paramagnetic $\text{NiCRMe}(\text{DMF})_2^{2+}$ species.

Table XLVII

Proton line broadening for $\text{NiCR}(\text{BF}_4)_2$ in water (Figure 20). Frequency: 60 MHz.

*Frequency: 100 MHz.

10 x complex concn, molal	t, °C	$\frac{10^3}{T}, ^\circ\text{K}^{-1}$	x_p (a)	$\Delta\nu_{\text{obsd}}, \text{Hz}$	$10^{-3} \times (T_{2P_M})^{-1}, \text{sec}^{-1}$
4.87	90	2.75	0.46	6.4	1.9
	80	2.83	0.52	7.0	2.0
	60	3.00	0.65	9.0	2.1
	40	3.19	0.78	12.6	2.52
	2.5	3.63	0.94	25.2	4.38
4.35	95	2.72	0.43	8.7*	3.53*
	85	2.79	0.49	10.2*	3.66*
	67	2.94	0.61	13.6*	3.99*
	47	3.12	0.74	19.1*	4.71*
	40	3.19	0.78	11.1	2.39
	38	3.22	0.79	24.2*	5.72*
	23.5	3.37	0.86	15.5	3.08
	20	3.41	0.88	16.2	3.18
	10	3.53	0.91	20.1	3.77
	0	3.66	0.94	25.0	4.68

Table XLVII

10 x complex concn, molal	t, °C	$\frac{10^3}{T}, ^\circ\text{K}^{-1}$	x_p (a)	$\Delta\nu_{\text{obsd}}, \text{Hz}$	$10^{-3}x(T_{2P_M})^{-1}, \text{sec}^{-1}$
5.20	80	2.83	0.52	7.9	2.0
	70	2.92	0.59	8.9	2.1
	60	3.00	0.65	10.0	2.16
	50	3.10	0.72	11.4	2.26
	40	3.19	0.78	13.3	2.44
	22.5	3.38	0.86	19.0	3.22
	12	3.51	0.91	22.4	3.66
	0	3.66	0.94	29.8	4.75
	40	3.19	0.78	15.4*	5.42*
	30	3.30	0.83	18.8*	6.30*
2.80	28.5	3.32	0.84	9.8	2.8
	20	3.41	0.88	23.5*	7.52*
	18	3.44	0.88	11.8	3.39
	12	3.51	0.91	12.8	3.58
	10	3.53	0.91	29.3*	9.18*
	0	3.66	0.94	18.0	5.03
				36.2*	11.0*

(a) Mole fraction of paramagnetic $\text{NiCR}(\text{OH}_2)_2^{2+}$ species.

Table XLVIII

Proton chemical shifts for $\text{NiCR}(\text{BF}_4)_2$ in
water at 60 MHz (Figure 21).

complex concn, m	t, °C	$10^3/T,$ °K ⁻¹	(a) x_p	(b) obsd shift, Hz	$10^{-3} \times (\Delta\omega_{\text{obsd}}/P_M),$ rad sec ⁻¹
0.469	80	2.83	0.52	- 5.5	-3.9
	35	3.25	0.81	-10.8	-4.92
	24.5	3.36	0.86	-12.0	-5.14
	2.5	3.63	0.93	-14.5	-5.68
0.487	90	2.75	0.46	- 5.0	-3.9
	80	2.83	0.52	- 6.3	-4.3
	60	3.00	0.65	- 8.5	-4.6
	50	3.10	0.72	- 9.5	-4.7
	40	3.19	0.78	-11.0	-5.0
	24.5	3.36	0.86	-13.0	-5.4
	2.5	3.63	0.94	-15.5	-5.8
0.495	40	3.19	0.78	-10.5	-4.69
	22.5	3.38	0.86	-13.0	-5.21
	12	3.51	0.91	-14.0	-5.36
	2	3.64	0.94	-15.5	-5.74

(a) Mole fraction of paramagnetic $\text{NiCR}(\text{OH}_2)_2^{2+}$ species.

(b) Shifts were obtained using DSS as the internal standard.

Table XLIX

Proton line broadening for $\text{NiCRMe}(\text{BF}_4)_2$ in water (Figure 22).

Frequency: 60 MHz. *Frequency: 100 MHz.

complex concn, m	t, °C	$10^3/T,$ °K ⁻¹	(a) x_p	$\Delta\nu_{\text{obsd}},$ Hz	$10^{-3} \times (T_{2P_M})^{-1},$ sec ⁻¹
0.376	42	3.18	0.42	8.0	3.7
	33	3.27	0.47	9.8	4.1
	20	3.41	0.55	13.0	4.87
	11	3.52	0.61	16.0	5.43
	0	3.66	0.68	23.0	7.06
0.450	85	2.80	0.23	4.8	3.0
	74	2.88	0.25	5.5	3.2
	64	2.97	0.31	6.7	3.4
	50	3.10	0.37	8.2	3.5
0.326	73	2.89	0.27	5.5*	4.3*
	57	3.03	0.33	7.3*	4.8*
	42	3.18	0.42	10.6*	5.83*
	20	3.41	0.55	18.6*	8.24*
	2	3.64	0.67	34.8*	13.0*

(a) Mole fraction of paramagnetic $\text{NiCRMe}(\text{OH}_2)_2^{2+}$ species.

Table I

Proton line broadening for $\text{NiCR}(\text{PF}_6)_2$ in acetonitrile at 60 and at 100 MHz (Figure 23).

complex concn, molal	t, °C	$\frac{10^3}{T}, ^\circ\text{K}^{-1}$	x_p	(a)	$\Delta\nu_{\text{obsd}}, \text{Hz}$		$10^{-2} \times (T_{2P_M})^{-1}, \text{sec}^{-1}$	
					60 MHz	100 MHz	60 MHz	100 MHz
0.630	60	3.00	0.66		2.2		1.1	
	50	3.10	0.71		2.5		1.2	
	40	3.20	0.75		3.0		1.4	
	39.5	3.20	0.75			5.3		3.2
	21	3.40	0.82			7.7		4.5
	19	3.42	0.83		3.7		1.8	
	10	3.53	0.86		4.3		2.0	
	6	3.58	0.87			9.5		5.5
	0	3.66	0.89		5.3	11.6	2.6	6.72
	-7	3.76						
	-12	3.83	0.92			15.2		8.63
	-15	3.88	0.93		7.4		3.7	
	-23	4.00	0.94			23.1		13.1
	-25	4.03	0.94		10.0		5.01	
	-33.3	4.17	0.96			40.5		23.3
	-34	4.18	0.96		14.8		7.76	

Table L (Cont'd).

complex concn, molal	t, °C	$\frac{10^3}{T}, ^\circ\text{K}^{-1}$	x_p (a)	$\Delta\nu_{\text{obsd}}, \text{Hz}$		$10^{-2}x(T_{2P_M})^{-1}, \text{sec}^{-1}$	
				60 MHz	100 MHz	60 MHz	100 MHz
0.630	-45	4.39	0.97	29.5	86.0	16.3	49.8
0.525	60	3.00	0.66	2.2		1.1	
	40	3.20	0.75	3.2		1.4	
	20	3.41	0.82	3.4		1.6	
	0	3.66	0.89	5.2		2.8	
	-10	3.80	0.91	6.0		3.3	
	-20	3.95	0.94	7.6		4.2	
	-30	4.12	0.95	10.6		6.08	
	-40	4.29	0.97	17.0		10.6	
	-42.5	4.34	0.97	23.5		15.2	
	-46	4.41	0.97	29.6		19.4	

(a) Mole fraction of paramagnetic $\text{NiCR}(\text{CH}_3\text{CN})_2^{2+}$ species.

Table LI

Proton chemical shifts for $\text{NiCR}(\text{PF}_6)_2$ in acetonitrile at 60 MHz and at 100 MHz (Figure 24).

complex concn, molal	t, °C	$\frac{10^3}{T}, ^\circ\text{K}^{-1}$	x_p	(a)		$10^{-4} \times \Delta\omega_M / P_M, \text{rad sec}^{-1}$
				obsd shift, Hz		
				60 MHz	100 MHz	60 MHz 100 MHz
0.630	61	2.99	0.66		-100	-1.78
	60	3.00	0.66	-61.8		-1.09
	50	3.10	0.71	-67.3		-1.12
	40	3.20	0.75	-73.8		-1.15
	39.5	3.20	0.75		-123.2	-1.92
	21	3.40	0.82		-142.6	-2.02
	19	3.42	0.83	-86.8		-1.22
	10	3.53	0.86	-93.0		-1.26
	6	3.58	0.87		-158.5	-2.11
	0	3.66	0.89	-99.0	-164.6	-2.15
	-7	3.76			-175.0	-2.23
	-12	3.83	0.92		-179.5	-2.26
	-15	3.88	0.93	-108.5		-1.36
	-20	3.95	0.94	-114.0		-1.41
	-23	4.00	0.94		-192.8	-2.37
	-25	4.03	0.94	-117.0		-1.43

Table LI (Cont'd).

complex concn, molal	t, °C	$\frac{10^3}{T}, ^\circ\text{K}^{-1}$	x_p (a)	obsd shift, Hz		$10^{-4} \times \Delta\omega_M / P_M, \text{rad sec}^{-1}$	
				60 MHz	100 MHz	60 MHz	100 MHz
0.630	-33.3	4.17	0.96		-206		-2.48
	-34	4.18	0.96	-124.5		-1.50	
	-45	4.39	0.97	-133.5	-216	-1.58	-2.56
0.525	60	3.00	0.66	- 53.0		-1.13	
	40	3.00	0.75	- 64.5		-1.22	
	20	3.41	0.82	- 74.0		-1.26	
	0	3.66	0.89	- 84.0		-1.33	
	-10	3.80	0.91	- 89.0		-1.36	
	-20	3.95	0.94	- 95.0		-1.42	
	-30	4.12	0.95	- 99.5		-1.46	
	-40	4.29	0.97	-106.0		-1.53	
	-42.5	4.34	0.97	-108.5		-1.56	
	-46	4.41	0.97	-112.0		-1.61	

(a) Mole fraction of paramagnetic $\text{NiCR}(\text{CH}_3\text{CN})_2^{2+}$ species.

Table LII

Proton line broadening for $\text{NiCR}(\text{BF}_4)_2$ in methanol (Figures 25 and 26).

Frequency: 60 MHz. *Frequency: 100 MHz.

10 x complex concn, molal	t, °C	$10^3/T$	(a) X_p	$\Delta\nu_{\text{obsd}}$, Hz	$10^{-3} \times (T_{2P_M})^{-1}$, sec^{-1}	OH	CH ₃
1.981	63.5	2.97	0.62	5.0	1.7	0.39	
	52	3.08	0.68	6.0	1.9	0.45	
	40	3.19	0.73	7.0	2.1	0.51	
	38	3.22	0.74	14.9*	4.71*	1.1*	
	25	3.36	0.79	8.0	2.23	0.62	
	19	3.42	0.81	20.0*	5.56*	1.3*	
	7	3.57	0.86	10.5	2.72	0.74	
	0	3.66	0.88	11.2	2.87	0.78	
	0	3.66	0.88	25.5*	6.75*	1.7*	
	-10	3.80	0.91	13.0	3.23	0.96	
	-19	3.94	0.93	32.0*	8.03*	3.17*	
1.206	-13.5	3.85	0.92	8.0	3.1	0.92	
	-19	3.94	0.93		9.3*	3.3*	
	-29	4.10	0.95	10.2	5.9	3.86	1.7

Table LII (Cont'd).

10 x complex concn, molal	t, °C	10 ³ /T	(a) x _p	Δν _{obsd} , Hz	10 ⁻³ x (T _{2P_M}) ⁻¹ , sec ⁻¹	OH	CH ₃
1.206	-39	4.27	0.96	25.9*	24.4*	10.2*	9.41*
	-40	4.29	0.96	12.0	9.6	4.47	3.2
	-48.5	4.45	0.98	28.0*	35.0*	11.0*	13.6*
	-50	4.48	0.98	15.0	18.0	5.60	6.53
	-54	4.57	0.98		21.5		7.90
	-57	4.63	0.98	25.5*	34.0*	9.86*	13.1*
	-60	4.70	0.98	17.0	25.4	6.30	9.41
	-63.5	4.77	0.99		24.0		8.78
0.798	7	3.57	0.86	4.5		2.6	
	-37.5	4.25	0.96	8.0	6.1	4.2	2.7
	-56.5	4.62	0.98	19.0*	26.0*	10.9*	14.7*
	-57.5	4.64	0.98	18.5*	24.0*	10.5*	13.4*
	-60	4.70	0.98	12.0	17.0	6.45	9.06
	-62	4.74	0.99	16.0*	19.0*	8.86*	10.2*
	-64	4.78	0.99	11.2	17.0	5.88	8.66
	-66	4.83	0.99	13.8*	14.0*	7.44*	7.35*
	-67	4.85	0.99	10.0	13.1	5.10	6.45

Table LII (Cont'd).

10 x complex concn, molal	t, °C	$10^3/T$	(a)		$\Delta\nu_{\text{obsd}}$, Hz	$10^{-3} \times (T_{2P_M})^{-1}$, sec ⁻¹	
			x_P		OH	CH ₃	CH ₃
0.798	-69	4.90	0.99		9.4	11.1	4.7
	-70	4.93	0.99		8.8	10.6	4.3
	-72.5	4.99	0.99			9.8	4.2
	-73.5	5.01	0.99			9.0	3.8
2.113 (b)	47	3.12	0.72		7.0	2.8	2.0
	32.5	3.27	0.76		7.8	3.0	2.1
	-10	3.80	0.91		13.5	5.0	3.16
	-22	3.98	0.94		16.0	6.5	3.65
	-43.5	4.36	0.97		23.2	19.0	5.15
	-54	4.57	0.98		28.0	38.0	6.19
	-65.5	4.82	0.99			38.0	8.20
1.90 (b)	64	2.97	0.62		10.5*	4.0*	4.03*
	54	3.06	0.67		11.9*	4.8*	4.30*
	44	3.15	0.71		12.6*	4.5*	4.28*
	8	3.56	0.85		21.0*	6.5*	6.01*
							1.53*

Table LII (Cont'd).

10 x complex concn, molal	t, °C	$10^3/T$	(a) x_p	$\Delta\nu_{\text{obsd}}$, Hz		$10^{-3} \times (T_{2P_M})^{-1}$, sec ⁻¹	
				OH	CH ₃	OH	CH ₃
1.90 ^(b)	-10	3.80	0.91	28.0*	10.0*	7.59*	2.36*
	-20	3.95	0.93	30.0*	13.5*	7.92*	3.24*
0.917 ^(b)	- 8.5	3.78	0.90	13.2*	5.2*	7.18*	2.2*
	-17	3.91	0.92	14.5*	7.0*	7.71*	3.1*
	-30	4.12	0.95	16.5*	10.0*	8.65*	4.92*
	-34	4.18	0.96	17.5*	13.0*	9.07*	6.17*
	-45	4.39	0.97	21.0*	25.5*	10.7*	12.8*
	-48.5	4.45	0.98	11.2	12.2	5.39	5.53
	-56	4.61	0.98	13.0	18.5	6.28	8.76
	-59	4.67	0.98	14.0	19.0	6.69	8.95
	-60	4.70	0.98	13.0	19.0	6.15	8.95
	-62	4.74	0.99	13.2	19.0	6.20	8.89
0.746 ^(b)	-65	4.81	0.99		18.0		8.28
	-66.5	4.84	0.99	14.5*	16.0*	6.85*	7.20*
	-22.5	3.99	0.94	12.5*	7.5*	8.05*	3.7*
	-42	4.33	0.97	16.5*		10.0*	
	-48	4.44	0.97	18.0*	26.0*	10.8*	15.3*

Table LII (Cont'd).

10 x complex concn, molal	t, °C	$10^3/T$	(a) x_p	$\Delta\nu_{\text{obsd}}$, Hz	$10^{-3} \times (T_{2P_M})^{-1}$, sec ⁻¹	CH ₃
				OH	OH	CH ₃
0.746 (b)	-55	4.59	0.98	18.0*	10.7*	15.2*
	-61	4.72	0.98	16.0*	9.30*	12.0*
	-67	4.85	0.99	12.0*	6.61*	7.27*

(a) Mole fraction of paramagnetic $\text{NiCR}(\text{CH}_3\text{OH})_2^{2+}$ species.

(b) 2,4-dinitrobenzenesulfonic acid was added to this sample.

TABLE LIII

Proton chemical shifts for $\text{NiCR}(\text{BF}_4)_2$ in methanol (Figures 27 and 28).

Frequency: 60 MHz. *Frequency: 100 MHz.

10 x complex concn, m	t, °C	$10^3/T$, °K ⁻¹	(a) X_p	obsd shift, Hz		$10^{-3} \times (\Delta\omega_{\text{obsd}}/P_M)$, rad sec ⁻¹	
				OH	CH ₃	OH	CH ₃
1.98	63.5	2.98	0.62	- 4.3	14.2	- 3.3	11.2
	52	3.08	0.68	- 5.0	16.8	- 3.6	12.2
	40	3.20	0.73	- 5.5	19.5	- 3.7	13.1
	38	3.22	0.74	- 9.5*	32.6*	- 6.3*	21.7*
	25	3.36	0.79	- 7.5	22.0	- 4.6	13.6
	19	3.42	0.81	-12.9*	38.0*	- 7.76*	22.9*
	14	3.40	0.83	- 9.0	23.8	- 5.3	14.0
	7	3.57	0.86	- 9.2	25.0	- 5.3	14.3
	0	3.66	0.88	-10.0	26.3	- 5.56	14.6
	0	3.66	0.88	-16.5*	44.3*	- 9.18*	24.6*
	-10	3.80	0.91	-11.5	28.2	- 6.20	15.2
	-19	3.94	0.93	-21.7*	49.7*	-11.4*	26.2*
1.21	-13.5	3.85	0.92	- 7.0	16.5	- 6.2	14.5
	-19	3.94	0.93	-13.0*	29.4*	-11.3*	25.6*

Table LIII (Cont'd).

10 x complex concn, m	t, °C	$10^3/T$, °K ⁻¹	(a) x_p	obsd shift, Hz	10^{-3} x ($\Delta\omega_{\text{obsd}}/P_M$), rad sec ⁻¹	OH	CH ₃
1.21	-29	4.10	0.95	- 8.2	18.5	- 7.0	15.7
	-39	4.27	0.96	-15.8*		-13.2*	
	-40	4.29	0.96	- 9.5	19.0	- 8.0	15.9
	-48.5	4.45	0.98	-14.4*	21.5*	-11.9*	17.8*
	-50	4.48	0.98	- 9.5	17.5	- 7.9	14.5
	-54	4.57	0.98	- 9.0	15.2	- 7.4	12.6
	-57	4.63	0.98	-10.7*		- 8.79*	
	-60	4.70	0.99	- 7.0	9.5	- 5.7	7.8
	-63.5	4.77	0.99	- 5.5	4.5	- 4.5	3.7
0.798	7	3.57	0.86	- 4.0	10.0	- 5.7	14.3
	-37.5	4.25	0.96	- 6.0	12.5	- 7.6	15.9
	-56	4.61	0.98	- 5.8	7.8	- 7.2	9.6
	-57.5	4.64	0.98	- 7.0*	5.8*	- 8.7*	7.2*
	-60	4.70	0.98	- 4.5	4.5	- 5.6	5.6
	-62	4.74	0.99	- 3.8*	2.1*	- 4.7*	2.6*
	-66	4.83	0.99		1.3*		1.6*
	-67	4.85	0.99	- 3.0	1.5	- 3.7	1.8

Table LIII (Cont'd).

10 x complex concn, m	t, °C	$10^3/T$, °K ⁻¹	(a) x_p	obsd shift, Hz	$10^{-3} \times (\Delta\omega_{\text{obsd}}/P_M)$, rad sec ⁻¹	OH	CH ₃
2.11 (b)	60	3.00	0.64	16.8			12.0
	47	3.12	0.72	18.5			11.8
	32.5	3.27	0.76	- 6.5	- 3.9		13.0
	-10	3.80	0.91	-11.5	- 5.8		14.6
	-22	3.98	0.94				15.2
	-43.5	4.36	0.97	-17.0	- 8.0		15.4
	-54	4.57	0.98	-16.0	- 7.5		11.7
	-65.5	4.82	0.99	- 9.5	- 4.4		2.6
1.90 (b)	64	2.97	0.62	- 6.4*	- 5.3*		19.6*
	54	3.06	0.67	- 7.3*	- 5.6*		20.4*
	44	3.15	0.71	- 8.0*	- 5.8*		21.3*
	8	3.56	0.85	-15.0*	- 8.98*		23.9*
	-10	3.80	0.91	-18.7*	-10.5*		25.5*
	-20	3.95	0.93	-22.0*	-12.1*		25.8*
	60	3.00	0.64	9.6*			19.6*

Table LIII (Cont'd).

10 x complex concn, m	t, °C	$10^3/T$, °K ⁻¹	(a) x _p	obsd shift, Hz	$10^{-3} \times (\Delta\omega_{\text{obsd}}/P_M)$, rad sec ⁻¹	OH	CH ₃
0.746 (b)	42.5	3.17	0.72	- 3.0*	11.5*	-5.5*	21.0*
	0	3.66	0.88		16.0*		23.8*
	-10	3.80	0.91	- 7.3*	17.4*	-10.5*	25.1*
	-22.5	3.99	0.94		18.5*		25.9*
	-35	4.20	0.96	- 9.6*	18.6*	-13*	25.4*
	-42	4.33	0.97	-10.0*	17.3*	-13.5*	23.4*
	-48	4.44	0.97	- 9.0*	12.9*	-12*	17.3*
	-25	4.59	0.98	- 6.5*	7.5*	- 8.7*	10*
	-61	4.72	0.98		3.9*		5.2*
0.917 (b)	-30	4.12	0.95	-11.4*	22.9*	-12.8*	25.6
	-42.5	4.34	0.97	-11.6*	22.0*	-12.8*	24.2*
	-48.5	4.45	0.98	- 7.0	13.5	- 7.6	14.7
	-51	4.50	0.98	- 9.8*	15.7*	-10.7*	17.1*
	-54.5	4.58	0.98	- 8.8*	10.7*	- 9.5*	11.6*
	-56	4.61	0.98	- 7.5	10.0	- 7.6	10.8
	-58	4.65	0.98	- 7.4*	5.1*	- 8.0*	5.5*
	-59	4.67	0.98	- 5.5	8.0	- 5.9	8.6

Table LIII (Cont'd).

10 x complex concn, m	t, °C	$10^3/T$, °K ⁻¹	(a) X _p	obsd shift, Hz	$10^{-3} \times (\Delta\omega_{\text{obsd}}/P_M)$, rad sec ⁻¹	OH	CH ₃
0.917 ^(b)	-60	4.70	0.98	- 5.0	6.0	- 5.4	6.5
	-62	4.74	0.99	- 4.0	5.5	- 4.3	5.9
	-64	4.78	0.99	- 3.5*	2.3*	- 3.8*	2.5*
	-65	4.81	0.99	- 4.0	2.0	- 4.3	2.2
0.996 ^(c)	14	3.48	0.83	- 4.0	11.5	- 4.7	13.5
	-10	3.80	0.91	- 5.2	14.0	- 5.7	15.1
	-18	3.92	0.93	- 6.0	15.0	- 6.3	15.8
	-28	4.08	0.95	- 7.0	15.8	- 7.2	16.3
	-39	4.27	0.96	- 8.0	16.2	- 8.1	16.5
	-48.5	4.45	0.98	- 8.5	15.5	- 8.6	15.7
	-58	4.65	0.98	- 7.2	9.5	- 7.2	9.5
	-68	4.88	0.99	- 3.0	1.0	- 3.0	1.0
0.945 ^(d)	-38.5	4.26	0.96	- 7.0	15.8	- 7.5	16.9
	-53	4.54	0.98	- 7.0	12.5	- 7.4	13.2
	-65.5	4.82	0.99	- 4.4	1.5	- 4.6	1.6

Table LIII (Cont'd).

-
- (a) Mole fraction of paramagnetic $\text{NiCR}(\text{CH}_3\text{OH})_2^{2+}$ species.
- (b) This sample contained 2,4-dinitrobenzenesulfonic acid.
- (c) This sample was prepared from the nitrate salt of NiCR^{2+} .
- (d) This sample was prepared from the hexafluoroantimonate salt of NiCR^{2+} .

TABLE LIV

Proton line broadening and chemical shift for $\text{NiCR}(\text{PF}_6)_2$ in dimethylsulfoxide

(Figures 29 and 30). Frequency: 60 MHz. *Frequency: 100 MHz.

complex concn, m	t, °C	$10^3/T$ °K ⁻¹	$\Delta\nu_{\text{obsd}}$, Hz	(a)		
				$10^{-2} \times (T_2 P_M)^{-1}$, sec ⁻¹	obsd shift, Hz	$10^{-3} \times (\Delta\nu_{\text{obsd}}/P_M)$, rad sec ⁻¹
0.464	104	2.66	—	—	33.5	2.69
	101	2.68	5.0*	1.5*	56.3*	4.53*
	94	2.73	—	—	35.0	2.81
	84	2.80	2.8	0.60	37.0	2.97
	81.5	2.82	5.6*	1.7*	60.6*	4.87*
	74	2.88	3.0	0.71	38.0	3.05
	72.5	2.90	6.3*	2.0*	62.7*	5.05*
	64	2.96	3.2	0.71	38.8	3.12
	63	2.98	6.7*	2.1*	64.7*	5.20*
	54	3.06	3.5	0.77	40.0	3.22
	53.5	3.06	8.0*	2.6*	67.1*	5.40*
	45	3.14	4.0	0.92	42.0	3.38
	44	3.15	8.4*	2.7*	69.5*	5.59*
	32.5	3.28	5.0	1.2	43.5	3.50
	20.5	3.41	5.5	1.4	45.5	3.66

TABLE LIV (Cont'd).

complex concn, m	t, °C	$10^3/T$, °K ⁻¹	$\Delta\nu_{\text{obsd}}$ Hz	$10^{-2} \times (T_{2P_M})^{-1}$, sec ⁻¹	obsd shift, Hz	(a)	
						$10^{-3} \times (\Delta\omega_{\text{obsd}}/P_M)$, rad sec ⁻¹	
0.125 (b)	94	2.73			9.0	2.84	
	93	2.73			15.1*	4.76*	
	84	2.80			15.3*	4.82*	
	84	2.80			9.5	2.99	
	64	2.97			16.4*	5.17*	
	64	2.97			10.0	3.15	
	44	3.15			17.6*	5.55*	
	44	3.15			11.1	3.50	
	21	3.40			19.5*	6.15*	

(a) Calculated assuming NiCR^{2+} is six-coordinate in DMSO. The values given have not been adjusted for the temperature dependence of the diamagnetic-paramagnetic equilibrium.

(b) The line widths were small and inaccurate, and therefore, they are not given.

Table LV

Formyl proton line broadening for $\text{NiTRI}(\text{ClO}_4)_2$ in N,N -dimethylformamide at 60 MHz
and at 100 MHz (Figure 31).

$10^2 \times$ complex concn, molal	t, °C	$\frac{10^3}{T}, ^\circ\text{K}^{-1}$	$\Delta\nu_{\text{obsd}}, \text{Hz}$		$10^{-3} \times (T_{2P_M})^{-1}, \text{sec}^{-1}$	
			60 MHz	100 MHz	60 MHz	100 MHz
2.35	115	2.58	11.0		3.03	
	99	2.69		14.2		5.08
	95	2.72	12.0		3.94	
	94	2.72		16.0		6.35
	90	2.75	12.8	17.4	4.42	7.26
	85	2.78		20.0		9.07
	83	2.81	14.0		5.45	
	80	2.83		21.5		10.0
	76	2.87		23.0		10.9
	75	2.87	15.9		6.61	
	72	2.90	16.0		6.66	
	68.5	2.93	16.0		6.67	
	62	2.98	15.0		6.36	
	58	3.02	14.0		5.82	

Table LV (Cont'd).

10^2 x complex concn, molal	t, °C	$\frac{10^3}{T}, ^\circ\text{K}^{-1}$	$\Delta\nu_{\text{obsd}}, \text{Hz}$		$10^{-3} \times (T_{2P_M})^{-1}, \text{sec}^{-1}$	
			60 MHz	100 MHz	60 MHz	100 MHz
2.35	43	3.16		8.9		3.0
5.53	108	2.62		22.5		4.20
	105.5	2.64	19.0		3.33	
	101.5	2.67	20.0		3.61	
	100	2.68		25.0		4.99
	95	2.72	21.0		3.97	
	92.5	2.74		30.0		6.29
	84	2.80	26.0		5.37	
	77.5	2.85		46.0		10.5
	73	2.89	30.6		6.58	
	71	2.91		47.0		10.8
	67.5	2.94		45.0		10.3
	64	2.97	30.0		6.53	
8.70	62	2.98		38.5		
	53	3.07	23.0	26.0	4.86	5.58
	50	3.10	20.8		4.25	

Table IV (Cont'd).

$10^2 \times$ complex concn, molal	t, °C	$\frac{10^3}{T}, ^\circ\text{K}^{-1}$	$\Delta\nu_{\text{obsd}}, \text{Hz}$		$10^{-3} \times (T_{2P_M})^{-1}, \text{sec}^{-1}$	
			60 MHz	100 MHz	60 MHz	100 MHz
5.53	49	3.11		21.0		4.35
	48	3.12	18.0		3.58	
	43	3.16		16.0		3.07
	41.5	3.18	14.0		2.58	
	31.5	3.28		13.0		1.34
	20	3.41		9.0		0.79
	2	3.64		7.3		0.61
	-17.5	3.91				
	-36.5	4.23		7.0		1.0
9.95	53	3.07	39.0		4.93	
	43	3.16	22.0		2.53	
	41.5	3.18	20.5		2.34	
	37.5	3.22	18.0		2.01	
	31.5	3.28		13.0		1.34
	31	3.29	12.0		1.18	
	20			9.0		0.79

Table LV (Cont'd).

$10^2 \times$ complex concn, molal	t, °C	$\frac{10^3}{T}, ^\circ\text{K}^{-1}$	$\Delta\nu_{\text{obsd}}, \text{Hz}$		$10^{-3} \times (\tau_{2P_M})^{-1}, \text{sec}^{-1}$	
			60 MHz	100 MHz	60 MHz	100 MHz
9.95	19	3.42	9.0		0.80	
	7	3.57	7.1		0.59	
	2	3.64		7.3		0.61
	- 2.5	3.70	7.1		0.59	
	-17.5					
	-36.5	4.23	10.0		0.99	
	-46.5	4.42	11.5		1.20	
	-55	4.59	13.2		1.44	
	-57					
	-60.5	4.71	16.0		1.83	

Table LVI

Formyl proton chemical shifts for $\text{NiTRI}(\text{ClO}_4)_2$ in
N,N-dimethylformamide (Figure 32).

Frequency: 60 MHz. *Frequency: 100 MHz.

complex concn, m	t, °C	$10^3/T,$ °K ⁻¹	obsd shift, Hz	$10^{-3} \times \Delta\omega_{\text{obsd}}/P_M,$ rad sec ⁻¹
0.0235	115	2.58	8.8	10.6
	99	2.69	15.0*	18.2*
	95	2.72	9.0	10.9
	94	2.72	15.0*	18.2*
	90	2.75	8.5	14.5
	85	2.79	14.0*	17.0*
	80	2.83	12.4*	15.0*
	76	2.86	11.0*	13.3*
	75	2.87	7.5	9.1
	72	2.90	6.8	8.2
	68.5	2.93	5.5	6.7
	62	2.98	3.5	4.2
	58	3.02	2.5	3.0
0.0553	108	2.62	35.0*	17.9*
	105.5	2.64	21.0	10.8
	101.5	2.67	21.0	10.8
	100	2.68	35.5*	18.2*
	95	2.72	20.5	10.5
	92.5	2.74	35.0*	17.9*
	84	2.80	19.5	9.98
	77.5	2.85	27.8*	14.2*
	73	2.89	16.7	8.55
	67.5	2.94	16.1*	8.24*
	64	2.97	8.8	4.5

Table LVI (Cont'd).

complex concn, m	t, °C	$10^3/T,$ °K ⁻¹	obsd shift, Hz	$10^{-3} \times \Delta \omega_{\text{obsd}}/P_M,$ rad sec ⁻¹
0.0553	62	2.98	7.5*	3.8*
	53	3.07	3.6*	1.8*
	50	3.10	2.0	1.0
	49	3.11	1.5*	0.77*
	48	3.12	1.3	0.67
	43	3.16	1.3*	0.66*

Table LVII

Formyl proton line broadening for NiTAAB(ClO₄)₂ in
N,N-dimethylformamide (Figure 33).

Frequency: 60 MHz. *Frequency: 100 MHz.

complex concn, m	t, °C	$10^3/T,$ °K ⁻¹	$\Delta\nu_{\text{obsd}},$ Hz	$10^{-3} \times (T_{2P_M})^{-1},$ sec ⁻¹
0.0299	90	2.76	10.9*	3.86*
	80	2.83	11.0*	4.29*
	73	2.89	11.0	4.28
	71	2.91	11.0*	4.64*
	64	2.97	11.2	4.71
	62	2.98	11.6*	5.14*
	53	3.07	12.5*	5.92*
	44.5	3.15	12.6	6.06
	42.4	3.17	14.0*	7.14*
	32	3.28	13.0	6.56
	20.5	3.41	14.0	7.50
	6.5	3.58	14.0	7.86
	- 3	3.70	12.0	6.43
	- 17.5	3.91	7.0	2.86
0.0538	138	2.43	14.0	2.78
	136	2.44	14.2*	2.66*
	127	2.50	14.3*	2.89*
	122	2.53	14.5	3.17
	119	2.55	14.5*	3.17*
	111	2.60	14.0	3.17
	110	2.61	15.0*	3.37*
	102	2.67	15.0	3.76
	101.5	2.67	15.0	3.57
	98	2.70	15.0*	3.57*

Table LVII (Cont'd).

complex concn, m	t, °C	$10^3/T,$ °K ⁻¹	$\Delta\nu_{\text{obsd}},$ Hz	$10^{-3} \times (T_{2P_M})^{-1},$ sec ⁻¹
0.0538	96.5	2.71	14.5*	3.57*
	92	2.71	15.0	3.80
	83	2.81	15.5	4.00
	82	2.82	16.0	3.96
	77.5	2.85	16.2*	4.44*
	72	2.90	16.0	4.36
	67.5	2.94	17.0*	4.84*
	62	2.98	17.0	4.84
	61.5	2.99	18.5*	5.43*
	55	3.05	18.6*	5.75*
	52	3.08	17.5	5.20
	51.5	3.08	18.0	5.55
	49	3.11	20.4*	6.30*
	43	3.16	19.5	6.10
	34.4	3.25	25.0*	8.32*
	31.5	3.28	21.0	6.74
	27.5	3.33	21.0	6.94
	24.3	3.36	29.5*	10.3*
	17.5	3.44	24.0	7.94
	16	3.46	32.0*	11.3*
	10	3.53	24.0	8.14
	6	3.58	29.0*	10.2*
	2	3.63	22.0	7.54
	- 2	3.69	22.0*	7.33*
	- 4.8	3.73	18.0*	5.95*
	- 12	3.83	13.5*	4.16*
	- 19.5	3.94	10.0	2.78
	- 20	3.95	9.0*	2.38*
	- 35	4.20	6.5*	1.4*

Table LVII (Cont'd).

complex concn, m	t, °C	$10^3/T,$ °K ⁻¹	$\Delta\nu_{\text{obsd}},$ Hz	$10^{-3} \times (T_{2P_M})^{-1},$ sec ⁻¹
0.0538	- 39.5	4.28	6.5	1.4
	- 50	4.48	6.2	1.3
	- 54.5	4.58	7.5*	1.8*
	- 60	4.70	7.8	1.9

Table LVIII

Formyl proton line broadening for $\text{NiTAAB}(\text{NO}_3)_2$ in
N,N-dimethylformamide (Figure 33).

Frequency: 60 MHz. *Frequency 100 MHz.

complex concn, m	t, °C	$10^3/T,$ °K ⁻¹	$\Delta\nu_{\text{obsd}},$ Hz	$10^{-3} \times (T_{2P_M})^{-1},$ sec ⁻¹
0.0511	- 7.5	3.77	16.0	5.46
	-12.5	3.84	12.6	4.15
	-18	3.92	9.6	2.9
	-19	3.94	9.0	2.7
	-25	4.03	7.5	2.0
	-33	4.17	6.0	1.5
	-37	4.24	5.8	1.4
	-46.5	4.42	6.0	1.5
	-57	4.63	6.5	1.7
0.0311	- 7	3.76	10.0*	5.00*
	- 8	3.77	10.0	5.00
	-10.5	3.81	9.0	4.3
	-11	3.82	8.5*	4.1*
	-21.5	3.98	5.8	2.3
	-25	4.03	5.8*	1.9*
	-26.5	4.06	5.2	1.8
	-28.5	4.09	5.0	1.7
	-33	4.17	4.5	1.4
	-42	4.33	5.0*	1.4*
	-48	4.44	5.2*	1.5*
	-50.5	4.49	4.6	1.5
	-55	4.59	5.0	1.7
	-60.5	4.71	5.5	2.0
	-62	4.74	6.0*	2.1*

Table LIX

Formyl proton chemical shifts for NiTAAB(ClO₄)₂ in
N,N-dimethylformamide.

Frequency: 60 MHz. *Frequency: 100 MHz.

complex concn, m	t, °C	$10^3/T,$ °K ⁻¹	obsd shift, Hz	$10^{-3} \times \Delta\omega_{\text{obsd}}/P_M,$ rad sec ⁻¹
0.0299	90	2.75	10.1*	14.4*
	80	2.83	10.4*	14.8*
	73	2.89	6.2	8.9
	71	2.91	10.7*	15.3*
	64	2.97	6.5	9.3
	62	2.98	11.3*	16.2*
	53	3.07	11.5*	16.4*
	44.5	3.15	7.0	10
	42.4	3.17	11.7*	16.7*
	32	3.28	6.7	9.6
	20.5	3.41	5.7	8.1
	6.5	3.58	3.5	5.0
	- 3	3.70	1.5	2.1
	- 17.5	3.91	1.0	1.4
0.0538	138	2.43	9.0	7.1
	136	2.44	14.3*	11.3*
	127	2.50	15.2*	12.1*
	122	2.53	9.2	7.4
	119	2.55	15.5*	12.3*
	111	2.60	9.8	7.7
	110	2.61	16.1*	12.8*
	102	2.67	10.0	7.93
	98	2.70	17.0*	13.5*
	96.5	2.71	17.2*	14.0*

Table LIX (Cont'd).

complex concn, m	t, °C	$10^3/T,$ °K ⁻¹	obsd shift, Hz	$10^{-3} \times \Delta\omega_{\text{obsd}}/P_M,$ rad sec ⁻¹
0.0538	92	2.74	10.5	8.33
	83	2.81	10.5	8.33
	82	2.82	10.8	8.55
	77.5	2.85	19.5*	15.4*
	72	2.90	11.2	8.95
	71	2.90	11.0	8.71
	67.5	2.94	19.9*	15.8*
	61.5	2.99	19.4*	15.4*
	55	3.05	20.8*	16.5*
	52	3.08	12.0	9.50
	51.5	3.08	12.3	9.75
	49	3.11	20.7*	16.4*
	43	3.16	12.4	9.83
	34.4	3.25	20.0*	15.9*
	31.5	3.28	12.3	9.75
	27.5	3.33	11.5	9.12
	24.3	3.36	18.2*	14.4*
	17.5	3.44	10.5	8.32
	16	3.46	13.9*	11.0*
	10	3.53		
	6	3.58	7.2*	5.7*
	2	3.63	7.5	5.95
	- 2	3.69	4.0*	3.2*
	- 4.8	3.73	3.0*	2.4*
	- 12	3.83	1.0*	0.79*
	- 19.5	3.94	1.0	0.79

Table LX

Magnetic susceptibilities of the perchlorate and nitrate salts
of NiTAAB^{2+} in N,N -dimethylformamide.

$T, ^\circ\text{K}$	$\Delta f, \text{Hz}$ (a)		$10^3 \times \chi_{M(\text{cor})}, \text{mol}^{-1}$ (b)		$\mu_e, (c)$
	ClO_4^-	NO_3^-	ClO_4^-	NO_3^-	B_M
374.5	18.0		2.69		2.85
365		13.1		2.84	2.89
357	19.6		2.80		2.84
355		13.6		2.95	2.91
345		14.3		3.11	2.94
344	20.3		3.05		2.91
336		15.1		3.29	2.98
326		15.7		3.43	3.00
324.5	22.0		3.33		2.95
317		16.2		3.54	3.01
316	23.0		3.47		2.97
306.5		23.5*		3.73*	3.04
285		26.3*		4.18*	3.10
273.5		26.5*		4.21*	3.05
269.5		20.0		4.40	3.09
265.5		28.8*		4.58*	3.13
254		30.0*		4.79*	3.13
253.5	30.0		4.57		3.06
248		21.5		4.73	3.07
240		31.2*		4.99*	3.11
238		22.6		4.99	3.09
233.5	34.0		5.21		3.13
228		23.8		5.24	3.10
223	35.3		5.40		
219.5		25.0		5.52	3.12
213	38.0		5.83		3.16

Table LX (Cont'd).

T, °K	$\Delta f, \text{Hz}$ (a)		$10^3 \times \chi_{M(\text{cor})}, \text{mol}^{-1}$ (b)		$\mu_{e'}$ B_M (c)
	ClO_4^-	NO_3^-	ClO_4^-	NO_3^-	
212		26.0		5.75	3.13

(a) At 60 MHz for a $5.38 \times 10^{-2} \text{m}$ $\text{NiTAAB}(\text{ClO}_4)_2$ solution and two samples of $\text{NiTAAB}(\text{NO}_3)_2$: $3.71 \times 10^{-2} \text{m}$ and $5.11 \times 10^{-2} \text{m}^*$.

(b) A diamagnetic correction of -206×10^{-6} cgs. units for TAAB and two solvent DMF ligands has been applied.

(c) Calculated using $\mu_e = 2.839 \sqrt{\chi_{m(\text{cor})} T}$

Table LXI

Proton line broadening for $\text{Co}(\text{trans}[14]\text{diene})^{2+}$ in water
 (Figure 35). Frequency: 60 MHz. *Frequency: 100 MHz.

complex concn, m	t, °C	$10^{-3}/T,$ °K ⁻¹	$\Delta\nu_{\text{obsd}}, \text{Hz}$	$10^{-3} \times (T_{2P}^{PM})^{-1},$ sec ⁻¹
0.0647 (a)	80	2.83	3.6	2.9
	70	2.92	4.0	3.5
	60	3.00	4.9	4.4
	50	3.10	5.6	5.2
	40	3.20	6.6	6.4
	30	3.30	8.1	8.2
	30	3.30	8.5*	8.3*
	20	3.41	10.0	10.6
	20	3.41	10.0*	10.1*
	10	3.53	13.8	15.6
	10	3.53	13.8*	14.0*
	0	3.66	20.3	24.0
	0	3.66	18.9*	21.6*
0.0741 (a)	40	3.20	7.6	6.8
	30	3.30	9.1	8.4
	20	3.41	11.2	10.8
	10	3.53	15.3	15.4
	0	3.66	22.0	23.2
0.0628 (a)	80	2.83	3.5	2.9
	60	3.00	4.8	4.4
	40	3.20	7.0	7.2
	30	3.30	7.8	8.1
	20	3.41	10.2	11.2
	0	3.66	17.2	20.5

Table LXI (Cont'd).

complex concn, m	t, °C	$10^{-3}/T,$ °K ⁻¹	$\Delta\nu_{\text{obsd}}, \text{Hz}$	$10^{-3} \times (T_{2P_M})^{-1},$ sec ⁻¹
0.101 ^(b)	48.5	3.11	8.0	5.4
	35	3.25	10.3	7.20
	25	3.36	12.5	9.00
	10	3.53	19.3	14.7
	2	3.63	24.5	19.0

(a) Perchlorate salt.

(b) Tetrafluoroborate salt.

Table LXII

Magnetic susceptibilities of $\text{Co}(\text{trans}[14]\text{diene})(\text{ClO}_4)_2$ in water.

T, °K	$\Delta f, \text{Hz}$ (a)	$10^6 \times \chi_g,$	$10^3 \times \chi_{M(\text{cor})},$ (b)	μ_e, BM (c)
		gm^{-1}	mol^{-1}	
363	14.0	2.10	1.34	2.09
353	14.5	2.20	1.39	2.10
343	14.5	2.20	1.39	2.08
333	15.0	2.30	1.45	2.09
313	15.5	2.40	1.50	2.07
303	15.8	2.45	1.53	2.06
293	16.2	2.52	1.57	2.06
283	16.5	2.60	1.61	2.05
273	17.2	2.76	1.70	2.08
263	17.5	2.81	1.71	2.05

(a) At 60 MHz for a $7.34 \times 10^{-2} \text{M}$ solution containing 10 vol% acetone as the internal standard. Sample was prepared under vacuum.

(b) A diamagnetic correction of -213×10^{-6} cgs units was applied.

(c) Calculated using $\mu_e = 2.839 \sqrt{\chi_{M(\text{cor})} (T + \theta)}$, $\theta = 42^\circ \text{K}$.

Table LXIII

Proton line broadening for Co(trans[14]diene)(BF₄)₂ in
methanol at 60 MHz (Figure 35).

complex concn, m	t, °C	10 ³ /T, °K ⁻¹	Δν _{obsd} , Hz		10 ⁻³ × (T _{2P_M}) ⁻¹ , sec ⁻¹	
			OH	CH ₃	OH	CH ₃
0.121	35	3.25	16.0	4.5	6.11	1.3
	23.5	3.37	19.8	5.5	7.60	1.6
	0.5	3.66	30.6	8.0	11.9	2.7
0.121	53	3.07	11.4	4.0	4.31	1.2
	35	3.25	15.5	5.4	5.80	1.7
	13	3.50	24.5	7.2	9.56	2.4
	- 8	3.77	42.0	11.2	16.4	3.9
0.0914	-10	3.80	30.9	9.3	15.9	4.1
	-30	4.12	54.0	14.8	28.1	6.93
	-48.5	4.45	97.5	24.6	51.2	12.0
	-64	4.78		48.1		24.3

Table LXIV

Proton line broadening for Co(trans[14]diene) (ClO₄)₂ in
acetonitrile at 60 MHz (Figure 36).

complex concn, m	t, °C	$10^3/T,$ °K ⁻¹	$\Delta\nu_{\text{obsd}},$ Hz	$10^{-3} \times (T_{2P_M}^{\text{PM}})^{-1},$ sec ⁻¹
0.207	70	2.92	7.4	1.1
	60	3.00	8.7	1.3
	51	3.09	9.6	1.5
	40	3.20	11.4	1.82
	-29.5	3.31	13.0	2.11
	20	3.41	15.0	2.47
	0	3.66	20.5	3.47
	- 9.5	3.80	24.0	4.09
	-20	3.95	31.8	5.47
	-27	4.06	33.9	5.85
	-36	4.22	42.0	7.32
	-45.5	4.40	56.3	9.90
0.156	8	3.57	13.0	2.81
	-35	4.20	31.0	7.09
	-45	4.38	41.2	9.53

Table LXV

Proton chemical shifts of $\text{Co}(\text{trans}[14]\text{diene})^{2+}$ in
acetonitrile at 60 MHz (Figure 37).

complex concn, m	t, °C	$10^3/T, ^\circ\text{K}^{-1}$	obsd shift	$10^{-3}\Delta\omega_{\text{obsd}}/P_M$
0.207 (a)	51	3.09	-10.0	-3.64
	20	3.41	-11.5	-4.18
	11	3.52	-12.5	-4.55
	0	3.66	-12.5	-4.55
	- 9.5	3.80	-13.3	-4.82
	-20	3.95	-14.5	-5.27
	-27	4.06	-14.7	-5.34
	-36	4.22	-16.0	-5.82
	-45.5	4.40	-16.2	-5.91
0.156 (a)	-45	4.38	-12.0	-5.81
	-35	4.20	-11.5	-5.56
0.259 (b)	78	2.85	-11.5	-3.32
	63	2.98	-13.0	-3.76
	43	3.16	-13.5	-3.90
	20	3.41	-15.3	-4.42
	-32	4.16	-19.5	-5.65
	- 7	3.76	-17.5	-5.06

(a) Perchlorate salt.

(b) Tetrafluoroborate salt.

Table LXVI

Formyl proton line broadening for $\text{CoCR}(\text{ClO}_4)_2$ in
N,N-dimethylformamide (Figure 36).

Frequency: 60 MHz. *Frequency: 100 MHz.

complex concn, m	t, °C	$10^3/T,$ °K ⁻¹	$\Delta\nu_{\text{obsd}}, \text{Hz}$	$10^{-4} \times (T_{2P}^{PM})^{-1}, \text{ (a)}$ sec ⁻¹
0.0908	73	2.89	14.0	0.458
	63	2.98	15.4	0.531
	53	3.06	17.5	0.639
	43	3.16	20.5	0.787
	42	3.18	21.0*	0.810*
	16	3.46	32.5	1.38
	-15.5	3.88	63.0	2.83
0.0252	-26	4.05	25.0	3.82
	-31	4.13	30.9	4.83
	-40.5	4.30	40.0	6.37
	-53	4.54	58.0	9.42
	-60	4.70	66.0	10.8

(a) Calculated by assuming that $\text{CoCR}(\text{ClO}_4)_2$ is 5-coordinate in DMF.

Table LXVII

Proton line broadening for $\text{CuCR}(\text{BF}_4)_2$ in water (Figure 38).

Frequency: 60 MHz. *Frequency: 100 MHz.

Complex concn, m	t, °C	$10^3/T$, °K ⁻¹	$\Delta\nu_{\text{obsd}}$, Hz	$10^{-3} \times (T_{2P_M}^{P_M})$, sec ⁻¹ (a)
0.552	94	2.72	11.2	3.08
	87.5	2.77	12.0	3.30
	75	2.87	13.7	3.82
	63.5	2.97	16.0	4.50
	52.5	3.07	19.5	5.58
0.224	48.5	3.11	10.0	6.41
	35	3.24	11.8	7.64
	25	3.36	14.8	9.90
	14	3.48	18.8	12.9
	11	3.52	22.5*	15.6*
	0	3.66	29.2	20.8

(a) A value of one is assumed for n in the calculation of P_M .

Table LXVIII

Formyl proton line broadening for $\text{CuCR}(\text{BF}_4)_2$ in
 N,N-dimethylformamide (Figure 38).

Frequency: 60 MHz. *Frequency: 100 MHz.

Complex concn, m	t, °C	$10^3/T,$ °K ⁻¹	$\Delta\nu_{\text{obsd}},$ Hz	$10^{-4} \times (T_{2P}^{PM})^{-1},$ sec ⁻¹ (a)
0.311	94	2.72	18.0	0.169
	74	2.88	21.0	0.216
	53	3.07	25.0	0.279
	40	3.20	30.5	0.358
0.134	43	3.16	14.0	0.316
	24.5	3.36	17.8	0.452
	14	3.48	19.7	0.522
	- 8.5	3.78	29.6	0.846
	-17.5	3.92	37.3	1.09
	-27	4.06	48.0	1.44
0.0525	-10	3.80	13.6	0.856
	-31	4.14	21.8	1.58
	-41	4.31	29.0	2.16
	-50	4.49	41.5	3.18
	-60	4.70	65.0	5.10
0.0486	20	3.41	8.3*	0.46*
	- 2	3.69	11.1*	0.715*
	-17.5	3.92	14.0	1.00
	-23	4.00	17.3*	1.24*
	-39	4.28	25.0	1.98
	-45	4.38	33.9*	2.71*

Table LXVIII (Cont'd).

Complex concn, m	t,	$10^3/T,$	$\Delta\nu_{\text{obsd}},$	$10^{-4} \times (T_{2P_M})^{-1},$	(a)
	°C	°K ⁻¹	Hz	sec ⁻¹	
0.0486	-49.5	4.48	37.7	3.10	
	-55	4.59	50.0*	4.16*	
	-60	4.70	62.3	5.27	

(a) A value of one is used for n in the calculation of P_M .

Table LXIX

Formyl proton chemical shifts at 60 MHz for $\text{CuCR}(\text{BF}_4)_2$
in N,N-dimethylformamide (Figure 39).

Complex concn, m	t, °C	$10^3/T$, °K ⁻¹	obsd shift, Hz	$10^{-3} \times \Delta\omega_{\text{obsd}}/P_M$, ^(a) rad sec ⁻¹
0.311	94	2.72	5.5	1.5
	74	2.88	6.5	1.8
	53	3.07	7.5	2.0
	40	3.20	7.5	2.0
0.134	43	3.16	3.5	2.2
	24.5	3.36	3.5	2.2
	14	3.48	3.0	1.9
	- 8.5	3.78	3.5	2.2
	-17.5	3.92	5.5	3.5
	-27	4.06	5.0	3.2
0.0525	-31	4.14	2.5	4.1
	-41	4.31	2.8	4.3
	-50	4.49	3.0	4.9
	-60	4.70	6.0	9.8
0.0486	-17.5	3.92	2.0	3.5
	-39	4.28	2.8	4.8
	-49.5	4.48	3.0	5.3
	-60	4.70	6.0	10.6

(a) A value of one is used for n in the calculation of P_M .

SPECIAL COLLECTIONS
UNIVERSITY OF ALBERTA LIBRARY

REQUEST FOR DUPLICATION

I wish a photocopy of the thesis by

Len Rusnak (author)

entitled NMR of Schiff Base + Porphyrin complexes

The copy is for the sole purpose of private scholarly or scientific study and research. I will not reproduce, sell or distribute the copy I request, and I will not copy any substantial part of it in my own work without permission of the copyright owner. I understand that the Library performs the service of copying at my request, and I assume all copyright responsibility for the item requested.

B30008